GEORG-AUGUST-UNIVERSITÄT
GÖTTINGEN IN PUBLICA COMMODA SEIT 1737

The enzymatic product of SH2 domain-containing inositol 5-phosphatases supports the fitness of BCR-dependent Burkitt lymphoma cells by promoting the energy metabolism

Dissertation

for the award of the degree
"Doctor rerum naturalium"
of the Georg-August-Universität Göttingen

within the doctoral program of the IMPRS Molecular Biology
of the Georg-August University School of Science (GAUSS)

submitted by

Florian Mayr

from Kempten im Allgäu

Göttingen 2023

Thesis Advisory Committee

Prof. Dr. Jürgen Wienands, Institute of Cellular and Molecular Immunology, University Medical Center, Göttingen

Dr. Alex Faesen, Research Group Biochemistry of Signal Dynamics, Max Planck Institute for Multidisciplinary Sciences, Göttingen

Prof. Dr. Lutz Walter, Department of Primate Genetics, German Primate Center, Göttingen

Members of the Examination Board

Referee: Prof. Dr. Jürgen Wienands, Institute of Cellular and Molecular Immunology, University Medical Center, Göttingen

2nd Referee: Dr. Alex Faesen, Research Group Biochemistry of Signal Dynamics, Max Planck Institute for Multidisciplinary Sciences, Göttingen

Further Members of the Examination Board:

Prof. Dr. Michael Thumm, Department of Cellular Biochemistry, University Medical Center, Göttingen

Dr. Johannes Söding, Research Group Quantitative and Computational Biology, Max Planck Institute for Multidisciplinary Sciences, Göttingen

Prof. Dr. Argyris Papantonis, Institute of Pathology, University Medical Center, Göttingen

Date of Oral Examination: November 13th, 2023

Parts of this thesis are accepted for publication as **Mayr F**, Kruse V, Fuhrmann D C, Wolf S, Löber J, Alsouri S, Paglilla N, Lee K, Chapuy B, Brüne B, Zenz T, Häupl B, Oellerich T, Engelke M, SH2 domain-containing inositol 5-phosphatases support the survival of Burkitt lymphoma cells by promoting energy metabolism, *Haematologica*, 2023

Acknowledgements

This thesis would not have been possible without the collective support of many people and institutions, which have played a crucial role during this endeavour.

First, I want to convey my appreciation to Prof. Dr. Jürgen Wienands for affording me the chance to become part of his department, allowing me to pursue my interests and of course for being part of my thesis committee. I also want to sincerely thank the other members of my thesis committee, Dr. Alex Faesen and Prof. Dr. Lutz Walter, for their helpful advice and constructive feedback.

Michael, I am especially grateful to you for your unwavering support, guidance and, of course, patience. Also, that you have always have put up with my antics and motivated me to continue, thereby helping me grow as a researcher. I will miss our chats about sports and coffee.

Gabi, Ines and Anika, working on this thesis would have been impossible without your continuous support, be it technical or administrative. Thanks for always offering a helping hand and the possibility to talk.

Furthermore, I want to thank all the members of the institute, present and former, for the great time. Particularly Saed, Nadia, Matthias, Carolina, Richard, Cagil, Jens and Stela for the fun times in the lab, the mensa and especially the coffee breaks. I enjoyed our wine tastings, barbecues and humorous conversations. It was a pleasure to work with you.

Thanks to the Deutsche Krebshilfe for the financial support for this project. Also I want to thank my collaboration partners, Dr. Thomas Oellerich, Dr. Björn Häupl, Dr. Do-

minik Fuhrmann and Dr. Sebastian Wolf from the University Hospital Frankfurt and Dr. Jens Löber from the Charite in Berlin. Thanks also to my talented Lab rotation students, and in particular Cagil and Naomi for their contribution. I would also like to express my gratitude to Steffen and Kerstin from the IMPRS MolBio program for their great support.

I want to thank Max, Laura and Jan for sharing a rope with me and keeping me balanced throughout the years. Also a big shout out to my mates from the TS and my fellow "Laborknechte".

Lastly, a big thanks to my family and friends for their unconditional support and keeping me motivated. Especially also to my grandmother Gaby. None of this would have been possible without your support.
Katha, thank you so much for keeping me grounded during this journey, for the endless scientific discussions and your continuous encouragement. I am incredibly happy to have you at my side.

Abstract

Burkitt lymphoma (BL) is an aggressively growing neoplasm owing to an over expression of the *MYC* oncogene and exploitation of the tonic B cell receptor (BCR) signaling for its survival. While it is known that the survival signaling is mediated by the phosphoinositide-3-kinase (PI3K), the details of the rewired BL-specific BCR signaling network remain poorly understood. A small-hairpin RNA (shRNA) based loss of function screen revealed that the SH2 domain-containing 5-inositol phosphatase 2 (SHIP2) potentially influences the survival of BL cells. Generation and characterisation of multiple SHIP2-deficient BL cell lines revealed a perturbed proliferation and increased apoptosis. Furthermore, these effects could not be observed in a surface BCR-negative BL cell line, suggesting that SHIP2 activity is regulated by tonic BCR signaling. SHIP2 is generally described as a negative regulator of AKT activity, but the phosphorylation levels of AKT remained stable in the absence of SHIP2. Similarly, the activation of mitogen-activated protein kinases (MAPK) were unaltered. In contrast, SHIP2 deficiency attenuated the ATP production independently of glucose uptake. It was found that the enzymatic product of SHIP2, phosphatidylinositol-3,4-bisphosphate ($PI(3,4)P_2$), is required for an efficient energy metabolism. In addition, SHIP2-deficient cells exhibited lowered aspartate levels, possibly due to inefficient glycolysis. Further, interference with the function of SHIP1 mirrored the effects observed in SHIP2-deficient cells, indicating a redundant function. Consistently, interruption of SHIP1/2 activity in BL cell lines augmented the susceptibility to inhibition of survival signaling mediated by the PI3K. This study provides a molecular basis describing how tonic BCR signals are linked to an efficient energy metabolism, which is particularly necessary to fuel a fast growing tumor such as BL. Moreover, these discoveries may serve as a basis to potentially enhance the treatment efficiency of BL by targeting the energy supply through the inhibition of SHIP proteins, thus increasing the vulnerability to targeting survival signals.

Contents

1 Acknowledgements **i**

2 Abstract **iii**

3 Abbreviations **vii**

4 Introduction **1**

4.1 The human immune system at a glance 1

4.2 The intricacies of B cell antigen receptor signaling 3

4.2.1 Structure of the B cell antigen receptor 3

4.2.2 Stimulated BCR signaling 3

4.2.3 Tonic BCR signaling 7

4.3 Germinal center reactions 8

4.4 Burkitt Lymphoma 11

4.4.1 A short history 11

4.4.2 An epidemiological tumor 12

4.4.3 Molecular characteristics of BL 13

4.5 The world of 5-inositol phosphatases 15

4.6 Aims 17

5 Materials and Methods **19**

5.1 Materials 19

5.1.1 Cell Culture 19

5.1.2 Inhibitors 23

5.1.3 Antibodies 24

5.1.4 Enzymes 25

5.1.5 Chemicals 25

5.1.6 Instruments . . . 27
5.1.7 Consumables . . . 28
5.1.8 Buffers . . . 28
5.1.9 Kits . . . 29
5.1.10 Nucleic acids . . . 30
5.1.11 Plasmids . . . 31
5.1.12 Software and databases . . . 32
5.2 Methods . . . 33
5.2.1 Handling of cell cultures . . . 33
5.2.2 Biochemical methods . . . 37
5.2.3 Molecular Biology . . . 40
5.2.4 Flow cytometry . . . 43
5.2.5 Imaging flow cytometry . . . 48

6 Results **50**
6.1 SHIP2 is predicted as an important contributor to BL fitness . . . 50
6.2 Generation of SHIP2-deficient BL cell lines . . . 54
6.3 SHIP2 is an important contributor to BL cell fitness . . . 60
6.4 shRNA-mediated ablation of SHIP2 confirmed results of CRISPR targeting 68
6.5 SHIP2 deficiency does not affect the fitness of BCR-negative BL cells . . . 71
6.6 SHIP2 is not involved in the regulation of major tonic BCR signaling pathways . . . 74
6.6.1 SHIP2 does not control the signaling efficiency of MAPKs . . . 74
6.6.2 Phosphorylation of AKT remained stable in the absence of SHIP2 . 76
6.6.3 SHIP2 deficiency sensitized BL cells to inhibition of PI3K and mTOR 79
6.6.4 Phosphoproteome analysis did not reveal SHIP2-dependent changes in the tonic BCR signaling network . . . 88
6.7 SHIP2 is required for an efficient ATP production in BL cell lines . . . 90
6.8 The SHIP2 product PI(3,4)P_2 promotes BL fitness . . . 103
6.9 Down-regulation of SHIP1 mirrors SHIP2 deficiency . . . 114

7 Discussion **130**
7.1 SHIP2 activity may be dependent on tonic BCR signaling . . . 130
7.2 AKT signaling is not affected by absence of SHIP2 . . . 131

7.3 SHIP2 deficiency increases the sensitivity to inhibition of components of the PI3K-AKT axis 133
7.4 PI(3,4)P_2 contributes to BL fitness by promoting the energy metabolism . 136
7.5 SHIP2 could promote BL fitness via aspartate synthesis 139
7.6 SHIP1 and SHIP2 may be therapeutic targets due to their redundant functions in BL cells 141
7.7 Outlook 143
7.8 Conclusion 144

Abbreviations

2-DG	2-deoxy glucose
2-NBDG	2-deoxy-2-[(7-nitro-2,1,3-benzoxadiazol-4-yl)amino]-D-glucose
3AC	3-α-aminocholestane
7-AAD	7-amino-actinomycin D
AID	Activation-induced cytidin desaminase
APC	antigen-presenting cell
BCAP	B cell adapter for PI3K
BCR	B cell antigen receptor
BH3	BCL-2 homology 3
BL	Burkitt lymphoma
BTK	Bruton's tyrosine kinase
Caspase 3	Cysteine-dependent, aspartate-specific protease 3
Caspase-9	Cysteine-dependent, aspartate-specific protease 9
CCL	Cleared cellular lysates
CD19	Cluster of differentiation 19
CHOP	cyclophosphamid-hydroxydaunorubicin-vincristin-prednison
CIN85	CBL-interacting protein of 85 kDa
CL6	B cell lymphoma 6

Continued on next page

Table 3.0: (Continued)

CRISPR	Clustered regularly interspaced short palindromic repeat
crRNA	CRISPR RNA
DAG	Diacylglycerol
DMSO	Dimethylsulfoxid
DOK-3	Docking protein 3
EBV	Epstein-Barr virus
ECAR	Extracellular acidification rate
ERK	Extracellular signal-regulated kinase
FCS	Fetal calf serum
FDC	Follicular dendritic cells
FOXO	Forkhead transcription factors
GC	Germinal center
GEF	Guanine nucleotide exchange factor
gPome	global phosphatome
gProt	global proteome
GRB2	Growth factor receptor-bound protein 2
GSK3	Glycogen synthase kinase 3
HELZ	Helicase with zinc finger
HRPO	Horse reddish peroxidase
ID3	Inhibitor of binding 3
Ig	Immunoglobulin
IgH	Immunoglobulin heavy chain
IgL	Immunoglobulin light chain
ITAM	Immunoreceptor-tyrosine-based activation motifs
INPP5D	Inositol polyphosphate-5-phosphatase D
INPPL1	Inositol polyphosphate-phosphatase like 1

Continued on next page

Table 3.0: (Continued)

IP_3	Inositol-1,4,5-triphosphate
ITIM	Immunoreceptor-tyrosine based inhibitory motif
JNK	Jun N-terminal kinase
KDM5A	Lysine demethylase 5A
LZ-B cell	Light zone B cell
MHCII	Major histocompatibility complex class II
MOMP	Mitochondrial outer membrane permeabilisation
mRNA	messenger RNA
mTOR	mammalian target of rapamycin
mTORC1	mammalian target of rapamycin complex 1
mTORC2	mammalian target of rapamycin complex 2
NCK1	NCK adapter protein 1
NFκB	Nuclear factor of κ light polypeptide gene enhancer in B cells
nHL	non-Hodgkin lymphoma
OCR	Oxygen consumption rate
p38	Mitogen-activated protein kinase 38
PAMP	Pathogen-associated molecular patten
PBS	Phosphate buffered saline
PCR	Polymerase chain reaction
PDK1	Phosphoinositide dependent kinase 1
PH	Preckstrin homology
PI	Propidium iodide
$PI(3,4)P_2$	Phosphatidylinositol-3,4-bisphosphate
$PI(3,4,5)P_3$	Phosphatidylinositol-3,4,5-triphosphate
$PI(4,5)P_2$	Phosphatidylinositol-4,5-bisphosphate
PI3K	Phosphoinositide-3-kinase

Continued on next page

Table 3.0: (Continued)

PKB, AKT	Protein kinase B
PLCδ	Phospholipase C δ
PLCγ2	Phospholipase C γ2
PLEKHA1	Pleckstrin homology domain containing protein 1
PLEKHA2	Pleckstrin homology domain containing A2
PRR	Pattern recognition receptors
PTP	Protein tyrosine phosphatases
pYome	tyrosine phosphatome
SAM	Sterile alpha motif
SDS-PAGE	Sodium dodecyl sulfate polyacrylamide gel electrophoresis
SGK	Serum- and glucocorticoid-induced kinase
sgRNA	single guide RNA
SH2	Src-homology 2
SHIP1	SH2 domain-containing inositol 5-phosphatase 1
SHIP2	SH2 domain-containing inositol 5-phosphatase 2
shNTC	non-targeting control shRNA
SILAC	Stable isotope labeling with amino acids in cell culture
SIN1	Stress-activated protein kinase-interacting protein 1
SLP65	SH2 domain-containing leucocyte adapter protein of 65 kDa
SMARCA4	SWI/SNF related, matrix-associated, actin-dependent regulator of chromatin, subfamily A, member 4
SOS	Son-of-sevenless
SYK	spleen tyrosine kinase
TCA	Tricarboxylic acid cycle
TCF-3	transcription factor 3
TCR	T cell receptors

Continued on next page

Table 3.0: (Continued)

THF	Follicular T_H cell
TP53	Tumor protein 53
trcrRNA	Transactivating crRNA
UIM	Ubiquitin interacting motif
XTT	Sodium 3´-[1- (phenylaminocarbonyl)- 3,4- tetrazolium]-bis (4-methoxy6-nitro) benzene sulfonic acid hydrate

Introduction

4.1 The human immune system at a glance

The human body is safeguarded from a plethora of pathogens by a remarkably complex defense network in the form of its immune system. It comprises the innate and adaptive immune systems, which are both characterised by their distinct abilities and mechanisms.

The innate immune system is comprised of anatomic and physiologic barriers such as the skin, pH level and temperature, but also specialized cells predominantly stemming from the myeloid lineage. Depending on their specialization, these cells reside either in the tissue or circulate in the bloodstream and possess pattern recognition receptors (PRR) that facilitate the detection of pathogen-associated molecular patterns (PAMPs). Once a PAMP is identified, the innate immune cell may respond by phagocytosis of the pathogen, production of pro-inflammatory cytokines or direct elimination of the pathogen by secretion of destructive compounds. Furthermore, the uptake of a pathogen connects the innate with the adaptive immune system, as the pathogen is processed intracellularly and presented in the form of antigens to lymphocytes in the lymph nodes [1].

The adaptive immune system offers a more time-demanding, but highly specific and tailored response to individual pathogens that also comprises a memory function. It exclusively consists of cells of the lymphoid lineage, namely B and T cells. Activation of these cells is conducted by antigens, which in the case of T cells requires the presentation as peptides by antigen-presenting cells (APC). The activation of cytotoxic CD8+ T cells has a direct detrimental effect on the target cell, whereas the activation of CD4+ T helper cells leads to the secretion of cytokines. One function of these cytokines is shape the differentiation of B cells. B cells are responsible for humoral immunity, meaning the

production and secretion of their antigen-specific receptors, referred to as "antibodies" that bind to epitopes found in encountered antigens with high affinity. The binding of antibodies to antigens disturbs vital functions of pathogens, such as preventing the invasion into cells. Also it targets the pathogen for destruction by cells of the adaptive immune system by a process called opsonisation. In contrast to the adaptive immune system, the innate immune response incorporates a memory, thereby sustaining a specific and long-term immunity to a vast array of pathogens [1].

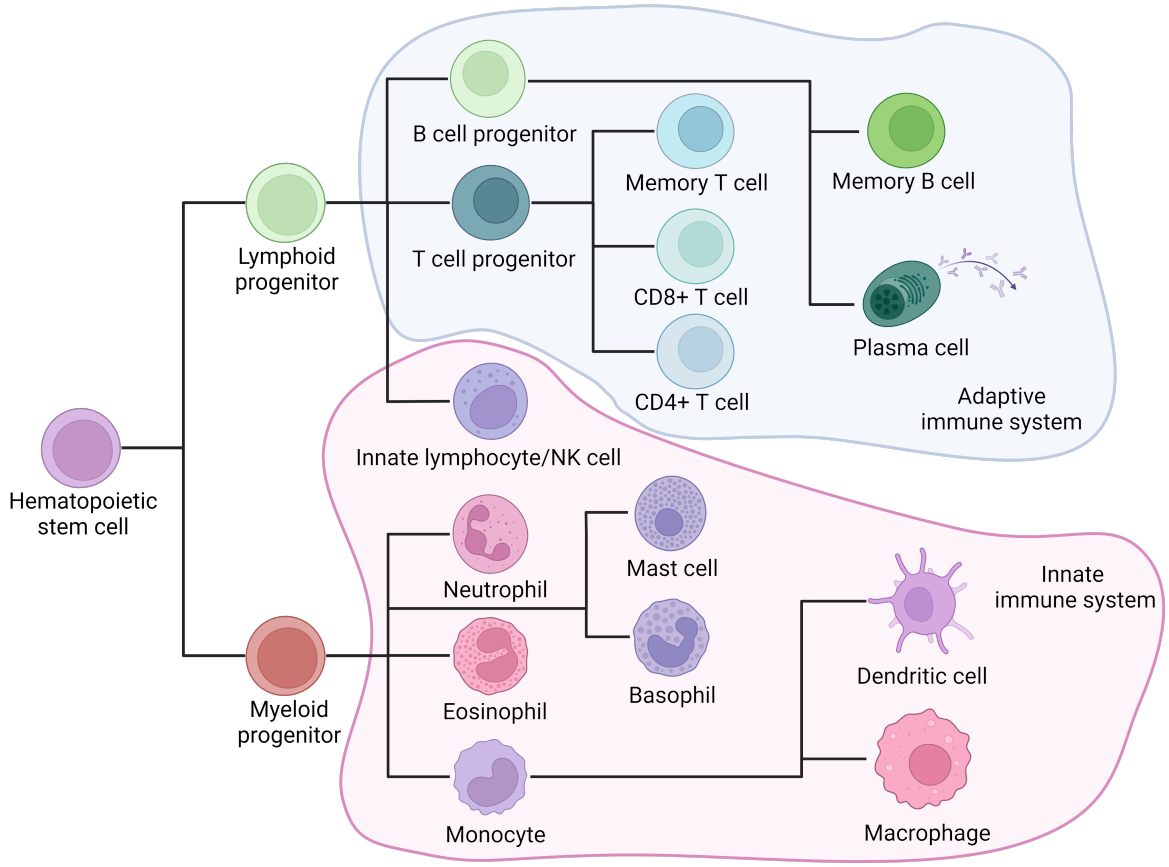

Figure 4.1: **Overview of the immune cells that compose the human immune system.** The overview shows the composition of the adaptive and innate immune system and how these cells differentiate from their lymphoid and myeloid progenitors, respectively. CD8+ T cell = cytotoxic T cell. CD4+ T cell = T helper cell. NK cell = natural killer cell.

4.2 The intricacies of B cell antigen receptor signaling

4.2.1 Structure of the B cell antigen receptor

The B cell antigen receptor (BCR) is composed of a transmembrane version of an immunoglobulin (Ig) formed by two identical heavy and light chains, respectively. These chains are connected by disulfide bonds between the two heavy chains and between the heavy and light chains. The gene segments encoding the heavy chain are designated as variable (V_H), diversity (D_H), joining (J_H) and constant (C_H), while the light chain-coding gene segments just comprise V_L, J_L and C_L. The rearrangement of these V(D)J genes enables a large antibody diversity, which in turn allows the immune system to recognize and respond to a wide range of antigens [2].

In addition to the transmembrane Ig, a functional BCR also requires the presence of CD79A and CD79B, also known as Igα and Igβ. CD79A and CD79B are directly connected by disulfide bonds and form a heterodimer that associates with the transmembrane Ig in a non-covalent manner [3]. Both, the surface expression of the BCR and the transduction of signals requires the presence of the whole complex. The signal transduction is facilitated by immunoreceptor-tyrosine-based activation motifs (ITAM) in the cytoplasmic tails of CD79A and CD79B [4]. Stimulation of the BCR triggers the phosphorylation of the tyrosine residues within the ITAMs, thereby initiating an orchestrated down-stream signaling by different pathways.

4.2.2 Stimulated BCR signaling

Several models compete to explain the BCR dynamics in resting, unstimulated B cells [5]. Yet, those models agree with the down-stream signaling processes initiated after binding of the cognate antigen to the BCR. This engagement leads to phosphorylation of the tyrosine residues in the ITAMs of the CD79A-CD79B heterodimer, as well as a non-ITAM tyrosine residue in CD79A, by Src-family kinases such as LYN[6, 7]. Phosphorylated ITAMs serve as *bona fide* binding sites for the spleen tyrosine kinase (SYK) and enable its full activation [8, 9].

Moreover, the SH2 domain-containing leucocyte adapter protein of 65 kDa (SLP65) is recruited to the phosphorylated non-ITAM tyrosine subsequently phosphorylated on multiple tyrosine residues by SYK [10, 11]. These phosphorylations on SLP65 then act as docking sites for Bruton´s tyrosine kinase (BTK) and phospholipase Cγ2 (PLCγ2) to form the Ca^{2+} initiation complex, which allows for the BTK-dependent activation of PLCγ2 [9, 12]. PLCγ2 then converts phosphatidylinositol-4,5-bisphosphate (PI(4,5)P_2) into inositol-1,4,5-triphosphate (IP_3) and diacylglycerol (DAG) [13]. IP_3 acts as a second messenger opening Ca^{2+} channels at the endoplasmic reticulum (ER) resulting in a Ca^{2+} flux into the cytoplasm [9, 14, 15]. Production of DAG eventually leads to activation of the transcription factor nuclear factor of κ light polypeptide gene enhancer in B cells (NFκB) that has importance in regulating genes controlling the proliferation, survival and differentiation of B cells [16, 17].

Engagement of the BCR also leads to activation of the mitogen-activated protein kinases of the extracellular signal-regulated kinase (ERK), Jun N-terminal kinase (JNK) and mitogen-activated protein kinase 38 (p38) types, which are important for the proliferation and survival of lymphocytes [18–20]. Activation of ERK can be facilitated by a complex consisting of SLP65, the adaptor protein growth factor receptor-bound protein 2 (GRB2) and the guanine nucleotide exchange factor (GEF) son-of-sevenless (SOS) that in turn activates the small G-protein RAS [10, 21–24]. In addition, SLP65 enables the activation of JNK by recruitment of the small GEF VAV, which activates the Rho-family GTPase RAC1, and PLCγ2 [25]. In contrast, p38 is activated by pathways targeted by DAG-dependent PKCβ [26].

Another important signaling pathway down-stream of the BCR is referred to as the phosphoinositide-3-kinase (PI3K) pathway. Engagement of the BCR results in phosphorylation of the co-receptor cluster of differentiation 19 (CD19) by SYK, FYN and BTK that provide docking sites for the B cell adapter for PI3K (BCAP) and the regulatory subunit p85 of PI3K [27]. The NCK adapter protein (NCK) is able to circumvent CD19 by binding to the phosphorylated non-tyrosine residue of CD79A to recruit BCAP and thereby commence signaling via the PI3K pathway [28]. The activated PI3K catalyses the conversion of PI(4,5)P_2 into phosphatidylinositol-3,4,5-triphosphate (PI(3,4,5)P_3) at the plasma membrane. PI(3,4,5)P_3 can be engaged by the PH domains of the protein kinase B (PKB, typically referred to as AKT), the phosphoinositide dependent kinase 1

(PDK1) and of the stress-activated protein kinase-interacting protein 1 (SIN1), which is part of the mammalian target of rapamycin (mTOR) complex 2 (mTORC2) [29–32]. The binding of AKT to PI(3,4,5)P_3 is preceded by its phosphorylation at serine 473 facilitated by mTORC2 [33]. This phosphorylation leads to a conformational change that exposes the PH domain, enabling the recruitment to the plasma membrane, and exposing the activation loop [33, 34]. AKT binding to PI(3,4,5)P_3 is further phosphorylated by PDK1 at threonine 308 in its activation loop, thereby becoming fully active [35–38].
In turn, activated AKT promotes survival by mediating the deactivation of pro-apoptotic BCL-2 related proteins, cysteine-dependent, aspartate-specific protease 9 (caspase-9) and forkhead transcription factors (FOXO) [39–41]. Moreover, it contributes to proliferation and metabolism by activation of mTORC1 and deactivation of glycogen synthase kinase 3 (GSK3) among many other targets [42–44]. PI(3,4,5)P_3 at the plasma membrane is converted by the SH2 domain-containing inositol 5-phosphatases (SHIP1/2) to phosphatidylinositol-3,4-bisphosphate (PI(3,4)P_2) [29, 45]. The SHIP proteins were long perceived as antagonists to AKT signaling due to the removal of membrane docking sites [46]. While this is true for some cases, recent studies could provide evidence that PDK1 and certain AKT isoforms can also bind to PI(3,4)P_2, suggesting that SHIP activity may diversify AKT signaling or even has AKT-independent functions [29–31, 47].

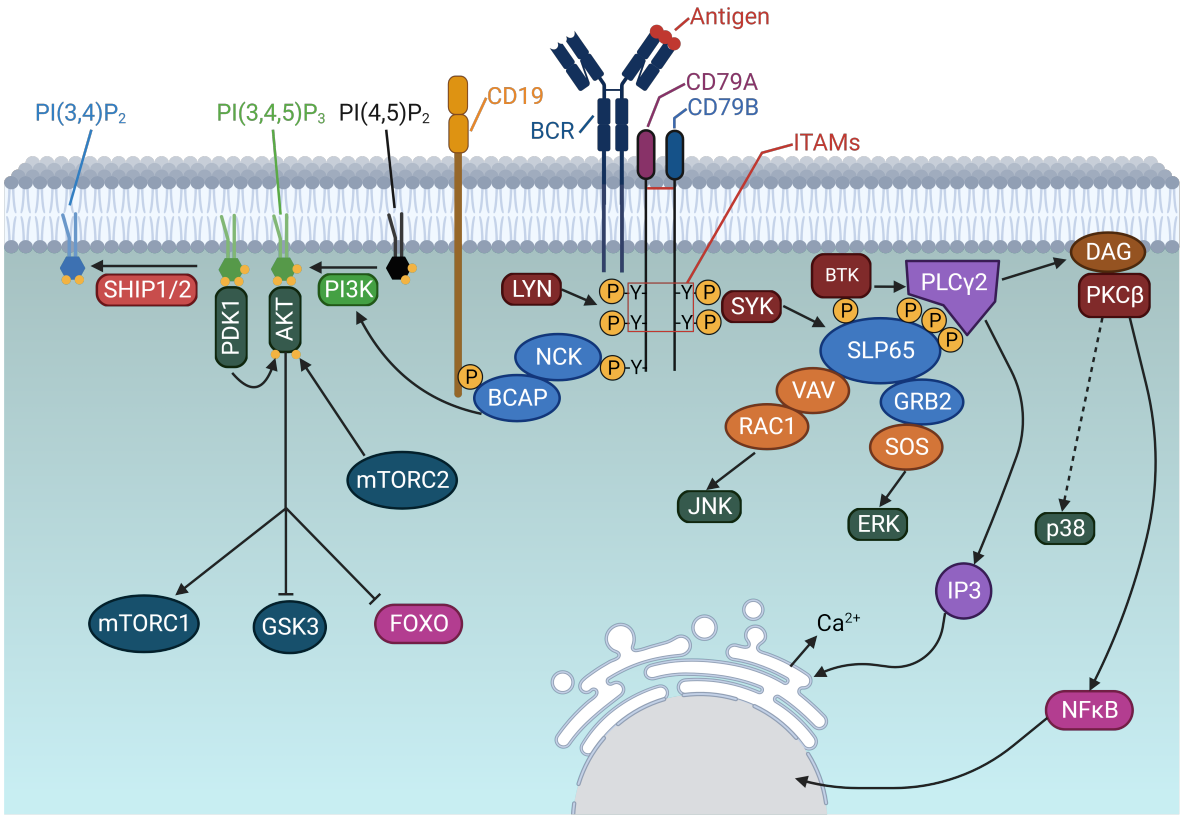

Figure 4.2: **Overview of the processes down-stream of the BCR after antigen engagement.** Binding of the cognate antigen to the BCR results in phosphorylation of the ITAM and non-ITAM tyrosine residues of the CD79A-CD79B heterodimer by LYN. The phospho-tyrosines of the ITAM act as a docking site for SYK, which in turn phosphorylates SLP65. These phosphorylations serve as a binding motif for BTK and PLCγ2. BTK activates PLCγ2, which produces DAG and IP3. IP3 acts as a second messenger on Ca^{2+} channels at the endoplasmic reticulum causing release of Ca^{2+} into the cytoplasm. DAG serves as an anchor for PKCβ that enables activation of p38 and NFκB, allowing the latter to translocate into the nucleus. SLP65 also serves as starting point for the activation of JNK via VAV and RAC1, as well as ERK by GRB2 and SOS. Moreover, LYN and SYK phosphorylate CD19, which enables the binding of BCAP and recruitment of the PI3K. CD19 can also be recruited independently of phosphorylations by recruitment of NCK to the non-ITAM phospho-tyrosine of CD79A. The activated PI3K catalyses the conversion of $PI(4,5)P_2$ to $PI(3,4,5)P_3$. This phosphoinositide serves as an anchor point for the PH domains of AKT and PDK1. AKT is phosphorylated at serine 473 by mTORC2 and threonine 308 by PDK1, leading to full activation, thereby inhibiting GSK3 and FOXO and promoting mTORC1 activity. $PI(3,4,5)P_3$ is converted by SHIP1 and SHIP2 into $PI(3,4)P_2$.

4.2.3 Tonic BCR signaling

The BCR is able to also transduce a signal in the absence of a cognate antigen, which is referred to as tonic BCR signaling. Studies from Wienands *et al* in 1996 already revealed that the inhibition of protein tyrosine phosphatases (PTP) in resting B cells leads to activation of SYK followed by BCR signaling independently of antigen engagement, implicating the presence of preformed BCR transducer complexes [48]. Quickly thereafter, Lam *et al* showed in an *in vivo* ablation experiment that the presence of surface BCR is essential for the survival of mature B cells [49]. Stimulated BCR signaling is $\tilde{4}.3$ times stronger than tonic BCR signaling. Moreover, the strength of the tonic BCR signaling correlates with the number of BCRs found on the cell surface [50].

Three models compete for the best explanation of the tonic BCR signaling. The Homotypic pre-BCR-binding model proposes that the self-aggregation of BCR facilitates down-stream signaling. This model is based on the existence of oligomeric BCR complexes on the cell surface, which are facilitated by non-covalent interactions between polar amino acid residues located in the heavy chains [51]. Indeed, mutation of these amino acids results in tonic signaling incompetent BCRs [52]. However, the clear evidence for the existence of these oligomeric BCR complexes is still pending [53].

The lipid raft compartmentalisation model suggests that a portion of the surface BCRs are compartmentalised in lipid rafts. This promotes LYN activity leading to ITAM-dependent down-stream signaling [54]. Supported is this model by the finding that BCRs increasingly associate with lipid rafts during antigen engagement [55].

In contrast to the previous models, the equilibrium model is based on individual BCRs and not on aggregation. Instead, the model postulates a homeostatic, dynamic equilibrium of positively and negatively regulating factors that come into proximity of monomeric BCRs on the cell surface. The positive regulation is facilitated by the close proximity of CD45 to the BCR, thereby triggering LYN followed by phosphorylation of the ITAMs in CD79A-CD79B and activation of SYK [6–8, 56]. The negative regulation is based on the close proximity of CD22 that enables the recruitment of PTPs to their immunoreceptor-tyrosine based inhibitory motifs (ITIM) that deactivate the signal by dephosphorylation of the ITAMs and SYK [57]. In summary, the model proposes a continuous toggling be-

tween the active and inactive states of the BCR, leading to a persistent signaling baseline within the cell [58].

While the upstream process that initiates the tonic BCR signaling is still under discussion, some of the down-stream processes that are necessary to maintain B cell survival have been addressed. Neither over-activation of NFκB, the ERK activating kinase MEK nor over expression of BCL-2 could rescue the survival of mature B cells after ablation of the BCR [49]. Instead, only the over-activation of the PI3K pathway resulted in an AKT-dependent phosphorylation of FOXO1 could rescue the survival [59].

4.3 Germinal center reactions

The germinal center (GC) reaction occurs within secondary lymphoid organs, such as lymph nodes and the spleen, during the adaptive immune response [60]. It is essential for the generation of specialized B cells, including memory B cells and plasma cells, which play a critical role in the immune system's ability to respond to pathogens effectively. The processes involved in the germinal center reactions are shown in a simple overview in figure 4.3.

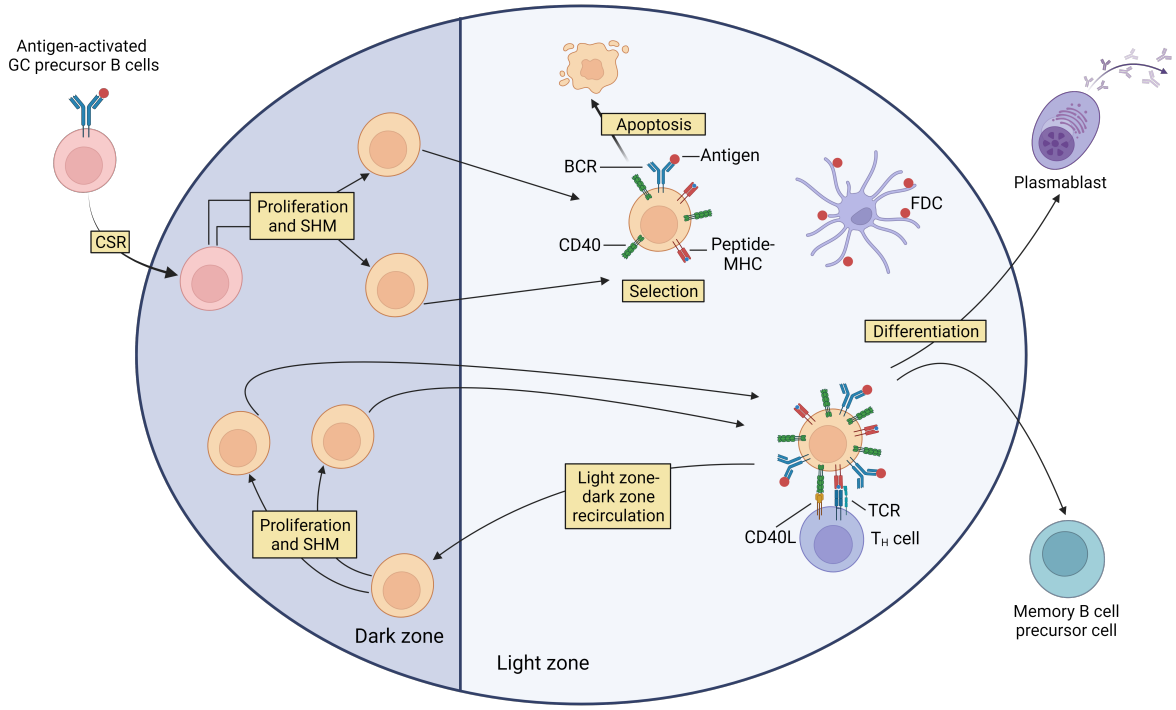

Figure 4.3: **Overview of the dynamics of B cells in the germinal center.** Activated germinal center (GC) precursor B cells undergo class switch recombination (CSR) followed by clonal expansion leading to the formation of dark zone of the GCs. Afterwards, the clonal B cells undergo somatic hypermutation (SHM), which introduces random mutations in the exons encoding for the variable regions of the antibodies. Afterwards these cells migrate into the light zone where they are positively selected according to the affinity of their BCR to engage and internalise the antigen presented by follicular dendritic cells (FDC). Furthermore, the light zone B cells present the antigen via their major histocompatibility complex class II to the follicular T_H cell. Positively selected cells recirculate into the dark zone where they again proliferate and mutate to increase their affinity for the antigen. This process is repeated until the affinity is sufficient to allow differentiation into either memory B cell precursors or plasmablasts that produce and secrete high affinity antibodies. Adapted from DeSilva & Klein [61]. TCR = T cell receptor.

As soon as the BCR on a B cell is engaged by its specific antigen in secondary lymphoid organs, the B cell becomes activated, leading to internalisation of the antigen and presentation of peptides on major histocompatibility complex class II (MHCII). Once a type 2 T helper cell binds to the MHCII-peptide complex, the B cell gets activated and migrates into lymphoid follicles within the secondary lymphoid organs [60, 62–64]. The activated

cell undergoes class switch recombination to enable production of functionally optimised antibody isotypes [65]. Furthermore, and the activated B cell clonally expand, thereby generating a germinal center. These centers consist of a transient and dynamic microenvironment with specific regions, dark zone and light zone, each full filing a distinct role [66].

In the dark zone, the clones of the initially activated B cell proliferate further and undergo somatic hypermutation. In this process, the activation-induced cytidin desaminase (AID) catalyses the conversion of cytidin to uracil in the complementary-determining regions of the exons that encode for the immunoglobulin heavy (IgH) and immunoglobulin light (IgL) chains [67]. The generated uracil-guanine mismatches are repaired by an interplay of uracil-DNA-glycosylases and DNA polymerases, which eventually creates single point mutations [68]. These random mutations introduce a diversity into the clonal B cell population, resulting in BCRs with varying affinities for the initially encountered antigen. These BCRs are displayed on the cell surface and the cell migrates into the light zone of the germinal center [69]. Errors in the somatic hypermutation process can result in tumorigenesis of several lymphomas [70]

In the light zone, the B cell (LZ-B cell) undergoes an antigen- and T cell-dependent selection process that tests the affinity of the LZ-B cell's BCR [71, 72]. First, the LZ-B cell bind via their BCR to an antigen supplied by follicular dendritic cells (FDC), which are able to retain and display antigens in the form of immune complexes [73]. The binding of the BCR results in the internalisation of the BCR-antigen complex, followed by subsequent processing and loading of the antigen onto MHCII proteins [74–77]. The resulting antigen-MHCII complex is presented to follicular T_H (THF) cells, which are located at the LZ of GCs [78, 79]. This triggers the expression of *MYC* to mark it as a positively selected LZ-B cell [80]. Whether antigen engagement of the BCR leads to BCR-dependent survival signaling in LZ-B cells is still a matter of debate [81, 82]. However, the affinity of its BCR to the antigen is tested, because the higher the affinity is the more antigen can be internalized, eventually leading to more efficient help by the THF [83, 84]. If the LZ-B cell is not able to engage an antigen via its BCR due to low affinity, it is not receiving any survival signaling eventually leading to apoptosis [85, 86]. A similar fate awaits those LZ-B cells that display no CD40 on their cell surface, as they are unable to receive T cell help [87, 88]. In addition, LZ-B cells that respond to antigen binding with too strong BCR signaling also enter apoptosis, presumably to maintain self-tolerance [89–91].

The positively selected cells undergo different fates. Some cells can recirculate into the dark zone where they again undergo proliferation and somatic hypermutation followed by re-circulation into the light zone and selection [92, 93]. This process is repeated multiple times to refine the affinity of the B cell, a process called affinity maturation [94, 95]. On the other hand, positive selection can also lead to the differentiation of the cell into specialized B cells. Positively selected LZ-B cells that experience increased help from the THF and exhibit a high affinity for the antigen may differentiate into short-lived plasma blasts or longer-lived plasma cells [96–100]. In contrast, LZ-B cells that differentiate into memory B cell precursors are characterised by relative quiescence and the current understanding is that these cells require less THF help [101, 102]. However, the details of the differentiation process in the LZ of GCs remain to be elucidated.

4.4 Burkitt Lymphoma

4.4.1 A short history

Burkitt lymphoma (BL) is a malignant non-Hodgkin lymphoma first described in 1958 by the Irish surgeon Denis Parson Burkitt while working in equatorial Africa [103]. He outlined an extremely fast-growing tumor in children that was unfailingly lethal and predominantly located at the jaw and head. While initially regarded as round-cell sarcoma, histological analyses revealed a remarkable similarity to other lymphomas, confirming that BL has a lymphoid origin [103, 104]. In contrast to most other types of cancer, it quickly became obvious that BL is primarily found in equatorial regions and in particular equatorial Africa, which suggested an association to endemic, infectious diseases [105]. It took only two years to confirm this theory, as the oncogenic Epstein-Barr virus (EBV) was discovered in lymphoblasts derived from BL patients [106, 107]. Further discoveries in BL were an increased size of chromosome 14 accompanied by a concurrent loss of genetic material on chromosome 8 [108, 109]. Detailed analyses of this abnormality revealed a translocation of the *MYC* oncogene from chromosome 8 to chromosomes 2,14 or 22 thereby causing an over expression of *MYC* that drives the rapid proliferation of BL [110, 111].

4.4.2 An epidemiological tumor

Apart from EBV, Kafuko and Burkitt quickly realised that BL is also prevalent in regions with endemic malaria, suggesting a connection that was confirmed by significantly lower BL cases in regions that successfully combated this infectious disease [112, 113]. On this basis, the occurrence of BL was categorized by the WHO according to its associated origin into endemic, spontaneous and immunodeficiency-associated BL [114]. While the three variants exhibit similar morphological and immunophenotypic characteristics, such as their "starry sky" appearance in histological preparations, they differ in terms of their epidemiological and clinical attributes [114, 115].

Endemic BL, also known as African-type, commonly occurs in regions holoendemic for *Plasmodium falciparum* [113]. As stated in the initial discovery, it predominantly manifests as a fast-growing tumor in the head and neck, but can also be found in the abdominal region [103, 116]. Endemic BL occurs virtually always in young children, with a high burden of parasites being associated with an increased risk of developing BL [117–119]. Though, asymptomatic malaria also increases the likelihood of emerging BL [120]. Moreover, endemic BL is almost exclusively associated with an EBV infection [121, 122]. Similar to malaria, increased titers of antibodies targeting EBV are linked to an increased risk [123]. In contrast to the other types of BL, endemic BL occurs in large numbers, especially in sub-Saharan countries and Papua-New Guinea where it accounts for 50 - 75 % of childhood cancers [124–126].

Sporadic BL, also known as spontaneous, American-type or non-Africa, is the type of BL most commonly found in regions without endemic malaria such as Europe and North America [127]. Compared to endemic BL, it has low incidence numbers, yet it is the most common sub type of non-Hodgkin lymphoma in the USA [128]. The median patient age lays at 10 years, while there is a second patient group between 40 and 75 years old [129]. Males exhibit a higher likelihood to develop sporadic BL compared to women [129]. In contrast to endemic BL, sporadic BL typically manifests in the abdominal region and is associated with EBV in only 20 - 30 % of the cases, predominantly in the older patient group, and is not a defining feature of the sporadic type [130]. Furthermore, there is mounting evidence suggesting that the paediatric form of sporadic BL differs strongly from the one occurring in older patients, indicated by the increased association to EBV and accumulated mutations [130, 131]. Sporadic BL is histologically indistinguishable from endemic BL and both types show only slight alterations in their gene expression

profiles [132–134].
Immunodeficiency-associated BL is usually found in patients suffering the acquired immunodeficiency syndrome (AIDS) but also occurs in post-transplant patients [135–137]. While incidence numbers are low compared to endemic BL, the immunodeficiency-associated BL accounts for $\tilde{4}0$ % of lymphomas in AIDS patients [138]. Apart from the association to immunodeficiency, this type of BL does not differ from the previous types in terms of EBV involvement or clinical manifestation [139]. The major difference compared to the other types is found in the higher median age of the patient group at 40 - 45 years old [140].

BL is treated with a variety of different chemotherapies which consist of a mix of DNA damaging, immunosuppressive compounds and recently also including monoclonal antibodies [141–143]. While the efficiency of the therapy is rising constantly and the overall cure rate is excellent, it still lacks an efficient application in elderly patients and those with lacking medical care [127, 144]. Moreover, relapsed or refractory patients have a poor prognosis highlighting the need for novel therapeutic approaches [145].

4.4.3 Molecular characteristics of BL

The hallmark of BL cells is the over expression of the *MYC* oncogene, which encodes for the c-MYC transcription factor [146]. This over expression of *MYC* is caused by a translocation event in germinal center B cells. According to the current opinion, this translocation is an accidental process that takes place during somatic hypermutation or class switch recombination and is based on an abnormal expression of AID that induces chromosomal breaks [147–150]. In more detail, the *MYC* gene is placed under the regulatory control of the promoters of either the Ig-heavy chain (t(8;14)(q23;q32)), the kappa- (t(2;8)(p12;q24)) or lambda- (t(8;22)(q24;q11)) light chain, with the first being the most prevalent translocation as depicted in figure 4.4.

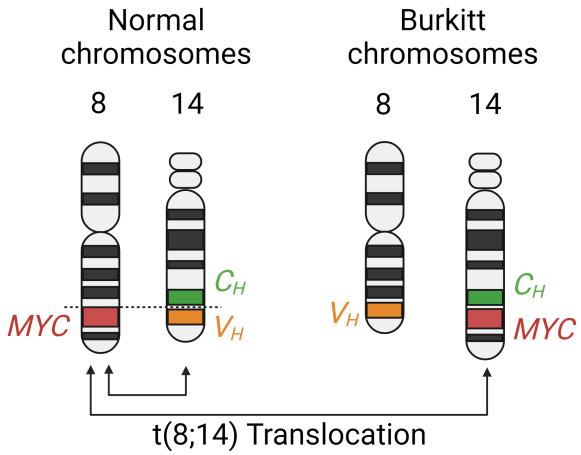

Figure 4.4: **Depiction of the most prevalent *MYC* translocation in BL.** The t(8;14)(q23;q32) translocation transfers the *MYC* oncogene from chromosome 8 to chromosome 14 and brings it under control of the promoter of the Ig heavy chain gene locus.

c-MYC facilitates the activation of ~15 % of the human genes, many of those involved in metabolism and cell cycle [151]. Moreover, *MYC* is often mutated in its transactivation domain further contributing to tumorigenesis [152, 153]. However, the deregulation of *MYC* alone is not sufficient for the generation of BL, which rely on further mutated genes [152, 154]. The reason for this is that while some *MYC* mutations facilitate survival signaling, over expression of *MYC* generally leads to the activation of p53-mediated apoptosis [153, 155]. Consequently, the encoding gene *TP53* experiences inactivating mutations in ~35 % of BL cases [156, 157].

BL cells typically display an IgM-based BCR, suggesting that BL cells undergo somatic hypermutation but not class switch recombination [158]. In fact, a large portion of BL cells relies on an intact BCR to transduce a tonic BCR signaling, which they exploit for their survival [152, 159]. Accordingly, a substantial part of BL cells harbor mutations in the transcription factor 3 (*TCF-3*) and inhibitor of binding 3 (*ID3*) genes [152, 160]. *TCF-3* encodes for a transcription factor that facilitates a transcriptional program similar to dark zone germinal center cells ensuring the survival and proliferation of BL cells [161]. Partly this is due to the promotion of continuous BCR signaling caused by down regulation of factors that negatively regulate the BCR signaling network [57, 152]. *ID3* encodes for a repressor of *TCF-3* and as such often carries inactivating mutations in BL [162]. In addition, it was shown that specifically the tonic BCR signaling-dependent

PI3K pathway is important to ensure the survival of BL cells [152]. An extensive, mass spectrometry-based analysis of the phospho-proteome of BCR-dependent BL cell lines unveiled an intricate and expansive tonic BCR signaling network that extends well beyond the PI3K pathway [163]. Moreover, it was shown that SYK is stabilised by the chaperone heat-shock protein 90 (HSP90), thereby maintaining the BL-specific tonic BCR survival signaling ([164]. The one-carbon metabolism is another factor BL cells use to sustain survival as it was shown by increased apoptosis upon inhibition of the key one-carbon metabolism enzyme serine hydroxymethyltransferase 2 (SHMT2) [165].

In terms of association with EBV, it is still unclear if EBV is an uninvolved passenger virus due to its extremely high incidence of almost 90 % of the human population [166]. However, its high association with BL, especially in the endemic type, and the fact that EBV+ BL cells exhibit different mutations compared to non-EBV BL suggests some contribution to lymphomagenesis from the virus [131, 167]. This is further supported by the fact that EBV was shown to transform cells on its own [168, 169]. Furthermore, the latent EBV infection leads to the production of anti-apoptotic proteins such as EBNA1, which ensures the survival of the host cell and thus contributes to the formation or severity of BL [170].

Due to its mutational landscape, exploitation of diverse survival signaling pathways and association to infectious diseases, BL can be regarded as an extremely heterogeneous tumor.

4.5 The world of 5-inositol phosphatases

The two 5-phospho inositol phosphatases SHIP1 and SHIP2, now designated as SHIPs, are encoded by two separate genes, inositol polyphosphate-5-phosphatase D (*INPP5D*) and inositol polyphosphate-phosphatase like 1 (*INPPL1*) respectively [171]. The proteins share a 51 % sequence homology thus exhibiting a similar domain structure, especially in the N-terminus [47]. Both proteins possess an N-terminal Src-homology 2 (SH2) domain that facilitates a regulated interaction with phosphorylated tyrosine residues of other proteins, though the SH2 domains show significant sequence alterations between SHIP1 and SHIP2 [47]. The SH2 domains exhibit the same ligand specificity but SHIP1 showed

an extremely fast association and dissociation rates compared to SHIP2 [172]. The SHIP proteins contain the same enzymatic core consisting of a PH domain to bind $PI(3,4,5)P_3$, the catalytic phosphatase domain followed by a C2 domain to transiently bind $PI(3,4)P_2$ [173]. The largest differences are located in the C-terminal regions. Here, SHIP1 retains one additional tyrosine phosphorylation (NPXY)-motif and proline-rich (PXXP)-motif that enable binding to SH3 domain-containing proteins [174, 175]. In contrast, SHIP2 has a ubiquitin interacting motif (UIM) that regulates the activity [176]. Moreover, the sterile alpha motif (SAM) of SHIP2 enables homotypic or heterotypic interactions with other SAM-containing proteins [177, 178]. An overview of the structure of SHIP proteins is given in figure 4.5.

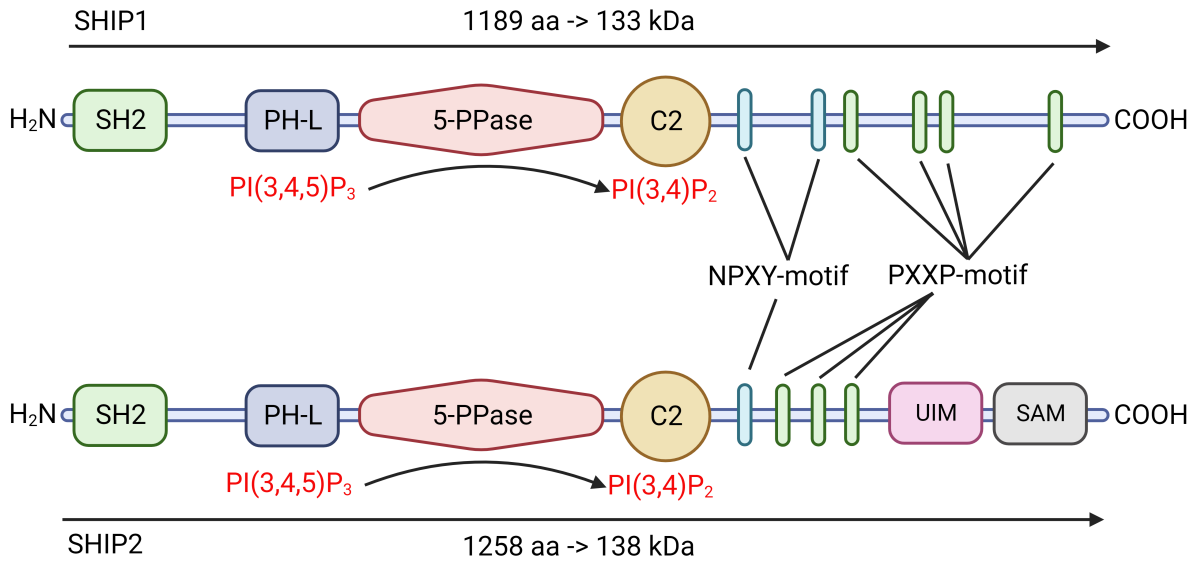

Figure 4.5: **Domain structure of the 5-inositol phosphatases SHIP1 and SHIP2.** Both proteins possess a N-terminal Src-homolgy 2 (SH2) domain to facilitate protein interactions as well as a Pleckstrin homology (PH-L) domain, catalytic phosphatase domain (5-PPase) and C2 domain to facilitate its enzymatic function. SHIP1 and SHIP2 differ in their C-terminal domains. SHIP1 contains two distinct NPXY-motifs and an additional PXXP-motif compared to SHIP2. In contrast, the C-terminus of SHIP2 is composed of an ubiquitin interacting motif (UIM) and a sterile alpha motif (SAM). Adapted from Pedicone *et al* [47].

SHIP1 is mainly expressed in cells of the hematolymphoid lineage which includes central nervous system resident microglia cells, mesenchymal stem cells and osteoblasts where it is a proven modulator of cell proliferation [179–185]. In contrast, owing to the more ubiquitous expression of *INPPL1*, SHIP2 is found in almost all cells of the human body

[186]. In the literature, SHIP2 is predominantly associated with the negative regulation of insulin signaling [187, 188].

As mentioned in the previous chapter, both SHIPs primarily facilitate the enzymatic conversion of PI(3,4,5)P_3 to PI(3,4)P_2 and are the sole proteins to do so at the plasma membrane [29, 45]. However, SHIP1 has also been shown to occasionally use PI(4,5)P_2 and phosphatidyl inositol-1,3,4,5-tetrakisphosphate (PI(1,3,4,5)P_4 as substrate [189–191]. The recruitment process that targets SHIP1 to the plasma membrane in B cells is relatively well understood. SHIP1 is mandatory for negative regulation of the activated BCR signaling either by interaction with FCγRIIB or in a receptor-independent way via interaction with docking protein 3 (DOK-3) and GRB2 [192–195]. Consequently, the absence of SHIP1 in B cells leads to hyper reactivity indicated by a strongly increased Ca^{2+} mobilisation after stimulation of the BCR [195] In contrast to SHIP1, the regulation and function of SHIP2 in B cells is less understood.

4.6 Aims

The exact mechanisms employed by BL cells to exploit the tonic BCR signaling are still poorly understood and require an in-depth analysis of the involved factors. Recent studies revealed that both SHIPs possess phosphosites that are activated during tonic BCR signaling, suggesting a potential regulatory function [163]. Moreover, a shRNA screen comparing BL cell lines with non-blood cell lines indicated a high relevance of SHIP2, but not SHIP1 for the survival of BL cell lines [196]. Furthermore, the latest in-house study demonstrated that SHIP2 is important for survival and proliferation in a single BL cell line, though the underlying mechanisms are yet to be unraveled [197].

To improve the understanding of how SHIP2 could contribute to the fitness of tonic BCR-dependent BL cells, I pursue the following goals:

(i) Validate that SHIP2 contributes to BL fitness by perturbation of SHIP2 function via small molecule inhibitors and genetic targeting

(ii) Replication of SHIP2-dependent effects in multiple cell lines to represent the heterogeneity of BL

(iii) Assess if the SHIP2 effects are based on tonic BCR signaling

(iv) Reveal the fitness-promoting mechanisms mediated by SHIP2

(v) Identify if SHIP2 is a promising drug target in BL

To achieve these goals I plan to generate SHIP2-deficient BL cell lines representing different BL entities by utilizing the clustered regularly interspaced short palindromic repeat (CRISPR) system. These SHIP2-deficient cell lines will be reconstituted with a Citrin-SHIP2 fusion protein to exclude potential clonal effects. The generated cell lines will be assessed for effects regarding proliferation and apoptosis. In addition, the signal transduction in the absence of SHIP2 will be analysed in detail by analysis of single targets but also phosphoproteomics to identify global changes. The results will be validated by the application of selective small molecule inhibitors and induced expression of shRNA targeting the SHIP2 coding gene.
The overarching goal of this study is to provide molecular details that may give rise to new therapeutic approaches in the treatment of BL, since small molecule-based inhibition of 5-inositol phosphatases may be a feasible option and such inhibitors have already been established.

Materials and Methods

5.1 Materials

5.1.1 Cell Culture

5.1.1.1 Eukaryotic cell lines

Ramos

The Ramos cell line was derived from the ascitic fluid of a 3-year-old Caucasian male, showing symptoms of an American-type Burkitt lymphoma. The cell line is tested negative for presence of EBV [198]. Ramos cells contain the characteristic BL t(8;14)(q22;32) translocation of the *MYC* gene. Further, the cells express an IgM with a λ-light chain and the cell line is proven to be BCR-dependent [163, 199]. In addition, Ramos cells carry mutations in tumor protein 53 (*TP53*) and other oncogenes such as B cell lymphoma 6 (*BCL6*), the BCR regulator *TCF3* and SWI/SNF related, matrix-associated, actin-dependent regulator of chromatin, subfamily A, member 4 (*SMARCA4*) [156, 200, 201]. Ramos cells were kept at a concentration of 0.6-1.2*10^6 cells/ml and split every day 1:3.5 or every second day 1:10.

Daudi

The Daudi cell line was derived in 1967 from B lymphoblasts isolated from peripheral blood of a black, 16-year-old male. These cells exhibit the characteristic t(8;14)(q22;32) translocation of *MYC* and express an IgM and ϰ-light chain on the cell surface [199, 202]. Furthermore, Daudi cells have been shown to be BCR-dependent [163]. Moreover, the cell line carries mutations in *TP53*, the BCR regulator *ID3* and *FOXO1* among many others [156, 200, 201]. In addition, Daudi cells are tested positive for a latent EBV infection [203]. Prior to this thesis, *INPPL1*$^{-/-}$ as well as *INPPL1*$^{-/-}$ + CitSHIP2 cells were generated by

Dr. Vanessa Kruse [197]. Daudi cells were kept at a concentration of 0.8-1.4*10^6 cells/ml and split every second day 1:5.

DG75

DG75 cells were established in 1975 from the pleural effusion of a 10-year-old Caucasian male with clinical symptoms of Burkitt lymphoma[204]. This cell line also possesses the typical t(8;14)(q22;32) translocation of *MYC* but are tested EBV-negative [205]. DG75 cells express an IgM paired with a κ-light chain on their cell surface and show no signs of EBV infection [204]. Moreover, this cell line lacks BAK and BAX proteins which effectively prevents their entry into apoptosis [206]. Further, *TP53*, *TP53B1*, *TCF3* and the PI3K pathway proteins *PIK3CG*, *PIK3C2G* and *PIK3CB* are mutated [207]. DG75 cells were kept at a concentration of 0.6-1.2*10^6 cells/ml and split every day 1:3.5 or every second day 1:10.

Raji

The Raji cell line was established in 1963 from a black 12-year-old male suffering from Burkitt lymphoma [208]. The cells exhibit the classical t(8;14)(q22;32) translocation of *MYC* [199]. In addition, Raji cells carry a latent EBV infection [209]. Raji cells produce mainly cytoplasmic IgM and show no BCR on their cell surface [210, 211]. The cell line exhibits mutations in *TP53*, *PIK3C2G* and *PIK3R3* [200, 201]. Raji cells were kept at a concentration of 0.6-1.2*10^6 cells/ml and split every day 1:3.5 or every second day 1:10.

Cell lines

Cell lines used and generated as well as their genotype and modifications are shown in table 5.1. Table 5.2 shows the different cell culture medias and the added components while the suppliers of the supplements are listed in table 5.3.

Table 5.1: Used and generated cell lines.

Name	**Genotype**	**Description**	**Biosafety level**	**Reference**
Ramos	WT	Wild type	1	ATCC CRL-1596TM

Ramos	*INPPL1*$^{-/-}$	CRISPR/Cas9 induced SHIP2 deficiency	1	This work
Ramos	*INPPL1*$^{-/-}$+CitSHIP2	Reconstitution of a Citrine-SHIP2 construct via PiggyBac	1	This work
Ramos	shNTC	Tet-On inducible shRNA construct for a non-targeting control transfected via PiggyBac	1	This work
Ramos	sh*INPP5D* #1-2	Tet-On inducible shRNA targeting *INPP5D* transfected via PiggyBac	1	This work
Ramos	sh*INPPL1* #1-3	Tet-On inducible shRNA targeting *INPPL1* transfected via PiggyBac	1	This work
Ramos	WT GFP	Stable GFP expression transfected via PiggyBac	1	This work
Ramos	WT GFP-2xTAPP1-PH	Stable GFP-2xTAPP1-PH expression transfected via PiggyBac	1	This work
Ramos	WT Tet-On GFP	Tet-On GFP construct transfected via PiggyBac	1	This work
Ramos	WT Tet-On GFP-2xTAPP1-PH	Tet-On GFP-2xTAPP1-PH construct transfected via PiggyBac	1	This work
Ramos	*INPPL1*$^{-/-}$ GFP	Stable GFP expression transfected via PiggyBac	1	This work
Ramos	*INPPL1*$^{-/-}$ GFP-2xTAPP1-PH	Stable GFP-2xTAPP1-PH expression transfected via PiggyBac	1	This work
Ramos	*INPPL1*$^{-/-}$ Tet-On GFP	Tet-On GFP construct transfected via PiggyBac	1	This work
Ramos	WT	Tet-on Myr-Cer-INPP4A construct transfected via PiggyBac	1	N. Elbing
Ramos	WT	Tet-on Cer-PLCδ-PH construct transfected via PiggyBac	1	M. Engelke
Ramos	*INPPL1*$^{-/-}$ Tet-On GFP-2xTAPP1-PH	Tet-On GFP-2xTAPP1-PH construct transfected via PiggyBac	1	This work
Daudi	WT	Wild type	2	ATCC CCL-213TM

Daudi	*INPPL1*$^{-/-}$	CRISPR/Cas9 induced SHIP2 deficiency	2	V. Kruse
Daudi	*INPPL1*$^{-/-}$+CitSHIP2	Reconstitution of a Citrine-SHIP2 construct via PiggyBac	2	V. Kruse
Daudi	shNTC	Tet-On inducible shRNA construct for a non-targeting control transfected via PiggyBac	2	This work
Daudi	sh*INPP5D* #1-2	Tet-On inducible shRNA targeting *INPP5D* transfected via PiggyBac	2	This work
Daudi	sh*INPPL1* #1-3	Tet-On inducible shRNA targeting *INPPL1* transfected via PiggyBac	2	This work
Raji	WT	Wild type	2	ATCC CCL-86TM
Raji	*INPPL1*$^{-/-}$ #1-2	CRISPR/Cas9 induced SHIP2 deficiency	2	This work
DG75	WT	Wild type	1	ATCC CRL-2625TM
DG75	*INPPL1*$^{-/-}$	CRISPR/Cas9 induced SHIP2 deficiency	1	This work
DG75	*INPPL1*$^{-/-}$+CitSHIP2	Reconstitution of a Citrine-SHIP2 construct via PiggyBac	1	This work
DG75	WT Tet-On GFP	Tet-On GFP construct transfected via PiggyBac	1	This work
DG75	WT Tet-On GFP-2xTAPP1-PH	Tet-On GFP-2xTAPP1-PH construct transfected via PiggyBac	1	This work
DG75	*INPPL1*$^{-/-}$ Tet-On GFP	Tet-On GFP construct transfected via PiggyBac	1	This work
DG75	*INPPL1*$^{-/-}$ Tet-On GFP-2xTAPP1-PH	Tet-On GFP-2xTAPP1-PH construct transfected via PiggyBac	1	This work

5.1.1.2 Cell culture media

Table 5.2: Used Cell culture media and added components. Labeled and unlabeled amino acids were obtained from Sigma.

Medium	Manufacturer	FCS %	Other components
RPMI-1640 Gluta-Max	Gibco	0, 1, 5, 10, 20	1 % Penicillin/Streptomycin, 50 mM L-glutamine, 50 µM β-mercaptoethanol
DMEM	Gibco	10	50 mM L-glutamine
SILAC RPMI-1640 "light"	Gibco	10, dialyzed	1 % Penicillin/Streptomycin, 50 mM L-glutamine, 50 µM β-mercaptoethanol, non labeled 0.0115 mM L-arginine, 0.27 mM L-lysine, 0,2 g/l L-proline
SILAC RPMI-1640 "heavy"	Gibco	10, dialyzed	1 % Penicillin/Streptomycin, 50 mM L-glutamine, 50 µM β-mercaptoethanol, 0.0115 mM L-arginine, ($^{13}C_3$,$^{15}N_4$)(+10) and 0.27 mM l-lysine ($^{13}C_3$,$^{15}N_2$)(+8), 0.2 g/l l-proline
RPMI glucose-free	Gibco	0	Penicillin/Streptomycin, 50 µM β-mercaptoethanol

Table 5.3: List of supplements for the cell culture media.

Supplement	Supplier
β-mercaptoethanol	Sigma-Aldrich
L-Glutamine	Roth
Penicillin/Streptomycin	Sigma-Aldrich
Fetal Calf Serum	Biochrom
Fetal Calf Serum, dialyzed	PAN Biotech
L-Arginine:HCl $^{13}C_6$ $^{15}N_4$ (Arg+10)	Cambridge Isotope Lab.
L-Lysine:2HCl $^{13}C_6$ $^{15}N_2$ (Lys+8)	Cambridge Isotope Lab.
L-Arginine	Sigma-Aldrich
L-Lysine	Sigma-Aldrich
L-Proline	Sigma-Aldrich

5.1.2 Inhibitors

Table 5.4: Inhibitors with their respective targets.

Inhibitor	Target	Supplier
AS1949490	SHIP2	Tocris
3AC	SHIP1	MedChemExpress

GSK2334470	PDK1	MedChemExpress
Capivasertib	AKT	CaymanChemicals
Ipatasertib	AKT	MedChemExpress
2-deoxy glucose	GPI and HK	MedChemExpress
Copanlisib	PI3K	MedChemExpress

5.1.3 Antibodies

The antibodies and their specifications are listed according to their application either in table 5.5 for Western Blot analysis or table 5.6 for flow cytometry.

Table 5.5: List of antibodies used for Western Blot analysis of proteins. Primary antibodies were diluted 1:1000 while secondary antibodies were diluted 1:10000.

Antibody	**Clone / Identification**	**Supplier**
α-SHIP2	C76A7	CST
α-SHIP1	C40G9	CST
α-JNK	9252	CST
α-p-JNK(T183/Y185)	G9	CST
α-ERK	Clone16	BD
α-p-ERK(T202/Y204)	D13144E	CST
α-p-p38(T180/Y182)	Clone36	BD
α-pan-AKT	40D4	CST
α-p-AKT(S473)	D9E	CST
α-p-AKT(T308)	244F9	CST
α-β-Actin	8H10D10	CST
α-mouse IgG-HRPO	1030-05	Southern Biotech
α-mouse IgG1-HRPO	1071-05	Southern Biotech
α-mouse IgG2a-HRPO	1081-05	Southern Biotech
α-mouse IgG2b-HRPO	1091-05	Southern Biotech
α-rabbit IgG-HRPO	4030-05	Southern Biotech

Table 5.6: List of antibodies used for flow cytometry.

Antibody	**Clone / Identification**	**Supplier**
α-hIgM-AF647	109-606-129	Jackson ImmunoResearch
α-Glut1	A-4	SantaCruz
α-Glut4	IF8	SantaCruz
α-cleaved Caspase 3-APC	C92-605(RUO)	BD
α-p-AKT(S473)-APC	D9E	CST

α-p-AKT(T308)-AF647	B-5	SantaCruz
α-Cytochrome C-AF647	6H2.B4	BioLegend
α-mouse IgG1-AF647	1072-31	Southern Biotech

5.1.4 Enzymes

Table 5.7: List of enzymes utilized in this study.

Enzyme	Manufacturer
Phusion®DNA polymerase	NEB
Taq DNA polymerase	NEB
Taq PCR Master Mix	Quiagen
T4 DNA ligase	NEB
Calf intestinal phosphatase (CIP)	NEB
Restriction endocnucleases	NEB
Proteinase K	Macherey-Nagel
RNAse H	NEB

5.1.5 Chemicals

Table 5.8: List of utilized chemicals.

Chemical	Manufacturer
10x CutSmart buffer	NEB
6x DNA loading buffer	NEB
2-NBDG	Thermo Fisher
4-(2-hydroxyethyl)-1-piperazineethanesulfonic acid (HEPES)	Roth
7-Aminoactinomycin D (7-AAD)	Invitrogen / BioLegend
Acrylamide/bis-acrylamide Rotiphorese Gel 30	Roth
Agarose	Peqlab
Alamethicin	Enzo Life Sciences
Ammonium persulfate (APS)	Roth
Ampicillin	Serva
BH3-peptides	JPT Peptide Technologies
Bovine serum albumin (BSA)	Roth
Deoxynucleoside triphosphate (dNTP) mix	NEB
Digitonin	Sigma-Aldrich
Dimethyl sulfoxide (DMSO)	Thermo Fisher
Di-sodium hydrogen phosphate (Na_2HPO_4)	Roth

Dithiothreitol (DTT)	Roth
DNALadder GeneRuler 1 kb	Roth
Doxycycline	Thermo Fisher
Ethidium bromide	NEB
Ethylendiaminetetraacetate (EDTA)	Roth
4 % formaldehyde solution	Süsse Labortechnik
Glycerol	Roth
Glycine	Roth
Cytofix^{TM} fixation buffer	BD
Hoechst33342	Sigma-Aldrich
Hydrochloric acid (HCl)	Roth
Hydrogen peroxide (H_2O_2)	Roth
INDO-1 AM	Life Technologies
Isopropanol	Roth
Luminol	Sigma-Aldrich
Magnesium chloride ($MgCl_2$)	Roth
Methanol	Roth
MitoTracker$_{TM}$ Deep Red	Thermo Fisher
N-ethylmaleimide	Sigma-Aldrich
PageRuler Plus protein ladder	Thermo Fisher
p-coumaric acid	Sigma-Aldrich
5x Phusion HF buffer	NEB
Pluronic F-127	Life Technologies
Perm/Wash buffer I	BD
Potassium chloride (KCl)	Roth
Potassium dihydrogen phosphate (KH_2PO_4)	Merck
Propidium iodide	Sigma-Aldrich
Protease Inhibitor cocktail	Sigma-Aldrich
Puromycin	InvivoGen
Sodium azide (NaN_3)	Roth
Sodium deoxycholate ($C_{24}H_{39}O_4Na$)	Roth
Sodium dodecyl sulfate (SDS)	Roth
sodium fluride (NaF)	Roth
Sodium orthovanadate (Na_3VO_4)	Sigma-Aldrich
Sodium pyrophosphate ($Na_4P_2O_7$)	Roth
T4 DNA Ligase buffer	NEB
Tetramethylethylendiamine (TEMED)	Roth
Tris(hydroxymethyl)-aminomethane (Tris)	Sigma-Aldrich
Tween20	Roth
Trypan Blue solution (0.4 %)	Sigma-Aldrich

Tryptone/peptone	Roth
Yeast extract	Roth
Urea	Thermo Fisher
Ethanol	Roth
Triton X-100	Roth

5.1.6 Instruments

Table 5.9: List of instruments.

Instrument	Manufacturer
Agarose Gel electrophoresis system	Peqlab
Balance BP61	Sartorius
Balance H95	Sartorius
Cell culture incubator HeraCell150	Heraeus
CellDrop BF	DeNovix
Centrifuge 5417R	Eppendorf
Centrifuge 5430R	Eppendorf
Centrifuge Multifuge 3SR	Heraeus
Chemi Lux gel imager	Intas Systems
Electrophoresis Power Supply EPS 301	Amersham Biosciences
Electrophoresis Power Supply EPS 601	Amersham Biosciences
Flow cytometer FACSCelesta	Becton Dickinson
Flow cytometer LSR II	Becton Dickinson
Flow cytometer LSRFortessa^{TM} X-20	Becton Dickinson
Freezer Platilab 340	Angelantoni Industrie
Ice machine	Ziegra
ImageStream X Mark II	Amnis
Laminar flow cabinet HERA safe	Heraeus
Light microscope TELAVAL 31	Zeiss
Magnetic stirrer m21/1	Framo
Mastercycler epgradient	Eppendorf
Microplate reader PowerWave 340	BioTek
Mini PROTEAN®Tetra Cell	Bio-Rad
MiniSpin	Eppendorf
Neon Electroporation System MPK500	Thermo Fisher
pH-Meter inoLab	WTW
Photometer NanoDrop 200	Thermo Fisher
Pipettes	Eppendorf
Semi-Dry transfer unit TE 77	GE Healthcare

Shaking incubator 3005	GFL
Thermomixer C	Eppendorf
Thermomixer comfort	Eppendorf
ThermoStat plus	Eppendorf
UV-illuminator ChemoCam	Intas Systems
Vortex Genie 2	Scientific industries
Water bath	GFL
Water bath	Memmert
Water Purification System Milli-Q Millipore	Sartorius

5.1.7 Consumables

Table 5.10: List of consumables.

Consumable	Supplier
Blotting Paper Whatman	GE Healthcare
CELLSTAR 96/48/24/12/6-well suspension culture plates	Greiner bio-one
CELLSTAR culture dishes 60 mm, 100 mm, 145 mm diameter	Greiner bio-one
CELLSTAR serological pipettes 2 ml, 5 ml, 10 ml, 25 ml	Greiner bio-one
CELLSTAR tubes 15 ml, 50 ml	Greiner bio-one
384-well plates	Corning®
Cryo tubes	Greiner bio-one
Electroporation curvettes	Invitrogen
Electroporation tips 10 µl, 100 µl	Invitrogen
Filter pipette tips	Greiner bio-one
Flow cytometry tubes, 5 ml	Sarstedt
Luer-Lok™ Syringe 50 ml	BD
Nitrocellulose membrane Protran™ supported 0.45 µm	Amersham
PCR tubes 0.2 ml	Sarstedt
Pipette tips	Greiner bio-one
Reaction tubes 1.5 ml, 2 ml	Greiner bio-one
Sterile filter Filtropur S 0.2 µm	Sarstedt

5.1.8 Buffers

Table 5.11: List of buffers and their respective composition.

Name	Composition

5x Laemmli buffer	150 mM Tris-HCl pH 6.8, 15 % SDS, 50 % glycerol, 0.05 % bromophenol blue, 0,5 M DTT, in ddH_20
Krebs-Ringer solution	140 mM NaCl pH 7.4, 10 mM D-glucose, 10 mM HEPES, 4 mM KCl, 1 mM $MgCl_2$, add fresh: 1 mM $CaCl_2$
1x PBS	137 mM NaCl, 2.7 mM KCl, 4.3 mM NA2HPO4x12H2O, 1.4 mM KH_2PO_4, in ddH_20
Cleared cellular lysis buffer	Produce fresh: 2x RIPA buffer, 1 % NP-40, 1 mM sodium orthovanadate, 5 mM NaF, 1:50 protease inhibitor cocktail, in ddH_20
Urea lysis buffer	20 mM HEPES pH 8.0, 9 M urea, 1 mM sodium orthovanadate, 2.5 mM sodium pyrophosphate, 1 mM beta-glycerophosphate
TAG lysis buffer	10 mM Tris pH 8.0, 50 mM KCl, 0.45 % NP-40, 0.45 % Tween20, in ddH_20
Blocking and antibody dilution solution	5 % BSA, 0.01 % NaN_3, in 1x TBS-T
Stacking gel buffer	0.5 M Tris-HCl pH 6.8, 14 mM SDS, in ddH_20
Resolving gel buffer	1.5M Tris-HCl pH 8.8, 14 mM SDS, in ddH_20
SDS-PAGE buffer	25 mM Tris, 192 mM glycine, 0.1 % SDS, in ddH_20
1x TBS-T	20 mM Tris pH 7.6, 137 mM NaCl, 0.1 % Tween20, in ddH_20
1x TAE	40 mM Tris, 20 mM glacial acetic acid, 1 mM EDTA, in ddH_20
ECL solution	4 ml ECL SA, 400 µl ECL SB, 1.2 µl 30 % H_2O_2
ECL SA	100 mM Tris-HCl pH 8.6, 0.28 mM luminol in ddH_20
ECL SB	6.7 mM p-coumaric acid in DMSO
Annexin staining buffer	2 % BSA, 0.01 % NaN_3, in 1x PBS
MEB2 buffer	150 mM mannitol, 150 mM KCl, 10 mM HEPES-KOH, 5 mM succinate, 1 mM EGTA, 1 mM EDTA, 0.1 % BSA, pH 7.5, 0.002 % digitonin
N2 buffer	1.7 M Tris base, 1.25 M glycin, pH 9.1
BH3 profiling staining solution	10 % BSA, 2 % Tween20, in 1x PBS
Blotting buffer	48 mM Tris, 39 mM glycine, 0.0375 % SDS, 0.001 % Na_3, 20 % methanol, in ddH_2O
Lysogeny broth (LB) medium	10 g/l tryptone/peptone, 5 g/l yeast extract, 5 g/l NaCl, pH 7, in ddH_2O

5.1.9 Kits

Table 5.12: List of utilized ready to use kits and their respective manufacturers.

Kit	Manufacturer
Nucleospin®Gel and PCR Clean-up Kit	Macherey-Nagel
Nucleobond®XTRA Midi EF Plasmid Kit	Macherey-Nagel

Nucleospin®Plasmid easy pure Kit	Macherey-Nagel
TA^{TM} cloning Kit with pCR^{TM}2.1	Invitrogen
APC Annexin-V apoptosis detection Kit with 7-AAD	BioLegend
XTT Proliferation Assay	Serva
Neon Transfection System 10 µl Kit	Thermo Fisher
Neon Transfection System 100 µl Kit	Thermo Fisher

5.1.10 Nucleic acids

5.1.10.1 CRISPR RNAs

The custom made CRISPR RNAs (crRNA) used for CRISPR/Cas9 targeting of genes are shown in table 5.13 along with their sequence and target exon.

Table 5.13: List of custom made crRNAs obtained from IDT.

Sequence	**Target gene**	**Target site**	**Designer**
5'-GGTCCGAGACAGCGAGAGCG-3'	*INPPL1*	Exon 1	V. Kruse
5'-GTCTCGCACGACTACCTGAA-3'	*INPPL1*	Exon 5	F. Mayr

5.1.10.2 shRNAs

The shRNAs used for inducible silencing of genes are listed in table 5.14. Designs of the shRNAs were obtained from [212].

Table 5.14: List of shRNAs used in this study. All shRNAs were ordered as 97mer oligos from Eurofins.

shRNA	**Sequence**	**Target**
sh*INPPL1* # 1	CCAAGTTCTTCATCGAGTTCTA	*INPPL1*
sh*INPPL1* # 2	GCGGCGTGATGTCTTCAATAAA	*INPPL1*
sh*INPPL1* # 3	GCCGCACCAAGTTCTTCATCGA	*INPPL1*
sh*INPP5D* # 1	GCAGCTCATTAAGTCACAGAAA	*INPP5D*
sh*INPP5D* # 2	TCAGGTGCTATGCCACATTGAA	*INPP5D*

5.1.10.3 Primers

The primers used in this thesis are shown in table 5.15. The primers were designed using Primer3Plus to have a melting temperature (T_M) between 55 and 65 °C. While the primer length varied according to application, the primer design adhered to the guidelines published by Howard Judelson [213] in terms of 3'-binding, dimerization and hairpin formation.

Table 5.15: List of primers and their respective sequence and application. Primers were ordered from Eurofins.

Primer	Sequence 5'-3'	Application
INPPL1_E5_for	cactgaacaggagacccttttct	CRISPR/Cas9 targeting validation
INPPL1_E5_rev	agagatcatgccaccttcttct	CRISPR/Cas9 targeting validation
INPPL1_E1_for	atatcattgggagaactgagaagc	CRISPR/Cas9 targeting validation
INPPL1_E1_rev	atttttcgtcatcacagtcacact	CRISPR/Cas9 targeting validation
Citrine_XhoI_for	TAATCTCGAGATGGTGAG-CAAGGGCGAG	CitSHIP2 into PB
INPPL1_AsiSI_rev	TAATgcgatcgcTCACTTGCT-GAGCTGCAGG	CitSHIP2 into PB
2xGFP-PH-TAPP1_AgeI_for	TAATaccggtatggtgagcaagggcgag	GFP-2x-TAPP1-PH into PB
2xGFP-PH-TAPP1_NotI_rev	TAATgcggccgccgtgcgcttctgcctca	GFP-2xTAPP1-PH into PB
GFP-2x-TAPP1-PH_NheI_for	TAATgctagcatggtgagcaagggcgag	GFP-2x-TAPP1-PH into PB-TRE
GFP-2x-TAPP1-PH_AgeI_rev	TAATaccggtcgtgcgcttctgcctca	GFP-2x-TAPP1-PH into PB-TRE
miRseq5	TGTTTGAATGAGGCTTCAGTAC	Sequencing primer for the inducible shRNA construct
miRE-Xho-for	TGAACTCGAGAAG-GTATATTGCTGTTGACAGT-GAGCG	Amplification of 97mer oligos for the inducible shRNA construct
miRE-EcoOligo-rev	TCTCGAATTCTAGCCC-CTTGAAGTCCGAGGCAGTAGGC	Amplification of 97mer oligos for the inducible shRNA construct

5.1.11 Plasmids

Table 5.16: List of plasmids generated in this study. PB=PiggyBac, TRE=Tetracycline regulated element. Referenced constructs were supplied by Addgene.

Plasmid	Generated from	Reference
PB-CitSHIP2	F. Mayr	Insert is a Gift from Christophe Erneux
PB-TRE-shRNA	S. Alsouri	shRNA construct obtained from [212]
PB-TRE-GFP	F. Mayr	Original construct obtained from [214]
PB-GFP-2xTAPP1-PH	F. Mayr	Original construct obtained from [215]

PB-GFP	F. Mayr	F. Mayr
PB-TRE-2xTAPP1-PH	F. Mayr	Original construct obtained from [215]
PB-TRE-Myr-Cer-INPP4a	N. Elbing	Generated by Naomi Elbing
PB-TRE-Cer-PLCδ-PH	M. Engelke	Generated by Michael Engelke

5.1.12 Software and databases

The software and databases used in this thesis are listed in table 5.17 and table 5.18.

Table 5.17: List of software used to generate this study.

Software	**Application**	**Developer**
FlowJo V10.6.2	Analysis of flow cytometry data	Treestar
GraphPad Prism 10	Statistics and generation of graphs	Dotmatics
SnapGeneViewer	Cloning and plasmid management	Dotmatics
Fiji	Image processing	W.Rasband, NIH
FACSDiva	Flow cytometry data acquisition	BD
BioRender	Generation of illustrations	biorender.io
Overleaf	Text processing	Overleaf
Chemostar Professional	Western Blot image acquisition	Intas
Citavi 6	Citation management	Swiss Academic Software
Microsoft Excel 2016	Data management	Microsoft
NEBioCalculator	Ligation calculator	NEB
Python	Bioinformatics	Python Software Foundation
MetaboAnalyst 5.0	Metabolomic analysis	Wishart Research Group, University of Alberta
metassist	Metabolomic analysis	MetaSys
Ideas 6.2	Analysis of imaging flow cytometry data	Luminex

Table 5.18: List of databases consulted for this study.

Database	**Application**	**Website**
Primer3Plus	Primer Design	https://www.bioinformatics.nl/cgi-bin/primer3plus/primer3plus.cgi

Uniprot	Protein data	http://www.uniprot.org/
STRING-db	Protein-Protein interactions	https://string-db.org/
Basic Local Alignment Search Tool (BLAST)	Sequence alignment	https://blast.ncbi.nlm.nih.gov/Blast.cgi
Ensembl	Genomic and RNA data	https://www.ensembl.org/index.html
Genebank	Genomic and RNA data	https://www.ncbi.nlm.nih.gov/genbank/
Pubmed	Literature search	https://pubmed.ncbi.nlm.nih.gov/
Protein atlas	Protein expression	https://www.proteinatlas.org/
cBioPortal	Cancer genomics	https://www.cbioportal.org/
KEGG Pathway Database	Biological pathway analysis	https://www.genome.jp/kegg/pathway.html
DepMap Portal	Cancer genomics	https://depmap.org/portal/
canSAR.ai	Cell line data	https://cansar.ai/
Genomic Data Commons Data Portal	Cancer genomics and distribution	https://portal.gdc.cancer.gov/
Genotype-Tissue Expression (GTEx)	Gene expression mapping	https://gtexportal.org/home/

5.2 Methods

5.2.1 Handling of cell cultures

5.2.1.1 Cell culture conditions

All cell lines were incubated in a humidified cell culture incubator at 37 °C and 5 % CO_2. Suspension cells were cultured in RPMI1640 GlutaMax medium (Gibco) with FCS concentrations varying from 0 to 20 %, 1 % Penicillin/Streptomycin, 1 mM L-glutamine and 50 µM β-mercaptoethanol. Under normal conditions, the cells were cultivated in medium containing 10 % FCS (R10). All centrifugations in the cell culture were carried out at room temperature, 300 g and 4 min if not indicated otherwise. Adherent cells were cultivated in DMEM containing 10 % FCS, 1 % Penicillin/Streptomycin and 1 mM L-glutamine. Splitting was carried out by first washing with 1x PBS followed by detaching with 0.05 % trypsin. Cells were frozen by resuspending 3-5*10^6 cells in 1 ml of ice cold freezing medium followed by 48 h at -80 °C and -150 °C for long term storage. Thawing was carried out by incubating a cryo tube at 37 °C in the water bath with subsequent dilution of the thawed cell suspension in 5 ml R10. The resulting cell suspension was

centrifuged, the supernatant removed and the cell pellet was resuspended in fresh R10.

5.2.1.2 Cell counting

Cell counting was prepared by mixing cell suspension 1:2 with 0.4 % trypan blue to allow discrimination between living and dead cells. The counting was then performed either with a Neubauer improved counting chamber or with the automated cell counter DeNovix CellDrop™.

5.2.1.3 Electroporation of suspension cells

Electroporation of CRISPR/Cas9-complexes

The clustered regularly interspaced short palindromic repeat (CRISPR)/Cas9 system uses a single guide (sgRNA) to form a complex with the endonuclease Cas9. This RNA-protein complex is then targeted to the DNA-sequence complementary to the sgRNA where the Cas9 generates a double strand break in the DNA. This kind of DNA damage is repaired by a complex, template-free mechanism called non-homologous end joining which typically trims the 3'- and 5'-ends in the double strand break until the damaged nucleotides are removed and the strands can rejoin. However, since this repair mechanism lacks a template strand compared to other mechanisms, it always causes sequence alterations at the damaged site. If the system targets an exon, this usually results in the formation of a premature stop codon which leads to a shortened messenger RNA (mRNA) and a non-functional protein.

Electroporations were carried out with the Neon™ Transfection system (Thermo Fisher Scientific) and its associated buffers and materials. Prior to the electroporation procedure, the CRISPR RNA (crRNA) (IDT), transactivating crRNA (trcrRNA) (IDT) and enhancer (IDT) were diluted to 200 µM with IDT buffer pH 7.5. The enhancer is further diluted to a working concentration of 10.8 µM with nuclease free water. Afterwards, the crRNA/trcrRNA duplex mix is prepared by mixing 0.88 µl of crRNA and trcrRNA with 2.24 µl IDT duplex buffer followed by incubation at 95 °C for 5 min. Meanwhile, the Cas9 mix is prepared by adding 0.4 µl resuspension buffer (Buffer R) to 0.6 µl Cas9 nuclease (IDT). For each following electroporation 1 µl of duplex- and Cas9-mix are mixed together and incubated for 20 min at room temperature. The final electroporation mix consists of 4 µl diluted enhancer, 2 µl Cas9/duplex-mix and $1*10^6$ cells in 16 µl buffer R. 10 µl of the final electroporation mix were taken up with the electroporation pipette and added

into the electroporation curvette containing 3 ml of buffer E. The electroporation is then carried out according to the parameters for each cell line in table 5.19. After electroporation the cells were carefully added to a 24-well containing pre-warmed R20 medium. The electroporated cells were then given time to recover for up to 3 days.

Table 5.19: Parameters for the electroporation of the referenced cell lines. Voltage indicates the intensity and width the duration of each respective pulse.

Cell line	Voltage [v]	Number of pulses	Width [ms]
Ramos	1400	2	20
Daudi	1400	1	20
DG75	1350	1	30
Raji	1500	1	30

Electroporation of PiggyBac-transposon-transposase constructs

The PiggyBac-transposon-transposase system was employed for transfection and stable integration of constructs into human-derived BL cell lines. The principle was first described by Malcom Fraser in 1989 [216]. In this system, cells are electroporated with two plasmids; one coding for the CitSHIP2 construct under control of a CMV promoter and a puromycin selection marker, the other one expresses a transposase. In cells positive for both plasmids, the transposase is expressed and identifies the inverted terminal repeat sequences flanking the gene of interest and the selection marker. The transposase then transposes the sequence into TTAA chromosomal sites [217], which, due to the CMV promoter, should enable a constitutive expression of the gene of interest.

As for the CRISPR/Cas9 system, the Neon^{TM} Transfection system and its associated buffers and materials were used. The cells were counted and washed with warm 1x PBS. Each electroporation reaction requires $3*10^6$ cells, 1 µg transposase plasmid and 2 µg construct plasmid in a total of 120 µl buffer R. To achieve this mixture, the cells and plasmids mixes are separately prepared in 60 µl of buffer R each. After joining of both mixtures, the resulting cell-plasmid mix is taken up in a 100 µl electroporation pipette tip and the cells were electroporated according to table 5.19. After successful electroporation, the cells were carefully added into 4 ml of pre-warmed R20 in a 6-well. The cells were allowed to recover for up to three days, followed by selection and/or sorting.

5.2.1.4 Single cell dilution

Single cell dilution was performed to generate clones with identical genotypes. After cells have recovered from electroporation they were counted. Afterwards, 60 cells were transferred from the cell suspension to 50 ml of R20. The resulting diluted cell suspension was then transferred in a 96-well plate by adding 200 µl cell suspension into each well. The plate was then monitored for growth for up to 14 days. If cells proliferated in a well, the cells were expanded and the successful targeting was validated by Western Blot analysis before freezing and storage of clones.

5.2.1.5 Cell sorting

Cell sorting was conducted at the cell sorting facility of the university medical center Göttingen. At least $5*10^6$ cells of the respective cell lines were collected and pipetted through a Cell-Strainer cap (Falcon) to avoid aggregation of cells. The sorting was then performed according to the intensity of the selection markers using a BD FACS Aria II. The obtained cells were allowed to recover for multiple days in R20 containing 1 % Penicillin/Streptomycin.

5.2.1.6 Stable isotope labeling with amino acids in cell culture

Ramos cells were subjected to stable isotope labeling with amino acids in cell culture, which allows assessing their proteome and phospho-proteome. Therefore, Ramos *INPPL1*$^{-/-}$ + CitSHIP2 cells were cultivated in SILAC medium containing "heavy" isotopes of the amino acids L-arginine and L-lysine while SHIP2-deficient cells received non-isotope amino acids (see table 5.2). After 7 days, the labeling process was finished and the cells were heavily expanded. Once a sufficient amount of cells was reached, the cells were collected and cells were lysed in urea lysis buffer with a concentration of $5*10^6$ cells per 20 µl buffer. The lysates were stored at -80 °C until shipment to the Johann Wolfgang Goethe University in Frankfurt am Main for mass spectrometric analysis conducted by Dr. Björn Häupl. Phosphoproteomic and proteomic analysis was performed according to [165, 218, 219].

5.2.2 Biochemical methods

5.2.2.1 XTT Proliferation assay

The proliferation of cells can be monitored by using the colorimetric XTT proliferation assay [220, 221]. This assay is based on the conversion of the yellowish tetrazolium salt XTT (sodium 3´-[1- (phenylaminocarbonyl)- 3,4- tetrazolium]-bis (4-methoxy6-nitro) benzene sulfonic acid hydrate) into orange formazan. This conversion can only be carried out in living, metabolically active cells by mitochondrial dehydrogenases. Hence, the conversion rate is a measure of cell proliferation [222]. The absorption rate of the formazan can be measured at 450 nm and the reference at 650 nm. Therefore, cells have to be seeded in 96-well plates in R5 medium, as a higher content of FCS can interfere with the XTT reagents. Seeding densities depend on cell line and expected incubation time. To assess the proliferation after 24 h, 2000 cells/well of Ramos/DG75 cells, 4000 cells/well Raji or 8000 cells/well Daudi cells were seeded. After the intended cultivation time, 50 µl/well of the XTT assay mix, consisting of reagent A (XTT salt) and 1:50 reagent B (N-methyl dibenzopyrazine methyl sulfate) which is an electron coupling reagent, were added on top of the medium and the plate was further incubated for h in the cell culture incubator to allow conversion of the XTT. After the incubation, the plate is immediately measured in an plate reader (BioTek Powerwave). For final evaluation, the reference is subtracted from the 450 nm readings and normalised to a control.

5.2.2.2 Seahorse Assay

The Seahorse assay is used to quantify the ATP production rate of living cells is a proprietary assay developed by Agilent. The ATP production rate is the combination of the glycolytic ATP production given by the extracellular acidification rate (ECAR) and the mitochondrial ATP production indicated by the oxygen consumption rate (OCR). These assays were performed by Dr Dominik Fuhrmann at the University Hospital in Frankfurt am Main.

5.2.2.3 Cleared cellular lysates

The preparation of cleared cellular lysates (CCL) was performed by first spinning cells down at 4 °C followed by washing with cold 1x PBS. All further steps are carried out at 4 °C or on ice to limit protein degradation in the samples. After centrifugation, the

cells were lysed using 20 µl of freshly produced cleared cellular lysis buffer for every $1*10^6$ cells in the sample. The lysate was then incubated on ice for at least 15 min and up to 60 min depending on the pellet size. Afterwards, the nuclei are pelleted by spinning down at full speed for 15 min and 4 °C. Subsequently, the supernatant is carefully transferred into a fresh tube and 5 µl pre-warmed 5x Laemmli-buffer are added for every 20 µl of lysate. The SDS in the Laemmli-buffer reduces disulfide bonds in the protein causing linearization of the amino acid chain and, through accumulation on the protein, increases the negative charge which allows analysis by gel electrophoresis [223]. The resulting mixture is incubated for 10 min at 95 °C and stored at -20 °C.

5.2.2.4 SDS-PAGE

Sodium dodecyl sulfate polyacrylamide gel electrophoresis (SDS-PAGE) is a technique used to separate denatured proteins on a gel according to their size [224]. First, the polyacrylamide gel has to be casted. This gel consists of an upper stacking gel which focuses the sample at the interface to the separation gel due to the lower percentage of acrylamide and the resulting faster traveling of the linearized proteins. The higher acrylamide content in the separation gel enables then the separation of the proteins according to the length of the amino acid chains due to the different traveling times through the gel. The gels were prepared as shown in table 5.20.

Table 5.20: Composition of the stacking and separation gel used for SDS-PAGE. The indicated volumes are sufficient for one gel. The polymerisation reagents TEMED and APS were added as the final components directly before pouring the gel.

Reagent	**Stacking gel**	**Separation gel**
Stacking gel buffer	934 µl	-
Separation gel buffer	-	2 ml
Acrylamide/bis-acrylamide Rotiphorese Gel 30	600 µl	2.65 ml
TEMED	3.75 µl	7.5 µl
10 % APS	37.5 µl	50 µl
ddH_2O	2.2 ml	3.275 ml

After the polymerisation of the gel was finished, it was inserted into the Mini PROTEAN®Tetra cell SDS-PAGE system. The electrophoresis chamber was filled with SDS-PAGE running buffer and 25 µl of the samples obtained from the cell lysis were added per pocket in the gel. Besides the samples, Page Ruler Prestained protein ladder was added, which later allows determination of the molecular weight of the bands. Initially, the gel was run at 10 mA/gel until the running front entered the separation gel, after which

the electric current was increased to 25 mA/gel. Once the running front has left the gel and diffuses into the running buffer, the electrophoresis was stopped. The electrophoresis chamber was disassembled and the gel could be prepared for blotting.

5.2.2.5 Western Blot analysis

The Western Blot technique enables the selective visualization of proteins on a membrane by utilizing specific antibodies. This method requires a transfer of proteins from a polyacrylamide gel onto the membrane, which is called "blotting". The blotting on nitrocellulose membranes widely used today was first described in 1979 [225]. To assemble the blot for a semi-dry transfer of proteins, the nitrocellulose membrane and the Whatman papers were first equilibrated in blotting buffer. The final stack consists of a Whatman paper at the bottom followed by the membrane, the gel and another Whatman paper at the top. The assembled stack was carefully squeezed by rolling a roller across the top to remove air bubbles. Afterwards, the lid of the blotting chamber was pressed on top of the stack and weighed. Blotting was then conducted for 70 min at 16 V and 240 mA. After the transfer was completed, the stack was disassembled and the membrane quickly washed in 1x TBS-T followed by blocking in blocking buffer for 30 min on a rocking incubator. The membrane was incubated with primary antibody over night at 4 °C and constant agitation. The next day, the membrane was washed three times for 5 min with 1x TBS-T followed by incubation with secondary antibody for 1 h at room temperature and agitation. Excessive secondary antibody was removed from the membrane by washing four times with 1x TBS-T for 10 min each. Finally, the membrane was incubated for 1 min with ECL solution and imaged in a gel imager. The horse reddish peroxidase (HRPO)-coupled to the secondary antibody, catalyzes the oxidation of luminol in the presence of H_2O_2 which leads to emission of light. Images were acquired using the "Sequential Integration" option, which acquires a series of images in a time interval manner and stacks the obtained signal of each image onto the next one. In case that another primary antibody was to be used on the same membrane, the HRPO had to be inactivated by incubation of the membrane in 1x TBS-T containing 0.1 % NaN_3 for 10 min followed by two 5 min washing steps with 1x TBS-T. Quantification of the protein bands in the acquired images (.raw data format is required) was carried out with Fiji by measuring the signal intensity of each band, followed by normalization to the respective reference band on the same lane.

5.2.3 Molecular Biology

5.2.3.1 Plasmid purification

Plasmid purifications were carried out according to the manufacturers´ protocol. The Nucleospin®Plasmid easy pure Kit was used for normal plasmid purification while the Nucleobond®Midi EF plasmid Kit was used when larger amounts of plasmid were required as it was the case for electroporation.

5.2.3.2 Restriction digest

Recombining of different genomic elements required utilization of restriction enzymes that cut DNA at specific sequences [226]. Here, up to 500 ng of DNA (plasmid or PCR product) were mixed with 1 µl per enzyme, 1 µl 10x CutSmart®buffer (NEB) and filled with ddH_2O to a final volume of 10 µl. The mix was incubated at 37 °C for up to 60 min and if not directly used further, the enzymes were heat-inactivated according to the manufacturers´ requirements and stored at -20 °C.

5.2.3.3 DNA electrophoresis

DNA fragments can be separated in agarose gels according to their length. The DNA is pulled through the gel by an electric field, with larger fragments traveling slower through the pores of the gel due to their size. The DNA can be visualized in the gel by DNA intercalating dyes such as ethidium bromide which is visible under UV light [227]. Prior to electrophoresis, 1 % (w/v) agarose is dissolved in 1x TAE buffer by cooking, followed by addition of 0.5 µg/ml ethidium bromide once the gel has cooled down to around 50 °C. Subsequently, the gel was casted using a comb appropriate for the samples in number and size. Once the casted gel has fully cooled down, the sample was mixed with 6x DNA loading buffer and loaded. Agarose gels were run at 220 mA and 100 V for 25-45 min. Visualization of DNA bands was carried out using UV light.

5.2.3.4 Gel and PCR clean-up

Gel and PCR clean up was performed on agarose gel fragments containing DNA or after PCR to purify the DNA and remove unwanted protein contaminants. The clean-up was

conducted using the Nucleospin®Gel and PCR Clean-up kit according to the manufacturers´ protocol.

5.2.3.5 Ligation

DNA ligation is used to join DNA fragments, such as backbone and insert, together after restriction digest. For DNA ligation, 50 ng of backbone are mixed in a 1:3 ratio with the insert. The required insert mass was calculated using the NEB ligation calculator. Backbone and insert DNA were mixed with ddH_2O, T4 DNA-ligase buffer and T4 DNA-ligase to a final volume of 10 µl. The ligation mix was incubated for 15 min at 37 °C and stored at -20 °C if not used directly for transformation.

5.2.3.6 TA-cloning

TA-cloning was used for easy integration of DNA-fragments into the pCR.2.1 vector for further analysis of the fragments by sequencing. The cloning was carried out according to the manufacturers´ protocol.

5.2.3.7 DNA-sequencing

DNA sequencing was used to validate CRISPR/Cas9 targeting of genes as well as successful cloning of constructs. For sequencing, 80 ng/µl DNA in 12 µl ddH_2O were sent if standard sequencing primers can be used. Otherwise, 4 µM custom sequencing primer were added. Sequencing was performed by the Microsynth Seqlab using the Sanger sequencing technique.

5.2.3.8 Transformation of bacteria

Bacteria were used to amplify whole plasmids after generation of the constructs via restriction digest and ligation. First, 50 µl of chemically competent bacteria were thawed on ice and carefully mixed with either the whole ligation approach or mixed with up to 5 ng of plasmid DNA in case of a re-transformation of an existing plasmid. Subsequently, the bacterial-plasmid suspension was incubated for 30 min on ice. Afterwards, the transformation of plasmids into the bacterial cells was carried out by heat-shock at 42 °C for 1 min. Following the heat-shock, the bacterial cell suspension was placed back on ice for 5 min followed by addition of 200 µl LB-medium (without antibiotics) and incubation at 37 °C and 450 rpm for up to 20 min to allow recovery of the bacteria. Finally, 200 µl of the bacterial cell suspension was distributed on a LB-agar plate containing either ampicillin

or kanamycin depending on the resistance gene of the transformed plasmid. Plates were then incubated over night at 37 °C and checked for single colonies on the next day. The different bacterial strains used are listed below in table 5.21.

Table 5.21: Bacterial strains used for cloning of constructs. TOP10F' were used until plasmid sizes of ~10 kb and GeneHog once plasmids were larger than 10 kb. Competent bacteria were stored at -80 °C.

Bacterial strain	**Supplier**
One Shot TOP10F'^{TM} chemically competent *E.coli*	Invitrogen
Electrocomp Gene^{TM} Hogs®*E.coli*	Invitrogen

Single colonies were picked and placed in 4 ml of LB-medium (containing respective antibiotic) followed by incubation at 37 °C in a rocking incubator.

5.2.3.9 Polymerase chain reaction

The polymerase chain reaction (PCR) allows amplification of a stretch of DNA using specific primers and a DNA polymerase. The PCR requires a cycling of different temperatures which allow annealing of the primers to the template strand followed by amplification via the DNA polymerases and finally degradation of the resulting double strand into single strands. In this study, the PCR technique was used to prepare inserts for restriction digest by adding specific restriction sites on 5' and 3' ends of the inserts and to amplify genomic regions of DNA to validate CRISPR-targeting of genes. Shorter DNA sequences up to ~1000 bp were amplified using a *Taq* polymerase. The composition of this approach is shown in table 5.22.

Table 5.22: Composition of the PCR reaction using a *Taq* polymerase.

Reagent	**Volume [µl]**	**Final concentration**
Taq PCR master mix	5	1x
Primer forward (100 µM)	0.1	1 µM
Primer reverse (100 µM)	0.1	1 µM
Template	1	50-200 ng/µl
ddH_2O	fill up to 10 µl	

The Phusion®polymerase was utilized to amplify DNA fragments longer than ~1000 bp due to its higher fidelity and can be applied on fragments up to 5000 bp long. The respective composition of the PCR mix is shown in table 5.23.

Table 5.23: Composition of the PCR reaction using the Phusion polymerase.

Reagent	Volume [µl]	Final concentration
5x Phusion HF buffer	10	1x
dNTPs (10 mM)	1	200 µM
Primer forward (10 µM)	2.5	0.5 µM
Primer reverse (10 µM)	2.5	0.5 µM
Template	1	50 ng
Phusion polymerase (2000 U/ml)	0.5	1 U/reaction
ddH_2O	fill up to 50 µl	

The PCR cycle program used for the *Taq*- and Phusion®-PCR are shown in table 5.24.

Table 5.24: PCR program for *Taq*- and Phusion®-PCRs. The "X" acts as placeholder for the primer dependent annealing temperature which was determined using the NEB T_M calculator.

	Step	Taq PCR	Phusion®PCR
	Initial denaturation	94 °C, 120 s	98 °C, 30 s
35x	Denaturation	94 °C, 20 s	98 °C, 10 s
	Annealing	X °C, 30 s	X °C, 30 s
	Extension	72 °C, 60 s/kb	68 °C, 30 s/kb
	Final extension	72 °C, 2x extension time	68 °C, 2x extension time
	Stop	20 °C, ∞	20 °C, ∞

5.2.3.10 Extraction of genomic DNA

In the first step, up to $1*10^6$ cells were harvested by centrifugation at 400 g for 4 min followed by washing with 1x PBS. The cell lysis was performed by resuspension of the cells in 200 µl TAG buffer containing 100 µg/ml proteinase K followed by incubation for 3 h at 56 °C. After lysis, the proteinase K was heat-inactivated at 95 °C for 15 min and the DNA concentration and purity was measured via NanoDrop. The extracted genomic DNA was stored at 4 °C.

5.2.4 Flow cytometry

5.2.4.1 Staining for cell surface proteins

For staining of cell surface proteins, $1*10^6$ cells were harvested per sample. The cells were washed twice with cold 1x PBS and subjected to staining. Primary antibody was diluted

in 1x PBS and cells were resuspended in the staining solution and placed on ice for up to 45 min. If the primary antibody was conjugated to a fluorophore, the sample was washed twice with 1x PBS followed by analysis via flow cytometry. If a secondary staining was required, the cells were washed twice followed by 30 min staining with secondary antibody on ice. Afterwards, the samples were washed again and analysed via flow cytometry.

5.2.4.2 Intracellular staining

To allow staining of intracellular proteins, $1*10^6$ cells were harvested for each sample. The cells were fixed by resuspending in 200 µl of Cytofix diluted 1:2 with FCS-free medium and incubation for 15 min at 37 °C and 450 rpm. Afterwards, the cells were centrifuged for 6 min at 500 g which was used for the rest of the protocol. The fixed cells were permeabilised in 200 µl of Perm/Wash buffer I containing 1 % BSA at RT. After 10 min, another 200 µl of Perm/Wash buffer I was added to dilute the BSA. The cells were spun down after 10 min and resuspended in staining solution. The primary antibody was diluted in Perm/Wash buffer I and the cells were resuspended in the staining solution. The incubation was carried out at room temperature for 45 min and 450 rpm. Once staining was complete, 1 ml of Perm/Wash buffer I was added to dilute the staining, followed by centrifugation and another washing step. Finally, the pellet was resuspended in 300 µl Perm/Wash I and analysed via flow cytometry.

5.2.4.3 Cell cycle analysis

For the analysis of the cell cycle, $1*10^6$ cells were harvested by centrifugation at 400 g for min at 4 °C. Afterwards, cells were washed with cold 1x PBS and fixed. Fixation was carried out by thoroughly resuspending the cell pellet in 300 µl ice cold 70 % ethanol followed by incubation on ice for 60 min. Every 20 min the sample is gently vortexed to avoid aggregation of fixed cells. The fixed cells were centrifuged for 4 min at 600 g and 4 °C followed by a washing step with cold 1x PBS. Afterwards, the cells were stained for 1 h at 37 °C and 550 rpm in 300 µl 1x PBS containing 20 µg/ml PI, 0.05 % Triton X-100 and 100 µg/ml RNAse A. PI is a non-membrane-permeable, DNA intercalating dye that increases its fluorescence upon intercalation which allows the analysis of the cell cycle phases based on the intercalated dye in the cells. The dye is excited at 488 nm and shows its maximum emission at 617 nm [228]. Triton X-100 is used to permeabilise the membranes, which allows passage of PI into the cells. The RNAse A is used to

eliminate RNA, as it is also stained by PI and would falsify the analysis [228]. After the staining, the cells were washed twice with cold 1x PBS and were finally resuspended in 300 µl 1x PBS for analysis via flow cytometry. The resulting data was analysed in FlowJo and the PI profile of each sample was subjected to cell cycle analysis using the Watson-Pragmatic model, which allows an unbiased determination of the cell cycle phases[229]. The underlying algorithm identifies the first peak of the PI profile as the G_1/G_0 peak and assumes a normal distribution. It then models the rest of the PI profile accordingly to produce an objective fit to the data [229].

5.2.4.4 Apoptosis assay

To assess apoptosis levels of suspension cells, $1*10^6$ cells were first collected by centrifugation at 500 g for 4 min. All centrifugations were carried out with these parameters to also collect the lighter apoptotic cells. Afterwards, the pellet was washed with Annexin-V-staining buffer followed by staining. Staining was performed in 100 µl Annexin-V-binding buffer containing 0.5 µl of Annexin-V-APC and 1.5 µg/ml 7-AAD. Annexin-V is a small peptide, which selectively binds to phosphatidyl serine which is flipped to extracellular leaflet of the plasma membrane upon early apoptosis [230]. 7-AAD is a DNA intercalating dye that cannot pass intact membranes [231]. Upon late apoptosis, membranes lose integrity which allows 7-AAD to enter the cell. Cells were resuspended in the staining solution and incubated at RT in the dark for 20 min. Subsequently, the stained cells were diluted with 200 µl Annexin-V-binding buffer and measured at the LSRII using the PerCP-Cy5 channel for 7-AAD and APC channel.

5.2.4.5 BH3-profiling

The BH3-profiling is used to identify the apoptotic pathway of cells and to determine the sensitivity to enter apoptosis. Apoptosis is regulated on the mitochondrial level by proteins that have either pro- or anti-apoptotic function, depending on their different BCL-2 homology (BH) domains [232]. The BH3-profiling assay uses peptides that mimic components of this complex regulation system to agonize or antagonize the pro- or anti-apoptotic proteins. The effect of the peptides is measured by assessing the cytochrome c release from the mitochondria, which is caused by mitochondrial outer membrane permeabilisation (MOMP) and triggers the formation of the apoptosome [233]. In addition, using different concentrations allows to determine the sensitivity to certain peptides. The

BH3-profiling in this study was performed by Dr. Jens Löber at the University Medical Center Göttingen using an established protocol described below [234, 235].

384-well plates were coated in quadruplicates for each cell line and condition with 15 µl of 1:50 diluted BH3-peptides in MEB2 buffer containing controls DMSO and alamethicin. $1*10^6$ cells were harvested and washed in MEB2 buffer, followed by incubation of 15 µl cell suspension for 1 h at 25 °C in each well of the prepared plate. Afterwards, cells were fixed for 10 min at 25 °C by addition of 10 µl 4 % formaldehyde solution, followed by quenching with 10 µl buffer N2 for 10 min at 25 °C. Staining was performed over night by adding 10 µl 10x staining solution containing 25 µg/ml Hoechst33342 and 1.25 µg/ml Alexa Fluor® 647 α-Cytochrome C. Cells were subjected to flow cytometry the following day (LSRFortessa™ X-20). After gating on single cells and viability, the DMSO control was used as negative control (no induced apoptosis) while alamethicin served as positive control for complete cytochrome C release due to BAX/BAK-independent MOMP formation. Concentration of the peptides (JPT Peptide Technologies) and controls used: BIM 10/1/0.1 µM, BAD 10/1 µM, HRKγ 10/1 µM, MS1 10/1 µM, FS1 10/1 µM, PUMA 10 µM, DMSO 1 %, Alamethicin 25 µM.

5.2.4.6 Glucose uptake assay

The glucose uptake assay is based on the uptake of the fluorescent glucose derivative 2-deoxy-2-[(7-nitro-2,1,3-benzoxadiazol-4-yl)amino]-D-glucose (2-NBDG). 2-NBDG is transported across the cell membrane in a similar manner to normal D-glucose and has an excitation/emission maxima of 475/550 nm respectively [236, 237]. Therefore, the amount of accumulated 2-NBDG and its resulting fluorescence are an indication of the physiological glucose uptake of the assessed cells. For this assay, $1{,}25*10^6$ cells are harvested by centrifugation at 400 g for 4 min. The pellet was washed with 500 µl pre-warmed glucose free RPMI followed by another centrifugation step. The cells were resuspended in 1050 µl glucose-free RPMI and split into five sub-samples of 200 µl containing approximately $0.25*10^6$ cells. Subsequently, the cells were starved for 60 min at 37 °C and 450 rpm. Afterwards, 100 µl of glucose-free RPMI containing 300 µM 2-NBDG were added to each subsample for a final concentration of 100 µM. Simultaneously, 100 µl of Glucose-free RPMI are added to the unstained control. The glucose uptake was then terminated by addition of 1 ml of cold 1x PBS at indicated time points of 5, 10, 20 or 30 min followed

by centrifugation at 4 °C. The pellet was again washed with cold 1x PBS followed by resuspension in 100 µl of cold 1x PBS containing 5 µg/ml 7-AAD as counter stain for dead cells. The samples are then incubated for 20 min at 4 °C in the dark followed by addition of 200 µl cold 1x PBS and analysis at the BD FACSCelesta using the blue laser, the FITC channel and a 530/30 nm filter (2-NBDG) and the PerCP-Cy5-5 channel and a 695/40 nm filter (7-AAD). The unstained cells were used as negative control to set up gates for 2-NBDG and 7-AAD. Only cells which appeared 7-AAD negative were included in the final gate.

5.2.4.7 Cell counting proliferation assay

The proliferation of cells in culture can be measured by the increase of cell number over time. Here, cells were seeded with a constant cell density in 48-well plates (5000 Ramos/DG75/Raji cells/well; 10000 Daudi cells/well; 1,5 ml R10/well) with two wells/cell line for every planned day. Every day, including the seeding day, two wells of each cell line were resuspended and 500 µl of the cell suspension were transferred into a FACS tube and subjected to flow cytometry. The cells were counted by using a 30 sec acquisition time, a constant flow rate throughout the whole experiment and by gating on living cells only as indicated by the FSC-SSC. This ensures, that only the living cells were counted every day which were normalised to the number of living cells at the seeding day. The resulting fold-change in cell number over time was then used as a measure of proliferation.

5.2.4.8 GFP-tracking assay

The inducible shRNA expression system produced not only the shRNA upon induction but also GFP, which allowed the tracking of GFP-positive, and therefore shRNA producing, cells over time using flow cytometry. For this purpose, the shRNA cells including the non-targeting control were seeded with a constant cell density in 48-well plates (5000 Ramos cells/well; 10000 Daudi cells/well; 1,5 ml R10/well). Each day, including the seeding day, two wells of each cell line were resuspended and 500 µl of the cell suspension were transferred into a FACS tube. The respective number of GFP-positive cells was then assessed by flow cytometry using a 30 sec acquisition time, a constant flow rate throughout the whole experiment and by gating on GFP-positive cells only. This experimental setup enabled a combined readout of proliferation and apoptosis over time, indicated by increase and/or decrease of the GFP signal and number of GFP-positive cells as GFP is lost during

apoptosis [238]. For evaluation, the number of GFP-positive cells is normalised to the initial cell number measured on the seeding day.

5.2.5 Imaging flow cytometry

5.2.5.1 MitoTracker assay

To determine the mitochondrial quantity in living cells, $3*10^6$ cells were harvested by centrifugation at 400 g for 5 min. Afterwards, the cell pellet was washed with room temperature 1x PBS and stained in 500 µl FCS-free RPMI containing 5 nM MitoTracker™ DeepRed. The MitoTracker™ are cell permeable allowing the staining of mitochondria in living cells. The dyes bind specifically thiol-reactive chloromethyl groups found in the mitochondrial membranes [239, 240]. The cells were incubated with the staining solution for 30 min at 37 °C and 500 rpm, followed by another washing step with 1x PBS. For the image stream analysis, the cell pellet was resuspended in 60 µl 1x PBS and analysed using the Amnis Image Stream X MKII. Assessed was the overall signal intensity of the MitoTracker™ DeepRed and the signal area of each individual cell. Moreover, the MitoTracker™ DeepRed signal relative to the respective cell size was measured.

5.2.5.2 Quantification of PI(3,4)P_2 on the plasma membrane

To measure the amount of PI(3,4)P_2 at the intracellular leaflet of the plasma membrane, $3*10^6$ GFP-2xTAPP1-PH expressing Ramos WT and Ramos *INPPL1*$^{-/-}$ cells were harvested by centrifugation at 400 g, 4 °C and for 4 min. Afterwards, the pellets were washed with ice-cold 1x PBS, resuspended in cold Krebs-Ringer (K-R) buffer containing 1 mM $CaCl_2$ and placed on ice until measurement at the Amnis Image Stream X MKII. After exclusion of the cell debris and cell aggregates, only the cells in an optimal focus were regarded for further analysis. The cells were then gated for a homogeneous GFP signal, excluding cells with a too high or low signal. Afterwards, the plasma membrane localization of GFP-2xTAPP1-PH was determined by blotting the entropy of the GFP signal on the H correlation. The entropy is a parameter describing the randomness of the signal intensities in an image. If an image has distinct areas with a focused intensity it has a lower entropy than an image with a widely distributed signal. The correlation measures how similar pairs of pixels are and can be regarded as the opposite of the contrast. Consequently, if the image has a high correlation, it is more homogeneous and lacking

variant texture. Collectively, the cells that exhibited a low entropy and correlation were measured.

Results

6.1 SHIP2 is predicted as an important contributor to BL fitness

The inositol phosphatase SHIP2 has been shown in previous studies to be involved in the tonic BCR signaling network, which is crucial for survival of several Burkitt lymphoma cell lines [152, 159]. However, the extent of the contribution of SHIP2 to this pathway and the underlying mechanisms are largely unknown. The Cancer Dependency Map database allowed for an extensive overview of the effects of targeting single genes in cell lines. The database combines multiple CRISPR/Cas9 or RNAi screens to evaluate the dependency of cell lines to specific genes as well as co-dependencies between genes [207]. The dependency to a certain gene is rated according to the relative effect on the cell line. This relative gene effect characterises the outcome of the gene targeting with a positive value representing improved proliferation and a negative value the opposite. Genes with a value smaller than -1 are considered as essential. In this approach, all cell lines in the database representing non-Hodgkins lymphoma, including BL cell lines, were analysed for the effect of targeting the SHIP2 coding gene *INPPL1* either by CRISPR/Cas9 or RNAi. In a second approach, a recently published shRNA screen comparing BL and non-blood cell lines was re-analysed for the effect of targeting the expression of *INPPL1* [196].

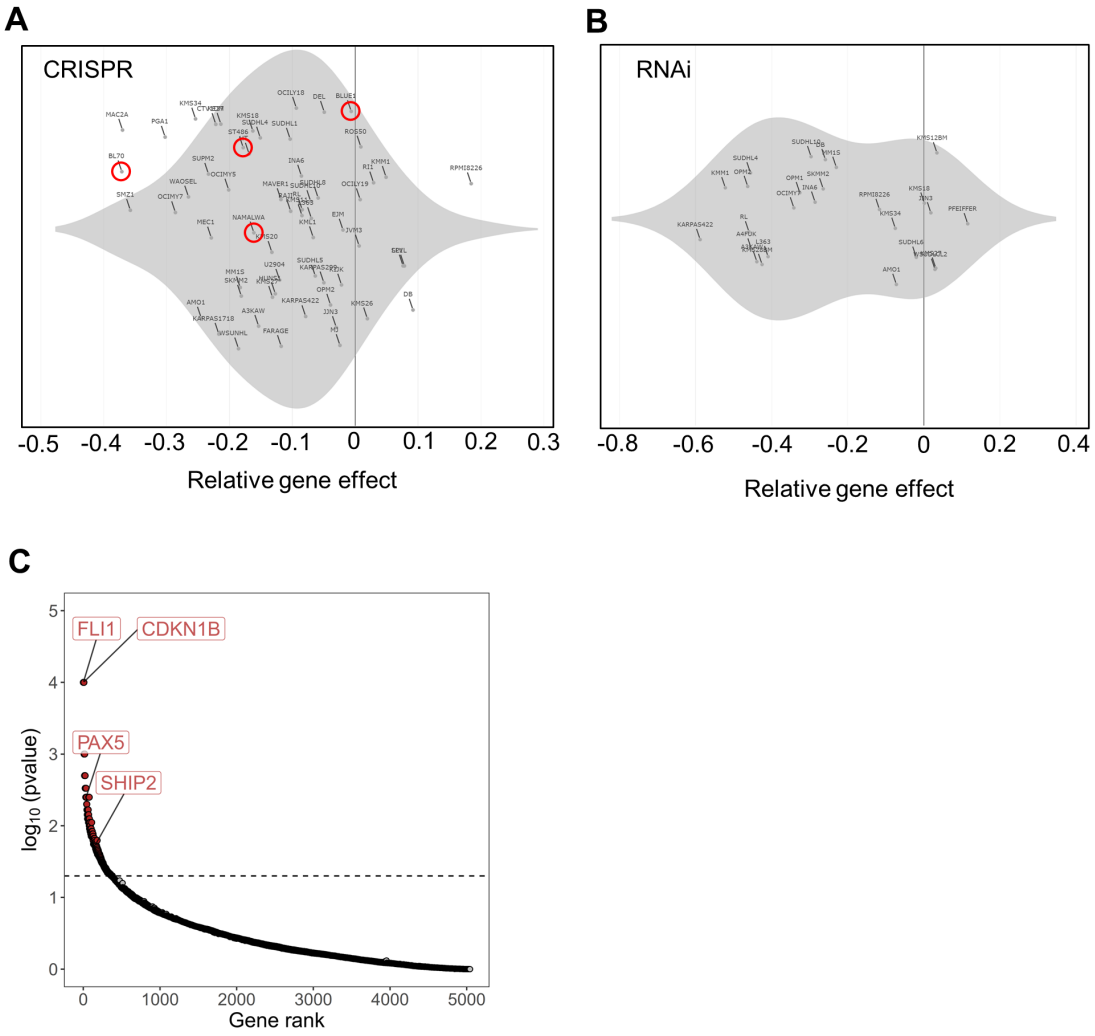

Figure 6.1: **SHIP2 is predicted as an important contributor to BL fitness.** Studies of **A.** CRISPR and **B.** RNAi targeting of *INPPL1* in multiple non-Hodgkin lymphoma cell lines. The data was extracted from the database of the Cancer Dependency Map [207]. Red circles indicate BL cell lines. The CRISPR database consists of three independent screens: DepMap Public2302, Score and Chronos. The RNAi databases consists of the Achilles, DRIVE, Marcotte and DEMETER2 screens. The gene effect describes the impact of the gene targeting on the growth of the respective cell line. A gene with a gene effect <-1 is considered as essential. **C.** Reassessment of the shRNA-based drop-out screen performed by Hüllein *et al.* [196] reveals SHIP2 as a potentially important contributor for BL fitness. The screen compared the importance of 5045 genes in n=8 BL cell lines with n=6 solid cancer cell lines.

The CRISPR screens demonstrated that a loss of SHIP2 led to a reduction of proliferation in almost all tested non-Hodgkin lymphoma cell lines, as indicated by a negative relative gene effect (Figure 6.1A). The RNAi screens validated these findings, indicating

that while not being lethal, the loss of SHIP2 has a negative effect on the proliferation of multiple non-Hodgkin cell lines (Figure 6.1B). Further corroborated are these findings by the re-analysis of the BL-specific shRNA screen conducted by Hüllein *et al.* Here, *INPPL1* was placed on rank 151 of 5045 genes relevant for BL fitness with a significance of p=0.019, which is two degrees of significance lower than that of the top-scoring gene *PAX5* with p=0.004 (Figure 6.1C) [196]. Hence, multiple studies provide evidence for an important role of SHIP2 in the fitness of BL cell lines.

I wanted to confirm these findings experimentally by assessing the proliferation of multiple BL cell lines after treatment with the SHIP2 inhibitor AS1949490. This inhibitor is characterised by a high selectivity for SHIP2 compared to other inositol-phosphatases and a sub-micromolar IC50 in a cell-free assay [241]. Four different cell lines were used to represent the heterogeneity of BL: The Ramos and DG75 cell lines both originate from spontaneous BL and possess the same t(8;14)(q22;32) translocation of *MYC* but differ in the accompanying mutations [156, 200, 201, 206]. In contrast, the Daudi and Raji cell lines have an endemic BL background and share the same *MYC* translocation, yet also differ in other mutations [156, 200, 201]. Apart from Raji cells, which do not display surface IgM levels, the other three cell lines are shown to be BCR-dependent [163]. The proliferation was measured by using the XTT proliferation assay. This colorimetric assay utilizes the conversion of the yellowish tetrazolium salt XTT into orange formazan by mitochondrial dehydrogenases in living cells. Therefore, measuring the absorption rate of formazan at 450 nm is an indicator for the amount of metabolically active, proliferating cells [222]. For the experiment, the different cell lines were seeded equally and incubated with increasing concentrations of AS1949490 for 24 h followed by determination of the proliferation via XTT assay.

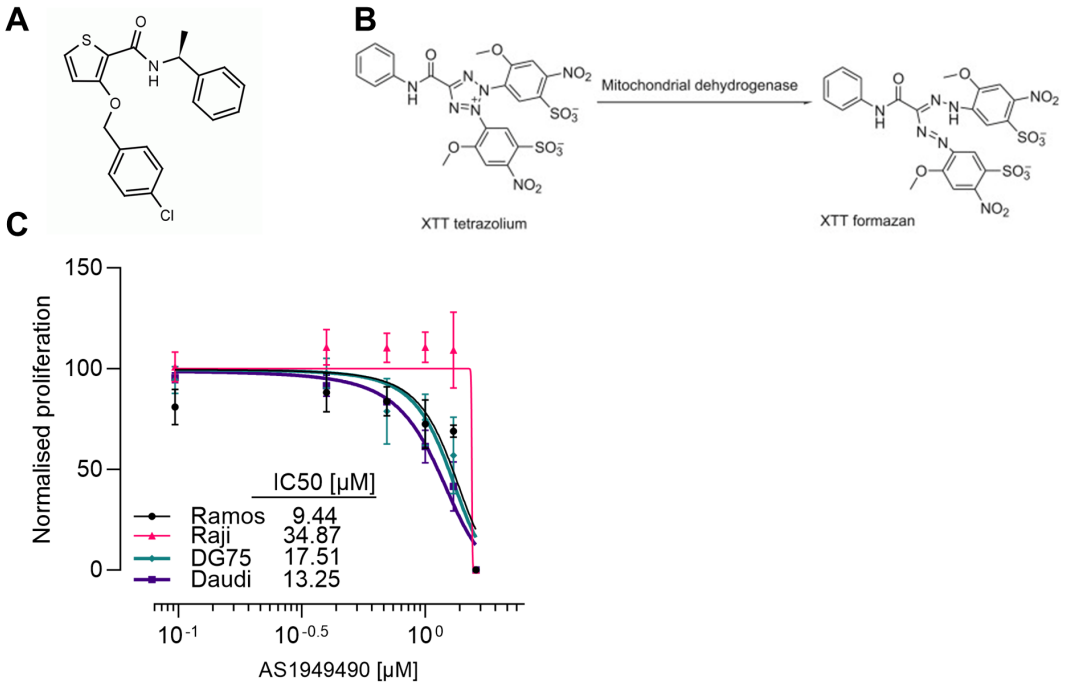

Figure 6.2: **Inhibition of SHIP2 decreases proliferation of multiple BL cell lines. A.** Molecular structure of the SHIP2 inhibitor AS1949490. **B.** Chemical principle of the XTT proliferation assay that relies on the conversion of the XTT tetrazolium salt to XTT formazan facilitated by mitochondrial dehydrogenases. **C.**. Dose-response curve of four different BL cell lines treated with increasing concentrations of AS1949490 for 24 h. The relative proliferation was assessed by XTT assay and normalisation to vehicle-treated samples. DMSO served as negative control. The dose-response curve was calculated using a non-linear regression model for normalised data. IC50 values were calculated using GraphPad Prism. Shown are the results of n≥3 independent experiments. Error bars indicate the standard deviation.

Treatment with AS1949490 (Figure 6.2A) led to a dose-dependent decrease of proliferation across all tested BL cell lines (Figure 6.2B,C). The strongest effect was observed in the Daudi cells as indicated by the comparably low concentration of inhibitor required for the decrease in proliferation. The proliferation of Ramos and DG75 cells was marginally less effected compared to Daudi while the Raji cells only exhibited a reaction at the highest concentration (Figure 6.2C). This experiment confirms that the loss of SHIP2 activity, either by targeting the expression or by inhibition, has a negative outcome on the proliferation of BL cells.

6.2 Generation of SHIP2-deficient BL cell lines

After it was confirmed that multiple Bl cell lines were dependent on SHIP2 activity, I aimed to generate a SHIP2-deficient cell line by utilizing the clustered regularly interspaced short palindromic repeat (CRISPR)/Cas9 system. As B cell lines are notoriously difficult to transfect, a novel delivery technique was used. Here, the custom-made and gene specific CRISPR-RNA (crRNA) was first hybridized with a generic trans-activating crRNA (trcrRNA). The resulting RNA hybrid is mixed with a recombinant Cas9 endonuclease to form a RNA-protein complex, which can be electroporated into cells with high efficiency. After electroporation, the cells were allowed to recover for up to 3 days followed by single cell dilution to generate single clones. These clones were expanded and cleared cellular lysates were screened for a loss of SHIP2 protein. Clones negative for SHIP2 were subjected to isolation of their genomic DNA and a PCR of the crRNA target site followed by sequencing were performed to confirm successful disruption of the gene on both alleles. Using this workflow, the SHIP2-coding gene *INPPL1* was targeted in Ramos and DG75 cells.

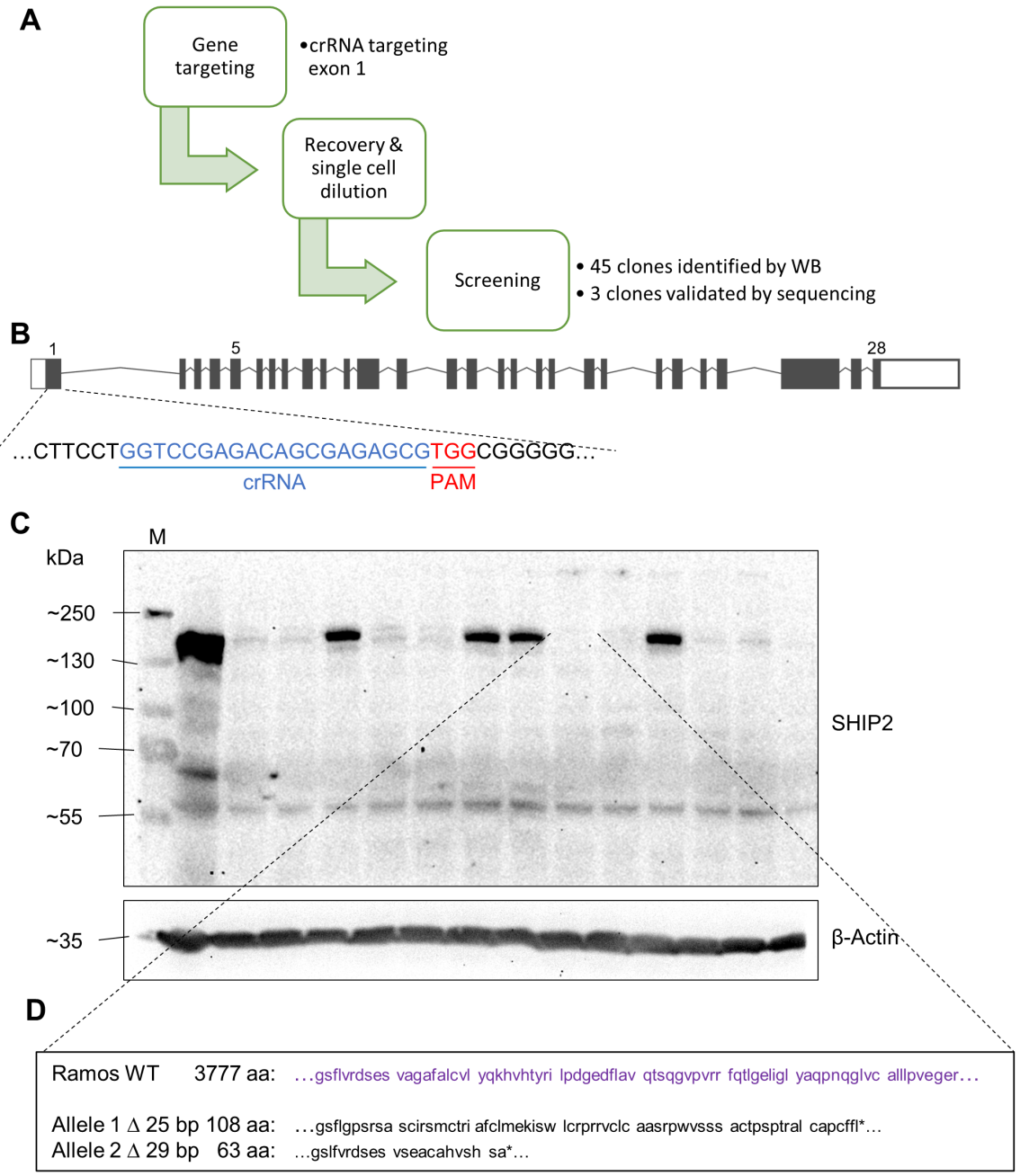

Figure 6.3: **Targeting of *INPPL1* in Ramos cells using CRISPR/Cas9. A.** Flow chart depicting the workflow required for generation of a SHIP2-deficient Ramos cell line. **B.** Exon structure of the *INPPL1* consensus gene with the respective target site of the crRNA (blue) and PAM site (red) in the first exon. **C.** Clones recovered from the single cell dilution were screened for protein deficiency via Western Blot analysis. The membranes were probed with α-SHIP2 and α-β-Actin as loading control. The apparent molecular weight is indicated as kDa. **D.** Genomic sequencing identified 3 clones with genomic aberrations on both alleles, of which one clone is shown. The clone exhibited 25 bp and 29 bp deletions on the two alleles, respectively, which led to formation of a premature stop codon after 108 aa or 63 aa.

Targeting the first exon of *INPPL1* resulted in the identification of 45 clones negative for SHIP2 protein as demonstrated by Western Blot analysis (Figure 6.3A-C). The DNA sequence alterations in three of these clones were analysed by Sanger sequencing, of which the alterations of one clone are shown as an example. This clone, further called Ramos *INPPL1*$^{-/-}$, was characterised by a loss of 25 bp and 29 bp on the two alleles, resulting in premature stop codons after 108 or 63 amino acids, respectively (Figure 6.3D).

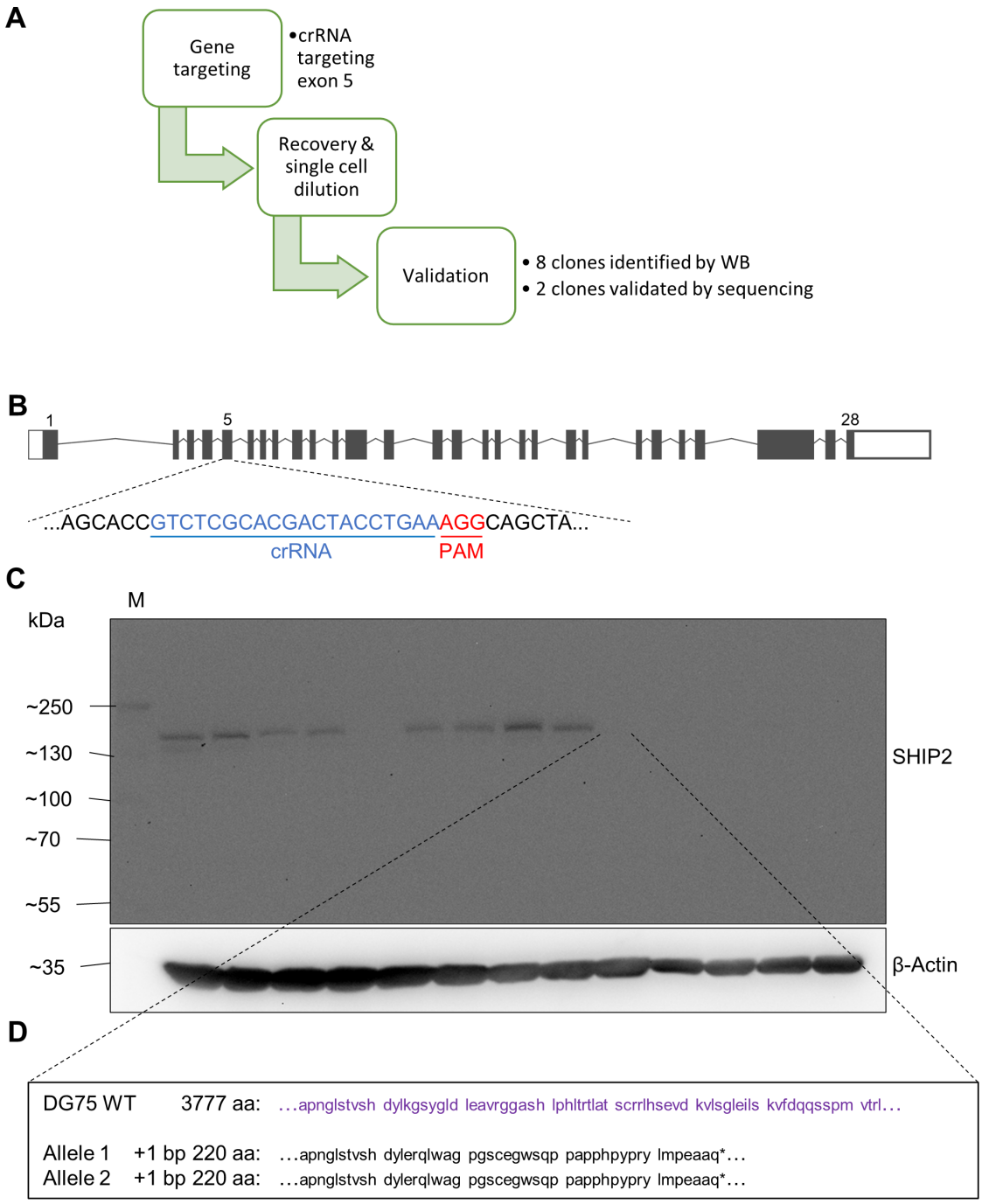

Figure 6.4: **Targeting of *INPPL1* in DG75 cells using CRISPR/Cas9. A.** Flow chart depicting the workflow required for generation of a SHIP2-deficient DG75 cell line. **B.** Exon structure of the *INPPL1* consensus gene with the respective target site of the crRNA (blue) and PAM site (red) in exon 5. **C.** Clones recovered from the single cell dilution were screened for protein deficiency via Western Blot analysis. The membranes were probed with α-SHIP2 and α-β-Actin as loading control. The apparent molecular weight is indicated as kDa.

Figure 6.4: Continued:

D. Genomic sequencing identified 2 clones with genomic aberrations on both alleles, of which one clone is shown.

In DG75, the SHIP2-coding gene was targeted at exon 5 using a different crRNA as for Ramos (Figure 6.4A,B). The Western Blot analysis of clones after single cell dilution identified 8 clones with a total loss of SHIP2 protein (Figure 6.4C). Two of these clones were further analysed by Sanger sequencing, of which one clone, now called DG75 *INPPL1*$^{-/-}$, is shown. DG75 *INPPL1*$^{-/-}$ exhibited the same addition of one nucleotide at the target site in both alleles (Figure 6.4D). No other alteration could be identified despite multiple Sanger sequencing runs leading to the conclusion that both alleles suffered the same alteration. The addition of one thymidin at the break site appeared to be a preferential alteration as it was sequenced in different clones across different cell lines (data not shown).

The lack of SHIP2 protein levels combined with the sequence alterations at the targeting sites and the predicted premature stop codons confirmed successful deletion of *INPPL1* expression in the respective Ramos and DG75 clones.
To address clonal effects, the SHIP2-negative cells were reconstituted with a wild type SHIP2 variant containing the fluorescent protein citrine [242] as an N-terminal tag (CitSHIP2). The constitutive expression of the CitSHIP2 construct was achieved by applying the PiggyBac-transposase-transposon system. The transfected cells were analysed for expression of CitSHIP2 by FACS and Western Blot analysis as well as for their surface IgM levels.

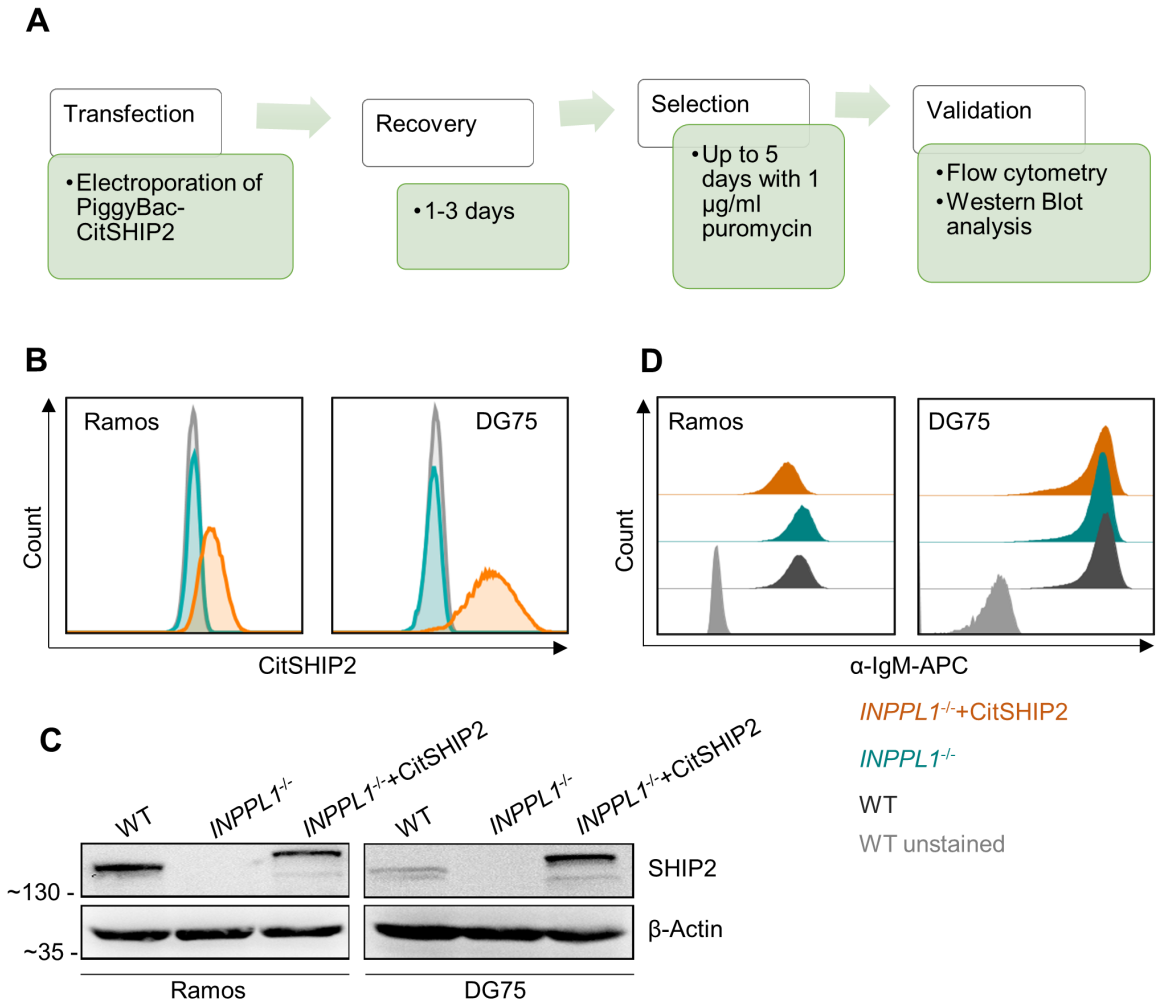

Figure 6.5: **Successful reconstitution of SHIP2-deficient Ramos and DG75 cells with a CitSHIP2 construct. A.** Workflow depicting the steps from the transfection of the cells with an N-terminally tagged Citrine-SHIP2 construct up to validation. **B.** FACS analysis showed a citrine signal in the reconstituted Ramos and DG75 cells indicating successful reconstitution of the CitSHIP2 construct. **C.** The Western Blot analysis validated the previous FACS analysis showing a SHIP2-specific band in the reconstituted cells that was slightly larger than wild type SHIP2. The membranes were probed with α-SHIP2 and α-β-Actin as loading control. The apparent molecular weight is indicated at kDa. **D.** Surface IgM levels of Ramos and DG75 cells remained unaffected by SHIP2-deficiency and reconstitution with CitSHIP2. The surface IgM levels were analysed by FACS analysis of α-IgM-AF647 stained living cells.

Flow cytometry of electroporated SHIP2-negative Ramos and DG75 cells showed a stable citrine signal indicating expression of the CitSHIP2 construct (Figure 6.5A,B). Western Blot analysis confirmed expression of the construct as indicated by the appearance of a SHIP2-specific band with increased molecular weight compared to WT SHIP2 due to the

citrine tag (Figure 6.5C). Furthermore, as this study is particularly interested in tonic BCR survival signaling, it was necessary to control the surface BCR levels, since changes in BCR surface expression could alter the activity of downstream signaling components. Hence, the full panel of each cell line, consisting of WT, *INPPL1*$^{-/-}$ and reconstituted cells was examined for their surface IgM levels, which directly reflect the surface BCR abundance [4, 243]. Flow cytometric analysis revealed that the surface BCR levels remained unaltered by loss of SHIP2 or re-introduction of CitSHIP2 (Figure 6.5D).
These data show that I was able to generate two different BL cell lines to study the effects of SHIP2-deficiency. The cell panel of each model consisted of the respective WT, the *INPPL1*$^{-/-}$ and the reconstituted cells expressing CitSHIP2. Furthermore, I could show that potential differences in tonic BCR signaling are not related to an altered surface abundance of the BCR. Hence, these cell lines were the basis for the characterization of SHIP2-specific effects as described in the following chapters.

6.3 SHIP2 is an important contributor to BL cell fitness

The BL fitness is the sum of the proliferation rate and the amount of survival signaling that the cell achieves. These parameters were addressed in the different generated BL cell lines by using different assays to specifically determine the proliferation and the apoptosis rates of the cells.
First, the proliferation was measured on a metabolic level by XTT assay. Previous studies with the Daudi cells had already indicated that SHIP2-deficiency compromised the growth of this BL cell line [197]. Hence, the Ramos and DG75 panels were tested for their proliferation in the same manner. The cells were seeded in equal cell concentrations in 96-well plates and the XTT assay was performed on the following day. In addition, cell counting was used as a simple but holistic approach to determine the proliferation of cell lines. For this purpose, the cells were seeded in equal cell concentrations and the number of living cells, indicated by FSC and SSC, were counted using flow cytometry. The cell count of 4 consecutive days was normalised to the starting cell count, which resulted in a fold-change of cell number that directly represents the proliferation. In this experimental approach, the Daudi cell lines were included.

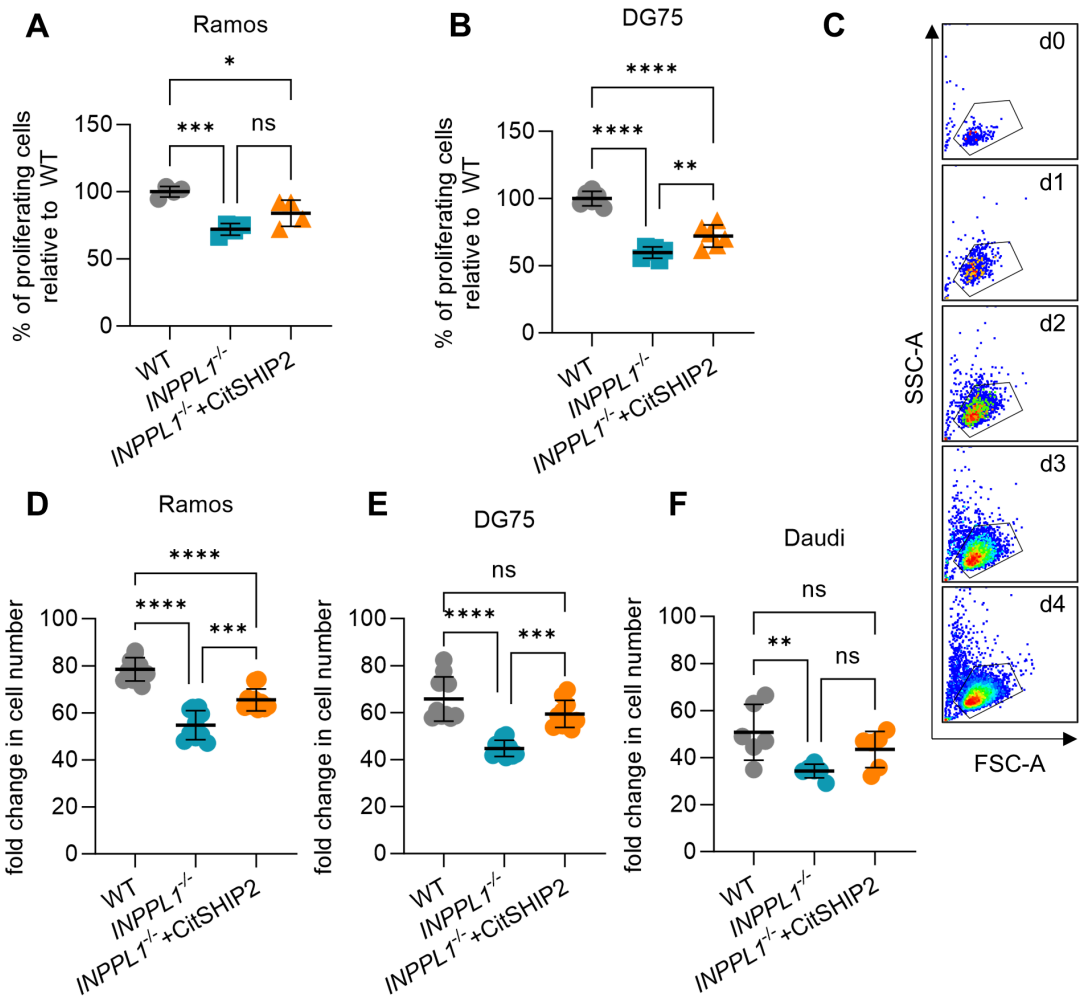

Figure 6.6: **SHIP2-deficiency decreases proliferation in Ramos and DG75 cells.** XTT assay based measurement of the proliferation of Ramos **A.** and DG75 **B.** cell lines. The proliferation was assessed after one day of cultivation and the obtained data was normalised to the respective WT controls. **C.** Gating strategy for the cell counting assay. Live cells were identified by SSC and FSC and counted on every indicated day. The proliferation of Ramos **D.**, DG75 **E.** and Daudi **F.** cell lines as revealed by the cell counting assay. Shown are the living cells counted on d4 (Ramos, DG75) or d7 (Daudi) followed by normalisation to d0. If not indicated otherwise experiments were performed n≥3. Error bars indicate the standard deviation. Statistics were performed using One-Way-ANOVA. Significance is indicated by $p<0.05$ *, $p<.0.01$ **, $p<0.001$ ***, $p<0.0001$ ****.

Loss of SHIP2 caused a decrease in proliferation in Ramos and DG75 cells as indicated by the XTT assay, which confirmed the results previously observed in Daudi [197]. While the reconstitution significantly rescued the proliferation in DG75 cells it only showed a moderate effect in Ramos cells (Figure 6.6A,B). However, the compromising effect of SHIP2

deficiency on the proliferation was validated in all three cell lines by the cell counting assay. The reconstitution with CitSHIP2 significantly rescued the proliferation in Ramos and DG75 cells while it only marginally improved the growth in Daudi cells (Figure 6.6C-F).

Since the proliferation, as one contributor to the fitness, was markedly reduced by SHIP2 deficiency, I also assessed the impact on cell survival. In a different study it was already shown that loss of SHIP2 increased the percentage of apoptotic cells in the Daudi cell lines ([197]). The apoptosis was assessed by combining the properties of Annexin-V and 7-amino-actinomycin D (7-AAD) to identify apoptotic cells. Annexin-V is a small protein which selectively binds to phosphatidyl serine, a phospho lipid, which upon early apoptosis is flipped from the intracellular leaflet of the plasma membrane to the extracellular leaflet ([230]). 7-AAD is a DNA intercalating dye, which is unable to pass intact membranes ([231]). During late apoptosis, cellular membranes lose integrity, which enables the 7-AAD to enter the cell and stain the nucleus. The combination of both reagents allows to distinguish between living (Annexin-V^-/7-AAD^-), necrotic (Annexin-V^-/7-AAD^+), early apoptotic (Annexin-V^+/7-AAD^-) and late apoptotic cells (Annexin-V^+/7-AAD^+). The DG75 cell lines are not suitable for this kind of apoptosis assay due to absence of the pro-apoptotic proteins BAK and BAX [206], which are essential to produce the alterations detectable by Annexin-V/7-AAD staining ([244]). Consequently, this assay was performed only in the Ramos cell lines, which were cultivated for 36 h in 1 % FCS medium prior to the assay to induce apoptosis by starvation.

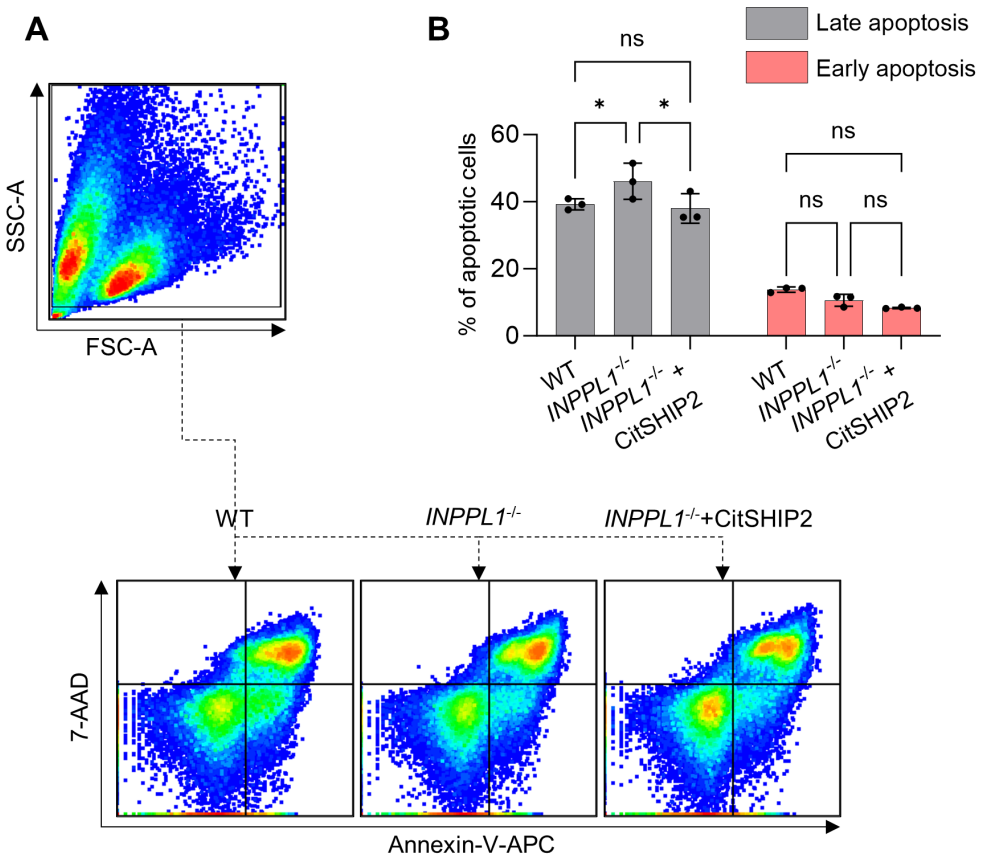

Figure 6.7: **Absence of SHIP2 increases apoptosis in Ramos cells. A.** Gating strategy for the Annexin-V-APC/7-AAD apoptosis assay. Cell debris was excluded and the cells were separated according to their Annexin-V-APC and 7-AAD signal. **B.** Percentage of late and early apoptotic Ramos WT, SHIP2-deficient and reconstituted cells. Apoptosis was induced by cultivation in 1 % FCS medium for 36 h prior to staining with 6 ng/sample Annexin-V-APC and 150 ng/sample 7-AAD. Late apoptosis is indicated by Annexin-V-APC$^+$/7-AAD$^+$ cells while early apoptotic cells are only Annexin-V-APC$^+$. If not indicated otherwise experiments were performed n≥3. Error bars indicate the standard deviation. Statistics were performed using Two-Way-ANOVA. Significance is indicated by p<0.05 *, p<.0.01 **, p<0.001 ***, p<0.0001 ****.

In the gating strategy, the cell debris was excluded and the remaining cells were separated according to their Annexin-V-APC and 7-AAD signal (Figure 6.7A). The assay revealed a marginal but significant elevation of late apoptosis in the *INPPL1*$^{-/-}$ cells compared to WT or reconstituted counterparts. No difference was observed in the level of early apoptosis (Figure 6.8B).

While there was a SHIP2-dependent apoptosis observable in two of three cell lines, two

questions remained. First, in both circumstances the increase was marginal and only in late apoptosis. Second, the utilized apoptosis assay was not suitable to detect apoptosis in the DG75 cells due to the mutations in this cell line. Therefore, the findings were validated by staining the intracellular levels of cleaved cysteine-dependent, aspartate-specific protease 3 (caspase 3) [245]. The sequential activation of caspases by cleavage plays a central role in apoptosis as these proteases hydrolyse essential proteins rendering the apoptosis irreversible [246]. Caspase 3 is one of the final caspases activated by the cascade as it indiscriminately hydrolyses any protein, which makes it a marker for late apoptosis [247]. Before the cells were intracellularly stained using α-cleaved caspase 3-APC they were starved for up to 72 h as explained above followed by fixation and permeabilisation. The results of this experiment are depicted in figure 6.8).

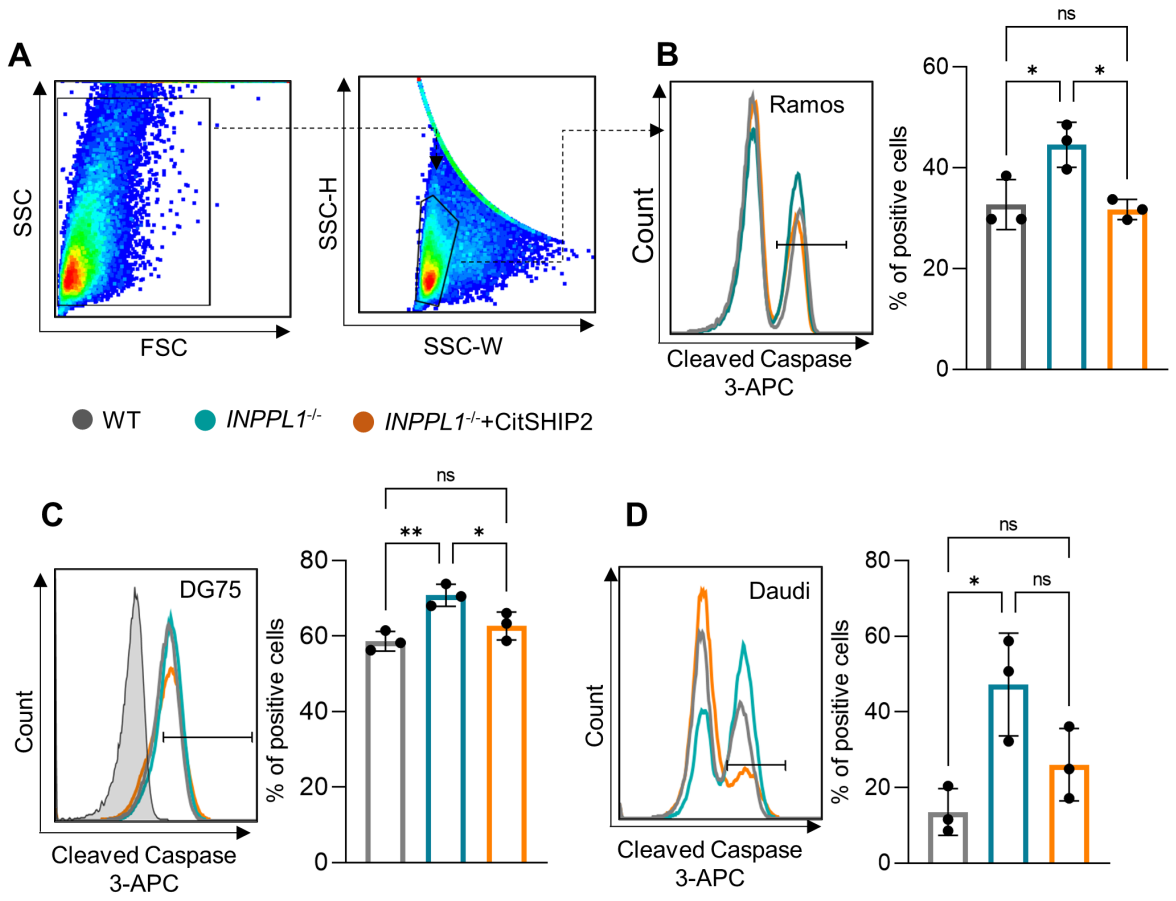

Figure 6.8: **Loss of SHIP2 coincided with increased activation of caspase 3 in BL cell lines. A.** Gating strategy for the intracellular staining of cleaved caspase 3 in fixed cells. Following the exclusion of cell debris the cells were gated on single cells only, which were then assessed for their cleaved caspase 3-APC signal. Levels of cleaved caspase 3 in Ramos **B.**, DG75 **C.** and Daudi **D.** cell lines. Apoptosis was induced by cultivation in 1 % FCS medium for 36 h (Ramos, DG75) or 72 h (Daudi) prior to fixation and staining with α-cleaved caspase 3-APC. If not indicated otherwise experiments were performed n$\geq$3. Error bars indicate the standard deviation. Statistics were performed using One-Way-ANOVA. Significance is indicated by p<0.05 *, p<.0.01 **, p<0.001 ***, p<0.0001 ****.

The gating strategy relied on the exclusion of cell debris followed by the analysis of the APC signal of single cells (Figure 6.8A). The loss of SHIP2 significantly increased the levels of active caspase 3 in all BL cell lines, especially in Daudi cells. The expression of CitSHIP2 decreased the cleavage of caspase 3 back on WT level, yet this rescue was not statistically significant in the Daudi cells (Figure 6.8B-D). Collectively, the increased activation of caspase 3 in SHIP2-negative cells corroborate the results of the Annexin-

V/7-AAD assay.

To assess the apoptotic pathways that are related to the function of SHIP2 in BL, the cells were subjected to a BH3 profiling. This assay focuses on the interaction of pro- and anti-apoptotic proteins of the BCL-2 family, which contain the BCL-2 homology 3 (BH3) domain [232, 248, 249]. The multi domain anti-apoptotic proteins such as BCL-2 and BCL-XL inhibit the multi domain pro-apoptotic proteins BAK and BAX, which themselves can be activated by engagement of their BH3 domain through BIM or BID [250–252] resulting in formation of mitochondrial outer membrane permeabilisation (MOMP) and cytochrome C release [233]. Similarly, the inhibition of apoptosis by the anti-apoptotic proteins can be prevented by binding of their BH3 domain to sensitizers such as BAD, HRK, MS-1, FS-1 and PUMA [253]. This principle is exploited by treatment of the cells with BH3-mimicking peptides, which represent either the activators of the pro-apoptotic proteins or the sensitizers binding to the anti-apoptotic proteins. The resulting response allows to determine dependencies on specific proteins, which may be deduced to the underlying signaling [234, 235].
Since the BH3 profiling measures the cytochrome C release, only the intrinsic apoptosis pathways can be addressed. Hence, the Daudi cell line was chosen due to its strong apoptosis and the lack of mutations in involved proteins. The DNA intercalating dye Hoechst33342 was used to determine cell viability [254]. Beyond the sensitising BH3 peptides, DMSO and alamethicin served as negative and positive control for MOMP, respectively [255, 256].

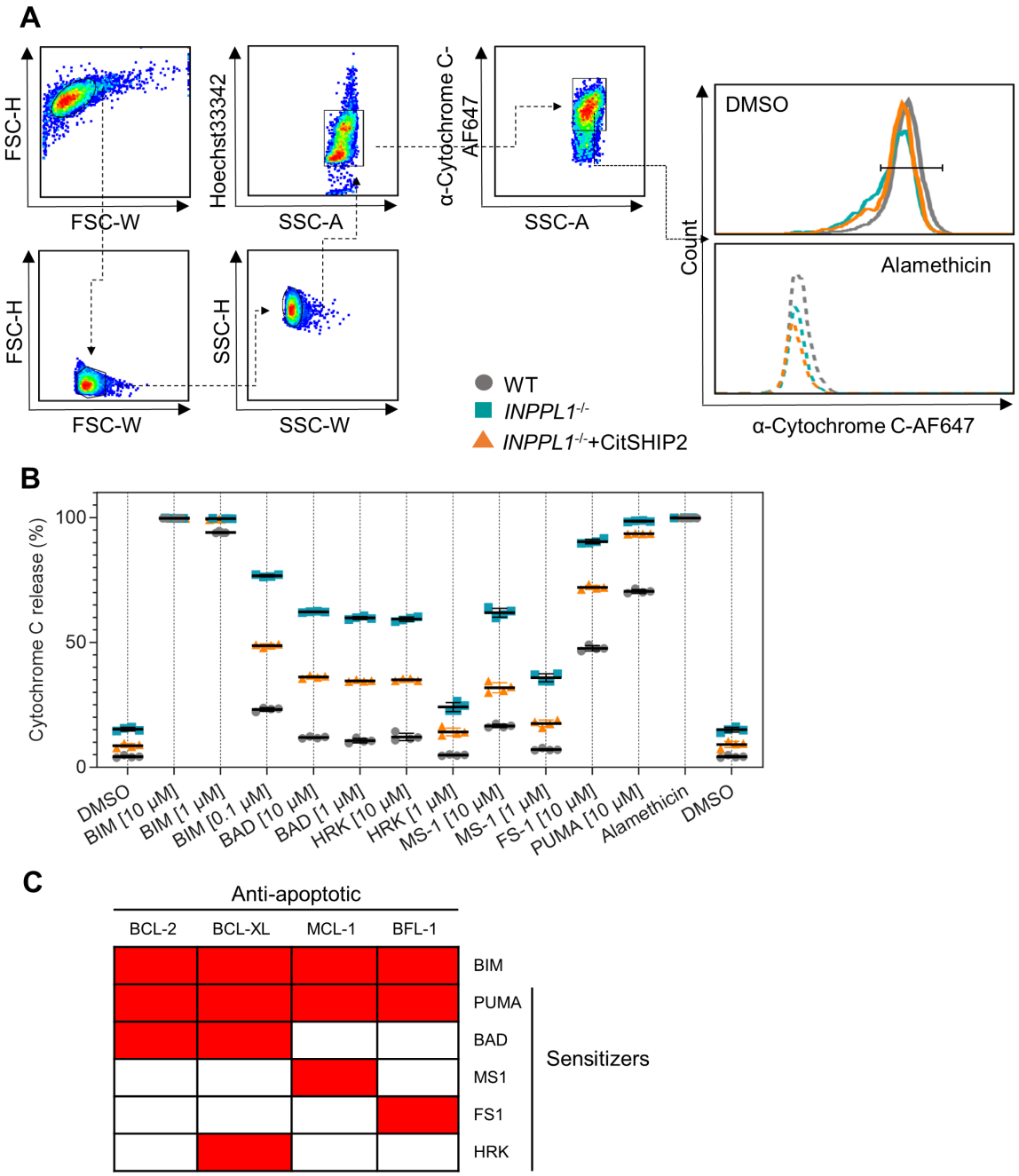

Figure 6.9: **Daudi cells exhibit increased sensitivity to apoptosis upon loss of SHIP2.** **A.** Gating strategy for the BH3-profiling. Cell debris was excluded and the single cells were assessed for their viability by Hoechst33342 signal followed by quantification of the released cytochrome C. The staggered histogram shows the cytochrome C release after DMSO or alamethicin treatment. **B.** BH3-profiling of Daudi WT, SHIP2-deficient and reconstituted cells. DMSO and alamethicin served as negative and positive control, respectively. Shown is one representative replicate. n=3 independent experiments were performed. Statistical analysis was conducted using Two-Way-ANOVA. Error bars indicate the standard deviation.

Figure 6.9: Continued:

C. The scheme depicts the specificity of the respective inhibitors for the anti-apoptotic proteins. Red cells indicate release of cytochrome C.

The gating strategy excluded cell debris, non-viable cells and doublets. The cytochrome C release is the inverse of the cytochrome C signal because release of cytochrome C, which rendered it unavailable for the α-Cytochrome C antibody (Figure 6.9A). The evaluation of the profiling confirmed a complete cytochrome C release by alamethicin in the whole Daudi panel. The negative control already revealed a significant increase of cytochrome C release in the SHIP2-deficient Daudi cells compared to WT or reconstituted. The same pattern was observable after treatment with any of the BH3 mimetic peptides, which indicates that the SHIP2 deficiency coincided with an increased sensitivity of these cells to enter apoptosis which was not dependent on one specific anti-apoptotic BCL2-family protein (Figure 6.9B). Though, the sensitivity for inhibition of BFL-1 by FS1 peptides showed the strongest overall potential to increase the sensitivity to apoptosis the ratio between the cells was comparable to inhibition of other anti-apoptotic proteins (Figure 6.9B,C).

Taken together, these data provide evidence that SHIP2 plays an important role for the fitness of tonic BCR signaling dependent BL cell lines by contributing to the proliferation and survival signaling.

6.4 shRNA-mediated ablation of SHIP2 confirmed results of CRISPR targeting

To exclude potential adaption effects caused by the complete disruption of the *INPPL1* expression in the SHIP2-negative cells, I aimed to generate cell lines with an inducible small hairpin RNA (shRNA) expression to down regulate the SHIP2 protein levels. After expression of a shRNA, it is modified by cellular enzymes producing a mature small interfering RNA (siRNA). The gene-specific guide strand of the siRNA allows the targeting and hybridisation to the messenger RNA (mRNA) of the selected gene. The hybridisation prevents the translation at the ribosome due to targeted degradation effectively silencing the gene expression [257]. Based on the PiggyBac system, constructs were generated

that allowed for a doxycycline-inducible, simultaneous expression of the shRNA targeting *INPPL1* (sh*INPPL1*) and a simultaneous GFP expression [212]. These plasmids were stably transfected into Ramos cells, which were examined for a functional shRNA expression by checking the cellular GFP levels via flow cytometry and the SHIP2 protein levels by Western Blot analysis. Following, proliferation and apoptosis were assessed after the induced silencing of *INPPL1* using the XTT and an Annexin-V staining. Cells with a non-targeting control shRNA (shNTC) served as control.

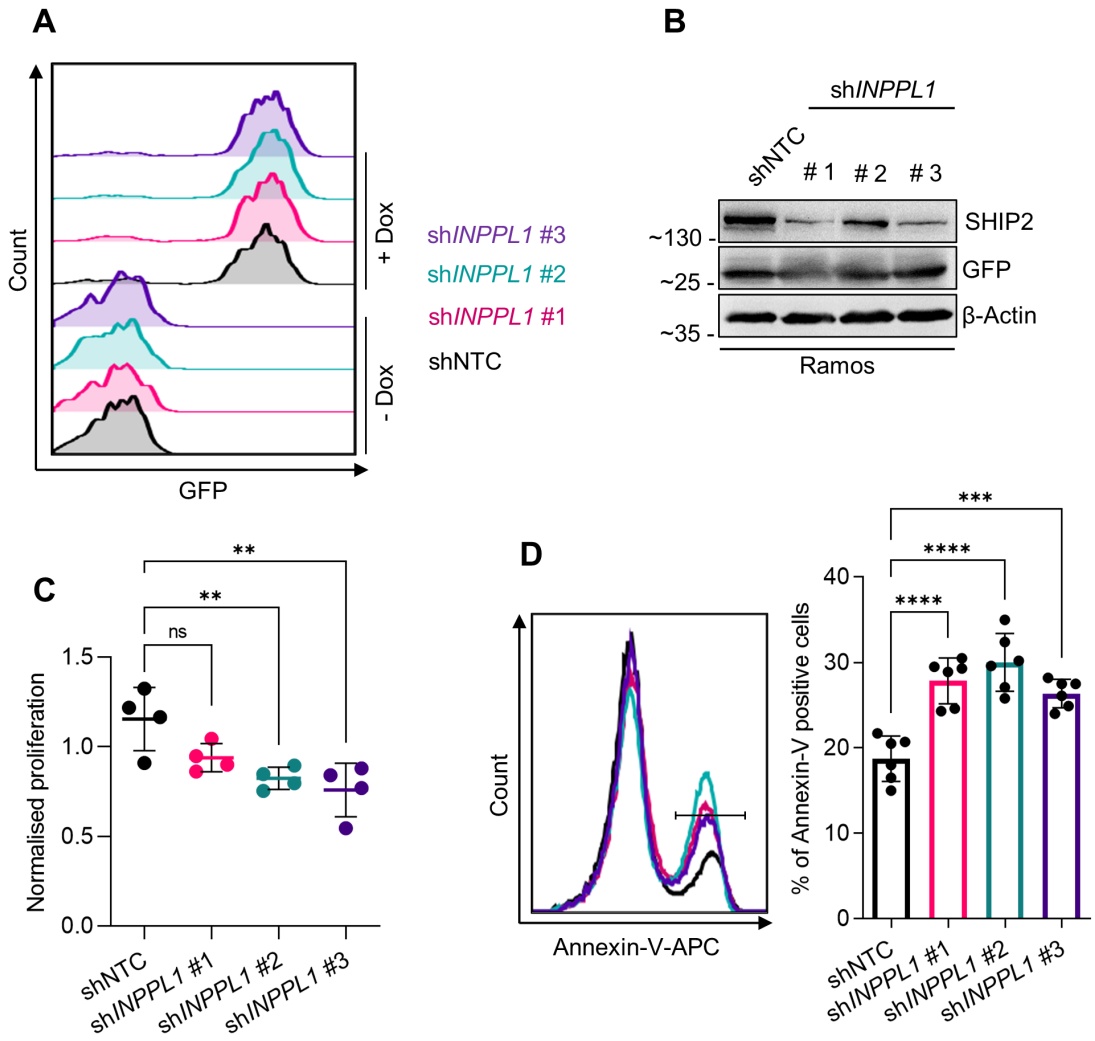

Figure 6.10: **shRNA-based ablation of SHIP2 attenuates the fitness of Ramos cells. A.** Histogram of Ramos cells carrying either a doxycycline-inducible non-targeting control shRNA (shNTC) or an shRNA targeting *INPPL1* (sh*INPPL1*#1-3) before and after one day of treatment with 250 ng/ml doxycycline. Induction of the constructs produces the respective shRNA and GFP, which allows monitoring of shRNA-positive cells. **B.** Western Blot analysis confirmed proper induction of the construct indicated by the GFP band and SHIP2 protein levels were reduced by induction of sh*INPPL1*#1-3. The cells were treated with 250 ng/ml doxycycline for 4 days followed by lysis and subjection to Western Blot analysis. The membranes were probed with α-SHIP2, α-GFP and α-β-Actin as loading control. The apparent molecular weight is indicated as kDa. **C.** Proliferation of Ramos cells after induced expression of sh*INPPL1*. The cells were treated with 250 ng/ml doxycycline for 5 days followed by a XTT assay and normalisation to non-induced cells. **D.** Percentage of Annexin-V-APC-positive cells after induced expression of sh*INPPL1*.

Figure 6.10: Continued:

The cells were induced in the before described manner followed by subjection to Annexin-V-APC staining. If not indicated otherwise experiments were performed n≥3. Error bars indicate the standard deviation. Statistics were performed using One-Way-ANOVA. Significance is indicated by p<0.05 *, p<.0.01 **, p<0.001 ***, p<0.0001 ****.

Addition of doxycycline to the transfected cells resulted in an increased GFP signal indicating that the shRNA system was functional and stably integrated (Figure 6.10A). In addition, induction of the three different sh*INPPL1* for 4 days reduced the SHIP2 protein levels markedly compared to the non-targeting control shRNA (shNTC), which confirmed the efficiency of the shRNAs (Figure 6.10B). The shRNA-mediated depletion of SHIP2 in the Ramos cells lowered the proliferation in a manner comparable to the respective *INPPL1*$^{-/-}$ cells (Figure 6.10C). Correspondingly, the induced silencing significantly elevated the percentage of Annexin-V-positive cells compared to the control (Figure 6.10D). The strong GFP expression in the induced cells prevented the use of 7-AAD due to spill over of the GFP signal.
Short-term ablation of SHIP2 produced the same effects observed in the *INPPL1*$^{-/-}$ cells, which further solidifies the evidence that SHIP2 is an important contributor to the fitness of BL cell lines.

6.5 SHIP2 deficiency does not affect the fitness of BCR-negative BL cells

While the BL cell lines that were analysed in this study have been reported to be BCR-dependent, this is not a proof that the effects observed in SHIP2-deficient cells are part of the tonic BCR signal network [163]. Hence, the *INPPL1* gene was targeted via the CRISPR/Cas9 system in the surface BCR-deficient Raji cell line to address this question [210, 211]. The disruption of the *INPPL1* gene was carried out using the same crRNA as in the DG75 cells, which targeted the fifth exon. The successful application of the CRISPR/Cas9 system was validated via Western Blot analysis and sequencing of the site of incision.

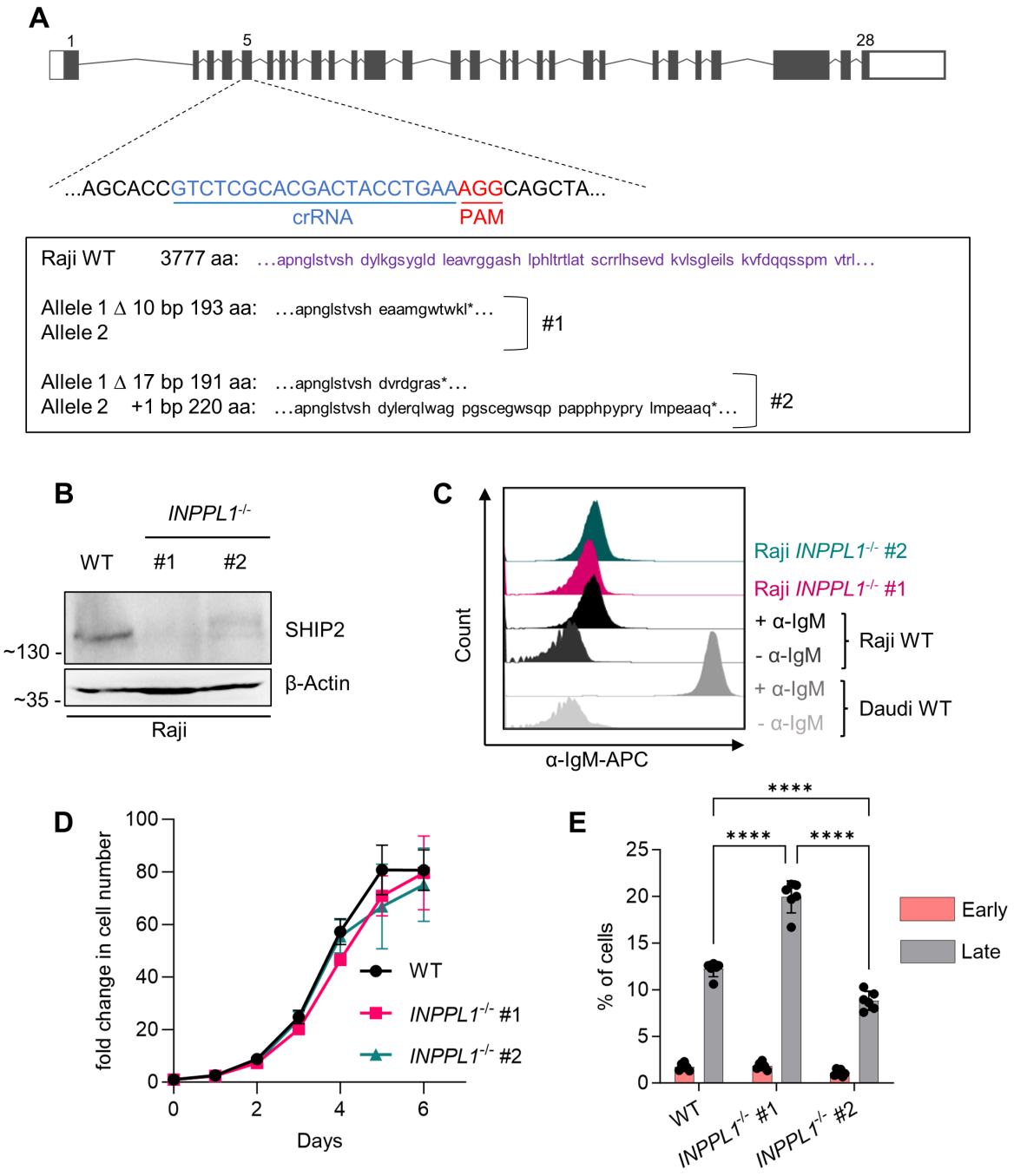

Figure 6.11: **Fitness of surface IgM-negative Raji cells remained unaltered upon loss of SHIP2. A.** Exon structure of the *INPPL1* consensus gene with the respective target site of the crRNA (blue) and PAM site (red) in the exon 5. Clones recovered from the single cell dilution were screened for protein deficiency via Western Blot analysis and subsequent genomic sequencing identified 2 clones with genomic aberrations. **B.** Western Blot analysis of the two clones confirmed the loss of SHIP2. The membranes were probed with α-SHIP2 and α-β-Actin as loading control. The apparent molecular weight is indicated as kDa.

Figure 6.11: Continued:

C. The surface IgM levels of Raji WT and SHIP2-deficient cells were quantified by FACS analysis of α-IgM-AF647 stained living cells. Unstained Daudi and Raji WT and stained Daudi WT served as negative and positive control respectively. **D.** Cell counting assay of SHIP2-deficient Raji cells compared to WT cells. Shown are the living cells on each day normalised to d0. **E.** Annexin-V-APC/7-AAD assay comparing the apoptosis of SHIP2-negative Raji cells with WT cells. Apoptosis was induced by cultivation in 1 % FCS medium for 48 h prior to staining with 6 ng/sample Annexin-V-APC and 150 ng/sample 7-AAD. Late apoptosis is indicated by Annexin-V-APC$^+$/7-AAD$^+$ cells while early apoptotic cells are only Annexin-V-APC$^+$. If not indicated otherwise experiments were performed n$\geq$3. Error bars indicate the standard deviation. Statistics were performed using Two-Way-ANOVA. Significance is indicated by p<0.05 *, p<.0.01 **, p<0.001 ***, p<0.0001 ****.

The screening for clones negative for SHIP2 protein level revealed two clones, which were further analysed by genomic sequencing. While two different sequence aberrations could be identified in *INPPL1*$^{-/-}$ #2, which led to the generation of premature stop codons only one mutation was found in clone #1. However, clone #1 appeared to be negative for *INPPL1* expression as indicated by the Western Blot analysis. Hence it was suspected that the sequence aberration on one allele spanned into the primers used for initial amplification of the target site, which prevented the sequencing (Figure 6.11A,B). As expected, the flow cytometric analysis of surface IgM-stained cells confirmed that Raji cells possess no BCR on the cell surface especially when compared to the Daudi cell line (Figure 6.11C). As revealed by cell counting, the proliferation of SHIP2-deficient Raji cells differed insignificantly compared to the WT, which sets it apart from the attenuated proliferation observed in the BCR-dependent cell lines (Figure 6.11D). The apoptosis assay showed ambiguous results with clone #1 exhibiting slightly increased and clone #2 decreased levels of late apoptosis compared to the parental Raji cells (Figure 6.11E).
These data imply that the BCR-negative BL cell line Raji is insensitive to SHIP2 deficiency, hence suggesting that the supportive role of SHIP2 is part of the tonic BCR signaling network.

6.6 SHIP2 is not involved in the regulation of major tonic BCR signaling pathways

6.6.1 SHIP2 does not control the signaling efficiency of MAPKs

The network of mitogen activated protein kinases (MAPK) influences the proliferation and survival in B cells [18, 258]. This network consists of three independent pathways named after the most downstream kinase: Jun N-terminal kinase (JNK), extracellular-signal regulated kinase (ERK) and p38 MAPK (p38). To test if SHIP2 regulates the activity of MAPKs I analyzed their regulating phosphosites in the generated Ramos cell lines.

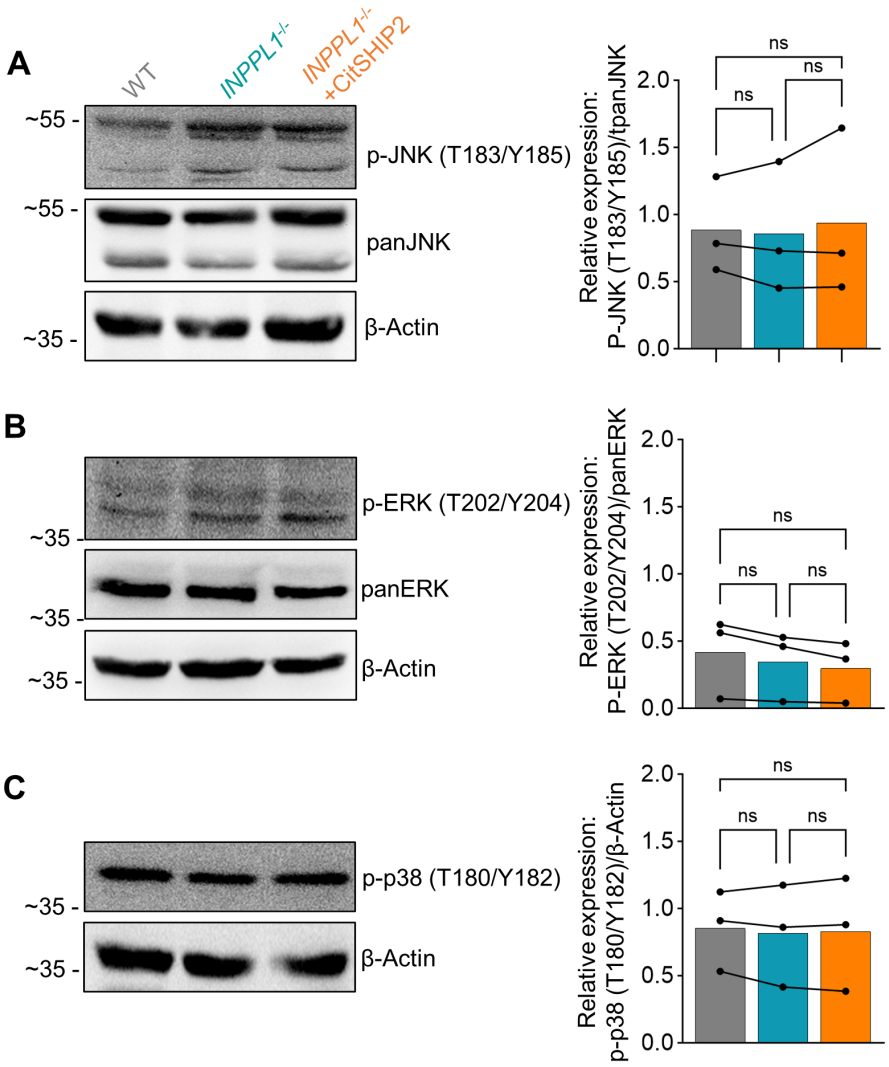

Figure 6.12: **MAPK signaling remained unaltered in SHIP2-deficient Ramos cells.** Western Blot analysis showing the phosphorylation levels of the MAP kinases **A.** JNK, **B.** ERK and **C.** p38 upon loss of SHIP2 in Ramos cells. Ramos WT, *INPPL1*$^{-/-}$ and reconstituted cells were subjected to lysis followed by Western Blot analysis. The membranes were probed with α-p-JNK (T183/Y185), α-panJNK, α-p-ERK (T202/Y204), α-panERK, α-p-p38 (T180/Y182) and α-β-Actin as loading controls. The apparent molecular weight is indicated as kDa. Relative expression was calculated after densiometric evaluation of the membranes and normalisation to either the non-phosphorylated protein or the loading control. If not indicated otherwise experiments were performed n$\geq$3. Error bars indicate the standard deviation. Statistics were performed using One-Way-ANOVA. Significance is indicated by p<0.05 *, p<.0.01 **, p<0.001 ***, p<0.0001 ****.

In contrast to previous findings in Daudi cells, SHIP2 deficiency did not influence the

phosphorylation levels of JNK as demonstrated by Western Blot analysis (Figure 6.12A). Also, the phosphorylation state of ERK and p38 remained stable (Figure 6.13B,C), showing that the activity of the MAPK signaling network remained unaffected by SHIP2 deficiency in Ramos cells, which suggests that the SHIP2-dependent regulation of JNK in Daudi might be cell line specific.

6.6.2 Phosphorylation of AKT remained stable in the absence of SHIP2

After having shown that MAPKs were not involved in the supportive function of SHIP2 in BL cells. other BCR-dependent signaling pathways were investigated. Of particular interest was the PI3K-AKT axis due to two different reasons: First, as mentioned above SHIP2 is considered as a negative regulator of AKT through its 5-inositol phosphatase activity [46]. Second, the tonic BCR-dependent survival signaling via AKT is crucial for the survival of B cells as it was shown that over-activation of the PI3K-AKT axis restored survival after ablation of the BCR [49]. Hence, the phosphorylation of AKT at serine 473 (p-AKT(S473)), which is facilitated by mTORC2 and directly responsible for the activation of the kinase was examined [33].

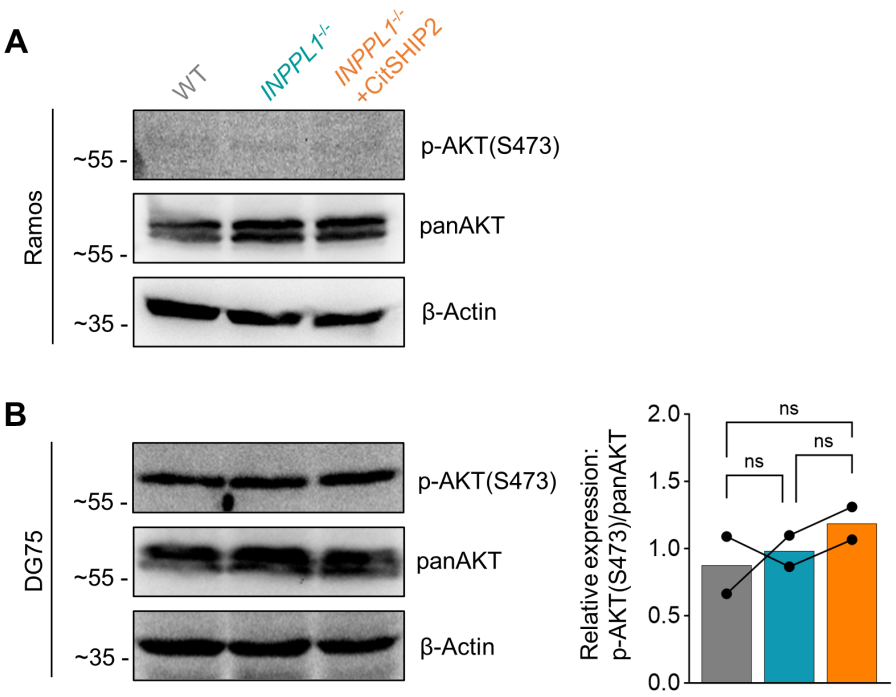

Figure 6.13: **AKT phosphorylation was unaffected by loss of SHIP2. A.** Western Blot analysis could not detect AKT phosphorylated at S473 in Ramos cells. **B.** p-AKT(S473) levels in the DG75 cells lines as revealed by Western Blot analysis. Ramos and DG75 WT, *INPPL1*$^{-/-}$ and reconstituted cells were subjected to lysis followed by Western Blot analysis. The membranes were probed with α-p-AKT(S473) and α-panAKT as well as α-β-Actin as loading control. The apparent molecular weight is indicated as kDa. Relative expression was calculated after densiometric evaluation of the membranes and normalisation to the non-phosphorylated protein. If not indicated otherwise experiments were performed n$\geq$3. Error bars indicate the standard deviation. Statistics were performed using One-Way-ANOVA. Significance is indicated by p<0.05 *, p<.0.01 **, p<0.001 ***, p<0.0001 ****.

The Western Blot analysis of the Ramos cells revealed very low phosphorylation levels in this cell line, which prevented the densiometric analysis (Figure 6.13A). However, p-AKT(S473) could be detected in cleared cellular lysates from the generated DG75 cell lines. Analysis of the obtained signals revealed similar intensities, which is against a function of SHIP2 in regulating AKT activity. Instead, the levels remained stable in the whole panel (Figure 6.13B).

To corroborate these findings, the different cell lines were subjected to intracellular staining of p-AKT(S473) and p-AKT(T308). AKT requires phosphorylation of two amino acid residues, serine at position 473 and threonine at 308, to be fully activated [38]. Therefore, the p-AKT(T308) levels were assessed by flow cytometry of intracellularly stained cells.

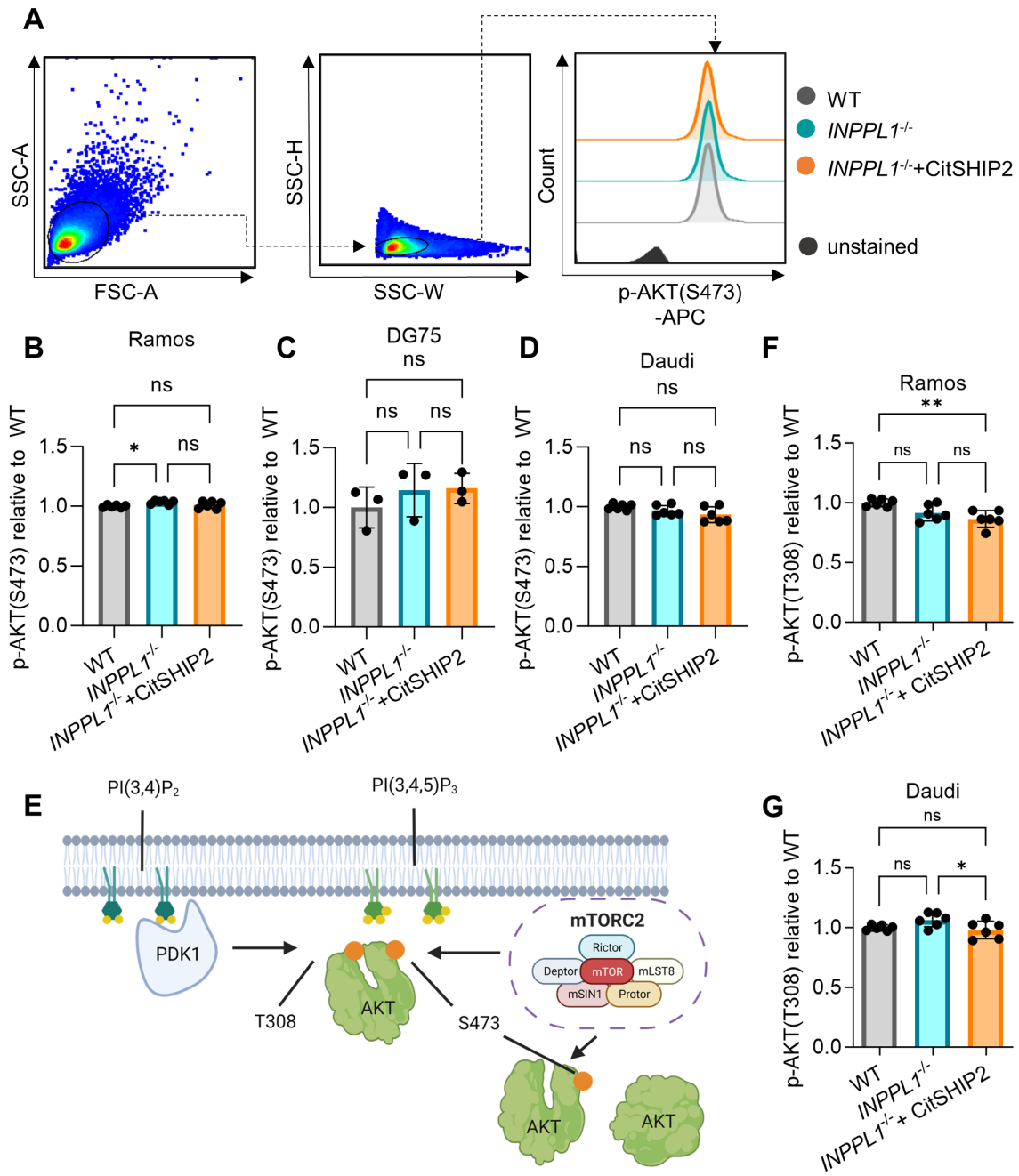

Figure 6.14: **Flow cytometry confirms the Western Blot analysis by showing no changes in intracellular p-AKT(S473,T308) in SHIP2-deficient BL cells. A.** Gating strategy for quantification of intracellular phosphorylated AKT(S473) in fixed cells. Following the exclusion of cell debris the cells were gated on single cells only which were then assessed for their p-AKT(S473)-APC signal. Quantification of the p-AKT(S473) levels in Ramos **B.**, DG75 **C.**, and Daudi **D.** cell lines relative to the respective WT cells. **E.** Cartoon depicting the regulation of the serine 473 and threonine 308 phosphosites of AKT by PDK1 and mTORC2. Intracellular staining for p-AKT(T308) in Ramos **F.** and Daudi **G.** cell lines.

Figure 6.14: Continued:

Prior to measuring, the cells were fixed, permeabilised and stained with α-p-AKT(S473)-APC or α-p-AKT(T308)-AF647 followed by FACS analysis. The obtained MFIs were normalised to the respective WT of each cell line. If not indicated otherwise experiments were performed n$\geq$3. Error bars indicate the standard deviation. Statistics were performed using One-Way-ANOVA. Significance is indicated by p<0.05 *, p<.0.01 **, p<0.001 ***, p<0.0001 ****.

The exemplary gating strategy for the Ramos cell lines showed how the inclusion of cell debris in the analysis was avoided (Figure 6.14A). Similar to Western Blot analysis, loss of SHIP2 did not alter the phosphorylation levels of AKT(S473) in any of the cell lines (Figure 6.14B-D). There is a minor, though statistically significant increase of p-AKT(S473) in the Ramos *INPPL1*$^{-/-}$ cells, which however is not altered by reconstitution. SHIP2-deficient Ramos and Daudi cells exhibited no dysregulations of p-AKT(T308) compared to the respective WT cells. While, the SHIP2-negative Daudi cells showed a slight but significant increase compared to the reconstituted cells, this does not correlate with reduced survival of these cells (Figure 6.14F,G).

These findings imply that SHIP2 does not regulated AKT activity in BL cell lines, thereby suggesting that the SHIP2-dependent survival function is AKT-independent.

6.6.3 SHIP2 deficiency sensitized BL cells to inhibition of PI3K and mTOR

Since the previous results indicate a pro-survival role of SHIP2 that is independent of the PI3K effector protein AKT, I assessed, if SHIP2 relies on PI3K activity in general to support BL cell fitness. The functions of PI3K and SHIP2 are directly connected as the PI3K generates PI(3,4,5)P_3, which serves as substrate for SHIP2 to produce PI(3,4)P_2 [46]. Hence, the next experiments aimed at elucidating, if the fitness of SHIP2-deficient cells converge with that of parental cells after inhibition of PI3K.
First, the effects of inhibition of PI3K by the small molecule copanlisib [259] were assessed in WT BL cells via the XTT assay. For this purpose, Ramos, Daudi and DG75 WT cells were treated with increasing concentrations of copanlisib for 24 h. Furthermore, it was validated whether the copanlisib treatment is PI3K-specific and does not affect other survival-related pathways such as the MAPK signaling [260–262]. Hence, the phospho-

rylation levels of ERK and JNK upon treatment with copanlisib were assessed via flow cytometry in the Ramos WT cells. In addition, the levels of p-AKT(S473) were quantified to see if the inhibition of PI3K led to the expected decrease of AKT activity, and which effects an additional inhibition of SHIP2 has. Therefore, parental and SHIP2-deficient Ramos, Daudi and DG75 cells were treated for 30 min with either 200 nM copanlisib, 5 µM AS1949490 or a combination of both.

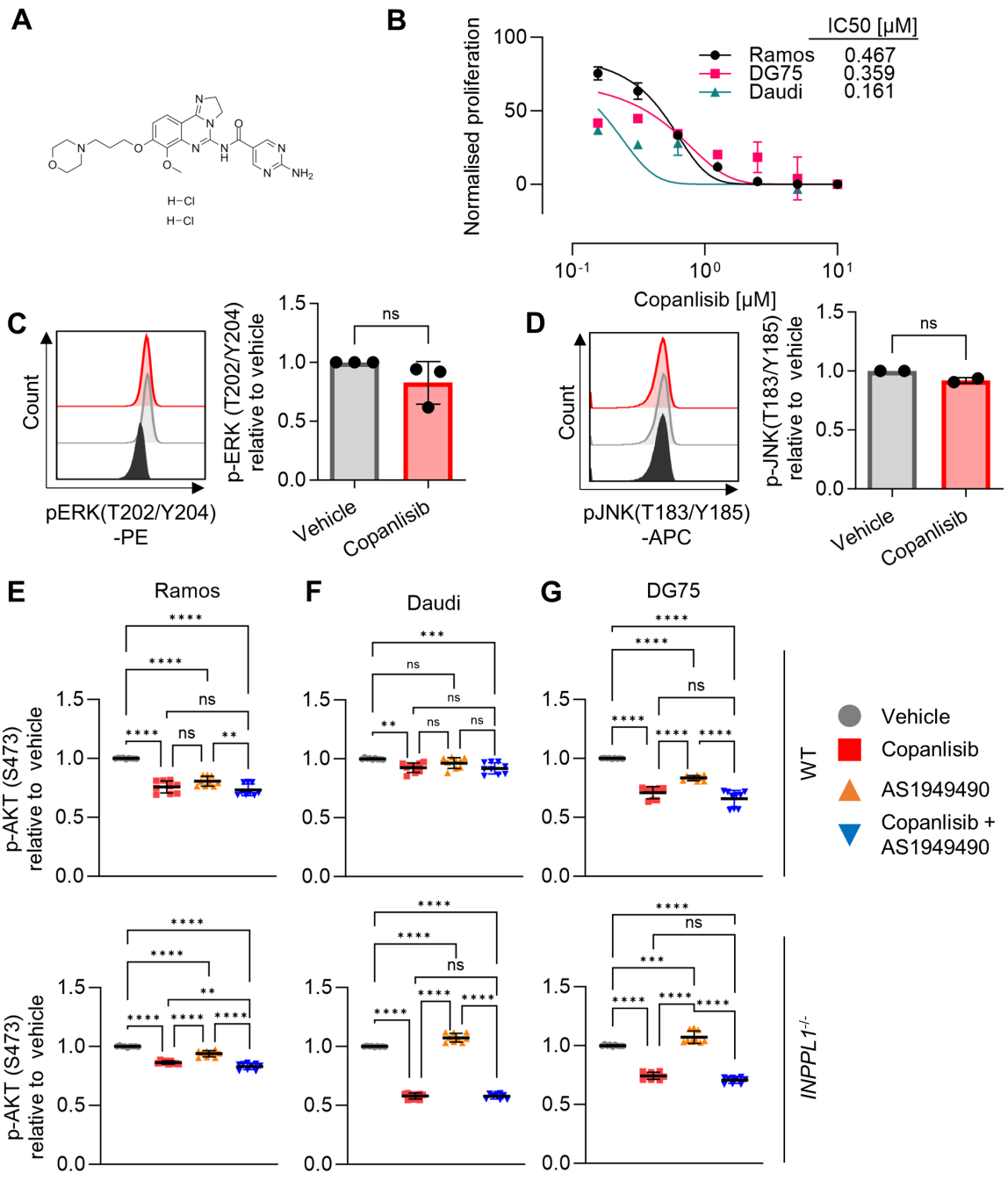

Figure 6.15: **Copanlisib decreases proliferation of BL cells in a dose- and PI3K-dependent manner and decreases AKT activity A.** Chemical structure of the selective PI3K inhibitor copanlisib. **B.** Proliferation of Ramos, DG75 and Daudi WT cells treated with increasing concentrations of copanlisib for 24 h. The relative proliferation was assessed by XTT assay and normalisation to vehicle-treated samples. The dose-response curve was calculated using a non-linear regression model for normalised data. IC50 values were calculated using GraphPad Prism.

Figure 6.15: Continued:

p-ERK(T202/Y204) **C.** and p-JNK(Ty183/Y185) **D.** levels of Ramos WT cells treated with copanlisib or 5 % TFA as vehicle control followed by fixation, permeabilisation and intracellular staining with either α-p-ERK(T202/Y204) or α-p-JNK(T183/Y185). p-AKT(S473) levels of Ramos **E.**, Daudi **F.** and DG75 **G.** cell lines after treatment with copanlisib, AS1949490 or a combination of both. The cells were treated as indicated with either a vehicle control (mixture of DMSO and 5 % TFA), 200 nM copanlisib, 5 µM AS1949490 or a combination of both inhibitors for 30 min followed by fixation, permeabilisation and intracellular staining with α-p-AKT(S473)-APC. MFIs of the respective signals were normalised to the vehicle control. If not indicated otherwise experiments were performed n≥3. Error bars indicate the standard deviation. Statistics were performed using paired t-test. Significance is indicated by p<0.05 *, p<.0.01 **, p<0.001 ***, p<0.0001 ****.

Treatment with copanlisib revealed a negative effect on proliferation in all three BL cell lines even at the starting concentration of 0.125 µM. The Ramos cells showed a particularly pronounced dose response while the effect was mild in the DG75 cells (Figure 6.15A,B). Consequently, a concentration of 200 nM of copanlisib was used for further experiments as this concentration ensured an effect on proliferation p-ERK(T202/Y202) and p-JNK(T183/Y185) levels (Figure 6.15C,D). Copanlisib treatment significantly reduced the p-AKT(S473) levels in all of the tested cell lines regardless of the SHIP2 status. Apparently for Daudi cells this effect was escalated by absence of SHIP2. Inhibition of SHIP2 decreased the p-AKT(S473) levels in parental cells while the inhibitor caused ambiguous, but minor alterations in the SHIP2-deficient cells. Combined use of both inhibitors did not yield an additional effect on p-AKT(S473) levels beyond copanlisib only treatment (6.15E-G).

To test for the effect of PI3K inhibition in the absence of SHIP2, the proliferation of the different BL cell lines after 48 h treatment with 200 nM copanlisib or TFA as vehicle control was assessed by XTT and cell counting assays. In addition, these experiments were complemented by treatment of WT cells for 48 h with with copanlisib or a combination of copanlisib and AS1949490. These experiments are depicted in figure 6.16.

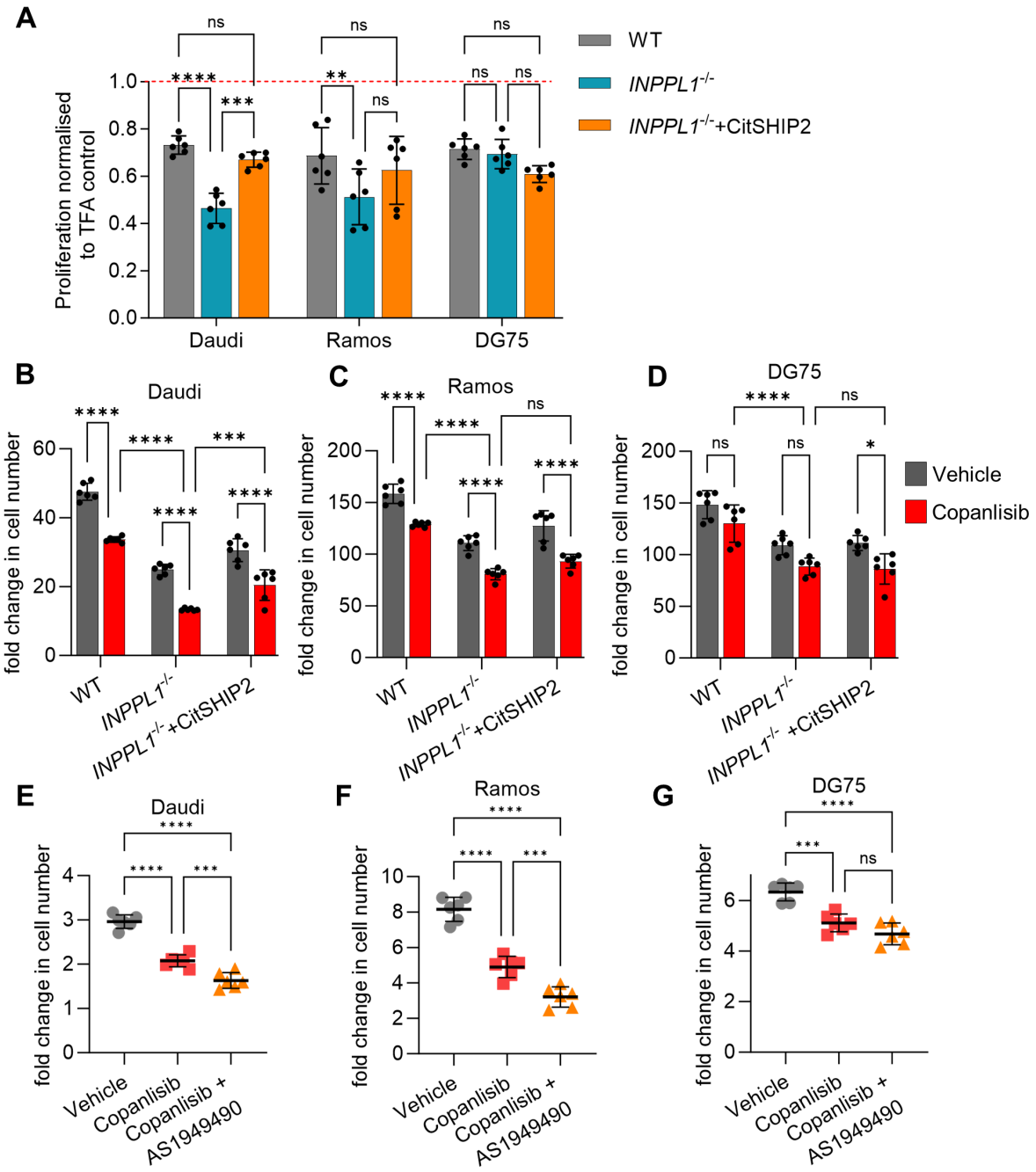

Figure 6.16: **Loss of SHIP2 sensitizes BL cell lines to inhibition of PI3K. A.** Proliferation of Daudi, Ramos and DG75 cell lines after treatment with the PI3K inhibitor copanlisib. The cells were treated with 200 nM copanlisib or 5 % TFA as negative control for 24 h followed by determination of the remaining proliferation by XTT assay. The proliferation of treated cells was normalised to the respective TFA controls. Cell counting assay of Daudi **B.**, Ramos **C.** and DG75 **D.** cell lines showing the fold change in cell number after treatment with 200 nM copanlisib for 48 h. Daudi **E.**, Ramos **F.** and DG75 **G.** WT cells were treated with either copanlisib or a combination of copanlisib and the SHIP2 inhibitor AS1949490.

Figure 6.16: Continued:

Shown are the living cells counted after 48 h of treatment with 200 nM copanlisib (B-G), 5 µM AS1949490 (E-G) or a combination of both (E-G). 5 % TFA (A-G) or DMSO (E-G) served as vehicle controls. Fold-change indicated the increase of living cells compared to d0. Shown are the results of n≥3 independent experiments. Error bars indicate the standard deviation. Statistics were performed using Two-Way-ANOVA. Significance is indicated by p<0.05 *, p<.0.01 **, p<0.001 ***, p<0.0001 ****.

Both assays showed that treatment with copanlisib affected the proliferation of SHIP2-deficient Daudi and Ramos cells significantly stronger, than parental and reconstituted cells (Figure 6.16A-C). Consistent with the low sensitivity to PI3K inhibition (Figure 6.15B), no changes in proliferation were observed in DG75 cells, regardless of SHIP2 expression (Figure 6.16A,D). The treatment with AS1949490 also sensitized for inhibition of PI3K confirming the observations in the SHIP2-deficient Ramos and Daudi but not DG75 cells (Figure 6.16E-G).
To corroborate these findings, the copanlisib-sensitive Daudi and Ramos cells were again treated with 200 nM copanlisib and the level of apoptotic cells was determined by an Annexin-V-APC staining.

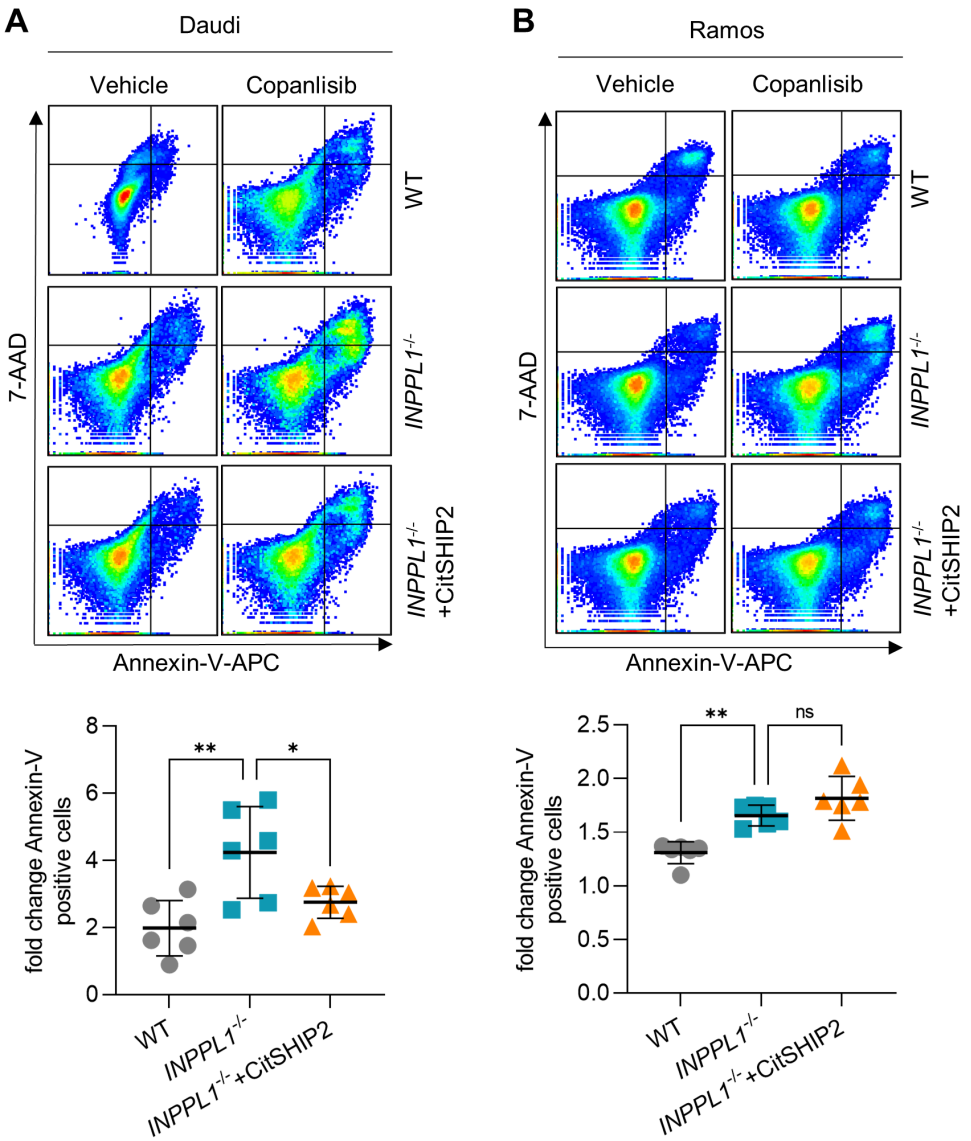

Figure 6.17: **SHIP2 deficiency renders BL cells more susceptible to apoptosis after copanlisib treatment.** Annexin-V-/7-AAD staining to assess the apoptosis of Daudi **A.** and Ramos **B.** cell lines after copanlisib treatment. The cells were treated for 48 h with 200 nM copanlisib or 5 % TFA as negative control followed by subjection to Annexin-V-APC/7-AAD staining. Fold-change indicates increase of Annexin-V-APC-positive cells compared to the negative control. If not indicated otherwise experiments were performed n≥3. Error bars indicate the standard deviation. Statistics were performed using One-Way-ANOVA. Significance is indicated by p<0.05 *, p<.0.01 **, p<0.001 ***, p<0.0001 ****.

In absence of SHIP2, copanlisib treatment led to a significantly stronger increase in Annexin-V-positive cells in Daudi compared to WT and reconstituted cells (Figure 6.17A).

While the same effect was observed in Ramos cells it could not be significantly rescued by reconstitution (Figure 6.17B).
The increased sensitivity of SHIP2-deficient cells to inhibition of PI3K suggests that the absence of SHIP2 rendered the cells more sensitive to inhibition of tonic BCR survival signaling. Consequently, the setup of the previous proliferation experiments was repeated with inhibition of AKT directly by using capivasertib [263] or by inhibition of the AKT activator mTOR with rapamycin [264, 265]. The cells were treated for 48 h with either 1 µM capivasertib, 100 nM rapamycin or DMSO as vehicle control followed by determination of the proliferation by cell counting.

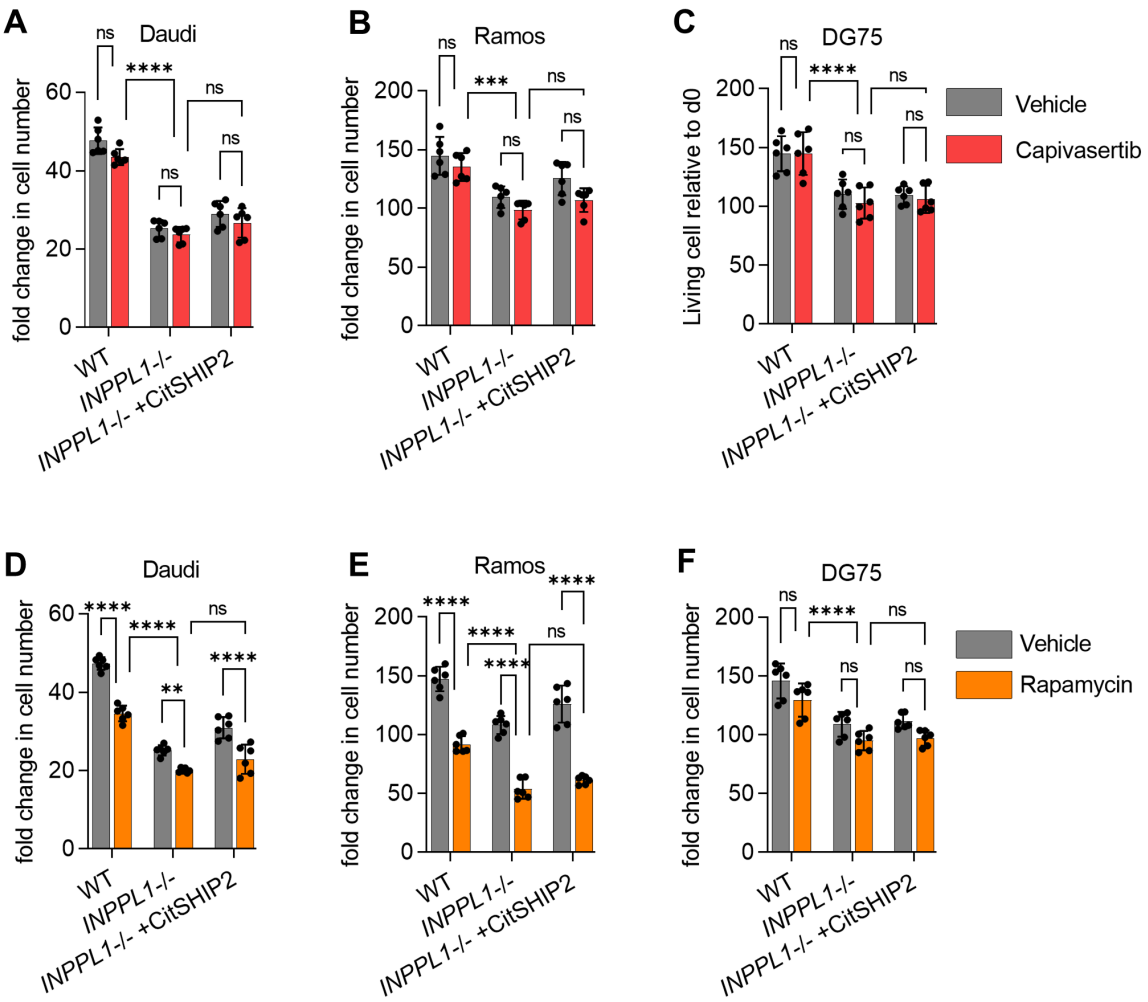

Figure 6.18: **Loss of SHIP2 sensitizes for mTORC2 inhibition but not AKT inhibition.** Cell counting assay to determine the proliferation of Daudi **A,D.**, Ramos **B,E.** and DG75 cell lines **C,F.** in response to inhibition of AKT by capivasertib or mTORC2 by rapamycin. Depicted are the living cells after treatment for 48 h with DMSO as vehicle control or 1 µM capivasertib (A-C) and 100 nM rapamycin (D-F). Fold-change indicated the increase of living cells compared to d0. If not indicated otherwise experiments were performed n≥3. Error bars indicate the standard deviation. Statistics were performed using Two-Way-ANOVA. Significance is indicated by p<0.05 *, p<.0.01 **, p<0.001 ***, p<0.0001 ****.

The cell counting reveals that inhibition of AKT had little to no effect on the proliferation of any of the BL cell lines. Moreover, SHIP2 deficiency did not increase the sensitivity to AKT inhibition (Figure 6.18A-C). In contrast, treatment with rapamycin lowered the proliferation of Daudi and Ramos cells, which was significantly exaggerated by absence of SHIP2 (Figure 6.18D,E). The DG75 cells remained insensitive to rapamycin treatment

regardless of SHIP2 presence (Figure 6.18F).

Taken together, Ramos and Daudi cells exhibited a SHIP2-dependently increased sensitivity to inhibition of PI3K and mTOR, which are both part of the tonic BCR survival signaling that contribute to the survival of BL cells. In contrast, inhibition of AKT did not affect the proliferation of BL cell lines regardless of *INPPL1* expression.

6.6.4 Phosphoproteome analysis did not reveal SHIP2-dependent changes in the tonic BCR signaling network

The previous experiments suggested that SHIP2 is part of the tonic BCR survival signaling, but the detailed mechanism remained elusive. Since activity of the key survival kinase AKT was not affected by SHIP2, I assessed if SHIP2 regulates other components of the tonic BCR signaling network. This was addressed by quantitative mass spectrometry of phospho-peptides. To achieve stable isotope labeling with amino acids in cell culture (SILAC), the cell lines were cultured in media containing normal amino acids ("light") and amino acids with carbon and nitrogen isotopes ("heavy"). By continuous culture, the supplemented amino acids were integrated into the proteome [266, 267]. Expanded cells were lysed and the lysates were mixed in a 1:1 ratio, followed by further processing and eventual subjection to mass spectrometry and analysis of the data according to [165, 218, 219]. The identified tyrosine phosphatome (pYome) and global phosphatome (gPome) consisting of the threonine and serine phosphosites were then cross-referenced via a Python script to a list of phosphosites known to be involved in tonic BCR signaling and extract matched phosphosites [163]. This complete workflow, including the SILAC, was carried out for the Ramos *INPPL1*$^{-/-}$ and reconstituted cells while the data obtained from Daudi cells in previous studies were re-evaluated.

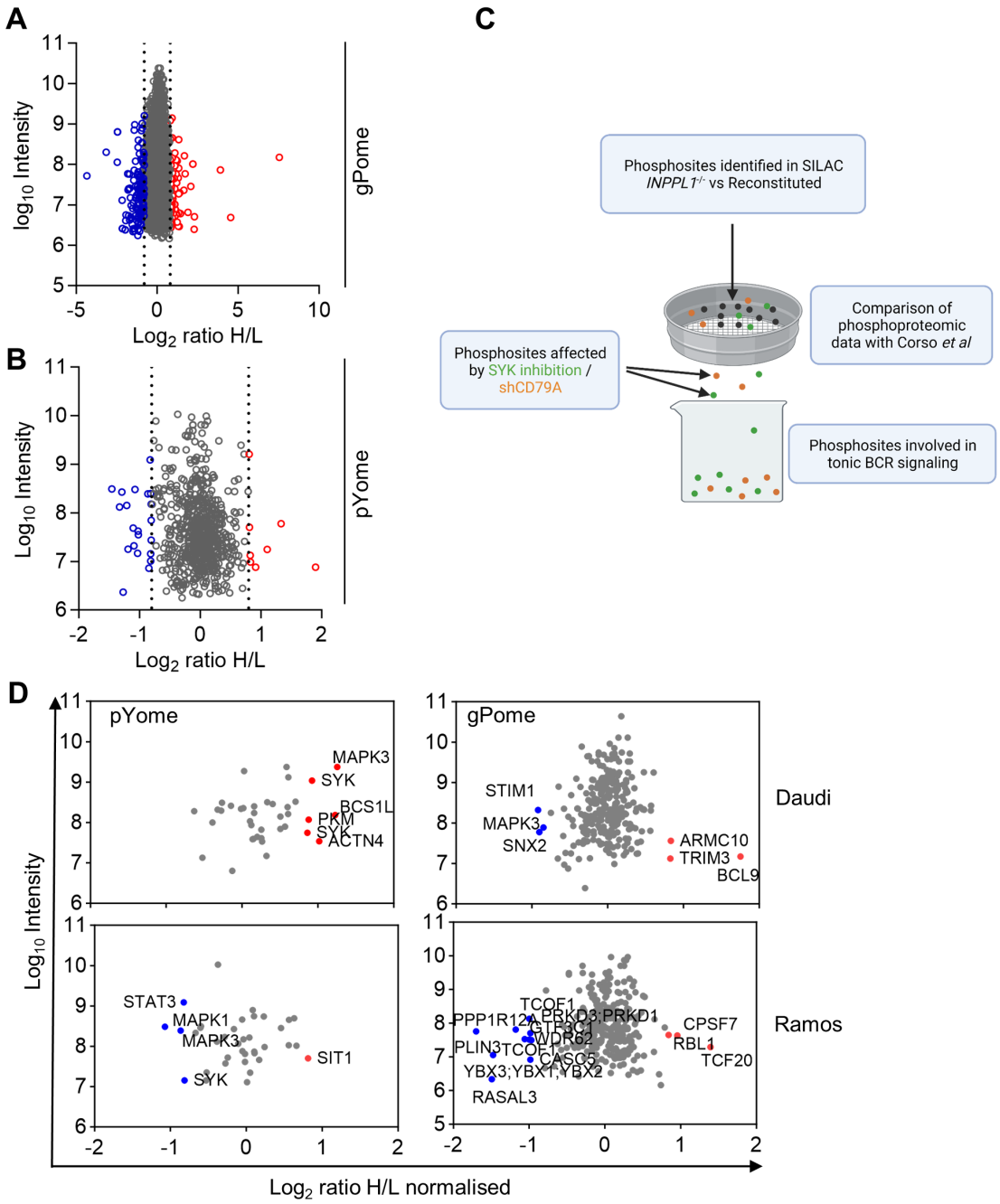

Figure 6.19: **Phospho-sites involved in tonic BCR signaling were not altered by SHIP2 deficiency in Ramos and Daudi cells. A.** Global phosphatome (gPome) and **B.** tyrosine phosphatome of Ramos *INPPL1*$^{-/-}$ cells versus reconstituted cells after SILAC and mass spectrometry. Log2 ratios >0.8 were considered as significant with red indicating down- and blue up-regulation of the respective phosphosite in the *INPPL1*$^{-/-}$ cells. **D.** Bioinformatic analysis of the phosphatome data from Ramos and Daudi cells. The data was searched for phosphosites published to be involved in tonic BCR signaling [163] and hits were extracted.

Figure 6.19: Continued:

E. The comparison revealed no consistent alterations in the phosphosites involved in the tonic signaling of SHIP2-negative cells. Red indicated down- and blue up-regulated phosphosites in *INPPL1*$^{-/-}$ compared to reconstituted cells.

The phosphoproteomic approach in Ramos identified a total of 7291 unique threonine or serine and 704 tyrosine phosphorylations. Many of these phosphosites were augmented in *INPPL1*$^{-/-}$ compared to reconstituted cells. Significant down regulation of a phosphosite in the SHIP2-negative cells is indicated by red colour and up regulation by blue (Figure 6.19A,B). The phosphoproteomic analysis did also not reveal augmented phosphorylation levels of ERK, JNK and AKT, which validated the previous results. The Ramos data set as well as the existing data from Daudi cells was then compared to the tonic BCR regulated phosphosites according to the cartoon (Figure 6.19C). As the plots for the tonic BCR signaling specific phosphosites revealed, only few phosphosites were significantly changed by SHIP2 deficiency. While some of the significantly changed phosphosites were found in crucial tonic BCR signaling proteins such as SYK [268], these changes were not consistent between the two BL cell lines 6.19D).
Consequently, this evaluation indicated that the absence of SHIP2 might not regulate known tonic BCR signaling processes, including the MAP kinases ERK and JNK as well as AKT, suggesting that the SHIP2-dependent contributions to BL cell fitness has a different cause.

6.7 SHIP2 is required for an efficient ATP production in BL cell lines

Complementary to the phospho-proteomic analysis, the global proteome (gProt) of the different Ramos cell lines was compared to address potential alterations of the tonic BCR signaling network on the protein abundance. The identified proteins were again compared to the proteins involved in the tonic BCR signaling [163] followed by a pathway analysis via the STRING database. For this purpose, the data set was analysed according to the alterations of the proteins and whether specific pathways were affected stronger in the *INPPL1*$^{-/-}$ or the reconstituted cells.

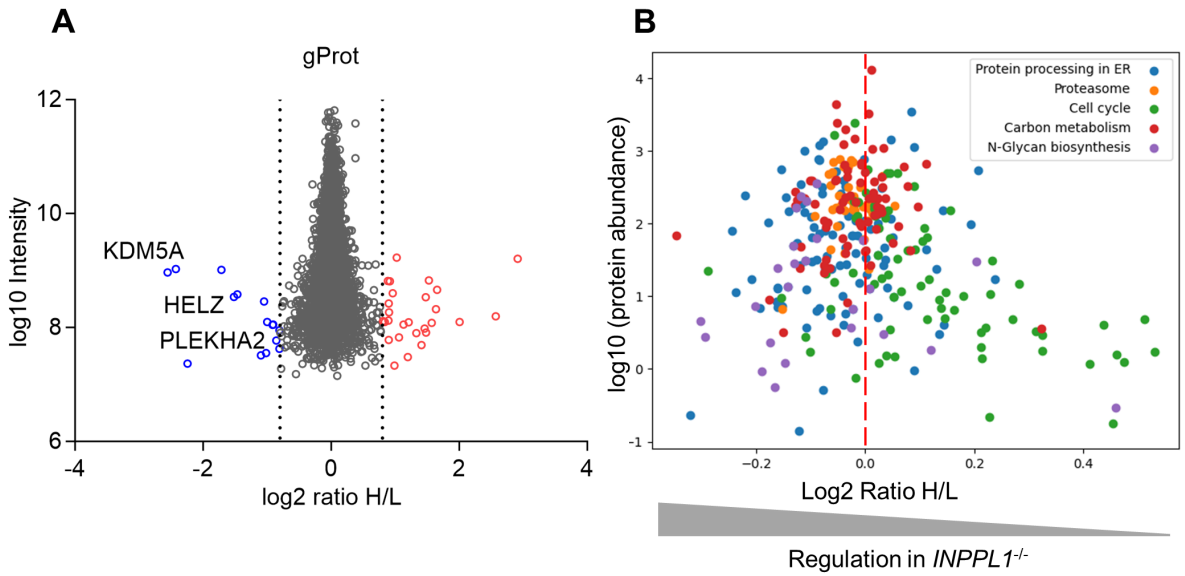

Figure 6.20: **Absence of SHIP2 altered the proteome of Ramos cells. A.** The previously labelled Ramos cells were used to analyse changes to the global proteome (gProt) of *INPPL1*$^{-/-}$ versus reconstituted cells. Red indicated up- and blue down-regulation of proteins in the *INPPL1*$^{-/-}$ cells. **B.** Cross-referencing of the Ramos gProt data set with the STRING database to search for dysregulated pathways. The significantly altered pathways were extracted. Each point represents a changed abundance of a protein involved in the respective pathway. The further a protein is located on the left side the higher is the abundance in SHIP2-deficient cells. The y-axis indicates the typical protein abundance in the human body.

The proteomic analysis identified a total of 4721 unique proteins with 42 having a significantly altered abundance in *INPPL1*$^{-/-}$ or reconstituted cells. Of these proteins only three corresponded to the list of proteins involved in the tonic BCR signaling and all of them were down regulated: The lysine demethylase 5A (KDM5A), the pleckstrin homology domain containing A2 (PLEKHA2) protein and the helicase with zinc finger (HELZ). In addition, the cross-reference with the STRING database revealed multiple significantly changed pathways, of which two were of particular interest, namely Cell cycle and carbon metabolism. Both would explain lowered proliferation levels and increased sensitivity to apoptosis, which prompted a detailed analysis of both pathways.

Changes in the cell cycle, also called arrests, can severely hamper cell proliferation as the cell is unable to progress from one cell cycle phase to the next. For analysis of the cell cycle staining with the DNA intercalating dye propidium iodide (PI) was performed. Based on the current stage of its cell cycle, the cell contains different amounts of DNA,

meaning twice as much in G_2/M phase than in G_1/G_0 due to the doubling of the genome required for cell division while the S phase is characterised by intermediate DNA levels. Accordingly, the PI signal reflects the DNA content of the cell and thus the current cell cycle phase [269]. To avoid subjectivity, the distribution of the cell cycle phases was analysed using the Watson pragmatic model. This model assumes that the data of the G_1/G_0 and G_2/M peak are normally distributed and the G_1/G_0 is clearly identifiable. The algorithm then objectively fits the data to the model allowing an unbiased discrimination between the phases [229].

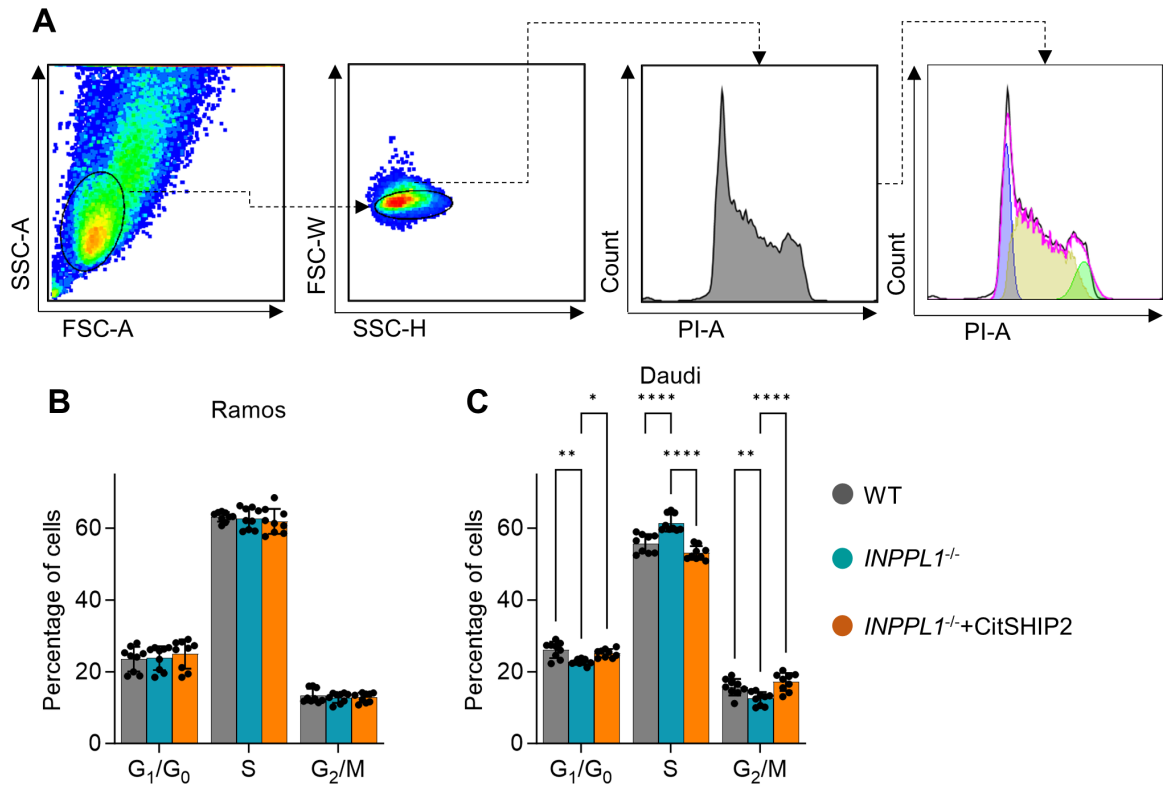

Figure 6.21: **The cell cycle remained unaffected by loss of SHIP2. A.** Gating strategy to evaluate the cell cycle phases in cell cultures. Cell debris was excluded and single cells were analysed for their PI signal followed by determination of the phases utilizing the Watson-Pragmatic model [229]. Quantification of the distribution of the different cell cycle phases of Ramos **B.** and Daudi **C.** WT, SHIP2-deficient and reconstituted cells. $1*10^6$ cells were fixed, permeabilised and stained with 20 µg/ml PI followed by FACS analysis. If not indicated otherwise experiments were performed n≥3. Error bars indicate the standard deviation. Statistics were performed using Two-Way-ANOVA. Significance is indicated by p<0.05 *, p<.0.01 **, p<0.001 ***, p<0.0001 ****.

After exclusion of cell debris the single cells were analysed for their PI signal followed by determination of the cell cycle phases (Figure 6.21A). SHIP2 deficiency did not cause any alterations of the cell cycle in the Ramos cell lines (Figure 6.21B), specifically no changes that could explain the reduced proliferation such as arrests in G_1 or G_2/M phase. In contrast, the absence of SHIP2 caused a mild but significant increase of cells in the S phase, which was recovered by reconstitution with CitSHIP2 (Figure 6.21C).

To assess SHIP2-dependent changes in energy metabolism I first analysed the glucose metabolism. The glycolytic pathways are based on a steady but controlled influx of glucose into the cell. The transport of glucose across the cell membrane is the starting point of glycolysis and the first rate limiting step [270]. A diminished import of glucose would coincide with a decreased energy supply and thus proliferation. The underlying basis of this connection is the Warburg effect, which describes cancer cells as notoriously dependent on the metabolism of vast amounts of glucose in the anaerobic glycolysis to satisfy their energy demand [271]. Therefore, the glucose import was analysed first by measuring the uptake of 2-(N-(7-nitrobenz-2-oxa-1,3-diazol-4-yl)amino)-2-deoxyglucose (2-NBDG), which is a fluorescent 2-deoxyglucose derivative often used to study the glucose import rate [236]. 2-NBDG is imported in a similar manner to normal D-glucose, however, it abrogates the glycolysis after the hexokinase step due to negative feedback inhibition. This leads to accumulation of 2-NBDG in the cell, which, when measured over time, is an indicator for the import rate of glucose [272]. For this assay, the cells were cultured in glucose free medium followed by addition of 2-NBDG for regular time intervals. At each indicated time point, the cells were harvested and counter stained with 7-AAD to exclude dead cells. The CitSHIP2 expressing cells were not included as the citrine strongly overlaps with the 2-NBDG emission spectrum.

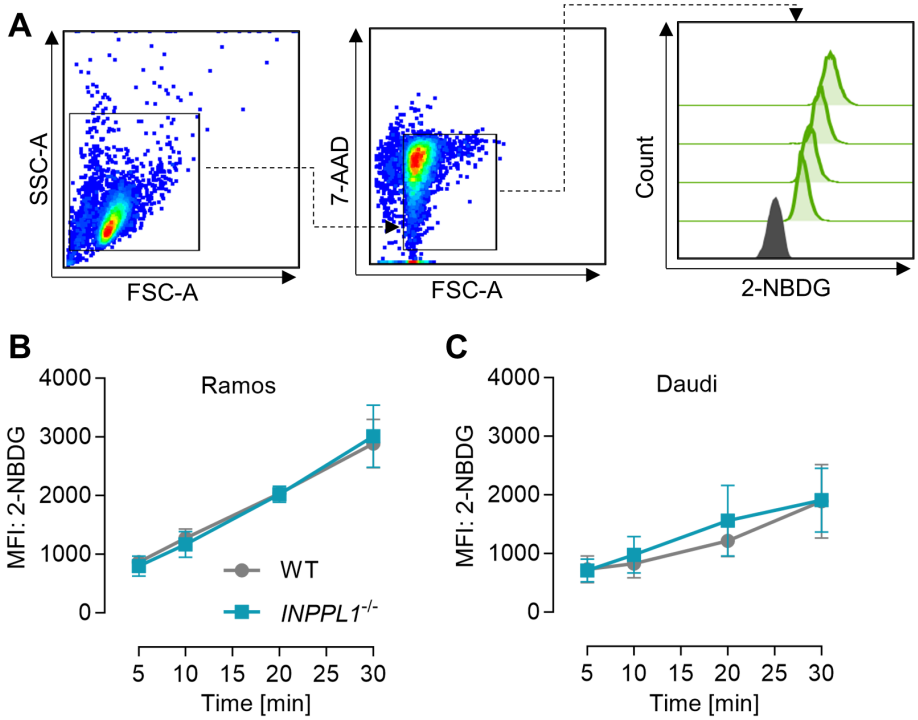

Figure 6.22: **Uptake of 2-NBDG is unaltered in SHIP2-deficient cells. A.** Gating strategy to quantify the uptake of 2-NBDG into cells. Cell debris was excluded and living cells indicated by a negative 7-AAD signal were analysed for their content of fluorescent 2-NBDG. Quantification of the uptake of 2-NBDG in Ramos **B.** and Daudi **C.** WT and SHIP2-deficient cells. The cells were starved in glucose-free medium followed by addition of 100 µM 2-NBDG. At indicated time points, the reaction was stopped with ice-cold 1x PBS and subsequent counter staining with 5 µg/ml 7-AAD followed by quantification of up taken 2-NBDG by FACS. If not indicated otherwise experiments were performed n≥3. Error bars indicate the standard deviation.

The gating strategy of an exemplary glucose uptake rate of Ramos WT cells is shown in Figure 6.22A, and the quantification of the results did not reveal SHIP2-dependent differences in the uptake of 2-NBDG in Ramos and Daudi cells (Figure 6.22B,C).
Complementary to the glucose import, the surface abundance of the glucose importers GLUT1 and GLUT4 was analysed. Both transporters are the predominant glucose transporters found on B cells [273]. To examine their surface expression, cells were stained with antibodies targeting either GLUT1 or GLUT4.

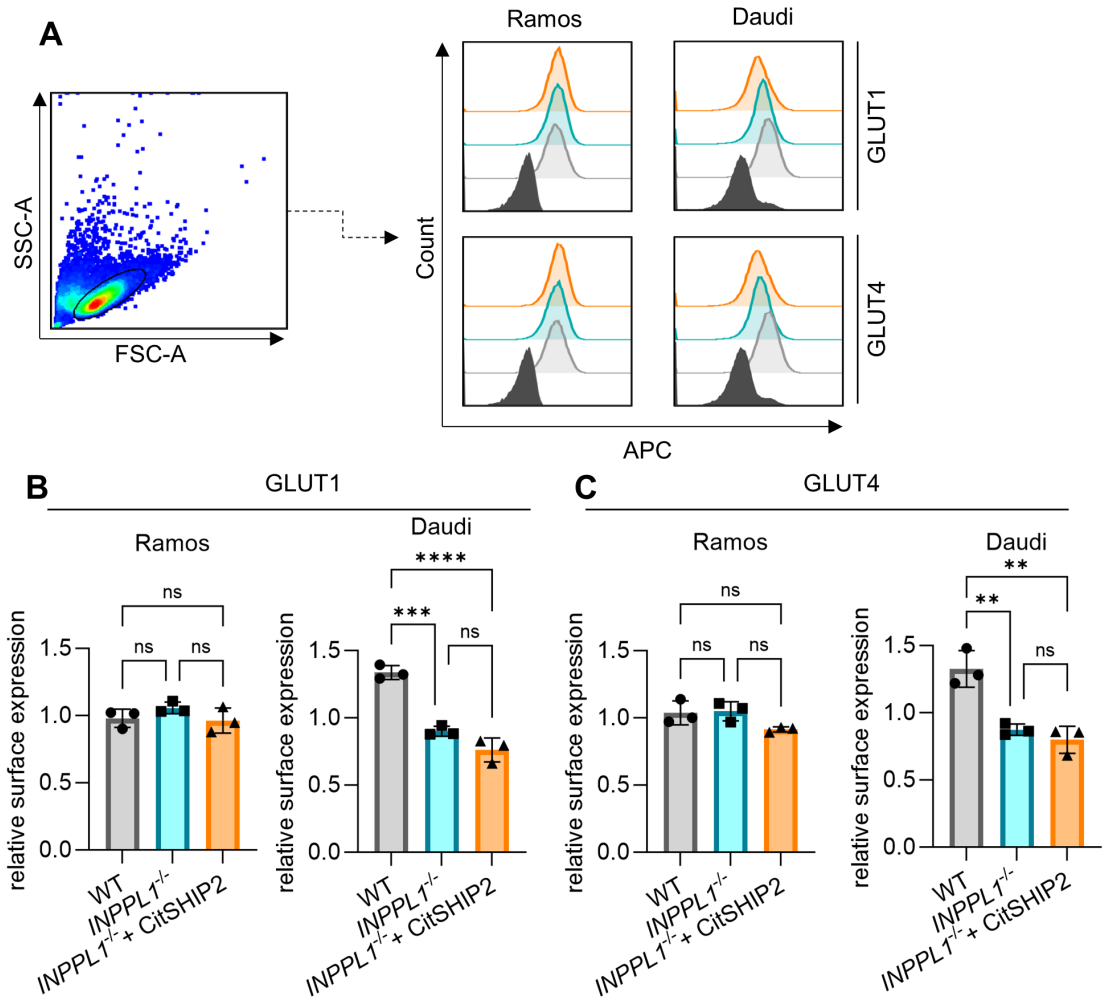

Figure 6.23: **Surface abundance of glucose transporters remained unchanged in absence of SHIP2. A.** Gating strategy for the surface staining of the glucose transporters GLUT1 and GLUT4. Cell debris of living cells was excluded followed by analysis of either GLUT1 or GLUT4 surface signal. Surface abundance of GLUT1 **B.** and GLUT4 **C.** on Ramos and Daudi WT, SHIP2-deficient and reconstituted cells. $1*10^6$ cells were washed, blocked and stained with either α-GLUT1-APC (B) or α-GLUT4-APC (C) followed by FACS analysis. If not indicated otherwise experiments were performed n$\geq$3. Error bars indicate the standard deviation. Statistics were performed using One-Way-ANOVA. Significance is indicated by p<0.05 *, p<.0.01 **, p<0.001 ***, p<0.0001 ****.

This approach revealed that the surface levels of GLUT1 and GLUT4 remained unaltered in the Ramos cell lines (Figure 6.23A-C). In the SHIP2-deficient Daudi cells the surface expression of both transporters was markedly reduced compared to parental cells, but this reduction was not reestablished after reconstitution (Figure 6.23B,C). These results

imply that SHIP2 does not regulate the import of glucose.

An important factor for energy metabolism are mitochondria, which also have important other functions such as regulation of oxidative stress and apoptosis [274]. The mitochondria of different Daudi cell lines were stained with MitoTracker^{TM}-Deep Red followed by imaging flow cytometry for the analysis. The MitoTracker^{TM} dyes are cell permeable and bind specifically thiol-reactive chloromethyl groups found in the mitochondrial membranes [239, 240]. MitoTracker^{TM} uptake correlates with the oxygen consumption and used to simultaneously assess mitochondrial mass and respiration [275, 276].

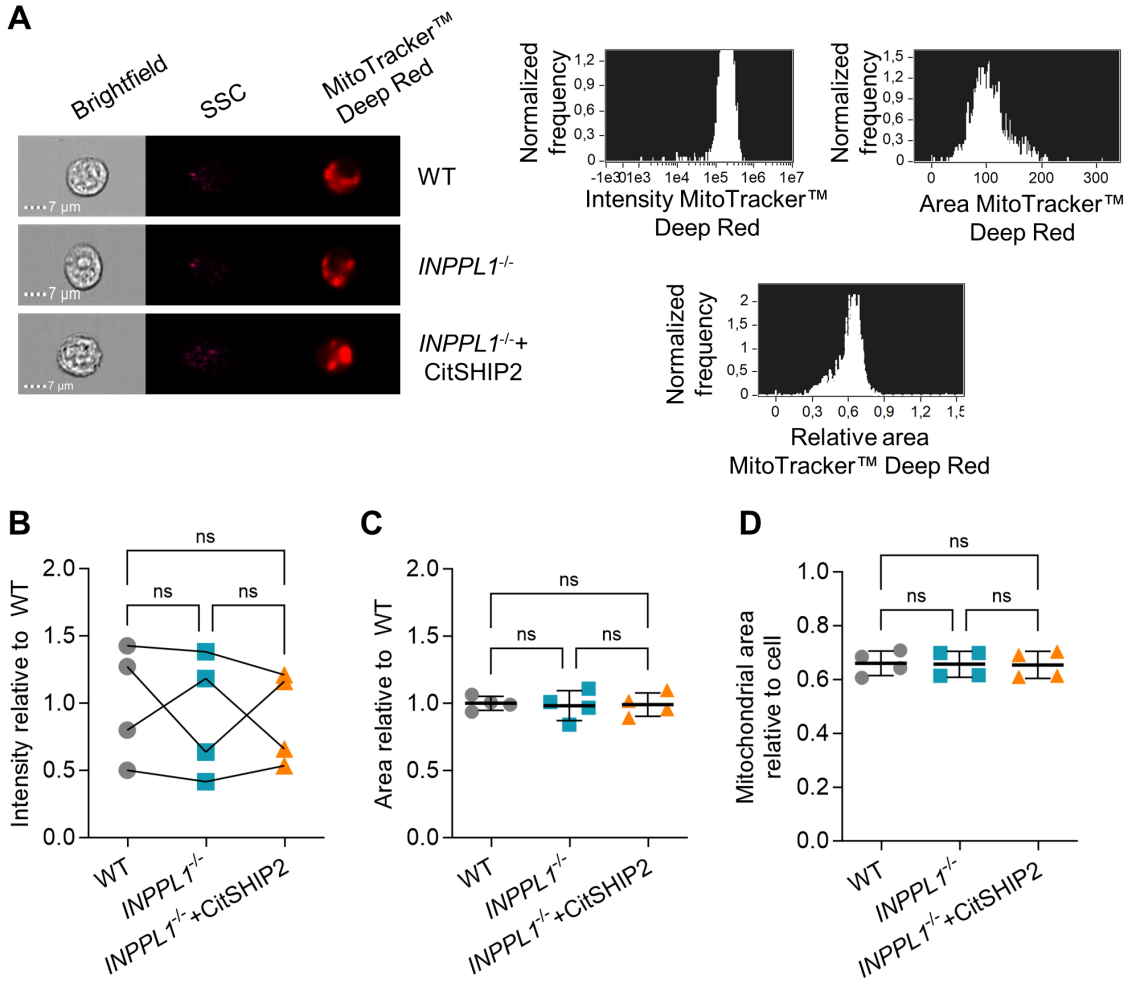

Figure 6.24: **Absence of SHIP2 did not alter the quantity of mitochondria in Daudi cells. A.** Images and gating strategy after exclusion of cell debris followed by quantification of the intensity, mitochondrial area and mitochondrial area relative to the cell Images of the cell lines from the Daudi cell lines include the bright field, the side scatter (SSC) and the MitoTracker™ Deep Red signal. Mitochondrial intensity relative to the WT **B.**, area relative to the WT **C.** and area relative to the cell **D.**. $3*10^6$ cells were washed and stained with 5 nM MitoTracker™ Deep Red followed by image-stream analysis. The intensity and area was normalised to WT cells. If not indicated otherwise experiments were performed n≥3. Error bars indicate the standard deviation. Statistics were performed using One-Way-ANOVA. Significance is indicated by p<0.05 *, p<.0.01 **, p<0.001 ***, p<0.0001 ****.

MitoTracker™ Deep Red signal intensity, signal area and area relative to the cell size were determined (Figure 6.24A). While the mitochondrial intensity was subject to strong variation, no consistent SHIP2-dependent alteration was observed between Daudi cell lines (Figure 6.24B). Accordingly, neither the mitochondrial area nor the area relative to the

cell size was changed by SHIP2 deficiency compared to the WT (Figure 6.24C-D). These data suggest that SHIP2 does not affect mitochondrial function.
To further assess, if energy-providing processes downstream of glucose uptake may be involved in the fitness-supporting function of SHIP2, the Ramos cell lines were treated with the glycolysis inhibitor 2-deoxy glucose (2-DG) and subjected to Annexin-V-APC/7-AAD staining. This inhibitor abrogates the glycolysis in the early stage after the hexokinase [277].

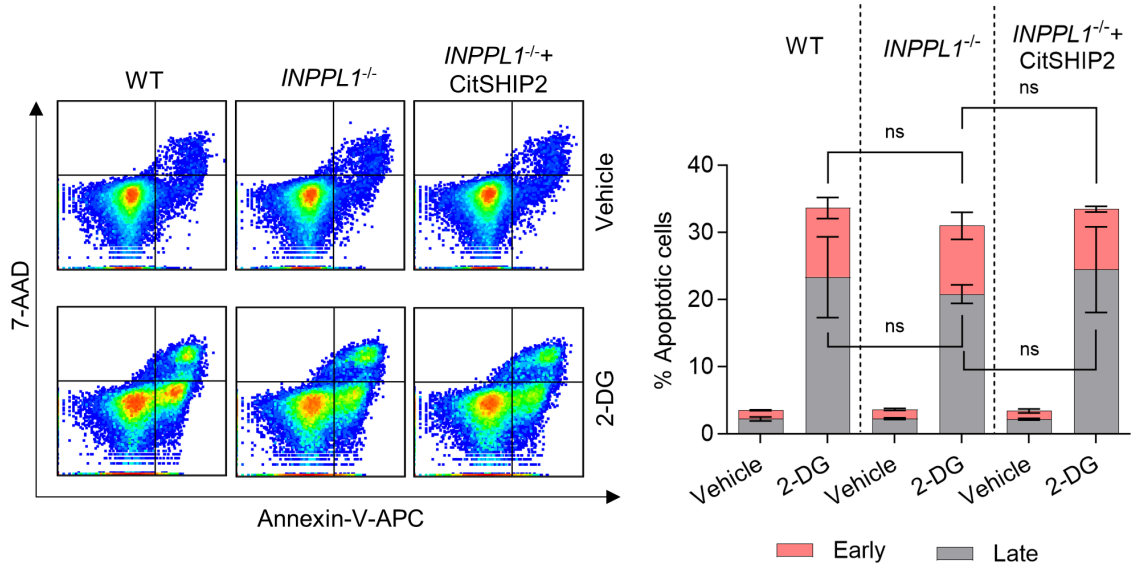

Figure 6.25: **SHIP2 deficiency did not correlate with increased sensitivity to inhibition of glycolysis.** The cells were treated for 24 h with 10 mM 2-DG or ddH_2O as negative control followed by staining with Annexin-V-APC and 7-AAD to distinguish between apoptotic phases. If not indicated otherwise experiments were performed n≥3. Error bars indicate the standard deviation. Statistics were performed using Two-Way-ANOVA. Significance is indicated by p<0.05 *, p<.0.01 **, p<0.001 ***, p<0.0001 ****.

Expectedly, the apoptosis assay showed a strong increase of apoptosis upon treatment in the whole cell panel. Notably, the inhibition of glycolysis resulted in similar apoptosis levels regardless of *INPPL1* expression, which indicates that the supporting SHIP2 function in BL cells involves processes downstream of glucose-6-phosphate production (Figure 6.25.
To validate this suggestion, a SHIP2 dependency of the general ATP production in the different cell lines was assessed. For this purpose, the Seahorse assay was employed [278]. The cellular ATP production rate is the sum of the glycolytic and mitochondrial activity.

The glycolytic activity is measured by the extracellular acidification rate (ECAR) while the mitochondrial activity is determined by the oxygen consumption rate (OCR). The ATP production rate was determined in all three BL cell lines in collaboration with Dr. Dominik Fuhrmann at the University Hospital in Frankfurt. The results of this assay are shown in 6.26.

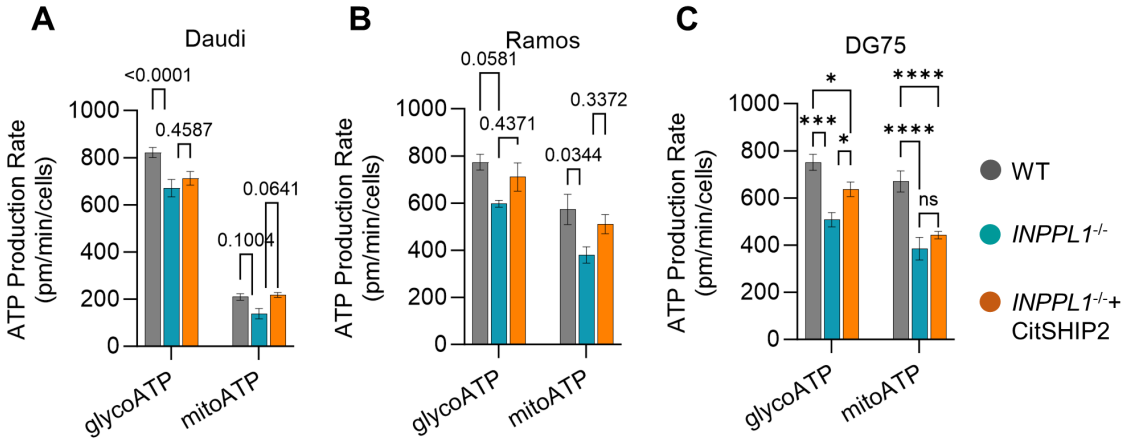

Figure 6.26: **Loss of SHIP2 coincided with a decreased ATP production.** Seahorse assay to determine the glycolytic (glycoATP) and mitochondrial (mitoATP) ATP production rate in Daudi **A.**, Ramos **B.** and DG75 **C.** WT cells compared to SHIP2-deficient and reconstituted cells. If not indicated otherwise experiments were performed n≥3. Error bars indicate the standard deviation. Statistics were performed using Two-Way-ANOVA. Significance is indicated by p<0.05 *, p<.0.01 **, p<0.001 ***, p<0.0001 ****.

SHIP2 deficiency impaired the glycolytic and mitochondrial ATP production compared to parental cells. The reconstitution revealed an improved albeit not complete re-establishment of ATP production compared to the SHIP2-deficient counterparts (Figure 6.26A-C).
To gain information about the processes underlying the more efficient ATP production in the presence of SHIP2, I employed a global approach utilizing mass spectrometry analysis of metabolic compounds in the Ramos and Daudi cell lines. First, the parental cells of both lines were compared with each other.

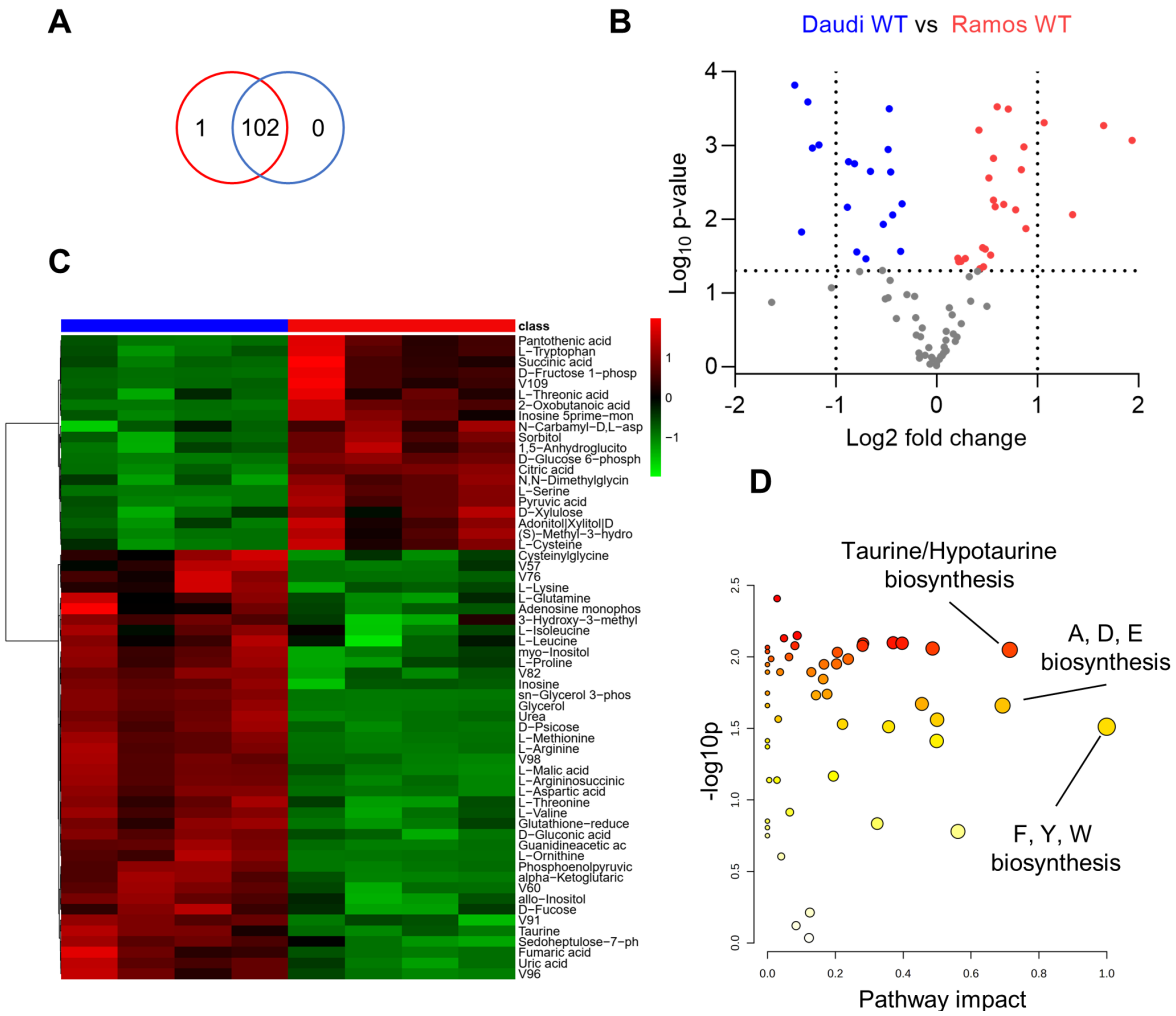

Figure 6.27: **The metabolomes of Daudi and Ramos cells exhibited a pronounced disparity. A.** The Venn diagram shows that 102 of the 103 identified unique metabolites are shared between Daudi (blue) and Ramos (red) cells. **B.** Volcano plot comparing the abundance of metabolites in Daudi and Ramos WT cells. Metabolites with a p-value <0.05 were regarded as significant. **C.** Heat-map and clustering of the previously identified, significantly altered metabolites. **D.** Pathway analysis revealed significant changes in multiple metabolic pathways particularly, the taurine/hypotaurine biosynthesis as well as biosynthesis of alanine (A), aspartate (D), glutamate (E), phenylalanine (F), tyrosine (Y) and tryptophan (W). The metabolome analysis was conducted with n=4. Evaluation of the data was performed with the web-based metassist tool from metaSysX. The heat-map and pathway analysis were generated using MetaboAnalyst 5.0 [279].

A total of 103 unique metabolites were identified, of which 102 were found in both cell lines (Figure 6.27A). Of these metabolites, 41 are significantly different in Ramos compared to Daudi cells (Figure 6.27B). Clustering of these significantly changed metabolites

for Daudi versus Ramos cells in a heat map revealed an increased abundance in all amino acids apart from tryptophan, serine and cysteine. In contrast, glucose-6-phosphate and fructose-1-phosphate, both intermediates of glycolysis, were over represented in the Ramos cells (Figure 6.27C). A pathway analysis of the identified metabolites concurred a different regulation of taurine/hypotaurine- and biosynthesis of multiple amino acids (Figure 6.27D).
The comparison of the metabolomes of Daudi and Ramos cells demonstrated the heterogeneity of Burkitt lymphoma on the metabolic level. In which way the presence of these metabolites is affected by SHIP2 was assessed by comparison of SHIP2-negative versus reconstituted cells.

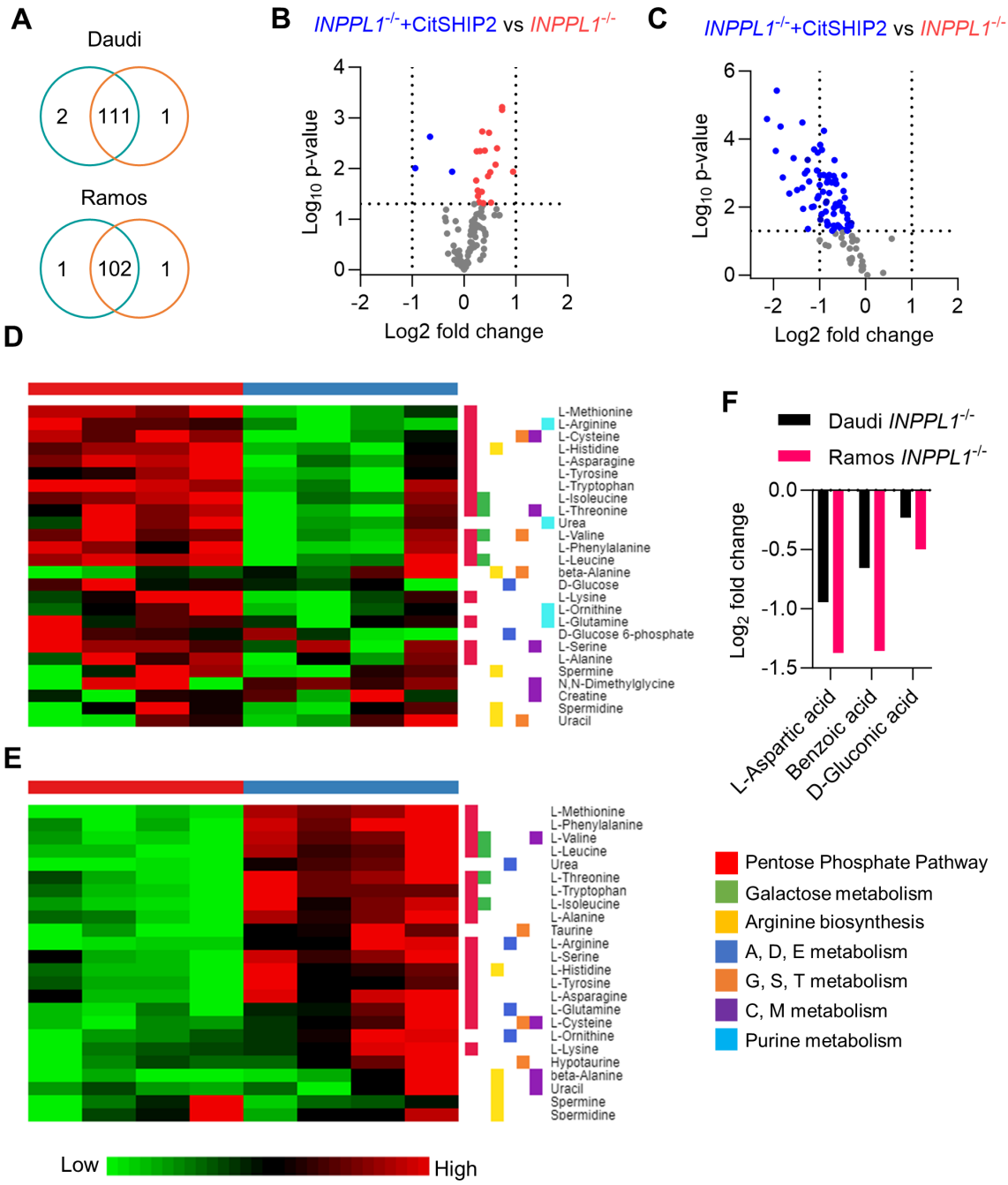

Figure 6.28: **Absence of SHIP2 causes dissimilarities in metabolic profiles of Ramos and Daudi cells. A.** Venn-diagrams show the identified metabolites shared between *INPPL1*$^{-/-}$ cells (turquoise) and SHIP2-negative cells reconstituted with CitSHIP2 (orange). **B.** Volcano plots of the metabolites identified in the Daudi **B.** and Ramos **C.** cells. Metabolites with a p-value <0.05 were regarded as significant. Heat-mapping of the identified metabolites in Daudi **D.** and Ramos **E.** cells with corresponding pathway analysis. Chosen were pathways with a p-value < 0.001.

Figure 6.28: Continued:

The pathway analysis revealed changes in the pentose phosphate pathway, galactose metabolism, arginine biosynthesis, alanine (A), aspartate (D), glutamate (E), glycin (G), serine (S) and threonine (T) metabolism. Additionally, the purine metabolism was affected only in the Daudi cells. **F.** SHIP2 deficiency led to a consistent decrease of L-aspartic acid, benzoic acid and D-gluconic acid in Ramos and Daudi cells. The metabolome analysis was conducted with n=4. Evaluation of the data was performed with the web-based metassist tool from metaSysX. Heatmaps and pathway analyses were generated using MetaboAnalyst 5.0[279].

111 and 102 metabolites were identified in the analysed Daudi and Ramos cells, respectively (Figure 6.28A). Most of the significantly changed metabolites in Daudi cells had an increased abundance in the absence of SHIP2 (Figure 6.28B). In contrast, in Ramos cells almost all metabolites had increased concentrations in the presence of SHIP2 (Figure 6.28C). Heat mapping and pathway analysis of the metabolites found in both cell lines revealed a SHIP2-dependent regulation of multiple metabolic pathways, of which those with a p-value < 0.001 were chosen for further analysis. In Daudi, the absence of SHIP2 coincided with enrichment of metabolites involved in the pentose phosphate pathway, galactose metabolism, biosynthesis and metabolism of various amino acids as well as purine metabolism (Figure 6.28D). The same pathways were affected in Ramos with the major differences that most of the metabolites were enriched in the reconstituted cells and no difference in the purine metabolism could be observed (Figure 6.28E). Comparison of SHIP2-deficient Daudi and Ramos cells with their reconstituted counterparts revealed three distinct amino acids, which were found in decreased abundance in both cell lines: L-aspartic acid, benzoic acid and D-gluconic acid.
While the metabolomic approach revealed certain SHIP2-dependent alterations, most of the observed differences were cell line specific. Hence, hampering a clear conclusion with regard to the role of SHIP2 in energy metabolism.

6.8 The SHIP2 product PI(3,4)P_2 promotes BL fitness

The enzymatic function of SHIP2 is to dephosphorylate the PI3K product PI(3,4,5)P_3 to PI(3,4)P_2 [46]. While the PI3K is the only producer of PI(3,4,5)P_3, PI(3,4)P_2 can be generated by the two SHIP proteins, SHIP1 and SHIP2. Therefore, I aimed at analysing the

impact of SHIP2 on PI(3,4)P_2 levels at the intracellular leaflet of the plasma membrane. For this purpose, a biological sensor was utilized that is composed of PI(3,4)P_2-specific tandem PH domains originating from the pleckstrin homology domain containing protein 1 (PLEKHA1 also known as TAPP1), conjugated with GFP [215](Figure 6.29A). The expression of the GFP-2xTAPP1-PH construct in parental and SHIP2-deficient Ramos cells, respectively, revealed a band close to an apparent molecular weight of 100 kDa, which corresponds to the computed molecular weight of 98.78 kDa. Moreover, the membrane did not exhibit free GFP, which could have indicated an instability of the construct and premature degradation (Figure 6.29B). To quantify the levels of membrane recruited biosensor, which correlates with the amount of PI(3,4)P_2 at the plasma membrane, cells were subjected to imaging flow cytometry.

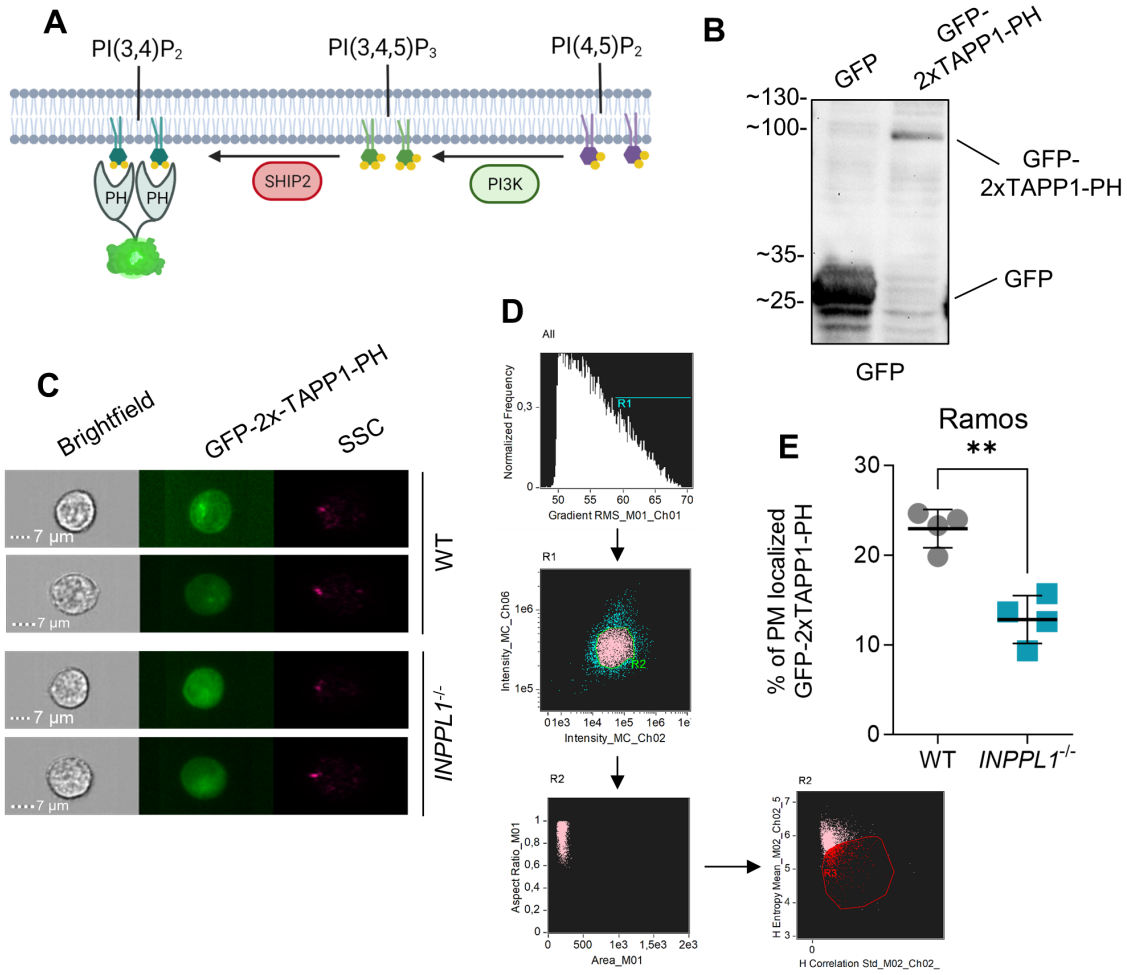

Figure 6.29: **Loss of SHIP2 concurs with decreased abundance of PI(3,4)P_2 on the intracellular leaflet of the plasma membrane. A.** Cartoon depicting the selectivity of the GFP-2xTAPP1-PH construct to exclusively bind to PI(3,4)P_2 generated by SHIP2. **B.** Western Blot analysis revealed a GFP specific band at ~100 kDa. Ramos cells, which constitutively expressed either GFP or GFP-2xTAPP1-PH were subjected to lysis and Western Blot analysis. The membrane was probed with α-GFP. The apparent molecular weight is indicated as kDa. **C.** Image-stream analysis showing the intracellular localization of GFP-2xTAPP1-PH in Ramos WT and SHIP2-deficient cells. **D.** These cells were analysed according to the depicted gating strategy. After exclusion of cell debris and cell aggregates, the cells in optimal focus were subjected to quantification of the signal at the plasma membrane using homogeneity and entropy parameters. **E.** Percentage of membrane localized GFP-2xTAPP1-PH in Ramos WT and SHIP2-deficient cells. Data shown consists of n=4 experiments with up to $1*10^5$ analysed cells. Error bars indicate the standard deviation and the statistics were performed using a paired t-test with significance indicated by $p<0.01$ **.

This analysis revealed a clear GFP signal in the transfected cells, which was not restricted

to the plasma membrane, but present to a large extent in the cytoplasm (Figure 6.29C). This could be caused by the low amounts of PI(3,4)P_2 in the plasma membrane which may result in unbound biosensor. To quantify the membrane-bound levels of GFP-2xTAPP1-PH the analysed cells, a specific gating was established. After exclusion of cell debris and aggregates, the cells in an optimal focus were gated on GFP-positive and side scatter-low cells. To assess the texture of the signal, the entropy and correlation parameters of the IDEAS software were utilized. A homogenous signal would reveal a high level of entropy, whereas a more specific structured localization emanating from plasma membrane-located biosensor correlates with a decrease in entropy. The correlation parameter increases with the signal´s homogeneity and is lower for signals with significant texture. Hence, for this analysis entropy^{low} and correlation^{low} images were considered to show cells with recruited biosensor (Figure 6.29D). As depicted in Figure 6.29E, this gate included less SHIP2-deficient cells compared to parental Ramos cells, thereby indicating compromised production of PI(3,4)P_2 in the absence of SHIP2.

During the generation of the biosensor-expressing cells, it appeared that the percentage of GFP-2xTAPP1-PH-positive cells constantly declined in a matter of days. This decline suggested a toxic property of the biosensor construct, which could be caused by shielding of PI(3,4)P_2-based binding motifs. To specifically monitor, if the constitutive expression of GFP-2xTAPP1-PH is toxic in BL cell lines, Ramos, DG75 and Raji cells were electroporated with constructs encoding either the biosensor construct or GFP as control followed by observation of the amount of GFP-positive cells in the following four days.

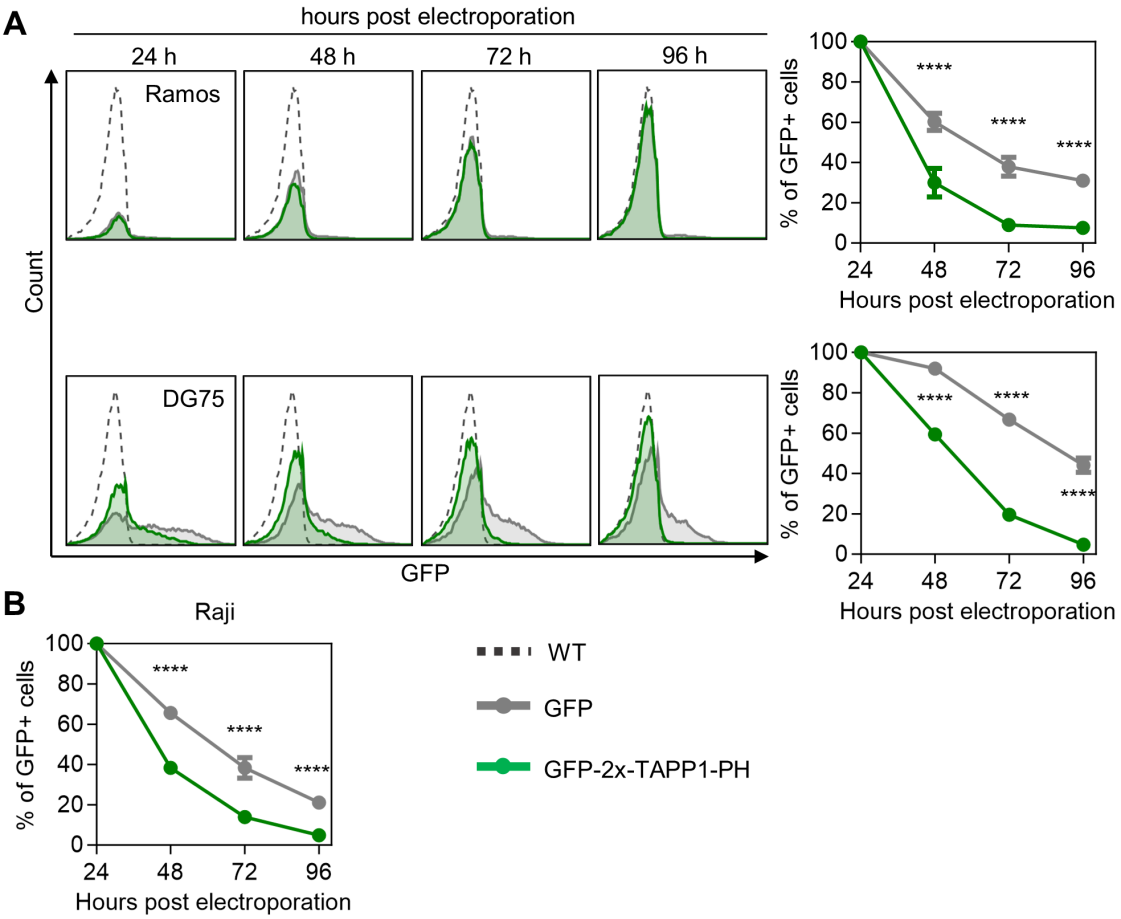

Figure 6.30: **Obstruction of PI(3,4)P_2 severely diminished the survival of BL cells. A.** Histograms depicting the GFP levels at indicated time points after electroporation of either GFP (grey) or GFP-2xTAPP1-PH (green) into Ramos and DG75 WT cells. Non-electroporated WT cells served as negative control (dashed line). The percentage of GFP+ cells of three independent replicates are shown on the right hand side **B.** Same experimental set up in the surface IgM-negative Raji WT cells. The cells were electroporated with a PiggyBac construct enabling constitutive expression of either GFP-2xTAPP1-PH or GFP-only. The transfected cells were then analysed for their GFP content at indicated time points followed by normalisation to the baseline at 24 h. No selection pressure was applied to the cultures. If not indicated otherwise experiments were performed n≥3. Error bars indicate the standard deviation. Statistics were performed using Two-Way-ANOVA. Significance is indicated by p<0.05 *, p<.0.01 **, p<0.001 ***, p<0.0001 ****.

This approach revealed that the GFP-positive proportion of biosensor-expressing cells declined markedly faster compared to the GFP-only control. This may reflect a negative impact of GFP-2xTAPP1-PH expression on BL cell survival, and hence these cells are overgrown by biosensor-negative cells (Figure 6.30A). Interestingly, the SHIP2-insensitive

and surface IgM-negative cell line Raji showed a similar effect suggesting that PI(3,4)P_2 has survival-related functions in BL independently of BCR activity (Figure 6.30B).
To exclude potential side effects caused by the electroporation process and constitutive expression, it was decided to validate these findings by generation of cell lines with a doxycycline-inducible GFP-2xTAPP1-PH or GFP-only expression. Therefore, the constructs were generated based on a PiggyBac backbone and containing a doxycycline-responsive element, which allowed for a controlled expression of the gene of interest. After generation of stable cell lines, the expression of the constructs was induced by addition of doxycycline followed by monitoring of GFP-positive cells as described in the prior experiment. In addition to the parental cells, their SHIP2-negative counterparts were also included to evaluate, if the absence of SHIP2 had an effect on the impact of GFP-2xTAPP1-PH expression.

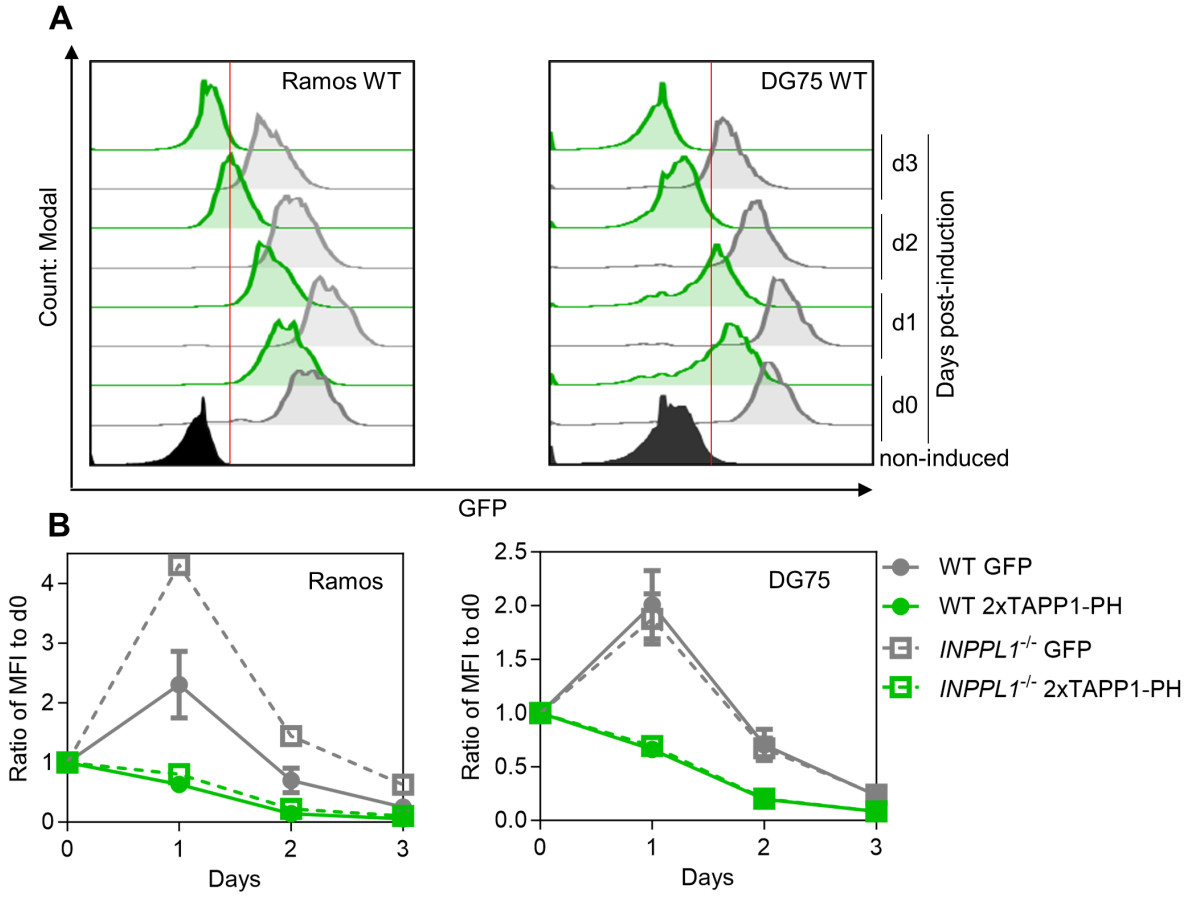

Figure 6.31: **Occluding PI(3,4)P_2 caused rapid loss of fitness in BL cell lines independent of SHIP2 activity. A.** Histograms showing the decrease of the GFP levels in Ramos and DG75 WT cells after induction of GFP-2xTAPP1-PH or GFP-only expression. **B.** Quantification of the median fluorescence intensity of the GFP signal in the Ramos and DG75 WT and SHIP2-deficient cells expressing either GFP or GFP-2xTAPP1-PH. Expression of GFP-2xTAPP1-PH and the GFP-only control was induced by addition of 250 ng/ml doxycycline for 4 h. Afterwards, the cells were washed vigorously to remove residual doxycycline and the GFP levels were measured at indicated time points to analyse the fate of GFP-positive cells. If not indicated otherwise experiments were performed n≥3. Error bars indicate the standard deviation. Statistics were performed using Two-Way-ANOVA.

In all generated cell lines the proportion of biosensor-positive cells decreased markedly faster than that of GFP-positive control cells. (Figure 6.31A,B). Notably, no additive effects of SHIP2 deficiency on the sensitivity to GFP-2xTAPP1-PH expression were observed indicating that shielding of PI(3,4)P_2 overrules the effects caused by absence of SHIP2 (Figure 6.31B). Collectively, these findings imply that SHIP2 promotes BL fitness via production of PI(3,4)P_2.

To exclude that the findings described above are not reflecting different stabilities of GFP and PH-GFP fusion proteins, I generated a biosensor-encoding construct with a different phosphoinositide specificity. The most abundant phosphoinositide at the inner leaflet of the plasma membrane is PI(4,5)P_2. I utilized the PI(4,5)P_2-selective properties of the PLCδ PH domain and expressed this domain with a N-terminally fused cerulean[280, 281]. After generation of a Ramos cell line with doxycycline-inducible expression of Cer Cer-PLCδ-PH, image stream analysis of doxycycline-induced cells was performed showing a cerulean signal, which is enriched at the plasma membrane (Figure 6.32A). The ensuing Western Blot analysis showed a GFP-specific band at $\tilde{4}5$ kDa corresponding to the calculated molecular weight of the construct, which, combined with the image stream analysis, demonstrated proper function of the biosensor (Figure 6.32B). A competitive growth assay was employed to compare the effects of GFP-2xTAPP1-PH to those of Cer Cer-PLCδ-PH expression. For this purpose, both cell lines were mixed in equal parts followed by induction of the constructs with doxycycline. The respective percentages of GFP- and cerulean-positive cells were determined via FACS in the following days followed by normalisation to the starting percentage.

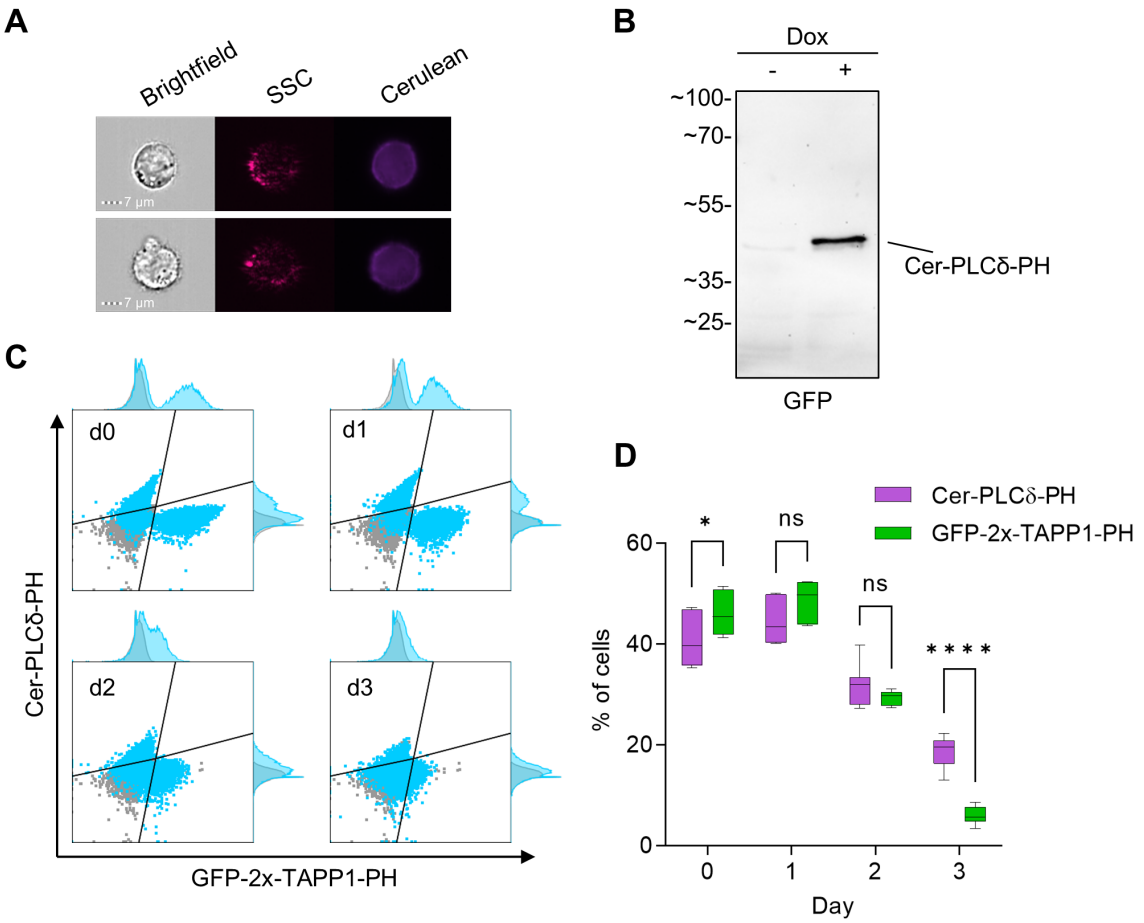

Figure 6.32: **PI(3,4)P_2 is more important for the fitness of Ramos cells than PI(4,5)P_2. A.** Image-stream analysis showing the localization of the Cer-PLCδ-PH construct in Ramos cells. The cells were induced with 250 ng/ml doxycycline 24 h prior to measurement. **B.** Western Blot analysis of Ramos cells expressing the Cer-PLCδ-PH construct revealing a band at 45 kDa. The cells were treated similar to **A.** followed by generation of cleared cellular lysates and Western Blotting. The membrane was probed with α-GFP. The apparent molecular weight is indicated as kDa. **C.** The scatter plots show a competitive growth assay of an equally mixed population consisting of cells expressing either GFP-2xTAPP1-PH or Cer-PLCδ-PH. **D.** Quantification of the GFP-2xTAPP1-PH or Cer-PLCδ-PH-positive populations. Both cell lines were mixed in equal parts followed by induction of both constructs through addition of 250 ng/ml doxycycline. After 4 h, the cells were washed vigorously to remove residual doxycycline and the GFP and cerulean levels were measured at indicated time points to analyse the fate of the respective positive cells. If not indicated otherwise experiments were performed n$\geq$3. Error bars indicate the standard deviation. Statistics were performed using Two-Way-ANOVA. Significance is indicated by p<0.05 *, p<.0.01 **, p<0.001 ***, p<0.0001 ****.

This approach revealed that obstruction of both phosphoinositides has toxic implications for the cells. However, because the percentage of GFP-positive cells declined markedly

faster than their cerulean-positive counterparts, shielding of $PI(3,4)P_2$ appears to be more toxic in this assay.

Since the previous experiments suggested that $PI(3,4)P_2$ is critical for BL fitness, it was tried to validate this finding by enzymatic targeting of the $PI(3,4)P_2$ pool at the plasma membrane. $PI(3,4)P_2$ is targeted with a high selectivity by two 4-inositol phosphatases, INPP4A and INPP4B, both generating PI(3)P [282, 283]. These phosphatases are widely distributed throughout the cell with INPP4A being present at endosomes and at the plasma membrane after growth factor stimulation [284, 285]. The selective phosphatase activity of INPP4A was exploited to artificially drain the $PI(3,4)P_2$ pool at the plasma membrane of BL cells. For this purpose, the INPP4A protein was N-terminally fused with the myristoylation sequence of LYN, which enables the localization to the plasma membrane and a cerulean to track the location of the construct in the cells [281]. The resulting Myr-Cer-INPP4A construct was expressed in Ramos cells in a doxycycline-inducible manner.

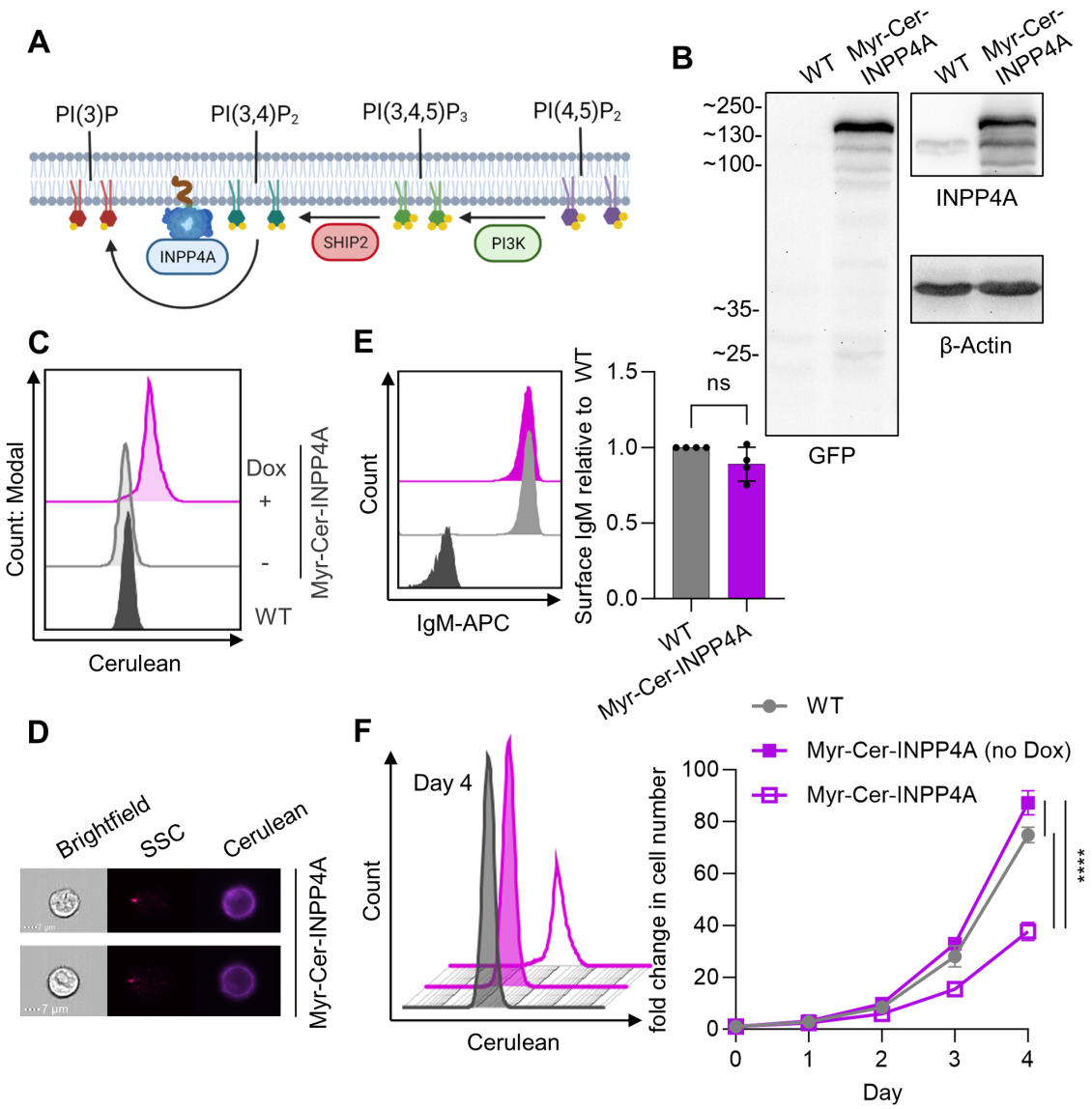

Figure 6.33: **Enzymatic reduction of PI(3,4)P_2 perturbed the fitness of Ramos cells comparable to obstruction. A.** Cartoon showing the intended function of the Myr-Cer-INPP4A construct. The myristoylation facilitates the anchoring of the cerulean-INPP4A construct to the intracellular leaflet of the plasma membrane were it dephosphorylates PI(3,4)P_2 to PI(3)P. **B.** Western Blot analysis showed a larger, INPP4A and GFP specific band at ĩ40 kDa in the Myr-Cer-INPP4A expressing cells compared to the WT. The cells were prepared as for the FACS analysis followed by generation of cleared cellular lysates and Western Blotting. The resulting membranes were probed with α-GFP, α-INPP4A and α-β-Actin as loading control. The apparent molecular weight is indicated as kDa. **C.** FACS analysis confirmed a cerulean signal after induction of the cells with 250 ng/ml doxycycline 24 h prior to measurement. **D.** Image-stream analysis giving the intracellular localization of the Myr-Cer-INPP4A construct after induction of the expression.

Figure 6.33: Continued:

E. The surface IgM levels of Myr-Cer-INPP4A expressing cells were determined by FACS analysis. The cells were induced with 250 ng/ml doxycycline 48 h prior to staining with α-hIgM-APC followed by FACS analysis. Obtained MFIs were normalised to the cerulean-negative WT control. **F.** Cell counting assay to assess the proliferation of Ramos WT cells compared to Ramos cells carrying Myr-Cer-INPP4A with or without induction by doxycycline. The histogram shows the cerulean signal and cell count after 4 days. The cells were induced at d0 with 250 ng/ml doxycycline followed by counting the living cells at the indicated time points. The cell counts of each day were normalised to the starting count at d0. If not indicated otherwise experiments were performed n$\geq$3. Error bars indicate the standard deviation. Statistics were performed using Two-Way-ANOVA. Significance is indicated by p<0.05 *, p<.0.01 **, p<0.001 ***, p<0.0001 ****.

The intended mode of action of the Myr-Cer-INPP4A fusion protein at the plasma membrane is depicted in (Figure 6.33A). Western Blot analysis of lysates from doxycycline-induced cells revealed a GFP band at 140 kDa that corresponded to the expected molecular weight (Figure 6.33B). Imaging flow cytometry confirmed a cerulean signal, located on the outer rim of the cells indicating proper localization of the fusion protein (Figure 6.33C,D). Furthermore, the expression of Myr-Cer-INPP4A had no significant impact on the surface IgM abundance (Figure 6.33E). Notably, the presence of Myr-Cer-INPP4A at the plasma membrane severely diminished the proliferation compared to parental cells (Figure 6.33F). Hence, this approach revealed further evidence that PI(3,4)P_2 supports the survival of BL cells.

6.9 Down-regulation of SHIP1 mirrors SHIP2 deficiency

Due to their equal enzymatic function, SHIP1 and SHIP2 both may contribute to the PI(3,4)P_2 pool and hence, contribute to the fitness of BL cells. To test this hypothesis, the published effects of targeting *INPP5D* gene expression in non-Hodgkin lymphoma via RNAi were explored using bioinformatics. Analysis of the Cancer Dependency Map revealed that down-regulation of *INPP5D* exhibited a negative effect on the proliferation of many, but not all tested non-Hodgkin lymphoma cell lines (Figure 6.34A). Notably, the relative gene effect of *INPP5D* appeared to be lower than for *INPPL1* suggesting that the loss of SHIP2 is more difficult to compensate for these cell lines (Figure 6.34A).

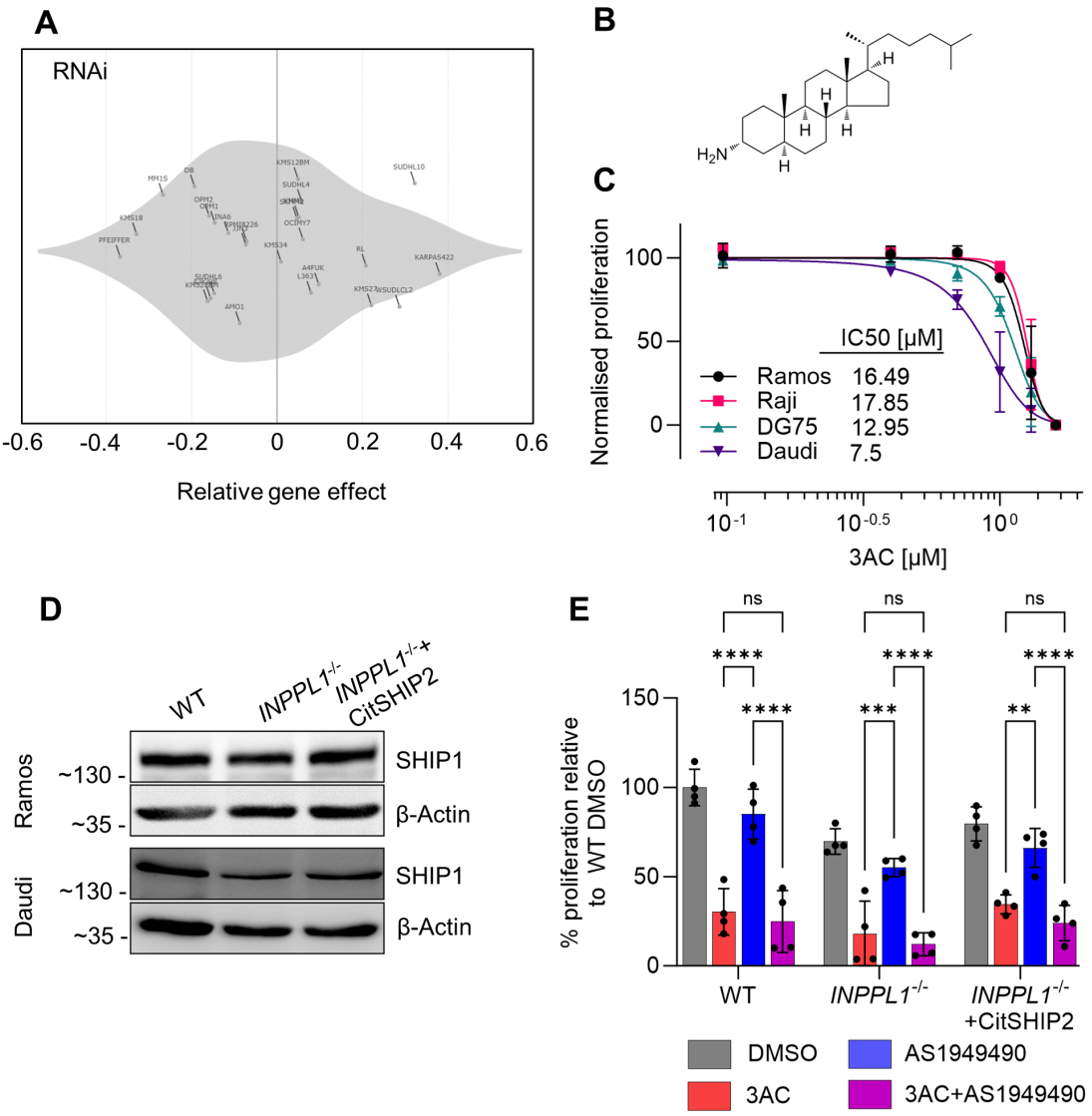

Figure 6.34: **Inhibition of SHIP1 lowered the proliferation of BL cell lines. A.** RNAi targeting studies of *INPP5D* showing the importance of *INPP5D* in nHL cell lines. The data was extracted from the database of the Cancer Dependency Map [207]. The RNAi databases consists of the Achilles, DRIVE, Marcotte and DEMETER2 screens. The gene effect describes the impact of the gene targeting on the growth of the respective cell line. A gene with a gene effect <-1 is considered as essential. **B.** Chemical structure of the small molecular inhibitor 3-α-aminocholestane (3AC) that selectively inhibits SHIP1. **C.** XTT assay based dose escalation of the SHIP1 inhibitor 3AC in multiple BL cell lines. The cells were treated with increasing concentrations of 3AC or DMSO as control 24 h prior to readout. The relative proliferation was established by normalisation to the DMSO control. The dose-response curve was calculated using a non-linear regression model for normalised data. IC50 values were calculated using GraphPad Prism. **D.** Western Blot analysis showing the SHIP1 protein levels in the SHIP2-deficient Ramos and Daudi cells.

Figure 6.34: Continued:

The membranes were probed with α-SHIP1 and α-β-Actin as loading control. The apparent molecular weight is indicated as kDa. **E.** Combination of 3AC and AS1949490 treatment in Ramos WT, SHIP2-deficient and reconstituted cells after XTT assay. The cells were treated with either 10 µM 3AC, 5 µM AS1949490, a combination of both or DMSO as control for 24 h followed by assessment of the proliferation through XTT assay. Proliferation was normalised to the DMSO control of the WT cells. If not indicated otherwise experiments were performed n$\geq$3. Error bars indicate the standard deviation. Statistics were performed using Two-Way-ANOVA. Significance is indicated by p<0.05 *, p<.0.01 **, p<0.001 ***, p<0.0001 ****.

In line with these findings, treatment of multiple BL cell lines with increasing concentrations of the small molecule inhibitor of SHIP1, 3-α-aminocholestane (3AC) [286], on the proliferation revealed sensitivity to the inhibition of SHIP1, especially for Daudi cells as indicated by their low IC50 value (Figure 6.34B,C). The SHIP1 protein levels remained stable in absence of SHIP2 in Ramos and Daudi cells, which indicated that the cells did not upregulate *INPP5D* expression to compensate for the loss of SHIP2 activity (Figure 6.34D). While 3AC treatment more efficiently compromised the proliferation of Ramos cells than SHIP2 inhibition with AS1949490, SHIP2 deficiency did not appear to result in a significantly higher sensitivity to 3AC treatment. Combined treatment with both SHIP inhibitors revealed an additive effect when compared to SHIP2 inhibition only (Figure 6.34E). However, the combination of inhibitors does not augment the 3AC effect, indicating either greater importance of SHIP1 or a lower selectivity of 3AC, also inhibiting SHIP2. Hence, the potential redundancy between SHIP1 and SHIP2 had to be addressed with an experimental setup with a higher degree of selectivity.
Consequently, the expression of *INPP5D* was down-regulated using the doxycycline-inducible shRNA system already utilized for transient targeting of *INPPL1*. Beyond single targeting of SHIP1, the system also enabled studying the effect of SHIP1 reduction in *INPPL1*$^{-/-}$ cells. The proliferation was assessed after induction of shRNA in parental as well as *INPPL1*$^{-/-}$ Daudi and Ramos cells.

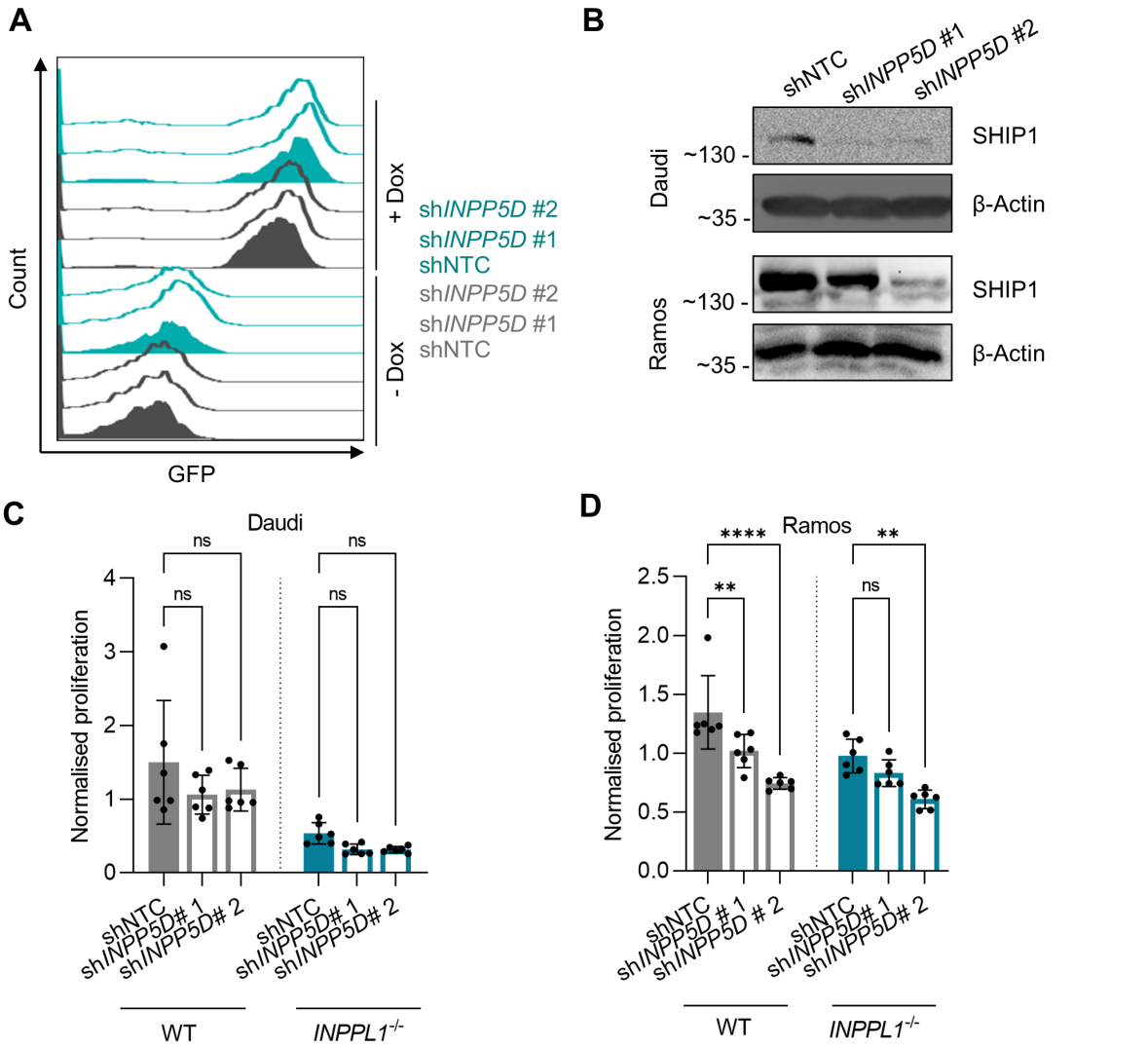

Figure 6.35: **Targeting SHIP1 by RNAi reduced the proliferation of Ramos and Daudi cells. A.** Example of Ramos WT (grey) and *INPPL1*$^{-/-}$ (turquoise) cells expressing either shRNA targeting the SHIP1 coding gene (sh*INPP5D*#1-2 or a non-targeting control (shNTC) under control of a doxycycline inducible promoter, which simultaneously produces GFP. The cells were treated 24 h prior with 250 ng/ml doxycycline. **B.** Western Blot analysis showed a reduction of SHIP1 protein levels by the induced expression of shRNA targeting *INPP5D*. The cells were treated with 250 ng/ml doxycycline for 4 days followed by generation of cleared cellular lysates and Western Blotting. The membranes were probed with α-SHIP1 and α-β-Actin as loading control. The apparent molecular weight is indicated as kDa. The proliferation of Daudi **C.** and Ramos **D.** WT and SHIP2-deficient cells expressing either sh*INPP5D* or shNTC was assessed by XTT assay. The cells were treated with 250 ng/ml doxycycline for 5 days to ensure reduction of SHIP1 protein levels followed by determination of the proliferation by XTT assay. The proliferation was normalised to the respective non-induced cells. If not indicated otherwise experiments were performed n$\geq$3.

Figure 6.35: Continued:

Error bars indicate the standard deviation. Statistics were performed using One-Way-ANOVA. Significance is indicated by p<0.05 *, p<.0.01 **, p<0.001 ***, p<0.0001 ****.

Flow cytometric analysis revealed a strong GFP expression indicating proper expression of the construct (Figure 6.35A). The Western Blot analysis of the same cells after 4 days of induction showed reduction of SHIP1 protein levels, which was more efficient in Daudi than in Ramos cells (Figure 6.35B). These reduced SHIP1 amounts had only minor impact on the proliferation of Daudi WT and *INPPL1*$^{-/-}$ cells as revealed by a XTT assay, whereas the proliferation of the Ramos cells was markedly compromised (Figure 6.35C,D). Notably, *INPP5D*#1 had a comparably lower effect on proliferation, which could be based on the inferior efficiency of protein depletion thereby suggesting a dose-dependent effect of depleting SHIP1 (figure 6.35B,D). Nevertheless, shRNA-mediated abrogation of SHIP1 appeared to further decrease the proliferation of *INPPL1*$^{-/-}$ cells, which suggests an additive effect of both 5-inositol phosphatases.
Because the XTT assay was brought to its methodical limits due to the long incubation times required for the efficient depletion of SHIP1 protein levels, the proportion of GFP-positive and therefore shRNA producing cells was directly determined by flow cytometry in regular time intervals after induction. This approach had multiple advantages: First, the cells could easily be cultured over longer time periods and directly analysed from the culture, and second, this assay only considers shRNA producing cells. Thus, I sought to confirm the previous proliferation assay using this "GFP tracking" approach.

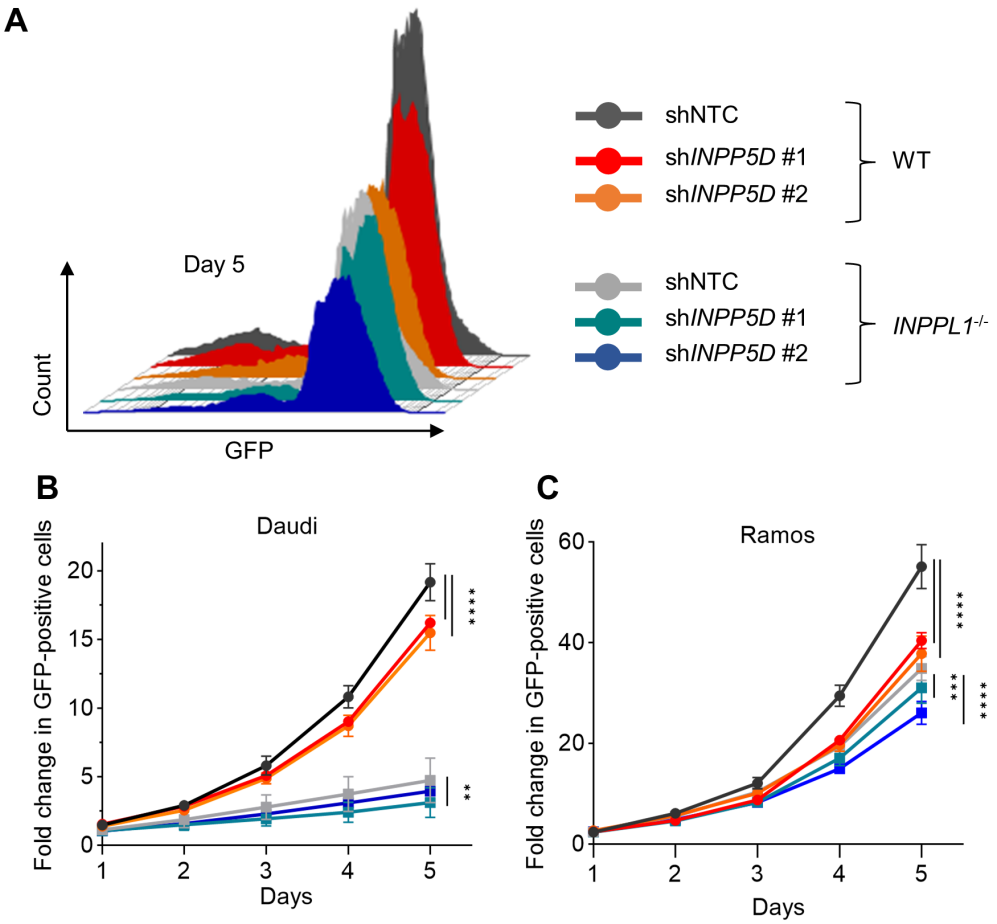

Figure 6.36: **SHIP1 and SHIP2 contribute to the fitness of BL cells. A.** Staggered histogram showing the distribution of GFP-positive, and therefore shRNA-positive, Ramos cells after 5 days of doxycycline treatment. The GFP-positive Daudi **B.** and Ramos **C.** cells were tracked over time to monitor the proliferation upon induction of the shRNA. The cells were seeded with equal cell numbers and induced with 250 ng/ml doxycycline followed by counting the GFP-positive cells at indicated time points. The fold-change represents the increase of GFP-positive cells compared to d0. If not indicated otherwise experiments were performed n≥3. Error bars indicate the standard deviation. Statistics were performed using Two-Way-ANOVA. Significance is indicated by p<0.05 *, p<.0.01 **, p<0.001 ***, p<0.0001 ****.

The induction of sh*INPP5D*s led to a decreased count of GFP-positive cells in the Ramos WT and *INPPL1*$^{-/-}$ cells compared to the control as visualized by the smaller peaks. Simultaneously, abrogation of SHIP1 also resulted in the formation of secondary peaks of increased size compared to the control, which suggested an increase of apoptosis (Figure 6.36A). The quantification of GFP-positive cells over time revealed a significantly lower fold change (normalised to d0) caused by reduction of SHIP1 compared to controls in the

Daudi and Ramos WT cells. In the SHIP2-deficient backgrounds, this effect was mild in Daudi cells, which appeared to be extensively affected by the loss of SHIP2, but pronounced in Ramos cells (Figure 6.36B,C).
In summary, these results indicate that the anti-proliferating effect in absence of SHIP2 is aggravated by down-regulation of the other PI(3,4)P_2 producing phosphatase, which further supports the crucial role of this phosphatidyl inositol for the fitness of Burkitt lymphoma.

To test, that the observed effect is not caused by affected survival signaling the p-AKT(S473) levels in the SHIP1 depleted cells were measured using flow cytometry. The obtained results are depicted in figure 6.37.

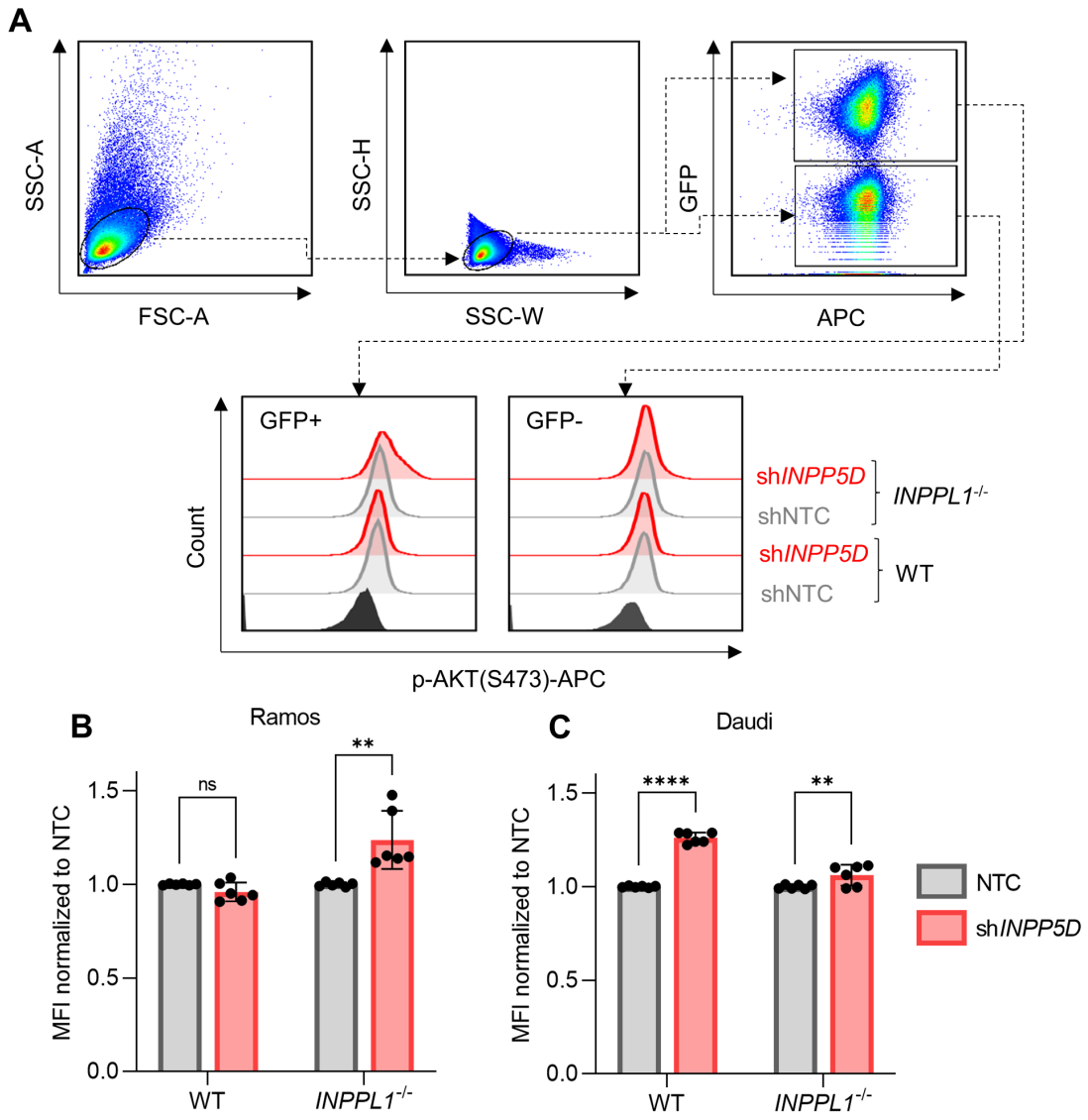

Figure 6.37: **Reduction of SHIP1 slightly elevated phospho-AKT levels. A.** Exemplary gating strategy of Ramos cells used to quantify the levels of phosphorylated AKT(S473) after induction of shRNA targeting *INPP5D*. Cell debris was excluded and single cells were categorized according to their GFP content followed by quantification of the p-AKT(S473)-APC signal. Quantification of the normalised median fluorescence intensity (MFI) of the p-AKT(S473)-APC signal in Ramos **B.** and Daudi **C.** cell lines. The cells were treated for 5 days with 250 ng/ml doxycycline prior to fixation and intracellular staining using α-phospho-AKT(S473)-APC followed by FACS analysis. The MFI of APC in the GFP-positive cells was normalised to the respective non-targeting controls. If not indicated otherwise experiments were performed n$\geq$3. Error bars indicate the standard deviation. Statistics were performed using Two-Way-ANOVA. Significance is indicated by p<0.05 *, p<.0.01 **, p<0.001 ***, p<0.0001 ****.

While analysis of the GFP- and APC-positive cells showed no effects after SHIP1 down-regulation in Ramos cells, a slight but significant increase of p-AKT(S473) in SHIP1 down-regulated and SHIP2-deficient Ramos cells was observed (Figure 6.37A,B). sh*INPP5D* expression in Daudi led to a slight overall increase of p-AKT(S473) levels regardless of SHIP2 (Figure 6.37C). While these results imply some regulation of p-AKT(S473) by SHIP1 the effects on the phosphorylation are mild and apparently opposed to the cell fitness. Hence, this data further supported that the SHIPs contribute to BL fitness not via modulation of AKT activity.

Since the loss of SHIP1 mirrored the effects caused by SHIP2 deficiency it was tested if it also sensitizes for inhibition of PI3K via copanlisib and if this effect could be exacerbated by loss of both SHIPs. Accordingly, the cells were subjected to GFP tracking for 6 days with addition of 200 nM copanlisib for the last two days.

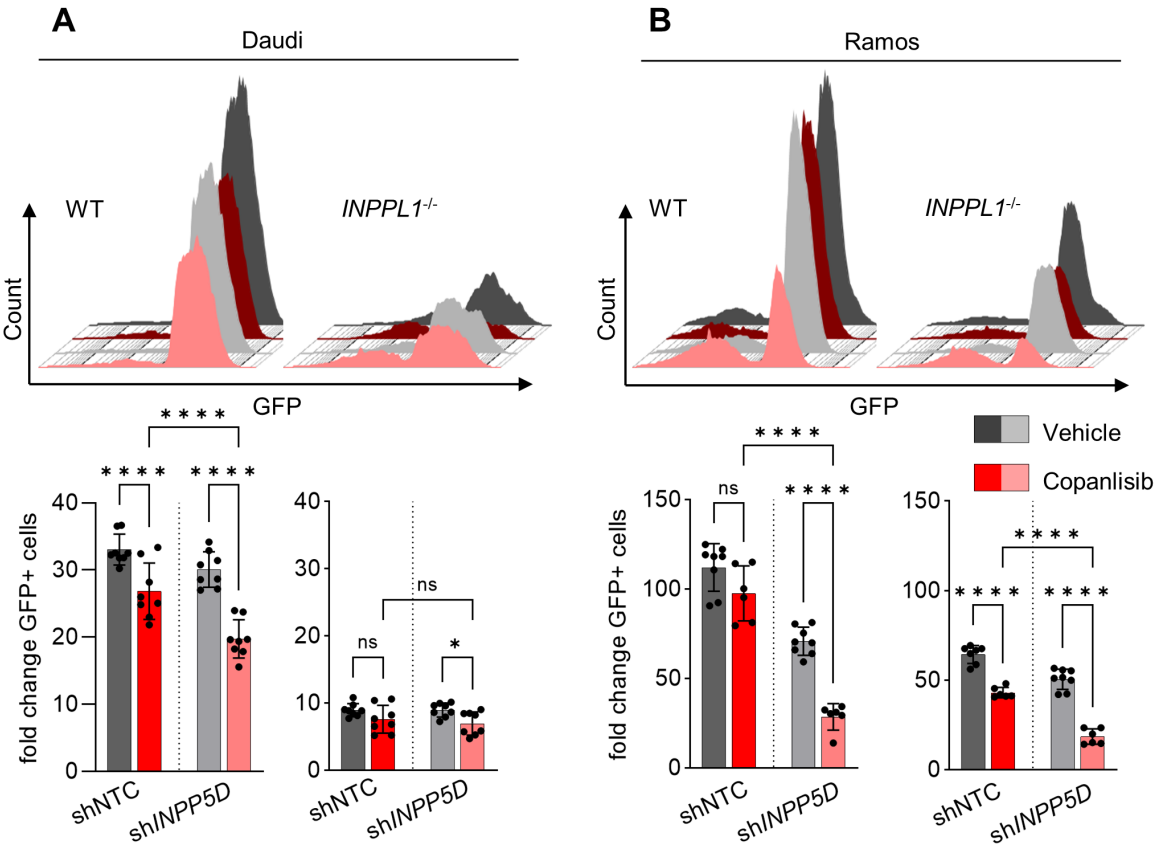

Figure 6.38: **Loss of SHIP1 led to an increase of sensitivity to copanlisib mirroring SHIP2 deficiency.** Daudi **A.** and Ramos **B.** WT and SHIP2-deficient cell lines expressing either a non-targeting control (shNTC) or a shRNA targeting *INPP5D* (sh*INPP5D*) were treated with copanlisib and subjected to GFP tracking assay to monitor the proliferation. The cells were induced with 250 ng/ml doxycycline for a total of 6 days with addition of 200 nM copanlisib or 5 % TFA as vehicle control on day 4. Shown in the column plots are the fold changes of the GFP-positive cells at day 6 relative to d 0. The histograms show the distribution of the GFP levels in the cells at day 6 with a notable increase of GFP-negative cells that underwent treatment and were missing both SHIPs. If not indicated otherwise experiments were performed n≥3. Error bars indicate the standard deviation. Statistics were performed using Two-Way-ANOVA. Significance is indicated by p<0.05 *, p<.0.01 **, p<0.001 ***, p<0.0001 ****.

The GFP tracking revealed an increased sensitivity to copanlisib treatment in the WT cells expressing sh*INPP5D*. SHIP1 down-regulation in SHIP2-deficient Ramos cells sensitised stronger to copanlisib treatment, while this sensitivity in SHIP2-deficient Daudi cells was not increased by down-regulation of SHIP1 (Figure 6.38A,B). This may be explained by an in general lower contribution of SHIP1 to the fitness of Daudi compared to Ramos cells. To corroborate these observation, cells were also subjected to an Annexin-V-APC

staining which enabled the selective monitoring of the proportion of apoptotic cells.

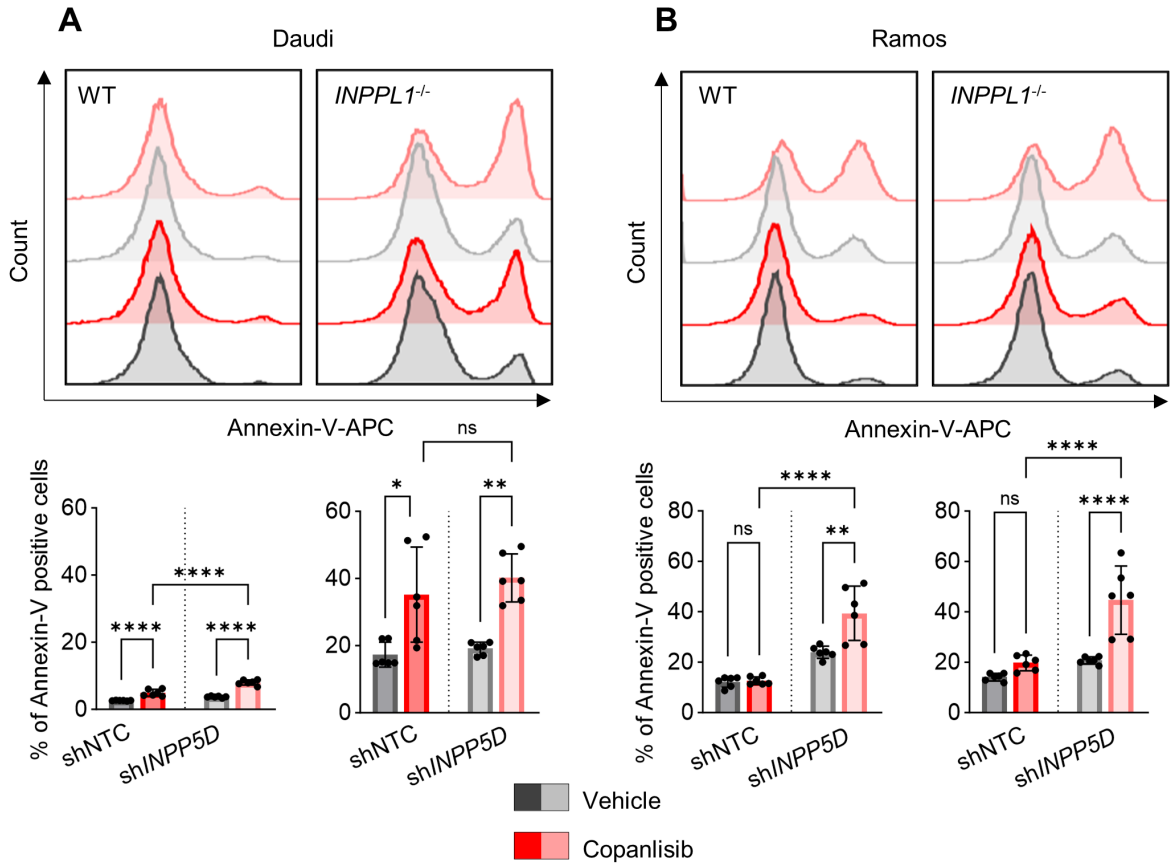

Figure 6.39: **Absence of SHIPs rendered cells more susceptible to copanlisib-induced apoptosis.** Daudi **A.** and Ramos **B.** WT and SHIP2-deficient cell lines expressing either a non-targeting control (shNTC) or a shRNA targeting *INPP5D* (sh*INPP5D*) were treated with copanlisib and subjected to Annexin-V-APC staining. The cells were induced with 250 ng/ml doxycycline for a total of 6 days with addition of 200 nM copanlisib or 5 % TFA as vehicle control on day 4. On day 6, the cells were subjected to Annexin-V-APC staining to assess the apoptosis. The histograms show the distribution of the Annexin-V-APC signal in the respective cells with a notable increase of APC-positive cells after loss of both SHIPs combined with copanlisib treatment. If not indicated otherwise experiments were performed n≥3. Error bars indicate the standard deviation. Statistics were performed using Two-Way-ANOVA. Significance is indicated by p<0.05 *, p<.0.01 **, p<0.001 ***, p<0.0001 ****.

Loss of *INPP5D* expression combined with copanlisib treatment correlated with an increase of Annexin-V-positive Daudi and particularly Ramos cells. Consistent with the results from the proliferation assay, SHIP2-deficient Ramos cells with down-regulated SHIP1 responded to copanlisib treatment with markedly elevated apoptosis levels com-

pared to either SHIP2-deficient or SHIP1 down-regulated cells (Figure 6.39A,B).

Based on these findings it was assessed how SHIP1 down-regulation affects the susceptibility of Ramos cells to inhibition of other components of the PI3K-AKT axis. First, the effect of AKT inhibition was assessed. The previously used capivasertib (6.18 was complemented with another ATP-competitive inhibitor, ipatasertib, which exhibits comparable selectivity and IC50 values for AKT [287]. The different Ramos cell lines were treated with both AKT inhibitors and the proliferation was determined by GFP tracking.

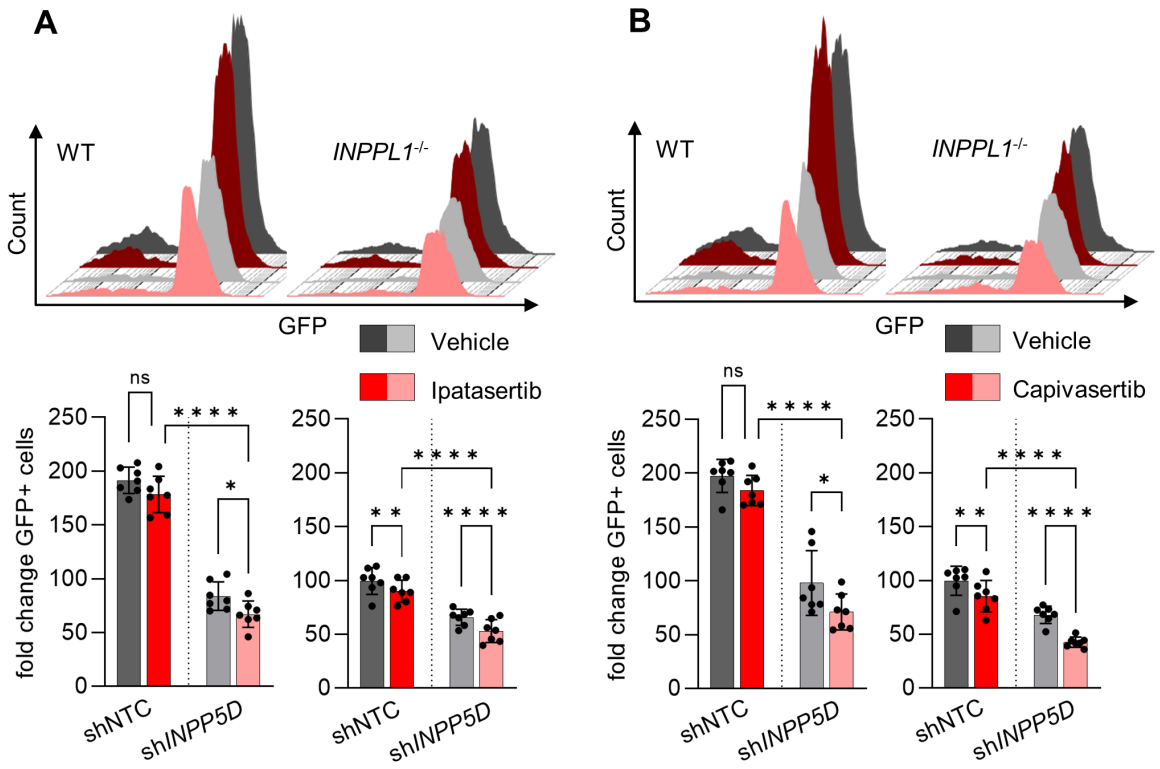

Figure 6.40: **shRNA targeting of *INPP5D* in Ramos cells moderately increased the sensitivity to AKT inhibition.** WT and SHIP2-deficient cell lines expressing either a non-targeting control (shNTC) or a shRNA targeting *INPP5D* (sh*INPP5D*) were treated with either ipatasertib **A.** or capivasertib **B.** and subjected to a GFP tracking assay to monitor the proliferation. The cells were induced with 250 ng/ml doxycycline for a total of 6 days with addition of 1 µM ipatasertib (A) and 1 µM capivasertib (B) or DMSO as vehicle control on day 4. Shown in the column plots are the fold changes of the GFP-positive cells at day 6 relative to d 0. The histograms show the distribution of the GFP levels in the cells at day 6 with a notable increase of GFP-negative cells that underwent treatment and were missing both SHIPs. If not indicated otherwise experiments were performed n≥3. Error bars indicate the standard deviation. Statistics were performed using Two-Way-ANOVA. Significance is indicated by p<0.05 *, p<.0.01 **, p<0.001 ***, p<0.0001 ****.

Inhibition of AKT with ipatasertib or capivasertib had little overall impact on the proliferation of the Ramos cells, confirming earlier results. Although, the effect of AKT inhibition on the proliferation was further augmented by SHIP1 down-regulation in SHIP2-deficient cells, the effect was marginal compared to copanlisib treatment (Figure 6.40A,B). These results further support the hypothesis that the survival promoting functions of both SHIPs are independent of AKT activity in BL cells.

Similar to the approach described for Figure 6.18, the sensitivity to the mTORC1 inhibitor rapamycin was assessed. Loss of SHIP1 increased the susceptibility to rapamycin treatment in a comparable manner to SHIP2 deficiency. However, the absence of both SHIPs almost completely diminished the proliferation. Also this loss of proliferation was accompanied by an extreme loss of GFP signal indicating that the cells suffered from elevated apoptosis in response to rapamycin treatment (Figure 6.41A). Another important effector in the survival signaling is phosphoinositide-dependent kinase 1 (PDK1), which facilitates the T308 phosphorylation of AKT and, moreover, activates PKC, S6K and SGK, which are all involved in promoting proliferation [36, 38, 288–291]. Its activity is dependent on prior recruitment to PI(3,4)P_2 [35, 37] and is selectively inhibited by GSK2334470 in sub-micromolar concentrations [292, 293]. The effect of GSK2334470 on the proliferation of the control cells was only moderate. However, all cells with targeted SHIP expression, particularly SHIP1 down-regulated and SHIP2-deficient cells were sensitive to PDK1 inhibition as revealed by almost complete abrogation of proliferation (Figure 6.41B).

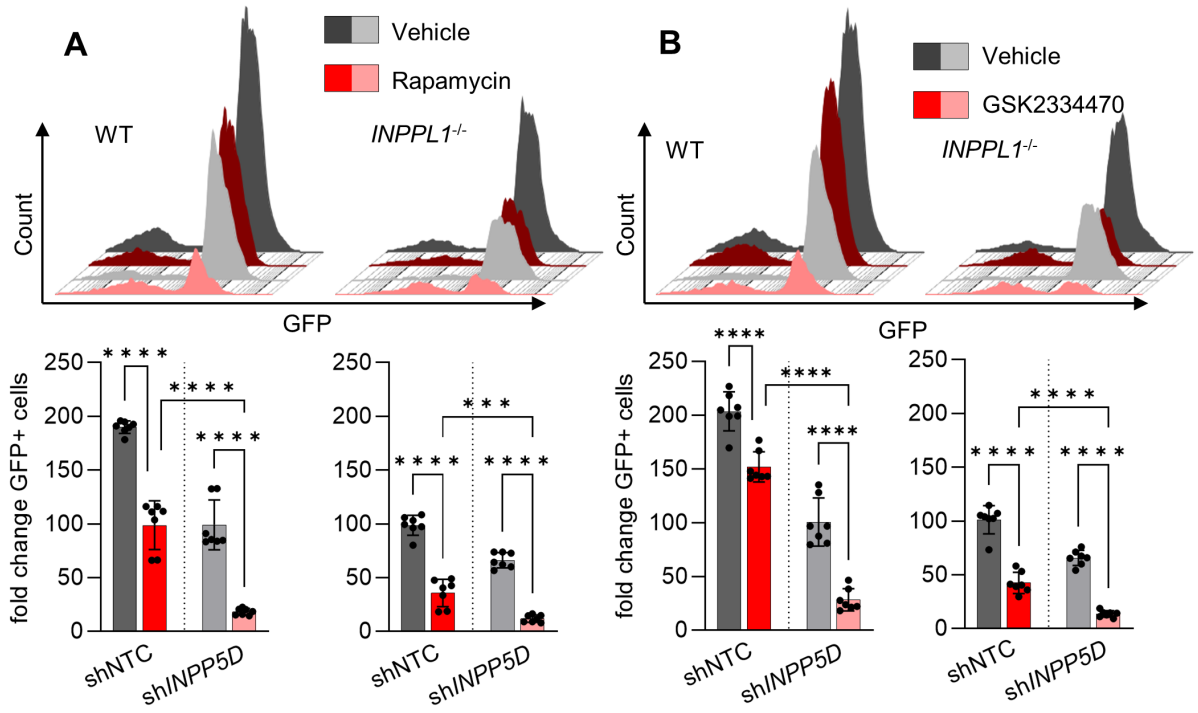

Figure 6.41: **Absence of SHIPs in Ramos cells increased the susceptibility to rapamycin treatment and PDK1 inhibition.** WT and SHIP2-deficient cell lines expressing either a non-targeting control (shNTC) or a shRNA targeting *INPP5D* (sh*INPP5D*) were treated with either rapamycin **A.** or GSK2334470 **B.** and subjected to a GFP tracking assay to monitor the proliferation. The cells were induced with 250 ng/ml doxycycline for a total of 6 days with addition of 100 nM rapamycin (A) and 2.5 µM GSK2334470 (B) or DMSO as vehicle control on day 4. Shown in the column plots are the fold changes of the GFP-positive cells at day 6 relative to d 0. The histograms show the distribution of the GFP levels in the cells at day 6 with a notable increase of GFP-negative cells that underwent treatment and were missing both SHIPs. If not indicated otherwise experiments were performed n≥3. Error bars indicate the standard deviation. Statistics were performed using Two-Way-ANOVA. Significance is indicated by $p<0.05$ *, $p<.0.01$ **, $p<0.001$ ***, $p<0.0001$ ****.

These findings provide evidence that interference with the activity of SHIP1 or SHIP2 and particularly a complete loss of $PI(3,4)P_2$ production due to absence of SHIPs increases the susceptibility to inhibition of multiple factors of the tonic BCR signaling network. Moreover, the results hint at a redundancy of SHIP proteins in their supporting function for BL cell fitness.

To test if down-regulation of SHIP1 also affects the cellular ATP production, the sh*INPP5D* expressing Daudi and Ramos cells were subjected to a Seahorse assay.

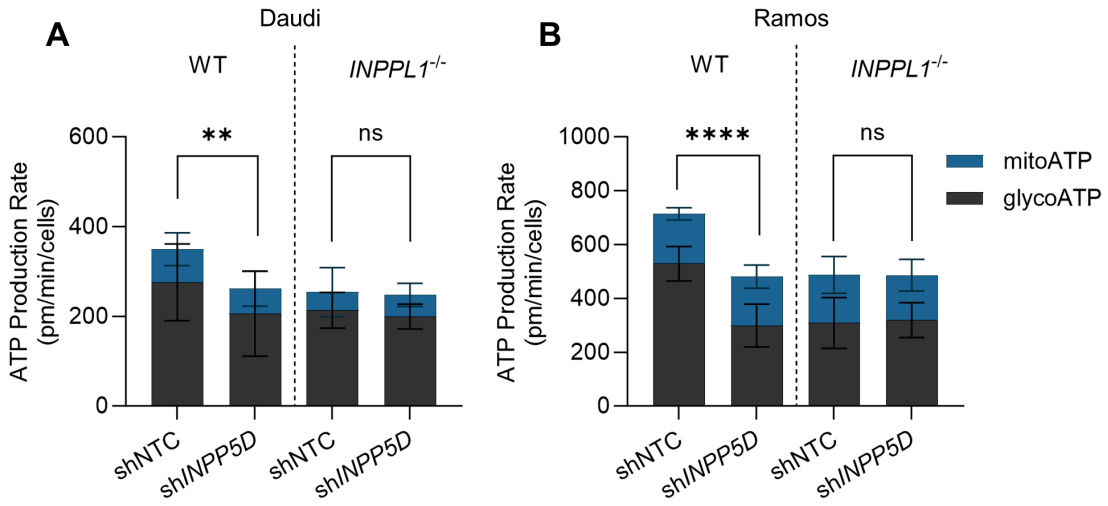

Figure 6.42: **SHIP1 contributes to energy metabolism mirroring SHIP2.** Daudi **A.** and Ramos **B.** WT and SHIP2-deficient cell lines expressing either a non-targeting control (shNTC) or a shRNA targeting *INPP5D* (sh*INPP5D*) were subjected to a Seahorse assay. The shRNA expression was induced by addition of 250 ng/ml doxycycline 5 days prior to the assay. The energy production is given by the mitochondrial (mitoATP) and glycolytic (glycoATP) ATP production. If not indicated otherwise experiments were performed n≥3. Error bars indicate the standard deviation. Statistics were performed using Two-Way-ANOVA only for the glycolytic ATP production. Significance is indicated by p<0.05 *, p<.0.01 **, p<0.001 ***, p<0.0001 ****.

Down-regulation of SHIP1 significantly decreased the glycolytic ATP production rate in Daudi and Ramos WT cells in a similar manner to SHIP2-deficient cells but had no effect on the mitochondrial ATP production rate. SHIP1 down-regulation in absence of SHIP2 did not further reduce the ATP production rate. Collectively, the fact that SHIP1 appears to have the same promoting effect on the ATP production like SHIP2 further highlights the importance of their enzymatic product PI(3,4)P_2 for the energy production of BL cells.

Discussion

A large portion of Burkitt lymphomas exploit the tonic BCR signaling network to maintain their survival. Therefore, identification and unravelling of the dysregulated processes and involved proteins could provide an opportunity for improved treatment strategies. This study provides evidence that the 5-inositol phosphatases SHIP1 and SHIP2 contribute to the fitness of BL cells by ensuring an efficient energy metabolism in dependency of the tonic BCR signaling.

7.1 SHIP2 activity may be dependent on tonic BCR signaling

Interfering with the activity of SHIP2 via CRISPR, RNAi or small molecule inhibitors markedly attenuated the proliferation and augmented the apoptosis of different tonic BCR signaling-dependent BL cell lines. Interestingly, SHIP2 deficiency in the surface IgM-negative cell line Raji did not yield similar effects. In addition, Raji cells remained almost unaffected by treatment with the SHIP2 inhibitor AS1949490. Collectively, these results suggested that the survival promoting function of SHIP2 is likely dependent on intact tonic BCR signaling. Indeed, there is evidence that the phosphorylation of the serine at position 132 of SHIP2 is part of the tonic BCR signaling network [163]. Moreover, this particular phosphosite is associated with an induction of enzymatic activity and switch of the intracellular localization, which suggests an active role of SHIP2 in the tonic BCR signaling network [294, 295]. While SHIP2 may be dependent on tonic BCR signaling, the phosphatome exhibited only few modulations of phosphosites involved in the tonic BCR signaling network. Collectively, this indicates that SHIP2 may be regulated by the tonic signaling but does not regulate other components of this network.

In contrast to SHIP2, SHIP1 is known as a negative regulator of the activated BCR signaling since SHIP1 deficiency is associated with hyper activation of B cells [193–195, 296]. However, the loss of SHIP1 mirrored strongly the effects observed in SHIP2-deficient cells, suggesting an involvement also in tonic BCR signaling. Interestingly, SHIP1 also exhibits tonic BCR signaling-dependent phosphorylation at the tyrosine 1021 and 1160 [163]. While the function of Y1160 is unknown, Y1021 is part of one of the NPXY-motifs of SHIP1 and an important regulatory site, as it enables protein-protein interactions that control the activity of SHIP1 [194, 297, 298]. In conjunction with its role in promoting the fitness, SHIP1 appears to have an important role in the tonic BCR signaling network of BL cells, similar to SHIP2.

7.2 AKT signaling is not affected by absence of SHIP2

After their discovery, the SHIP proteins were initially regarded as tumor suppressors owing to their apparent negative regulation of AKT. However, this view has changed in recent years as it was found that both SHIP proteins often promote tumorigenicity. High SHIP2 levels are associated with a poor prognosis in non-small lung cancer, breast cancer, laryngeal squamous cell carcinoma and also colorectal cancer among many others [299–302]. While the oncogenic role of SHIP2 has been shown mostly in solid tumors, this study is the first to describe it in a B cell lymphoma, particularly Burkitt lymphoma. Since SHIP1 is restricted to few tissues, predominantly hematopoietic cells, it was found as a promising target in acute myeloid leukemia and chronic lymphocytic leukemia [286, 303].

In contrast to SHIP2 being regarded as a negative regulator of AKT, the p-AKT levels of SHIP2-deficient BL cell lines were not altered. PI3K activity enables activation of AKT, known as the central kinase to trigger pro-survival and anti-apoptotic processes as well as induction of genes involved in energy metabolism [304]. Full activation of AKT is based on a two-step process. First, the phosphorylation at S473 in the carboxyl tail is facilitated by mTORC2 and is considered as the major factor that regulates AKT activity as it enables recruitment to the plasma membrane via its PH domain and exposes the activation loop [33, 34]. In addition, phosphorylation of T308 in the activation loop is facilitated by PDK1, which enables the full activation of AKT [35–37]. While the serine at

473 can be phosphorylated even when AKT is not recruited to the plasma membrane, the p-T308 is only present at plasma membrane-located AKT [33]. Since the plasma membrane localization of AKT was long thought to be directly dependent on PI(3,4,5)P_3, both 5-inositol phosphatases were regarded as tumor suppressors according to their enzymatic conversion of PI(3,4,5)P_3 to PI(3,4)P_2, which opposes PI3K and thus BL survival [305]. Accordingly, SHIPs were viewed similar to the 3-inositol phosphatase PTEN, which converts PI(3,4,5)P_3 to PI(4,5)P_2. PTEN has a tumor suppressor function in many cancers where it acts as a negative regulator of AKT signaling, thereby preventing uncontrolled growth and resistance to apoptosis [306–309].

The recent growing evidence is reported that SHIPs can be tumor-promoting proteins thus changing the view of inositol phosphatases as general tumor suppressors and giving rise to the "Two PIP Hypothesis" [310]. In this hypothesis, the PI(3,4)P_2 is not merely the product of hydrolysing PI(3,4,5)P_3 but rather a way to diversify and multiply the PI3K signaling by balancing the levels of PI(3,4,5)P_3 and PI(3,4)P_2 at the plasma membrane. The diversification is facilitated by PI(3,4,5)P_3 being regulated at the plasma membrane by two different classes of inositol phosphatases leading to two different outcomes as explained before. The multiplication is based on the specificity of the PH domains of the AKT isoforms. While AKT1 and AKT3 prefer binding to PI(3,4,5)P_3, AKT2 predominantly binds PI(3,4)P_2 [29]. Consequently, SHIP activity diversifies and thus promotes the anchoring and activation of AKT at the plasma membrane. In addition, the PH domain of PDK1 is able to bind to both phosphatidyl inositols, yet it prefers PI(3,4)P_2 and since PDK1 is required to fully activate AKT at the plasma membrane, this might be another level of regulation offered by the SHIPs [30, 31].

These findings may explain the observed stable p-AKT levels in SHIP2-deficient cells. In these cells, the increase of PI(3,4,5)P_3 could be accompanied with an elevation of phosphorylation of AKT1 and AKT3, while the opposite effect would be observed for AKT2. Accordingly, the total phosphorylation levels of AKT could remain stable, but the composition of activated AKT would have changed with potential consequences on downstream signaling. Since this theory is difficult to prove on a molecular level, the question remains, if this change in composition could explain the lowered fitness of SHIP2-deficient BL cells. However, inhibition of AKT using two different small molecule inhibitors exhibited mild to no effects on the proliferation of BL cells, which was exacerbated only slightly by absence

of both SHIPs. Therefore, even if the absence of SHIPs would change the composition of AKT isoforms at the plasma membrane, it is unlikely that this change concludes in the lowered fitness. Since AKT signaling is generally associated with increased survival, the low sensitivity to its inhibition opens the question whether AKT is actually important in BL cells.

While there is evidence that the inhibition of the PI3K-AKT axis has a negative effect in BL cells, a recent CRISPR/Cas9-based "drop-out" screen did not reveal any sensitivity of BL cell lines to AKT deficiency, as it is the case for other BCR-dependent lymphomas such as diffuse large B cell lymphoma cells [165, 311–313]. Moreover, over-activation of AKT was shown to be lethal in primary Burkitt lymphoma cells, indicating that the AKT signaling in BL cells needs to be tightly controlled [314]. On the other hand, refractory BL can gain sensitivity to AKT inhibition [315]. This suggests that their original survival signal is less dependent on AKT, while further adaption processes can lead to a change in the source of the survival signaling. In all BL cell lines used in this study, SHIP2-deficiency did not correlate with altered p-AKT levels as demonstrated by Western Blot analysis, intracellular staining and phosphoproteomic analysis. Consequently, the fitness-promoting effect of SHIP2 may be exerted beyond AKT signaling. Coincidentally, a recent review on targeting the SHIPs in cancer by Pedicone *et al* came to a similar conclusion, stating that "Thus, SHIP2 could be a cancer target independent of its ability to promote AKT activation by PI(3,4)P2 production." [47]. However, one should consider that even if AKT is not controlled by SHIPs in BL, this could be context-dependent since the inhibition of SHIP1 causes hyper activation of AKT in CLL cells [303]. In support of this, the p-AKT(S473) levels are not elevated in BL cells treated with the SHIP2 inhibitor AS1949490, which was shown to augment the p-AKT(S473) levels in the rat skeletal muscle cell line L6, as well as in podocytes [241, 316].

7.3 SHIP2 deficiency increases the sensitivity to inhibition of components of the PI3K-AKT axis

The PI3K inhibitor copanlisib was used to determine, if the supportive SHIP2 effect directly depends on active PI3K signaling, which was expected to cause a similar fitness of inhibitor-treated BL cells regardless of SHIP2 expression. SHIP2 deficiency increased the sensitivity to inhibition of PI3K, indicating that SHIP2 contributes to the fitness of BL

cells independently of PI3K activity. Consistently, the same effect was observed in the absence of SHIP1, followed by exacerbation through expression of sh*INPP5D* in SHIP2-deficient cells. These data further confirm that the survival-promoting functions of the SHIP proteins in BL cells occurs beyond regulation of the PI3K-AKT axis. Inhibitors targeting the PI3K are applied for the treatment of numerous different tumors due to the central role of this kinase in the survival signaling facilitated by receptor tyrosine kinases, G-protein coupled receptors and the B cell receptor [317–321]. Consequently, inhibition of PI3K has already found an efficient use in treatment of several other non-Hodgkin lymphomas, such as indolent, follicular and small lymphocytic lymphoma [116, 322, 323]. Furthermore, PI3K inhibitors are also under investigation for treatment of BL, as indicated by an ongoing clinical trial and experimental treatments with different inhibitors [324, 325]. Notably, there is indication that this sensitizing effect of SHIP deficiency is not restricted to BL cells, as a cross-reference of CRISPR- and drug-screens exhibited synergistic effects of SHIP2-deficiency and copanlisib treatment in many different cancer cell lines [207].

Interestingly, SHIP-deficient cells exhibited increased sensitivity to rapamycin, which may be contradictory to the findings discussed above, because mTORC1 is a major target of AKT. mTORC1 is an important regulator of cell growth as it is involved in the sensing of nutrient availability, cellular energy status, growth factor signaling and cellular stress responses among many other critical processes [326, 327]. Even though rapamycin selectively targets mTORC1 over mTORC2, prolonged exposure, which was the case in this study, can also inhibit mTORC2 [264]. However, mTORC2 can also facilitate survival signaling independently of AKT, for example via the direct activation of serum- and glucocorticoid-induced kinases (SGK) [328]. Consequently, a decreased activity of mTORC1 and 2 could explain the increased sensitivity to rapamycin of SHIP2-deficient BL cells. A SHIP2-dependent positive regulation of mTORC1 itself is unlikely, even though mTORC1 is able to bind to $PI(3,4)P_2$. However, this binding was reported to be restricted to endosomes and lysosomes where it has an inhibitory effect on mTORC1 activity [329].
Interestingly though, mTORC2 can directly localize to $PI(3,4,5)P_3$ at the plasma membrane through the PH domain of its component SIN1, which in turn leads to a PI3K-dependent activation of mTORC2 [32]. While this would not explain the lowered fitness of SHIP2-negative cells, it could contribute to the increased sensitivity to inhibition of

the PI3K. In absence of SHIP2, BL cells could still maintain some survival signals via PI3K-dependent activation of mTORC2. In line with this finding, rapamycin exhibits potent anti-cancer effects in BL. In a murine BL-like mouse model, rapamycin treatment significantly reduced the tumor burden [330]. In addition, combination of α-CD19 antibodies and rapamycin induced an autophagic cell death of the BL cell line SKW6.4 in a mouse xenocraft model and in patient-derived primary BL cells *in vitro* [331]. However, the mass spectrometry analysis revealed that SHIP deficiency does not cause alterations of the components of mTORC2 or any of its known substrates on protein or phosphorylation levels in the Ramos cell line. Thus, mTORC2 might facilitate a SHIP2-independent, but PI3K-dependent survival pathway in BL cells. This suggestion is supported by the fact that treatment of chemotherapy-sensitive and -insensitive BL models with a dual inhibitor of PI3K and mTOR showed strong anti-tumor capabilities *in vitro* and *in vivo* [332].

Intriguingly, SHIP deficiency particularly sensitises to inhibition of the serine/threonine kinase PDK1. The PDK1 coding gene *PDPK1* is over expressed in almost half the cases of acute myeloid leukemia and promotes tumorigenesis and growth of ovarian and breast cancer [333–335]. In addition, over expression of *PDPK1* is able to transform mammary epithelial cells [336]. Nevertheless, the mechanisms leading to activation of PDK1 are still poorly understood and are probably context-dependent. While there is evidence for PDK1 translocation and activation upon insulin- or growth hormone-induced signaling, there are also contradictory studies [337–340]. Apparently, PDK1 can also be activated in the absence of engaged receptors by auto phosphorylation dependent on phosphoinositides [37]. The PH domain of PDK1 shows affinity to PI(3,4,5)P_3 and PI(3,4)P_2, and accordingly SHIP2 could facilitate the plasma membrane localization and subsequent activation of PDK1. However, similar to mTORC2, the survival promoting function of PDK1 is suggested to be mainly facilitated by activating AKT [35, 341]. Yet, PDK1 has also shown the ability to maintain a survival signal in cells with low AKT activation via activation of SGKs and in particular SGK3 [342, 343]. In addition, PDK1 can directly activate p70S6K, p90RSK and members of the PKC family proteins, providing possibilities for a more diverse survival signaling maintained by PDK1 [288–291]. Therefore, modulation of PDK1 activity at the plasma membrane based on changes in the composition of phosphoinositides could not only increase the susceptibility to inhibition of PDK1 in SHIP-deficient BL cells, but also explain their generally lower fitness. However, the

protein and phosphorylation levels of PDK1 and the different SGKs were not affected by SHIP2 deficiency in Ramos cells, suggesting that the positive SHIP2 effect on BL survival does not rely on PDK1 activity. Nevertheless, the inhibition of PDK1 effectively reduced BL cell proliferation, indicating that PDK1 could be another mainstay of BL survival signaling. This theory is supported by the CRISPR- and RNAi-screens found in the Cancer Dependency Map, which highlights the role of PDK1 in many BL and non-Hodgkin lymphoma cell lines [207].

Beyond the PI3K-AKT axis, also MAPK may contribute to the fitness of BL cells. In activated BCR signaling, MAPK activation requires the recruitment of effector proteins such as PLCγ2, BTK and SOS, which all have PH domains binding to PI(3,4,5)P_3 [10, 23, 344]. Eventually this leads to activation of the MAPKs JNK, p38 and ERK that promote survival and proliferation in normal B cells [10, 18–20, 23, 26, 345]. An earlier study has shown that the JNK phosphorylation was down regulated in SHIP2-deficient Daudi cells [197]. Since JNK is required for maintenance of the c-MYC levels in Burkitt lymphoma and therefore necessary for the survival, it was reasoned that SHIP2 could modulate the JNK activity via an unknown mechanism, possibly recruitment of PI(3,4)P_2-specific membrane adaptors [197, 261]. However, I could not confirm these findings in other BL cell lines. Moreover, analysis of the phosphoproteome data of SHIP2-deficient Ramos and Daudi cells did not reveal substantial and consistent alterations in phosphorylation levels of these MAPKs. Based on this data, it is unlikely that SHIP2 promotes the fitness through regulation of the MAPK network, especially JNK.

Collectively, these data indicate that SHIP2 does not take part in regulation of any of the BCR pathways that are typically associated with increased survival and proliferation.

7.4 PI(3,4)P_2 contributes to BL fitness by promoting the energy metabolism

Instead of the described role of SHIPs in disrupting PI(3,4,5)P_3 to regulate plasma membrane-tethering of BCR effectors, the SHIP product PI(3,4)P_2 appears to contribute to the fitness of BL cells. Since it is exclusively produced from PI(3,4,5)P_3 at this localization, an important part of PI3K-mediated BL cell survival might be plasma membrane

localized PI(3,4,5)P_3 [29, 45]. This is already implied by the fact that SHIP1 and 2, which are the only producers of PI(3,4)P_2 at the plasma membrane, have redundant function. Evidently, shielding of PI(3,4)P_2 by GFP-2xTAPP1-PH had a remarkable effect on the survival of BL cell lines, also in the absence of SHIP2. The importance of PI(3,4)P_2 in BL cells was further highlighted by the decline in proliferation caused by its enzymatic conversion via a myristoylated, hence plasma membrane-located version of the inositol-4-phosphatase INPP4A. Consistently, INPP4A along with its sister protein INPP4B have been described as tumor suppressors, albeit because of a PI3K-opposing activity [346].

Moreover, the competitive growth assay demonstrated that blocking of PI(3,4)P_2 had a comparably stronger impact on the survival than the blocking of PI(4,5)P_2 through the PH domain of PLCδ. Nevertheless, Cer-PLCδ-PH-expressing cells also exhibited a mild survival disadvantage, indicating a role of PI(4,5)P_2 in the BL-specific survival signaling. In fact, PI(4,5)P_2 at the plasma membrane serves signaling-related and unrelated functions such as association to the actin cytoskeleton [347]. PI(4,5)P_2 serves as basis for two signaling networks: First, it is required as substrate for the PI3K to generate PI(3,4,5)P_3. Second, it is hydrolyzed by PLCγ2 to produce inositol-1,4,5-triphosphate (IP_3) and diacylglycerol (DAG), which enables the mobilization of Ca^{2+} and PKC activation, respectively [13, 14]. Therefore, in BL cells PI(4,5)P_2 may be required for maintenance of the PI3K pathway. Shielding of PI(4,5)P_2 could compromise the substrate pool of PI3K leading to a decrease in PI3K activity and thus down regulation of the associated survival signaling.

While the data provided in this thesis clearly imply that PI(3,4)P_2 is an important signaling component, it may appear peculiar that its contribution to the fitness of BL cells occurs without changes in associated signaling pathways.

Proteomics analysis revealed that SHIP2 deficiency correlated with an altered abundance of proteins involved in the carbon metabolism, indicating adaption processes of SHIP2-deficient BL cell clones. Abrogation of glycolysis by 2-DG strongly perturbed BL cell survival regardless of presence of SHIP2, indicating that the SHIP2 effect relies on intact energy metabolism. In addition, the loss of either SHIP resulted in a decrease of the cellular ATP production rate, particularly from glycolysis. BL is an aggressively growing lymphoma that requires an efficient energy metabolism to sustain its rate of proliferation. Hence, dysregulation of the energy metabolism could result in the observed phenotypes.

SHIP2 was shown to be an important modulator of the insulin signaling where it prevents type 2 diabetes [187, 348]. However, B cells do not rely on insulin signaling for glucose uptake. Instead, engagement of the BCR facilitates increased glucose uptake via the PI3K pathway, leaving the connection of SHIP2 and its enzymatic product to the energy metabolism in a AKT-independent manner elusive [273]. It has been reported that $PI(3,4)P_2$ is involved in trafficking of intracellular vesicles leading to alteration of glucose transporters on the plasma membrane [349]. In BL cells, however, despite exhibiting a lowered pool of $PI(3,4)P_2$ on the plasma membrane, SHIP2 deficiency does not alter the surface abundance of the glucose transporters GLUT1 and GLUT4. In line with these findings, no changes were observed in the glucose uptake. Nevertheless, this phosphoinositide could also be involved in trafficking of other transporters, for example to import certain amino acids that indirectly feed glycolysis.

In other cell types, $PI(3,4)P_2$ is inherently required for the formation of membrane ruffles and as such essential for clathrin-mediated and -independent endocytosis, particularly macropinocytosis, that enables scavenging of nutrients from the extracellular space [350, 351]. In this process, $PI(3,4)P_2$ is locally produced by SHIPs and facilitates the closure of the dorsal ruffles through membrane binding of TAPP1 and subsequent recruitment of cytoskeleton effectors and eventually dynamin to pinch off the macropinocytic vesicle [350, 352, 353]. The resulting early endosome is then still covered in $PI(3,4)P_2$, which is eventually targeted by 4-inositol phosphatases [352]. In fact, $PI(3,4)P_2$ is also found on lysosomal and late endosomal membranes where it is produced by different classes of PI3K [329, 354]. This may explain why the TAPP1-PH containing $PI(3,4)P_2$ biosensor is not exclusively localized at the plasma membrane, but is also found at in the cytoplasm, though without obvious vesicular localization. Nevertheless, a decrease in SHIP activity might restrict endocytosis in BL cells and as such also nutrient scavenging, which could reflect negatively on the ATP production rate. It is difficult to support this hypothesis due to the fact that very little is known about endocytosis in B cells, with the exception of BCR internalisation after antigen engagement [74, 75, 355, 356]. However, this process did not appear to be SHIP2-dependent because surface BCR levels were unaltered in absence of SHIP2.

Even though SHIP deficiency clearly correlated with a lowered glycolytic ATP production rate, mass spectrometry did not reveal alterations in protein- or phosphorylation levels of

proteins involved in the glycolysis. In fact, of the proteins involved in tonic BCR signaling, the expression of only three were significantly changed, more precisely down regulated, upon SHIP2 deficiency. The first was the lysine methyltransferase 5 A (KMT5A), which is a histone modifier associated with acute megakaryoblastic leukemia without down syndrome according to the MalaCards human disease database, but has no implication in BL or B cells in general [357]. Secondly, the helicase with zinc finger (HELZ), which was shown to promote cell proliferation by regulating the activity of the ribosomal protein S6 in HeLa cells, but has not been described in B cells [358]. Finally, the level of pleckstrin homology domain containing A2 (PLEKHA2, also known as TAPP2) protein was decreased in absence of SHIP2. PLEKHA2, is a sister protein of TAPP1 and exhibits the similar selectivity of its PH domain to bind $PI(3,4)P_2$. Consequently, its localization at the plasma membrane is dependent on PI3K and SHIP activity [359, 360]. The binding of the TAPP proteins to $PI(3,4)P_2$ at the plasma membrane is considered a negative feedback loop to constrict PI3K activity, as it was shown in the case of insulin signaling [360–362]. If this PI3K regulatory function of TAPPs can be translated to the BCR signaling, it would make sense for SHIP2-deficient cells to down regulate the expression of *PLEKHA1/2* to adapt to the already decreased $PI(3,4)P_2$ level. Moreover, membrane located TAPPs have been found to interact with actin-binding proteins, which suggests a role in signaling-dependent cytoskeleton remodeling [353]. Furthermore, PLEKHA2 is associated with some types of lymphoma, its tumor promoting role is poorly understood [357]. Despite the SHIP2-dependent changes in these proteins, they are not obviously involved in pathways that are associated to the energy metabolism. Therefore, based on the current knowledge it appears more likely that $PI(3,4)P_2$ affects the ATP production by controlling the transport of glycolysis- or TCA-feeding components but not glucose.

7.5 SHIP2 could promote BL fitness via aspartate synthesis

BL cells exhibit an increased consumption of glucose and glucose-derived carbon in the tricarboxylic acid cycle (TCA) based on the characteristic over expression of *MYC* [363]. In contrast to other B cell lymphomas such as DLBCL, BL cells appear to rely strongly on the one-carbon metabolism and show increased sensitivity to inhibition of this metabolic pathway [364, 365]. To gain a larger overview of the potential metabolic changes, the

Daudi and Ramos cell lines were subjected to a metabolome analysis, which revealed a pronounced difference in the biosynthesis of amino acids and taurine/hypotaurine. Dysregulation of the latter was found as an early marker for the diagnosis of breast cancer [366]. Consequently, the distinct metabolic profiles of Ramos and Daudi WT cells underline the heterogeneity of BL. Absence of SHIP2 caused alterations of several metabolic pathways, including amino acid metabolism and biosynthesis. However, the SHIP2-dependent differences were not consistent in Ramos or Daudi cells and gave no clear implication for a dysregulated one-carbon metabolism.

Nevertheless, SHIP2 deficiency in all analysed BL cell lines correlated with the down regulation of three metabolites: Benzoic acid, D-gluconic acid and D-aspartic acid. Little is known about benzoic acid in the context of cancer, however benzoic acid derivatives have been shown to possess anti-cancer abilities [367]. Similarly, D-gluconic acid is largely considered as physiologically inactive, though recent publications hint that it might be disadvantageous for cancer cells due to its ability to block the plasma membrane embedded citrate transporters [368]. More promising in the context of how $PI(3,4)P_2$ might regulate the BL-specific energy metabolism is the observed decrease in aspartic acid. This metabolite is known to be a limiting factor for the proliferation of tumor cells despite the ability to satisfy their aspartic acid supply via *de novo* synthesis [369, 370]. The production of aspartate in cancer is glucose-dependent and fueled by an efficient glycolysis and TCA [371]. The growth limiting aspect of aspartate is most likely based on the requirement of this amino acid for the production of nucleotides and protein biosynthesis [369, 372]. Consequently, a lower aspartate level could cause an altered cell cycle due to inadequate supply of nucleotides, which was not observed in SHIP2-deficient BL cell lines. On the other hand, the decrease in cellular aspartate might just be a symptom of the reduced efficiency of the glycolysis and has no direct physiological consequences as not all cancers are aspartate-dependent [369, 370]. Nevertheless, lower aspartate levels may be linked to the reduction in fitness found in SHIP2-deficient BL cells.

The details of how SHIP2 could influence aspartate levels is a matter of speculation, especially since the mass spectrometry analyses did not reveal major alterations in respective transporter proteins or proteins involved in glycolysis or the TCA. Potentially, BL cells may maintain their demand of important amino acids like aspartate by salvaging extracellular nutrients through phagocytosis or macropinocytosis as many other cancer

cells do [373–375]. While B cells in general are not known to perform phagocytosis or macropinocytosis like other antigen presenting cells, the exception to this rule are the follicular B cells in the germinal center. These cells have been observed to phagocytose antigen covered particles via internalisation of the BCR, a process implicated with a strong and efficient germinal center reaction [376]. Since BL cells originate from erroneous germinal center cells, one might think that these cells could have repurposed this ability to satisfy their nutrient demand. Despite the different implications discussed here, the exact role of $PI(3,4)P_2$ in energy metabolism needs to be further addressed, especially its putative role in the provision of amino acids that may be linked to the production of ATP.

7.6 SHIP1 and SHIP2 may be therapeutic targets due to their redundant functions in BL cells

Simultaneous interference with both 5-inositol phosphatases had an additive effect on proliferation and apoptosis compared to silencing of single SHIPs, which suggests that both enzymes exhibit a redundancy based on their enzymatic function. This is particularly interesting as these proteins are not isoforms, but proteins encoded from different genes located on different chromosomes [171]. Consistently, the redundancy of SHIP proteins has already been implicated as an important contributor to obesity due to the higher treatment efficiency of pan-SHIP inhibitors compared to single SHIP inhibitors [377]. This redundancy could also serve as an explanation as to why the SHIP1-coding gene *INPP5D* did not appear in the reported shRNA screens [196]. However, considering that the sh*INPP5D* expression had a comparably lower impact in Daudi than in Ramos implicates that cells could depend differently on the SHIPs. Nevertheless, loss of total SHIP activity was always associated with a negative outcome in the tested BL cell lines, suggesting a pharmacological potential in targeting SHIP proteins in in the treatment of BL. This potential was also subject of multiple reviews in recent years indicating that SHIPs could be an interesting target in other cancers besides BL [47, 378, 379].

This study is the first to describe an increased sensitivity to inhibition of multiple components of the PI3K-AKT pathway in the context of SHIP deficiency. In line with these findings, drug-perturbation screens in multiple BL cell lines have shown synergistic ef-

fects between a large variety of small molecule inhibitors targeting BTK but also especially mTOR and PI3K [380]. Combinatorial treatments are already in use and under investigation for a variety of different cancers, though BL is still often treated with a variation of the CHOP (cyclophosphamid-hydroxydaunorubicin-vincristin-prednison) scheme-containing potent cytostatic agents, which can be combined with the α-CD20 antibody rituximab to increase the efficiency [381]. Because SHIP proteins attenuate the energy metabolism, inhibition may be beneficial in combinatorial therapies. This is implied by my findings that the absence of SHIP markedly increased the sensitivity of BL cell lines to PI3K inhibition, which may be valid also for the combination with other, already established drugs. Here, SHIP inhibitors could be employed to lower the dosage of regimes to treat BL, thus possibly expanding the applicability to patient groups that were hitherto excluded from treatment due to the associated lethality [144].

Inhibitors selectively targeting either SHIP1 or SHIP2 or both simultaneously are currently under investigation for different tumors but also dietary-associated diseases such as diabetes and obesity [377, 382, 383]. However, the side effects of targeting the SHIP proteins in the human body are poorly understood and can only be speculated on based on animal and cell line models. SHIP1-deficient mice show increased mortality caused by an augmented infiltration of myeloid cells into the lungs followed by severe inflammation [384, 385]. While SHIP1 is restricted to hematopoietic and certain brain tissue, SHIP2 is ubiquitously expressed in the human body. Its role is particularly highlighted as a negative regulator of insulin signaling and thus, an important role for the insulin-dependent energy metabolism [187, 386–388]. Furthermore, SHIP2-deficient mice are resistant to obesity induced by high-caloric diets despite normal blood glucose levels and insulin tolerance, though exhibit mild skeletal defects [188]. Consequently, the use of small molecule inhibitors targeting SHIP2 are under investigation for the treatment of diabetes. In addition, it was also shown that the already used anti-diabetes drug metformin facilitates its pharmacological function partly through inhibition of SHIP2 [383, 389].
Collectively, inhibition of SHIP proteins may be a promising therapeutic target to treat BL patients, despite the yet unclear side effects. Especially the combination with established chemotherapeutics could strongly increase the efficiency of the treatment and thus include BL patients, such as the elderly or those with limited access to sufficient medical infrastructure.

7.7 Outlook

The mechanism that connects SHIP activity to the energy metabolism still requires further attention. While there are hints connecting $PI(3,4)P_2$ to metabolic processes, mostly by intracellular trafficking and endocytosis, it would be interesting to understand the underlying details. Especially in the case of endocytotic events such as macropinocytosis for scavenging of extracellular nutrient, which is so far unclear in B cells, and in particular in BL cells. For this purpose, the uptake of labeled dextran has been proven to be an excellent marker to ascertain the macropinocytotic processes in cell cultures [390–392]. To address if the lowered aspartate levels are a direct consequence of the deficient glycolysis it would be interesting to see if supplementation of aspartate or respective metabolic precursors could amend loss of fitness caused by absence of SHIPs.

The fact that limiting access to $PI(3,4)P_2$ at the plasma membrane proved to be lethal for multiple BL cell lines could be further corroborated. Coincidentally, PIT-1, a non-phosphoinositide small molecule agonist targeting $PI(3,4,5)P_3$ thereby preventing binding of PH domains, has displayed strong anti tumoral activity by induction of metabolic stress and apoptosis [393, 394]. This principle may also be exploited to target $PI(3,4)P_2$. While targeting of phosphoinositides could harbour enormous pharmacological potential it has to be noted that these phospho-lipids are significantly relevant for the cellular signal transduction, and unwanted side effects have to be considered.

Finally, the pharmacological potential of inhibition of the SHIP proteins to treat BL should be explored in more detail. Since the inhibition of SHIP2 caused the same increase in sensitivity to inhibition of PI3K as SHIP2 deficiency, the respective inhibitors appear to be specific and may be used in further studies. Consequently, the next step would be to replicate the results in mouse models to validate the cell culture findings before stepping into clinical trials. For this purpose, a genetically engineered mouse model with tumors that resemble BL could be employed to test the efficacy of SHIP2 inhibitors and combinatorial treatments *in vivo*. These tests may be spearheaded by xenocrafts of multiple BL cell lines in WT mice to enable a more realistic tumor microenvironment compared to cell cultures [395]

7.8 Conclusion

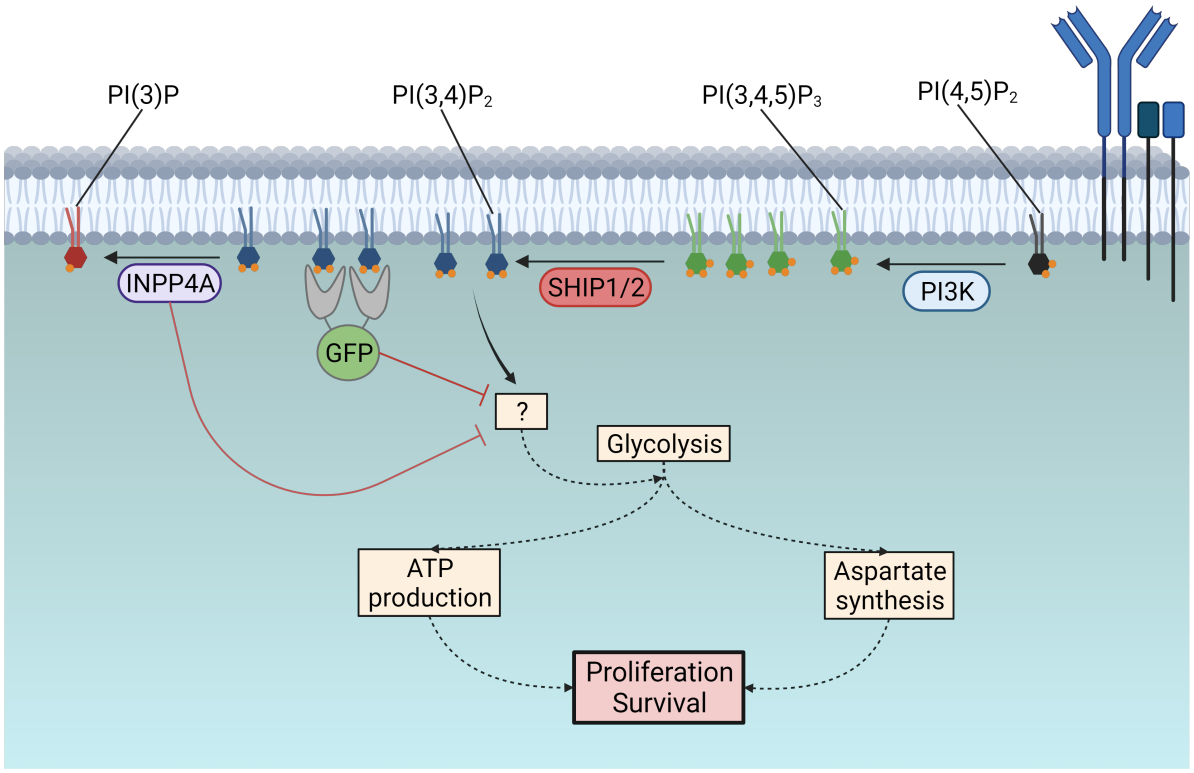

Figure 7.1: **The SHIP proteins contribute to BL fitness by production of PI(3,4)P_2.** Loss of PI(3,4)P_2 at the intracellular leaflet of the plasma membrane either by interfering with SHIP function, targeted degradation by INPP4A or obstruction by GFP-2xTAPP1-PH- negatively impacts BL fitness. While the specific mechanism that connects PI(3,4)P_2 to the glycolysis is yet to elucidate, a decreased pool of PI(3,4)P_2 at the plasma membrane restricts the ATP production and coincides with reduced aspartate levels.

Burkitt lymphoma is an aggressive neoplasm requiring equally aggressive chemotherapy, which cannot be applied to a large patient group. This study could prove a redundant survival and proliferation-promoting effect in tonic BCR signaling-dependent BL cells by SHIP1 and 2. Contrary to the current understanding, these positive effects on BL fitness were independent of AKT activity. Instead, stable plasma membrane levels of the SHIP product PI(3,4)P_2 proved to be crucial for multiple BL cell lines as demonstrated by targeted degradation and obstruction of PI(3,4)P_2 at the plasma membrane. Loss of SHIP2 caused a decrease in PI(3,4)P_2 levels at the plasma membrane, which coincided

with a deficient ATP production mainly via glycolysis. While the glucose uptake and mitochondria remained unchanged by SHIP2 deficiency, the reduced efficiency of the glycolysis may resulted in the observed lowered levels of aspartate, which is crucial for cancer cell proliferation (Figure 7.1). In addition, the loss of SHIP proteins rendered BL cell lines susceptible to inhibition of PI3K, mTOR and PDK1, which may facilitate the development of more efficient combinatorial therapies to combat BL (Figure 7.2).

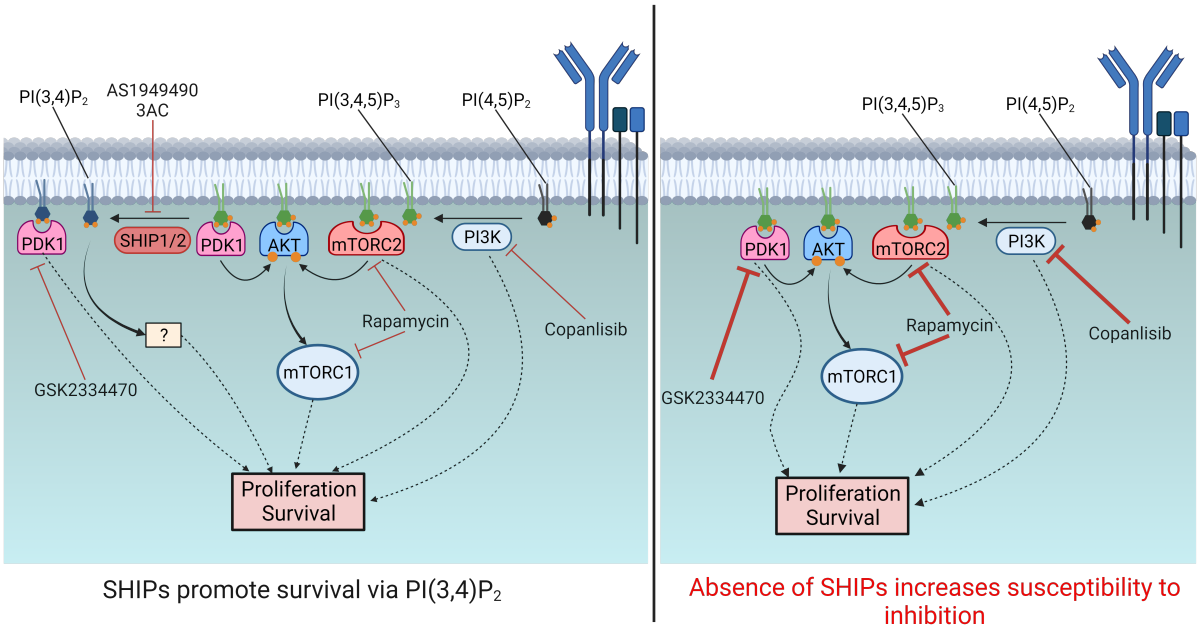

Figure 7.2: **SHIP1/2 deficiency sensitises BL cells to inhibition of other survival signals.** SHIP-deficient cells were markedly more susceptible to inhibition of the PI3K, PDK1 and rapamycin treatment. Despite SHIPs being regarded as negative regulators of AKT activity, the two major phosphorylations of AKT remained mostly unaffected in SHIP-negative cells.

Bibliography

1. Marshall, J. S., Warrington, R., Watson, W. & Kim, H. L. An introduction to immunology and immunopathology. eng. *Allergy, asthma, and clinical immunology : official journal of the Canadian Society of Allergy and Clinical Immunology* **14.** Journal Article Review, 49. ISSN: 1710-1484. eprint: 30263032 (2018).

2. Tonegawa, S. Somatic generation of antibody diversity. eng. *Nature* **302.** Journal Article Research Support, Non-U.S. Gov't Research Support, U.S. Gov't, P.H.S. Review, 575–581. ISSN: 0028-0836. eprint: 6300689 (1983).

3. Reth, M. *et al.* The B-cell antigen receptor complex. eng. *Immunology today* **12.** Journal Article Review, 196–201. ISSN: 0167-5699. eprint: 1878135 (1991).

4. Reth, M. Antigen receptor tail clue. eng. *Nature* **338.** Letter, 383–384. ISSN: 0028-0836. eprint: 2927501 (1989).

5. Treanor, B. B-cell receptor: from resting state to activate. eng. *Immunology* **136.** Journal Article Review, 21–27. eprint: 22269039 (2012).

6. Schmitz, R., Baumann, G. & Gram, H. Catalytic specificity of phosphotyrosine kinases Blk, Lyn, c-Src and Syk as assessed by phage display. eng. *Journal of molecular biology* **260.** Journal Article, 664–677. ISSN: 0022-2836. eprint: 8709147 (1996).

7. Pao, L. I., Famiglietti, S. J. & Cambier, J. C. Asymmetrical phosphorylation and function of immunoreceptor tyrosine-based activation motif tyrosines in B cell antigen receptor signal transduction. eng. *Journal of immunology (Baltimore, Md. : 1950)* **160.** Journal Article, 3305–3314. eprint: 9531288 (1998).

8. Fütterer, K., Wong, J., Grucza, R. A., Chan, A. C. & Waksman, G. Structural basis for Syk tyrosine kinase ubiquity in signal transduction pathways revealed by the crystal structure of its regulatory SH2 domains bound to a dually phosphorylated ITAM peptide. eng. *Journal of molecular biology* **281.** Journal Article Research Support, Non-U.S. Gov't Research Support, U.S. Gov't, P.H.S., 523–537. ISSN: 0022-2836. eprint: 9698567 (1998).

9. Engelke, M., Engels, N., Dittmann, K., Stork, B. & Wienands, J. Ca(2+) signaling in antigen receptor-activated B lymphocytes. eng. *Immunological reviews* **218.** Journal Article Research Support, Non-U.S. Gov't Review, 235–246. ISSN: 0105-2896. eprint: 17624956 (2007).

10. Wienands, J. *et al.* SLP-65: a new signaling component in B lymphocytes which requires expression of the antigen receptor for phosphorylation. eng. *The Journal of experimental medicine* **188.** Journal Article Research Support, Non-U.S. Gov't, 791–795. ISSN: 0022-1007. eprint: 9705962 (1998).

11. Engels, N., Wollscheid, B. & Wienands, J. Association of SLP-65 / BLNK with the B cell antigen receptor through a non-ITAM tyrosine of Ig-a. *European journal of immunology* **31,** 2126–2134. ISSN: 0014-2980 (2001).

12. Hashimoto, S. *et al.* Identification of the SH2 domain binding protein of Bruton's tyrosine kinase as BLNK–functional significance of Btk-SH2 domain in B-cell antigen receptor-coupled calcium signaling. eng. *Blood* **94.** Journal Article Research Support, Non-U.S. Gov't, 2357–2364. ISSN: 0006-4971. eprint: 10498607 (1999).

13. Kadamur, G. & Ross, E. M. Mammalian phospholipase C. eng. *Annual review of physiology* **75.** Journal Article Research Support, N.I.H., Extramural Review, 127–154. eprint: 23140367 (2013).

14. Taylor, C. W. & Tovey, S. C. IP(3) receptors: toward understanding their activation. eng. *Cold Spring Harbor perspectives in biology* **2.** Journal Article Research Support, Non-U.S. Gov't Review, a004010. eprint: 20980441 (2010).

15. Oh-hora, M. & Rao, A. The calcium/NFAT pathway: role in development and function of regulatory T cells. eng. *Microbes and infection* **11.** Journal Article Research Support, N.I.H., Extramural Research Support, Non-U.S. Gov't Review, 612–619. eprint: 19375514 (2009).

16. Hayden, M. S., West, A. P. & Ghosh, S. NF-kappaB and the immune response. eng. *Oncogene* **25.** Journal Article Research Support, N.I.H., Extramural Review, 6758–6780. ISSN: 0950-9232. eprint: 17072327 (2006).

17. Oeckinghaus, A. & Ghosh, S. The NF-kappaB family of transcription factors and its regulation. eng. *Cold Spring Harbor perspectives in biology* **1.** Journal Article Review, a000034. eprint: 20066092 (2009).

18. Khiem, D., Cyster, J. G., Schwarz, J. J. & Black, B. L. A p38 MAPK-MEF2C pathway regulates B-cell proliferation. eng. *Proceedings of the National Academy of Sciences of the United States of America* **105.** Journal Article Research Support, N.I.H., Extramural The authors declare no conflict of interest., 17067–17072. eprint: 18955699 (2008).

19. Yasuda, T. *et al.* ERKs induce expression of the transcriptional repressor Blimp-1 and subsequent plasma cell differentiation. eng. *Science signaling* **4.** Journal Article Research Support, Non-U.S. Gov't, ra25. eprint: 21505187 (2011).

20. Kyriakis, J. M. & Avruch, J. Mammalian mitogen-activated protein kinase signal transduction pathways activated by stress and inflammation. eng. *Physiological reviews* **81.** Journal Article Review, 807–869. ISSN: 0031-9333. eprint: 11274345 (2001).

21. Oh-hora, M., Johmura, S., Hashimoto, A., Hikida, M. & Kurosaki, T. Requirement for Ras guanine nucleotide releasing protein 3 in coupling phospholipase C-gamma2 to Ras in B cell receptor signaling. eng. *The Journal of experimental medicine* **198.** Journal Article Research Support, Non-U.S. Gov't, 1841–1851. ISSN: 0022-1007. eprint: 14676298 (2003).

22. Coughlin, J. J., Stang, S. L., Dower, N. A. & Stone, J. C. RasGRP1 and RasGRP3 regulate B cell proliferation by facilitating B cell receptor-Ras signaling. eng. *Journal of immunology (Baltimore, Md. : 1950)* **175.** Journal Article Research Support, Non-U.S. Gov't, 7179–7184. eprint: 16301621 (2005).

23. Aronheim, A. *et al.* Membrane targeting of the nucleotide exchange factor Sos is sufficient for activating the Ras signaling pathway. eng. *Cell* **78.** Journal Article Research Support, Non-U.S. Gov't, 949–961. eprint: 7923364 (1994).

24. Vanshylla, K. *et al.* Grb2 and GRAP connect the B cell antigen receptor to Erk MAP kinase activation in human B cells. eng. *Scientific reports* **8.** Journal Article Research Support, Non-U.S. Gov't The authors declare no competing interests., 4244. eprint: 29523808 (2018).

25. Ishiai, M. *et al.* BLNK required for coupling Syk to PLC gamma 2 and Rac1-JNK in B cells. eng. *Immunity* **10.** Journal Article Research Support, Non-U.S. Gov't Research Support, U.S. Gov't, P.H.S., 117–125. ISSN: 1074-7613. eprint: 10023776 (1999).

26. Hashimoto, A. *et al.* Involvement of guanosine triphosphatases and phospholipase C-gamma2 in extracellular signal-regulated kinase, c-Jun NH2-terminal kinase, and p38 mitogen-activated protein kinase activation by the B cell antigen receptor. eng. *The Journal of experimental medicine* **188.** Journal Article Research Support, Non-U.S. Gov't Research Support, U.S. Gov't, P.H.S., 1287–1295. ISSN: 0022-1007. eprint: 9763608 (1998).

27. Okada, T., Maeda, A., Iwamatsu, A., Gotoh, K. & Kurosaki, T. BCAP: the tyrosine kinase substrate that connects B cell receptor to phosphoinositide 3-kinase activation. eng. *Immunity* **13.** Journal Article Research Support, Non-U.S. Gov't, 817–827. ISSN: 1074-7613. eprint: 11163197 (2000).

28. Castello, A. *et al.* Nck-mediated recruitment of BCAP to the BCR regulates the PI(3)K-Akt pathway in B cells. eng. *Nature immunology* **14.** Journal Article, 966–975. eprint: 23913047 (2013).

29. Liu, S.-L. *et al.* Quantitative Lipid Imaging Reveals a New Signaling Function of Phosphatidylinositol-3,4-Bisphophate: Isoform- and Site-Specific Activation of Akt. eng. *Molecular cell* **71.** Journal Article Research Support, N.I.H., Extramural Research Support, U.S. Gov't, Non-P.H.S. DECLARATION OF INTERESTS. The authors declare no competing interests., 1092–1104.e5. eprint: 30174291 (2018).

30. DiNitto, J. P. & Lambright, D. G. Membrane and juxtamembrane targeting by PH and PTB domains. eng. *Biochimica et biophysica acta* **1761.** Journal Article Research Support, N.I.H., Extramural Review, 850–867. ISSN: 0006-3002. eprint: 16807090 (2006).

31. Manna, D., Albanese, A., Park, W. S. & Cho, W. Mechanistic basis of differential cellular responses of phosphatidylinositol 3,4-bisphosphate- and phosphatidylinositol 3,4,5-trisphosphate-binding pleckstrin homology domains. eng. *The Journal of biological chemistry* **282.** Journal Article Research Support, N.I.H., Extramural, 32093–32105. ISSN: 0021-9258. eprint: 17823121 (2007).

32. Liu, P. *et al.* PtdIns(3,4,5)P3-Dependent Activation of the mTORC2 Kinase Complex. eng. *Cancer discovery* **5.** Journal Article Research Support, N.I.H., Extramural Conflict of interest: None, 1194–1209. eprint: 26293922 (2015).

33. Sarbassov, D. D., Guertin, D. A., Ali, S. M. & Sabatini, D. M. Phosphorylation and regulation of Akt/PKB by the rictor-mTOR complex. eng. *Science (New York, N.Y.)* **307.** Journal Article Research Support, Non-U.S. Gov't Research Support, U.S. Gov't, P.H.S., 1098–1101. ISSN: 0036-8075. eprint: 15718470 (2005).

34. Chu, N. *et al.* Akt Kinase Activation Mechanisms Revealed Using Protein Semisynthesis. eng. *Cell* **174.** Journal Article Research Support, N.I.H., Extramural Research Support, Non-U.S. Gov't Research Support, U.S. Gov't, Non-P.H.S., 897–907.e14. eprint: 30078705 (2018).

35. Stephens, L. *et al.* Protein kinase B kinases that mediate phosphatidylinositol 3,4,5-trisphosphate-dependent activation of protein kinase B. eng. *Science (New York, N.Y.)* **279.** Journal Article Research Support, Non-U.S. Gov't, 710–714. ISSN: 0036-8075. eprint: 9445477 (1998).

36. Scheid, M. P., Marignani, P. A. & Woodgett, J. R. Multiple phosphoinositide 3-kinase-dependent steps in activation of protein kinase B. eng. *Molecular and cellular biology* **22.** Journal Article Research Support, Non-U.S. Gov't, 6247–6260. ISSN: 0270-7306. eprint: 12167717 (2002).

37. Levina, A., Fleming, K. D., Burke, J. E. & Leonard, T. A. Activation of the essential kinase PDK1 by phosphoinositide-driven trans-autophosphorylation. eng. *Nature communications* **13.** Journal Article Research Support, Non-U.S. Gov't The authors declare no competing interests., 1874. eprint: 35387990 (2022).

38. Hart, J. R. & Vogt, P. K. Phosphorylation of AKT: a mutational analysis. eng. *Oncotarget* **2.** Journal Article, 467–476. eprint: 21670491 (2011).

39. Datta, S. R. *et al.* Akt phosphorylation of BAD couples survival signals to the cell-intrinsic death machinery. eng. *Cell* **91.** Journal Article Research Support, Non-U.S. Gov't Research Support, U.S. Gov't, P.H.S., 231–241. eprint: 9346240 (1997).

40. Cardone, M. H. *et al.* Regulation of cell death protease caspase-9 by phosphorylation. eng. *Science (New York, N.Y.)* **282.** Journal Article Research Support, Non-U.S. Gov't Research Support, U.S. Gov't, Non-P.H.S. Research Support, U.S. Gov't, P.H.S., 1318–1321. ISSN: 0036-8075. eprint: 9812896 (1998).

41. Amin, R. H. & Schlissel, M. S. Foxo1 directly regulates the transcription of recombination-activating genes during B cell development. eng. *Nature immunology* **9.** Journal Article Research Support, N.I.H., Extramural, 613–622. eprint: 18469817 (2008).

42. Gingras, A. C., Kennedy, S. G., O'Leary, M. A., Sonenberg, N. & Hay, N. 4E-BP1, a repressor of mRNA translation, is phosphorylated and inactivated by the Akt(PKB) signaling pathway. eng. *Genes & development* **12.** Journal Article Research Support, Non-U.S. Gov't Research Support, U.S. Gov't, P.H.S., 502–513. ISSN: 0890-9369. eprint: 9472019 (1998).

43. Cross, D. A., Alessi, D. R., Cohen, P., Andjelkovich, M. & Hemmings, B. A. Inhibition of glycogen synthase kinase-3 by insulin mediated by protein kinase B. eng. *Nature* **378.** Journal Article Research Support, Non-U.S. Gov't, 785–789. ISSN: 0028-0836. eprint: 8524413 (1995).

44. Manning, B. D. & Toker, A. AKT/PKB Signaling: Navigating the Network. eng. *Cell* **169.** Journal Article Review Research Support, N.I.H., Extramural Research Support, Non-U.S. Gov't, 381–405. eprint: 28431241 (2017).

45. Goulden, B. D. *et al.* A high-avidity biosensor reveals plasma membrane PI(3,4)P2 is predominantly a class I PI3K signaling product. eng. *The Journal of cell biology* **218.** Journal Article Research Support, N.I.H., Extramural Research Support, U.S. Gov't, Non-P.H.S., 1066–1079. ISSN: 0021-9525. eprint: 30591513 (2019).

46. Liu, Q. *et al.* SHIP is a negative regulator of growth factor receptor-mediated PKB/Akt activation and myeloid cell survival. eng. *Genes & development* **13.** Journal Article, 786–791. ISSN: 0890-9369. eprint: 10197978 (1999).

47. Pedicone, C., Meyer, S. T., Chisholm, J. D. & Kerr, W. G. Targeting SHIP1 and SHIP2 in Cancer. eng. *Cancers* **13.** Journal Article Review W.G.K., C.P. and J.D.C. have patents on small molecules targeting of SHIP1 and SHIP2 in disease. W.G.K. is Chief Scientific Officer and J.D.C. serves on the Scientific Advisory Board of the company "Alterna Therapeutics" for development and commercialization of SHIP inhibitor therapeutics. The other authors have no conflicts to disclose. ISSN: 2072-6694. eprint: 33672717 (2021).

48. Wienands, J., Larbolette, O. & Reth, M. Evidence for a preformed transducer complex organized by the B cell antigen receptor. eng. *Proceedings of the National Academy of Sciences of the United States of America* **93.** Journal Article Research Support, Non-U.S. Gov't, 7865–7870. eprint: 8755568 (1996).

49. Lam, K. P., Kühn, R. & Rajewsky, K. In vivo ablation of surface immunoglobulin on mature B cells by inducible gene targeting results in rapid cell death. eng. *Cell* **90.** Journal Article Research Support, Non-U.S. Gov't, 1073–1083. eprint: 9323135 (1997).

50. Yasuda, S., Zhou, Y., Wang, Y., Yamamura, M. & Wang, J.-Y. A model integrating tonic and antigen-triggered BCR signals to predict the survival of primary B cells. eng. *Scientific reports* **7.** Journal Article Research Support, Non-U.S. Gov't The authors declare that they have no competing interests., 14888. eprint: 29097663 (2017).

51. Reth, M., Wienands, J. & Schamel, W. W. An unsolved problem of the clonal selection theory and the model of an oligomeric B-cell antigen receptor. eng. *Immunological reviews* **176.** Journal Article Research Support, Non-U.S. Gov't Review, 10–18. ISSN: 0105-2896. eprint: 11043764 (2000).

52. Pracht, C., Gimborn, K., Reth, M. & Huber, M. BCR mutants deficient in ligand-independent and more sensitive for ligand-dependent signaling. *European journal of immunology* **32,** 1614. ISSN: 0014-2980 (2002).

53. Monroe, J. G. Ligand-independent tonic signaling in B-cell receptor function. eng. *Current opinion in immunology* **16.** Journal Article Review, 288–295. ISSN: 0952-7915. eprint: 15134777 (2004).

54. Guo, B., Kato, R. M., Garcia-Lloret, M., Wahl, M. I. & Rawlings, D. J. Engagement of the human pre-B cell receptor generates a lipid raft-dependent calcium signaling complex. eng. *Immunity* **13.** Journal Article Research Support, Non-U.S. Gov't Research Support, U.S. Gov't, P.H.S., 243–253. ISSN: 1074-7613. eprint: 10981967 (2000).

55. Gupta, N. & DeFranco, A. L. Visualizing lipid raft dynamics and early signaling events during antigen receptor-mediated B-lymphocyte activation. eng. *Molecular biology of the cell* **14.** Journal Article Research Support, U.S. Gov't, P.H.S., 432–444. eprint: 12589045 (2003).

56. Thomas, M. L. & Brown, E. J. Positive and negative regulation of Src-family membrane kinases by CD45. eng. *Immunology today* **20.** Journal Article Research Support, Non-U.S. Gov't Research Support, U.S. Gov't, P.H.S. Review, 406–411. ISSN: 0167-5699. eprint: 10462740 (1999).

57. Cornall, R. J. *et al.* Polygenic autoimmune traits: Lyn, CD22, and SHP-1 are limiting elements of a biochemical pathway regulating BCR signaling and selection. eng. *Immunity* **8.** Journal Article Research Support, Non-U.S. Gov't Research Support, U.S. Gov't, P.H.S., 497–508. ISSN: 1074-7613. eprint: 9586639 (1998).

58. Monroe, J. G. ITAM-mediated tonic signalling through pre-BCR and BCR complexes. eng. *Nature reviews. Immunology* **6.** Journal Article Review, 283–294. eprint: 16557260 (2006).

59. Srinivasan, L. *et al.* PI3 kinase signals BCR-dependent mature B cell survival. eng. *Cell* **139.** Journal Article Research Support, N.I.H., Extramural Research Support, Non-U.S. Gov't, 573–586. eprint: 19879843 (2009).

60. MacLennan, I. C. Germinal centers. eng. *Annual review of immunology* **12.** Journal Article Review, 117–139. eprint: 8011279 (1994).

61. De Silva, N. S. & Klein, U. Dynamics of B cells in germinal centres. eng. *Nature reviews. Immunology* **15.** Journal Article Research Support, N.I.H., Extramural Review, 137–148. eprint: 25656706 (2015).

62. Garside, P. *et al.* Visualization of specific B and T lymphocyte interactions in the lymph node. eng. *Science (New York, N.Y.)* **281.** Journal Article Research Support, Non-U.S. Gov't Research Support, U.S. Gov't, P.H.S., 96–99. ISSN: 0036-8075. eprint: 9651253 (1998).

63. Okada, T. *et al.* Antigen-engaged B cells undergo chemotaxis toward the T zone and form motile conjugates with helper T cells. eng. *PLoS biology* **3.** Journal Article Research Support, N.I.H., Extramural Research Support, Non-U.S. Gov't Research Support, U.S. Gov't, P.H.S., e150. eprint: 15857154 (2005).

64. Qi, H., Cannons, J. L., Klauschen, F., Schwartzberg, P. L. & Germain, R. N. SAP-controlled T-B cell interactions underlie germinal centre formation. eng. *Nature* **455.** Journal Article Research Support, N.I.H., Intramural, 764–769. ISSN: 0028-0836. eprint: 18843362 (2008).

65. Roco, J. A. *et al.* Class-Switch Recombination Occurs Infrequently in Germinal Centers. eng. *Immunity* **51.** Journal Article Research Support, N.I.H., Extramural Research Support, Non-U.S. Gov't Competing interests. The authors declare no competing interests., 337–350.e7. ISSN: 1074-7613. eprint: 31375460 (2019).

66. Kepler, T. B. & Perelson, A. S. Cyclic re-entry of germinal center B cells and the efficiency of affinity maturation. eng. *Immunology today* **14.** Journal Article Research Support, Non-U.S. Gov't Research Support, U.S. Gov't, P.H.S. Review, 412–415. ISSN: 0167-5699. eprint: 8397781 (1993).

67. Muramatsu, M. *et al.* Class switch recombination and hypermutation require activation-induced cytidine deaminase (AID), a potential RNA editing enzyme. eng. *Cell* **102.** Journal Article Research Support, Non-U.S. Gov't, 553–563. eprint: 11007474 (2000).

68. Doseth, B. *et al.* Uracil-DNA glycosylase in base excision repair and adaptive immunity: species differences between man and mouse. eng. *The Journal of biological chemistry* **286.** Journal Article Research Support, Non-U.S. Gov't, 16669–16680. ISSN: 0021-9258. eprint: 21454529 (2011).

69. Beltman, J. B., Allen, C. D. C., Cyster, J. G. & de Boer, R. J. B cells within germinal centers migrate preferentially from dark to light zone. eng. *Proceedings of the National Academy of Sciences of the United States of America* **108.** Journal Article Research Support, Non-U.S. Gov't The authors declare no conflict of interest., 8755–8760. eprint: 21555569 (2011).

70. Basso, K. & Dalla-Favera, R. Germinal centres and B cell lymphomagenesis. eng. *Nature reviews. Immunology* **15.** Journal Article Review, 172–184. eprint: 25712152 (2015).

71. Allen, C. D. C., Okada, T. & Cyster, J. G. Germinal-center organization and cellular dynamics. eng. *Immunity* **27.** Journal Article Review, 190–202. ISSN: 1074-7613. eprint: 17723214 (2007).

72. Victora, G. D. & Nussenzweig, M. C. Germinal centers. eng. *Annual review of immunology* **30.** Journal Article Review, 429–457. eprint: 22224772 (2012).

73. Heesters, B. A., Myers, R. C. & Carroll, M. C. Follicular dendritic cells: dynamic antigen libraries. eng. *Nature reviews. Immunology* **14.** Journal Article Research Support, N.I.H., Extramural Review, 495–504. eprint: 24948364 (2014).

74. Salisbury, J. L., Condeelis, J. S. & Satir, P. Role of coated vesicles, microfilaments, and calmodulin in receptor-mediated endocytosis by cultured B lymphoblastoid cells. eng. *The Journal of cell biology* **87.** Journal Article Research Support, Non-U.S. Gov't Research Support, U.S. Gov't, P.H.S., 132–141. ISSN: 0021-9525. eprint: 6968316 (1980).

75. Guagliardi, L. E. *et al.* Co-localization of molecules involved in antigen processing and presentation in an early endocytic compartment. eng. *Nature* **343.** Journal Article Research Support, Non-U.S. Gov't Research Support, U.S. Gov't, Non-P.H.S. Research Support, U.S. Gov't, P.H.S. Review, 133–139. ISSN: 0028-0836. eprint: 2404209 (1990).

76. Bryant, P. & Ploegh, H. Class II MHC peptide loading by the professionals. eng. *Current opinion in immunology* **16.** Journal Article Review, 96–102. ISSN: 0952-7915. eprint: 14734116 (2004).

77. Batista, F. D., Iber, D. & Neuberger, M. S. B cells acquire antigen from target cells after synapse formation. eng. *Nature* **411.** Journal Article Research Support, Non-U.S. Gov't, 489–494. ISSN: 0028-0836. eprint: 11373683 (2001).

78. Rock, K. L., Benacerraf, B. & Abbas, A. K. Antigen presentation by hapten-specific B lymphocytes. I. Role of surface immunoglobulin receptors. eng. *The Journal of experimental medicine* **160.** Journal Article Research Support, U.S. Gov't, P.H.S., 1102–1113. ISSN: 0022-1007. eprint: 6207262 (1984).

79. Lanzavecchia, A. Antigen-specific interaction between T and B cells. eng. *Nature* **314.** Journal Article Research Support, Non-U.S. Gov't, 537–539. ISSN: 0028-0836. eprint: 3157869 (1985).

80. Dominguez-Sola, D. *et al.* The proto-oncogene MYC is required for selection in the germinal center and cyclic reentry. eng. *Nature immunology* **13.** Journal Article Research Support, N.I.H., Extramural Research Support, Non-U.S. Gov't, 1083–1091. eprint: 23001145 (2012).

81. Khalil, A. M., Cambier, J. C. & Shlomchik, M. J. B cell receptor signal transduction in the GC is short-circuited by high phosphatase activity. eng. *Science (New York, N.Y.)* **336.** Journal Article Research Support, N.I.H., Extramural, 1178–1181. ISSN: 0036-8075. eprint: 22555432 (2012).

82. Chen, S. T., Oliveira, T. Y., Gazumyan, A., Cipolla, M. & Nussenzweig, M. C. B cell receptor signaling in germinal centers prolongs survival and primes B cells for selection. eng. *Immunity* **56.** Journal Article Research Support, N.I.H., Extramural Research Support, Non-U.S. Gov't Declaration of interests The authors declare no competing interests., 547–561.e7. ISSN: 1074-7613. eprint: 36882061 (2023).

83. Batista, F. D. & Neuberger, M. S. Affinity dependence of the B cell response to antigen: a threshold, a ceiling, and the importance of off-rate. eng. *Immunity* **8.** Journal Article Research Support, Non-U.S. Gov't, 751–759. ISSN: 1074-7613. eprint: 9655489 (1998).

84. Schwickert, T. A. *et al.* A dynamic T cell-limited checkpoint regulates affinity-dependent B cell entry into the germinal center. eng. *The Journal of experimental medicine* **208.** Journal Article Research Support, N.I.H., Extramural, 1243–1252. ISSN: 0022-1007. eprint: 21576382 (2011).

85. Nakagawa, R. *et al.* MicroRNA-155 controls affinity-based selection by protecting c-MYC+ B cells from apoptosis. eng. *The Journal of clinical investigation* **126.** Journal Article Research Support, Non-U.S. Gov't, 377–388. eprint: 26657861 (2016).

86. Mayer, C. T. *et al.* The microanatomic segregation of selection by apoptosis in the germinal center. eng. *Science (New York, N.Y.)* **358.** Journal Article Research Support, N.I.H., Extramural Research Support, Non-U.S. Gov't. ISSN: 0036-8075. eprint: 28935768 (2017).

87. Kawabe, T. *et al.* The immune responses in CD40-deficient mice: impaired immunoglobulin class switching and germinal center formation. eng. *Immunity* **1.** Journal Article Research Support, Non-U.S. Gov't, 167–178. ISSN: 1074-7613. eprint: 7534202 (1994).

88. Renshaw, B. R. *et al.* Humoral immune responses in CD40 ligand-deficient mice. eng. *The Journal of experimental medicine* **180.** Journal Article, 1889–1900. ISSN: 0022-1007. eprint: 7964465 (1994).

89. Han, S., Zheng, B., Dal Porto, J. & Kelsoe, G. In situ studies of the primary immune response to (4-hydroxy-3-nitrophenyl)acetyl. IV. Affinity-dependent, antigen-driven B cell apoptosis in germinal centers as a mechanism for maintaining self-tolerance. eng. *The Journal of experimental medicine* **182.** Journal Article Research Support, U.S. Gov't, P.H.S., 1635–1644. ISSN: 0022-1007. eprint: 7500008 (1995).

90. Shokat, K. M. & Goodnow, C. C. Antigen-induced B-cell death and elimination during germinal-centre immune responses. eng. *Nature* **375.** Journal Article Research Support, Non-U.S. Gov't, 334–338. ISSN: 0028-0836. eprint: 7753200 (1995).

91. Pulendran, B., Kannourakis, G., Nouri, S., Smith, K. G. & Nossal, G. J. Soluble antigen can cause enhanced apoptosis of germinal-centre B cells. eng. *Nature* **375.** Journal Article Research Support, Non-U.S. Gov't Research Support, U.S. Gov't, P.H.S., 331–334. ISSN: 0028-0836. eprint: 7753199 (1995).

92. Sander, S. *et al.* PI3 Kinase and FOXO1 Transcription Factor Activity Differentially Control B Cells in the Germinal Center Light and Dark Zones. eng. *Immunity* **43.** Journal Article Research Support, Non-U.S. Gov't, 1075–1086. ISSN: 1074-7613. eprint: 26620760 (2015).

93. Inoue, T. *et al.* The transcription factor Foxo1 controls germinal center B cell proliferation in response to T cell help. eng. *The Journal of experimental medicine* **214.** Journal Article Research Support, Non-U.S. Gov't Research Support, N.I.H., Extramural, 1181–1198. ISSN: 0022-1007. eprint: 28351982 (2017).

94. Berek, C., Berger, A. & Apel, M. Maturation of the immune response in germinal centers. eng. *Cell* **67.** Comparative Study Journal Article Research Support, Non-U.S. Gov't, 1121–1129. eprint: 1760840 (1991).

95. Jacob, J., Kelsoe, G., Rajewsky, K. & Weiss, U. Intraclonal generation of antibody mutants in germinal centres. eng. *Nature* **354.** Journal Article Research Support, Non-U.S. Gov't Research Support, U.S. Gov't, P.H.S., 389–392. ISSN: 0028-0836. eprint: 1956400 (1991).

96. Victora, G. D. *et al.* Germinal center dynamics revealed by multiphoton microscopy with a photoactivatable fluorescent reporter. eng. *Cell* **143.** Journal Article Research Support, N.I.H., Extramural Research Support, Non-U.S. Gov't, 592–605. eprint: 21074050 (2010).

97. Turner, J. S., Ke, F. & Grigorova, I. L. B Cell Receptor Crosslinking Augments Germinal Center B Cell Selection when T Cell Help Is Limiting. eng. *Cell reports* **25.** Journal Article Research Support, N.I.H., Extramural DECLARATION OF INTERESTS. The authors declare no competing interests., 1395–1403.e4. eprint: 30403996 (2018).

98. Heise, N. *et al.* Germinal center B cell maintenance and differentiation are controlled by distinct NF-kB transcription factor subunits. eng. *The Journal of experimental medicine* **211.** Journal Article Research Support, N.I.H., Extramural, 2103–2118. ISSN: 0022-1007. eprint: 25180063 (2014).

99. Kräutler, N. J. *et al.* Differentiation of germinal center B cells into plasma cells is initiated by high-affinity antigen and completed by Tfh cells. eng. *The Journal of experimental medicine* **214.** Journal Article Research Support, Non-U.S. Gov't, 1259–1267. ISSN: 0022-1007. eprint: 28363897 (2017).

100. Phan, T. G. *et al.* High affinity germinal center B cells are actively selected into the plasma cell compartment. eng. *The Journal of experimental medicine* **203.** Journal Article Research Support, Non-U.S. Gov't, 2419–2424. ISSN: 0022-1007. eprint: 17030950 (2006).

101. Shinnakasu, R. *et al.* Regulated selection of germinal-center cells into the memory B cell compartment. eng. *Nature immunology* **17.** Journal Article Research Support, Non-U.S. Gov't, 861–869. eprint: 27158841 (2016).

102. Suan, D. *et al.* CCR6 Defines Memory B Cell Precursors in Mouse and Human Germinal Centers, Revealing Light-Zone Location and Predominant Low Antigen Affinity. eng. *Immunity* **47.** Journal Article Research Support, Non-U.S. Gov't, 1142–1153.e4. ISSN: 1074-7613. eprint: 29262350 (2017).

103. BURKITT, D. A sarcoma involving the jaws in African children. eng. *The British journal of surgery* **46.** Journal Article, 218–223. ISSN: 0007-1323. eprint: 13628987 (1958).

104. O'CONOR, G. T. & DAVIES, J. N. Malignant tumors in African children. With special reference to malignant lymphoma. eng. *The Journal of pediatrics* **56.** Journal Article, 526–535. ISSN: 0022-3476. eprint: 14428045 (1960).

105. BURKITT, D. A children's cancer dependent on climatic factors. eng. *Nature* **194.** Journal Article, 232–234. ISSN: 0028-0836. eprint: 13874900 (1962).

106. EPSTEIN, M. A., ACHONG, B. G. & BARR, Y. M. VIRUS PARTICLES IN CULTURED LYMPHOBLASTS FROM BURKITT'S LYMPHOMA. eng. *The Lancet* **1.** Journal Article, 702–703. ISSN: 01406736. eprint: 14107961 (1964).

107. Henle, W., Diehl, V., Kohn, G., zur Hausen, H. & Henle, G. Herpes-type virus and chromosome marker in normal leukocytes after growth with irradiated Burkitt cells. eng. *Science (New York, N.Y.)* **157.** Journal Article, 1064–1065. ISSN: 0036-8075. eprint: 6036237 (1967).

108. Manolov, G. & Manolova, Y. Marker band in one chromosome 14 from Burkitt lymphomas. eng. *Nature* **237.** Journal Article, 33–34. ISSN: 0028-0836. eprint: 4113130 (1972).

109. Zech, L., Haglund, U., Nilsson, K. & Klein, G. Characteristic chromosomal abnormalities in biopsies and lymphoid-cell lines from patients with Burkitt and non-Burkitt lymphomas. eng. *International journal of cancer* **17.** Journal Article, 47–56. ISSN: 0020-7136. eprint: 946170 (1976).

110. Dalla-Favera, R. *et al.* Human c-myc onc gene is located on the region of chromosome 8 that is translocated in Burkitt lymphoma cells. eng. *Proceedings of the National Academy of Sciences of the United States of America* **79.** Journal Article Research Support, Non-U.S. Gov't Research Support, U.S. Gov't, P.H.S., 7824–7827. eprint: 6961453 (1982).

111. Taub, R. *et al.* Translocation of the c-myc gene into the immunoglobulin heavy chain locus in human Burkitt lymphoma and murine plasmacytoma cells. eng. *Proceedings of the National Academy of Sciences of the United States of America* **79.** Journal Article Research Support, Non-U.S. Gov't, 7837–7841. eprint: 6818551 (1982).

112. Burkitt, D. P. Etiology of Burkitt's lymphoma–an alternative hypothesis to a vectored virus. eng. *Journal of the National Cancer Institute* **42.** Journal Article Review, 19–28. ISSN: 0027-8874. eprint: 4303830 (1969).

113. Kafuko, G. W. & Burkitt, D. P. Burkitt's lymphoma and malaria. eng. *International journal of cancer* **6.** Journal Article, 1–9. ISSN: 0020-7136. eprint: 4319231 (1970).

114. Swerdlow, S. H. *et al. WHO classification of tumours of haematopoietic and lymphoid tissues* (International agency for research on cancer Lyon, France, 2008).

115. Wright, D. H. Burkitt's lymphoma: a review of the pathology, immunology, and possible etiologic factors. eng. *Pathology annual* **6.** Journal Article Review, 337–363. ISSN: 0079-0184. eprint: 4342309 (1971).

116. Gopal, A. K. *et al.* Idelalisib is effective in patients with high-risk follicular lymphoma and early relapse after initial chemoimmunotherapy. eng. *Blood* **129.** Clinical Trial, Phase II Letter Multicenter Study Research Support, Non-U.S. Gov't, 3037–3039. ISSN: 0006-4971. eprint: 28325864 (2017).

117. Carpenter, L. M. *et al.* Antibodies against malaria and Epstein-Barr virus in childhood Burkitt lymphoma: a case-control study in Uganda. eng. *International journal of cancer* **122.** Journal Article Research Support, Non-U.S. Gov't Research Support, U.S. Gov't, P.H.S., 1319–1323. ISSN: 0020-7136. eprint: 18000823 (2008).

118. Mutalima, N. *et al.* Associations between Burkitt lymphoma among children in Malawi and infection with HIV, EBV and malaria: results from a case-control study. eng. *PloS one* **3.** Journal Article Research Support, Non-U.S. Gov't Competing Interests: The authors have declared that no competing interests exist., e2505. eprint: 18560562 (2008).

119. Aka, P. *et al.* Endemic Burkitt lymphoma is associated with strength and diversity of Plasmodium falciparum malaria stage-specific antigen antibody response. eng. *Blood* **122.** Journal Article Research Support, N.I.H., Intramural Research Support, Non-U.S. Gov't, 629–635. ISSN: 0006-4971. eprint: 23645841 (2013).

120. Redmond, L. S. *et al.* Endemic Burkitt lymphoma: a complication of asymptomatic malaria in sub-Saharan Africa based on published literature and primary data from Uganda, Tanzania, and Kenya. eng. *Malaria journal* **19.** Journal Article Review The authors declare that they have no competing interests., 239. eprint: 32718346 (2020).

121. zur Hausen, H. *et al.* EBV DNA in biopsies of Burkitt tumours and anaplastic carcinomas of the nasopharynx. eng. *Nature* **228.** Journal Article, 1056–1058. ISSN: 0028-0836. eprint: 4320657 (1970).

122. Shannon-Lowe, C., Rickinson, A. B. & Bell, A. I. Epstein-Barr virus-associated lymphomas. eng. *Philosophical transactions of the Royal Society of London. Series B, Biological sciences* **372.** Journal Article Review We declare that we have no competing interests. eprint: 28893938 (2017).

123. de-Thé, G. *et al.* Epidemiological evidence for causal relationship between Epstein-Barr virus and Burkitt's lymphoma from Ugandan prospective study. eng. *Nature* **274.** Journal Article Research Support, U.S. Gov't, P.H.S., 756–761. ISSN: 0028-0836. eprint: 210392 (1978).

124. Rainey, J. J. *et al.* Spatial distribution of Burkitt's lymphoma in Kenya and association with malaria risk. eng. *Tropical medicine & international health : TM & IH* **12.** Journal Article Research Support, Non-U.S. Gov't, 936–943. ISSN: 1360-2276. eprint: 17697088 (2007).

125. Hämmerl, L., Colombet, M., Rochford, R., Ogwang, D. M. & Parkin, D. M. The burden of Burkitt lymphoma in Africa. eng. *Infectious agents and cancer* **14.** Journal Article Competing interestsNo conflicts of interest., 17. ISSN: 1750-9378. eprint: 31388351 (2019).

126. Lavu, E. *et al.* Burkitt lymphoma in Papua New Guinea–40 years on. eng. *Annals of tropical paediatrics* **25.** Journal Article, 191–197. ISSN: 0272-4936. eprint: 16156984 (2005).

127. Molyneux, E. M. *et al.* Burkitt's lymphoma. eng. *Lancet (London, England)* **379.** Journal Article Review, 1234–1244. eprint: 22333947 (2012).

128. Ries, L. A. *et al. SEER cancer statistics review, 1975-2005* (ed U.S. National Institutes of Health) National Cancer Institute.

129. Mbulaiteye, S. M. *et al.* Trimodal age-specific incidence patterns for Burkitt lymphoma in the United States, 1973-2005. eng. *International journal of cancer* **126.** Journal Article Research Support, N.I.H., Intramural, 1732–1739. ISSN: 0020-7136. eprint: 19810101 (2010).

130. Satou, A. *et al.* Epstein-Barr virus (EBV)-positive sporadic burkitt lymphoma: an age-related lymphoproliferative disorder? eng. *The American journal of surgical pathology* **39.** Journal Article, 227–235. eprint: 25321330 (2015).

131. Grande, B. M. *et al.* Genome-wide discovery of somatic coding and noncoding mutations in pediatric endemic and sporadic Burkitt lymphoma. eng. *Blood* **133.** Journal Article Research Support, Non-U.S. Gov't Conflict-of-interest disclosure: The authors declare no competing financial interests., 1313–1324. ISSN: 0006-4971. eprint: 30617194 (2019).

132. Harris, N. L. *et al.* A revised European-American classification of lymphoid neoplasms: a proposal from the International Lymphoma Study Group [see comments]. *Blood* **84,** 1361–1392. ISSN: 0006-4971 (1994).

133. Diebold, J. Burkitt lymphoma. *Pathology and genetics of tumours of haematopoietic and lymphoid tissues,* 181–184 (2001).

134. Coffey, D. G. *et al.* Comparative Analysis of Endemic and Sporadic Burkitt Lymphoma By RNA Sequencing. *Blood* **126,** 3896. ISSN: 0006-4971 (2015).

135. Ziegler, J. L. *et al.* Outbreak of Burkitt's-like lymphoma in homosexual men. eng. *The Lancet* **2.** Case Reports Journal Article Research Support, Non-U.S. Gov't Research Support, U.S. Gov't, P.H.S., 631–633. ISSN: 01406736. eprint: 6125777 (1982).

136. Levine, A. M. Lymphoma complicating immunodeficiency disorders. eng. *Annals of oncology : official journal of the European Society for Medical Oncology* **5 Suppl 2.** Journal Article Review, 29–35. ISSN: 0923-7534. eprint: 8204517 (1994).

137. Mbulaiteye, S. M. *et al.* Burkitt lymphoma risk in U.S. solid organ transplant recipients. eng. *American journal of hematology* **88.** Journal Article Research Support, N.I.H., Intramural, 245–250. eprint: 23386365 (2013).

138. Lim, S. T. *et al.* AIDS-related Burkitt's lymphoma versus diffuse large-cell lymphoma in the pre-highly active antiretroviral therapy (HAART) and HAART eras: significant differences in survival with standard chemotherapy. eng. *Journal of clinical oncology : official journal of the American Society of Clinical Oncology* **23.** Comparative Study Journal Article, 4430–4438. ISSN: 0732-183X. eprint: 15883411 (2005).

139. Mbulaiteye, S. M. *et al.* Epstein-Barr virus patterns in US Burkitt lymphoma tumors from the SEER residual tissue repository during 1979-2009. eng. *APMIS : acta pathologica, microbiologica, et immunologica Scandinavica* **122.** Journal Article Research Support, N.I.H., Extramural Research Support, N.I.H., Intramural Research Support, Non-U.S. Gov't Research Support, U.S. Gov't, P.H.S. The authors reported no potential conflicts of interests., 5–15. eprint: 23607450 (2014).

140. Alderuccio, J. P. *et al.* HIV-associated Burkitt lymphoma: outcomes from a US-UK collaborative analysis. eng. *Blood advances* **5.** Journal Article, 2852–2862. eprint: 34283175 (2021).

141. Wästerlid, T. *et al.* Impact of chemotherapy regimen and rituximab in adult Burkitt lymphoma: a retrospective population-based study from the Nordic Lymphoma Group. eng. *Annals of oncology : official journal of the European Society for Medical Oncology* **24.** Journal Article Research Support, Non-U.S. Gov't, 1879–1886. ISSN: 0923-7534. eprint: 23446093 (2013).

142. Roschewski, M. *et al.* Multicenter Study of Risk-Adapted Therapy With Dose-Adjusted EPOCH-R in Adults With Untreated Burkitt Lymphoma. eng. *Journal of clinical oncology : official journal of the American Society of Clinical Oncology* **38.** Journal Article Research Support, N.I.H., Extramural Research Support, N.I.H., Intramural, 2519–2529. ISSN: 0732-183X. eprint: 32453640 (2020).

143. Smyth, L. *et al.* Burkitt leukaemia/lymphoma: R-CODOX-M/R-IVAC remains gold standard treatment in BL. eng. *Irish journal of medical science* **185.** Journal Article, 773–777. eprint: 25843016 (2016).

144. Intermesoli, T. *et al.* High cure rates in Burkitt lymphoma and leukemia: a Northern Italy Leukemia Group study of the German short intensive rituximab-chemotherapy program. eng. *Haematologica* **98.** Clinical Trial Journal Article Multicenter Study, 1718–1725. eprint: 23753030 (2013).

145. Manji, F. *et al.* Outcomes in Relapsed/Refractory Burkitt Lymphoma: A Multi-Centre Canadian Experience. *Blood* **138,** 2525. ISSN: 0006-4971 (2021).

146. Schmitz, R., Ceribelli, M., Pittaluga, S., Wright, G. & Staudt, L. M. Oncogenic mechanisms in Burkitt lymphoma. eng. *Cold Spring Harbor perspectives in medicine* **4.** Journal Article Review. eprint: 24492847 (2014).

147. Hardianti, M. S. *et al.* Expression of activation-induced cytidine deaminase (AID) in Burkitt lymphoma cells: rare AID-negative cell lines with the unmutated rearranged VH gene. eng. *Leukemia & lymphoma* **45.** Journal Article Research Support, Non-U.S. Gov't, 155–160. eprint: 15061213 (2004).

148. Robbiani, D. F. *et al.* AID is required for the chromosomal breaks in c-myc that lead to c-myc/IgH translocations. eng. *Cell* **135.** Journal Article Research Support, N.I.H., Intramural, 1028–1038. eprint: 19070574 (2008).

149. Scheller, H. *et al.* c-Myc overexpression promotes a germinal center-like program in Burkitt's lymphoma. eng. *Oncogene* **29.** Journal Article Research Support, Non-U.S. Gov't, 888–897. ISSN: 0950-9232. eprint: 19881537 (2010).

150. Shikata, H. *et al.* Role of activation-induced cytidine deaminase in the progression of follicular lymphoma. eng. *Cancer science* **103.** Journal Article, 415–421. eprint: 22168746 (2012).

151. Dang, C. V. *et al.* The c-Myc target gene network. eng. *Seminars in cancer biology* **16.** Journal Article Research Support, N.I.H., Extramural Review, 253–264. eprint: 16904903 (2006).

152. Schmitz, R. *et al.* Burkitt lymphoma pathogenesis and therapeutic targets from structural and functional genomics. eng. *Nature* **490.** Journal Article Research Support, N.I.H., Extramural Research Support, N.I.H., Intramural Research Support, Non-U.S. Gov't, 116–120. ISSN: 0028-0836. eprint: 22885699 (2012).

153. Hemann, M. T. *et al.* Evasion of the p53 tumour surveillance network by tumour-derived MYC mutants. eng. *Nature* **436.** Journal Article Research Support, N.I.H., Extramural Research Support, Non-U.S. Gov't Research Support, U.S. Gov't, P.H.S., 807–811. ISSN: 0028-0836. eprint: 16094360 (2005).

154. López, C. *et al.* Genomic and transcriptomic changes complement each other in the pathogenesis of sporadic Burkitt lymphoma. eng. *Nature communications* **10.** Journal Article Research Support, Non-U.S. Gov't The authors declare no competing interests., 1459. eprint: 30926794 (2019).

155. Evan, G. I. *et al.* Induction of apoptosis in fibroblasts by c-myc protein. eng. *Cell* **69.** Journal Article, 119–128. eprint: 1555236 (1992).

156. Farrell, P. J., Allan, G. J., Shanahan, F., Vousden, K. H. & Crook, T. p53 is frequently mutated in Burkitt's lymphoma cell lines. eng. *The EMBO journal* **10.** Journal Article, 2879–2887. ISSN: 0261-4189. eprint: 1915267 (1991).

157. Meyer, N., Kim, S. S. & Penn, L. Z. The Oscar-worthy role of Myc in apoptosis. eng. *Seminars in cancer biology* **16.** Journal Article Research Support, Non-U.S. Gov't Review, 275–287. eprint: 16945552 (2006).

158. Magrath, I. The pathogenesis of Burkitt's lymphoma. eng. *Advances in cancer research* **55.** Journal Article Review, 133–270. ISSN: 0065-230X. eprint: 2166998 (1990).

159. Young, R. M. & Staudt, L. M. Targeting pathological B cell receptor signalling in lymphoid malignancies. eng. *Nature reviews. Drug discovery* **12.** Journal Article Research Support, N.I.H., Intramural Review, 229–243. eprint: 23449308 (2013).

160. Richter, J. *et al.* Recurrent mutation of the ID3 gene in Burkitt lymphoma identified by integrated genome, exome and transcriptome sequencing. eng. *Nature genetics* **44.** Journal Article Research Support, Non-U.S. Gov't, 1316–1320. ISSN: 1061-4036. eprint: 23143595 (2012).

161. Kwon, K. *et al.* Instructive role of the transcription factor E2A in early B lymphopoiesis and germinal center B cell development. eng. *Immunity* **28.** Journal Article Research Support, Non-U.S. Gov't, 751–762. ISSN: 1074-7613. eprint: 18538592 (2008).

162. Kee, B. L. E and ID proteins branch out. eng. *Nature reviews. Immunology* **9.** Journal Article Research Support, N.I.H., Extramural Research Support, Non-U.S. Gov't Review, 175–184. eprint: 19240756 (2009).

163. Corso, J. *et al.* Elucidation of tonic and activated B-cell receptor signaling in Burkitt's lymphoma provides insights into regulation of cell survival. eng. *Proceedings of the National Academy of Sciences of the United States of America* **113.** Journal Article Research Support, Non-U.S. Gov't, 5688–5693. eprint: 27155012 (2016).

164. Walter, R. *et al.* HSP90 promotes Burkitt lymphoma cell survival by maintaining tonic B-cell receptor signaling. eng. *Blood* **129.** Journal Article Research Support, Non-U.S. Gov't, 598–608. ISSN: 0006-4971. eprint: 28064214 (2017).

165. Wilke, A. C. *et al.* SHMT2 inhibition disrupts the TCF3 transcriptional survival program in Burkitt lymphoma. eng. *Blood* **139.** Journal Article, 538–553. ISSN: 0006-4971. eprint: 34624079 (2022).

166. Dunmire, S. K., Verghese, P. S. & Balfour, H. H. Primary Epstein-Barr virus infection. eng. *Journal of clinical virology : the official publication of the Pan American Society for Clinical Virology* **102.** Journal Article Research Support, Non-U.S. Gov't Review, 84–92. eprint: 29525635 (2018).

167. Rezk, S. A., Zhao, X. & Weiss, L. M. Epstein-Barr virus (EBV)-associated lymphoid proliferations, a 2018 update. eng. *Human pathology* **79.** Journal Article Review, 18–41. eprint: 29885408 (2018).

168. Pope, J. H., Horne, M. K. & Scott, W. Transformation of foetal human keukocytes in vitro by filtrates of a human leukaemic cell line containing herpes-like virus. eng. *International journal of cancer* **3.** Journal Article, 857–866. ISSN: 0020-7136. eprint: 4894385 (1968).

169. Pattengale, P. K., Smith, R. W. & Gerber, P. Selective transformation of B lymphocytes by E.B. virus. eng. *The Lancet* **2.** Journal Article, 93–94. ISSN: 01406736. eprint: 4123640 (1973).

170. Lu, J. *et al.* Epstein-Barr Virus nuclear antigen 1 (EBNA1) confers resistance to apoptosis in EBV-positive B-lymphoma cells through up-regulation of survivin. eng. *Virology* **410.** Journal Article Research Support, N.I.H., Extramural, 64–75. ISSN: 0042-6822. eprint: 21093004 (2011).

171. Martin, F. J. *et al.* Ensembl 2023. eng. *Nucleic acids research* **51.** Journal Article Research Support, N.I.H., Extramural Research Support, Non-U.S. Gov't, D933–D941. eprint: 36318249 (2023).

172. Zhang, Y., Wavreille, A.-S., Kunys, A. R. & Pei, D. The SH2 domains of inositol polyphosphate 5-phosphatases SHIP1 and SHIP2 have similar ligand specificity but different binding kinetics. eng. *Biochemistry* **48.** Journal Article Research Support, N.I.H., Extramural, 11075–11083. ISSN: 0006-2960. eprint: 19839650 (2009).

173. Rohrschneider, L. R., Fuller, J. F., Wolf, I., Liu, Y. & Lucas, D. M. Structure, function, and biology of SHIP proteins. eng. *Genes & development* **14.** Journal Article Research Support, Non-U.S. Gov't Research Support, U.S. Gov't, P.H.S. Review, 505–520. ISSN: 0890-9369. eprint: 10716940 (2000).

174. Krystal, G. *et al.* SHIPs ahoy. eng. *The international journal of biochemistry & cell biology* **31.** Journal Article Review, 1007–1010. ISSN: 1357-2725. eprint: 10582334 (1999).

175. Osborne, M. A. *et al.* The inositol 5'-phosphatase SHIP binds to immunoreceptor signaling motifs and responds to high affinity IgE receptor aggregation. eng. *The Journal of biological chemistry* **271.** Journal Article Research Support, U.S. Gov't, P.H.S., 29271–29278. ISSN: 0021-9258. eprint: 8910587 (1996).

176. De Schutter, J. *et al.* SHIP2 (SH2 domain-containing inositol phosphatase 2) SH2 domain negatively controls SHIP2 monoubiquitination in response to epidermal growth factor. eng. *The Journal of biological chemistry* **284.** Journal Article Research Support, Non-U.S. Gov't, 36062–36076. ISSN: 0021-9258. eprint: 19880507 (2009).

177. Knight, M. J., Leettola, C., Gingery, M., Li, H. & Bowie, J. U. A human sterile alpha motif domain polymerizome. eng. *Protein science : a publication of the Protein Society* **20.** Journal Article Research Support, N.I.H., Extramural, 1697–1706. eprint: 21805519 (2011).

178. Leone, M., Cellitti, J. & Pellecchia, M. The Sam domain of the lipid phosphatase Ship2 adopts a common model to interact with Arap3-Sam and EphA2-Sam. eng. *BMC structural biology* **9.** Journal Article Research Support, N.I.H., Extramural, 59. eprint: 19765305 (2009).

179. Geier, S. J. *et al.* The human SHIP gene is differentially expressed in cell lineages of the bone marrow and blood. eng. *Blood* **89.** Journal Article Research Support, U.S. Gov't, Non-P.H.S. Research Support, U.S. Gov't, P.H.S., 1876–1885. ISSN: 0006-4971. eprint: 9058707 (1997).

180. Gloire, G., Erneux, C. & Piette, J. The role of SHIP1 in T-lymphocyte life and death. eng. *Biochemical Society transactions* **35.** Journal Article Research Support, Non-U.S. Gov't, 277–280. ISSN: 0300-5127. eprint: 17371259 (2007).

181. Erneux, C., Govaerts, C., Communi, D. & Pesesse, X. The diversity and possible functions of the inositol polyphosphate 5-phosphatases. eng. *Biochimica et biophysica acta* **1436.** Journal Article Research Support, Non-U.S. Gov't, 185–199. ISSN: 0006-3002. eprint: 9838104 (1998).

182. Hazen, A. L. *et al.* SHIP is required for a functional hematopoietic stem cell niche. eng. *Blood* **113.** Journal Article Research Support, N.I.H., Extramural Research Support, Non-U.S. Gov't, 2924–2933. ISSN: 0006-4971. eprint: 19074735 (2009).

183. Iyer, S., Viernes, D. R., Chisholm, J. D., Margulies, B. S. & Kerr, W. G. SHIP1 regulates MSC numbers and their osteolineage commitment by limiting induction of the PI3K/Akt/b-catenin/Id2 axis. eng. *Stem cells and development* **23.** Journal Article Research Support, N.I.H., Extramural Research Support, Non-U.S. Gov't, 2336–2351. eprint: 24857423 (2014).

184. Iyer, S., Brooks, R., Gumbleton, M. & Kerr, W. G. SHIP1-expressing mesenchymal stem cells regulate hematopoietic stem cell homeostasis and lineage commitment during aging. eng. *Stem cells and development* **24.** Journal Article Research Support, N.I.H., Extramural Research Support, Non-U.S. Gov't, 1073–1081. eprint: 25525673 (2015).

185. Brooks, R. *et al.* Coordinate expansion of murine hematopoietic and mesenchymal stem cell compartments by SHIPi. eng. *Stem cells (Dayton, Ohio)* **33.** Journal Article Research Support, N.I.H., Extramural Research Support, Non-U.S. Gov't, 848–858. eprint: 25402778 (2015).

186. Pesesse, X., Deleu, S., de Smedt, F., Drayer, L. & Erneux, C. Identification of a second SH2-domain-containing protein closely related to the phosphatidylinositol polyphosphate 5-phosphatase SHIP. eng. *Biochemical and biophysical research communications* **239.** Journal Article Research Support, Non-U.S. Gov't, 697–700. ISSN: 0006-291X. eprint: 9367831 (1997).

187. Clément, S. *et al.* The lipid phosphatase SHIP2 controls insulin sensitivity. eng. *Nature* **409.** Journal Article Research Support, Non-U.S. Gov't, 92–97. ISSN: 0028-0836. eprint: 11343120 (2001).

188. Sleeman, M. W. *et al.* Absence of the lipid phosphatase SHIP2 confers resistance to dietary obesity. eng. *Nature medicine* **11.** Journal Article, 199–205. eprint: 15654325 (2005).

189. Drayer, A. L. *et al.* Cloning and expression of a human placenta inositol 1,3,4,5-tetrakisphosphate and phosphatidylinositol 3,4,5-trisphosphate 5-phosphatase. eng. *Biochemical and biophysical research communications* **225.** Journal Article Research Support, Non-U.S. Gov't, 243–249. ISSN: 0006-291X. eprint: 8769125 (1996).

190. Kisseleva, M. V., Wilson, M. P. & Majerus, P. W. The isolation and characterization of a cDNA encoding phospholipid-specific inositol polyphosphate 5-phosphatase. eng. *The Journal of biological chemistry* **275.** Journal Article Research Support, Non-U.S. Gov't Research Support, U.S. Gov't, P.H.S., 20110–20116. ISSN: 0021-9258. eprint: 10764818 (2000).

191. Odai, H. *et al.* Purification and molecular cloning of SH2- and SH3-containing inositol polyphosphate-5-phosphatase, which is involved in the signaling pathway of granulocyte-macrophage colony-stimulating factor, erythropoietin, and Bcr-Abl. eng. *Blood* **89.** Journal Article Research Support, Non-U.S. Gov't, 2745–2756. ISSN: 0006-4971. eprint: 9108392 (1997).

192. Tridandapani, S. *et al.* Protein interactions of Src homology 2 (SH2) domain-containing inositol phosphatase (SHIP): association with Shc displaces SHIP from FcgammaRIIb in B cells. eng. *Journal of immunology (Baltimore, Md. : 1950)* **162.** Journal Article Research Support, Non-U.S. Gov't Research Support, U.S. Gov't, P.H.S., 1408–1414. eprint: 9973396 (1999).

193. Ono, M., Bolland, S., Tempst, P. & Ravetch, J. V. Role of the inositol phosphatase SHIP in negative regulation of the immune system by the receptor Fc(gamma)RIIB. eng. *Nature* **383.** Journal Article Research Support, Non-U.S. Gov't Research Support, U.S. Gov't, P.H.S., 263–266. ISSN: 0028-0836. eprint: 8805703 (1996).

194. Ono, M. *et al.* Deletion of SHIP or SHP-1 reveals two distinct pathways for inhibitory signaling. eng. *Cell* **90.** Journal Article Research Support, Non-U.S. Gov't Research Support, U.S. Gov't, P.H.S., 293–301. eprint: 9244303 (1997).

195. Manno, B. *et al.* The Dok-3/Grb2 adaptor module promotes inducible association of the lipid phosphatase SHIP with the BCR in a coreceptor-independent manner. eng. *European journal of immunology* **46.** Journal Article Research Support, Non-U.S. Gov't, 2520–2530. eprint: 27550373 (2016).

196. Hüllein, J. *et al.* MDM4 Is Targeted by 1q Gain and Drives Disease in Burkitt Lymphoma. eng. *Cancer research* **79.** Journal Article Research Support, Non-U.S. Gov't Journal Article Research Support, Non-U.S. Gov't, 3125–3138. ISSN: 0008-5472. eprint: 31000522 (2019).

197. Kruse, V. *Identification of therapeutic targets in the Burkitt's lymphoma specific B cell antigen receptor signalling network* Cellular and Molecular Immunology. Dissertation (Georg-August-University Göttingen, Göttingen, 2018).

198. Klein, G., Giovanella, B., Westman, A., Stehlin, J. S. & Mumford, D. An EBV-genome-negative cell line established from an American Burkitt lymphoma; receptor characteristics. EBV infectibility and permanent conversion into EBV-positive sublines by in vitro infection. eng. *Intervirology* **5.** Comparative Study Journal Article, 319–334. ISSN: 0300-5526. eprint: 181343 (1975).

199. Quentmeier, H. *et al.* The LL-100 panel: 100 cell lines for blood cancer studies. eng. *Scientific reports* **9.** Journal Article, 8218. eprint: 31160637 (2019).

200. Cerami, E. *et al.* The cBio cancer genomics portal: an open platform for exploring multidimensional cancer genomics data. eng. *Cancer discovery* **2.** Journal Article Research Support, N.I.H., Extramural Research Support, Non-U.S. Gov't Journal Article Research Support, N.I.H., Extramural Research Support, Non-U.S. Gov't, 401–404. eprint: 22588877 (2012).

201. Gao, J. *et al.* Integrative analysis of complex cancer genomics and clinical profiles using the cBioPortal. eng. *Science signaling* **6.** Journal Article Research Support, N.I.H., Extramural Research Support, Non-U.S. Gov't Competing interests: The authors declare that they have no competing interests., pl1. eprint: 23550210 (2013).

202. Klein, E. *et al.* Surface IgM-kappa specificity on a Burkitt lymphoma cell in vivo and in derived culture lines. eng. *Cancer research* **28.** Journal Article, 1300–1310. ISSN: 0008-5472. eprint: 4174339 (1968).

203. Gabay, C., Ben-Bassat, H., Schlesinger, M. & Laskov, R. Somatic mutations and intraclonal variations in the rearranged Vkappa genes of B-non-Hodgkin's lymphoma cell lines. eng. *European journal of haematology* **63.** Journal Article Research Support, Non-U.S. Gov't Journal Article Research Support, Non-U.S. Gov't, 180–191. ISSN: 0902-4441. eprint: 10485273 (1999).

204. Ben-Bassat, H. *et al.* Establishment in continuous culture of a new type of lymphocyte from a "Burkitt like" malignant lymphoma (line D.G.-75). eng. *International journal of cancer* **19.** Case Reports Journal Article Research Support, U.S. Gov't, P.H.S. Case Reports Journal Article Research Support, U.S. Gov't, P.H.S., 27–33. ISSN: 0020-7136. eprint: 188769 (1977).

205. Wiman, K. G., Magnusson, K. P., Ramqvist, T. & Klein, G. Mutant p53 detected in a majority of Burkitt lymphoma cell lines by monoclonal antibody PAb240. eng. *Oncogene* **6.** Journal Article Research Support, Non-U.S. Gov't Research Support, U.S. Gov't, P.H.S. Journal Article Research Support, Non-U.S. Gov't Research Support, U.S. Gov't, P.H.S., 1633–1639. ISSN: 0950-9232. eprint: 1923530 (1991).

206. Ierano, C. *et al.* Loss of the proteins Bak and Bax prevents apoptosis mediated by histone deacetylase inhibitors. eng. *Cell Cycle* **12.** Journal Article Journal Article Research Support, N.I.H., Extramural Research Support, Non-U.S. Gov't, 2829–2838. ISSN: 1538-4101. eprint: 23966164 (2013).

207. Tsherniak, A. *et al.* Defining a Cancer Dependency Map. eng. *Cell* **170.** Journal Article, 564–576.e16. eprint: 28753430. https://www.sciencedirect.com/science/article/pii/S0092867417306517 (2017).

208. Pulvertaft, R. CYTOLOGY OF BURKITT'S TUMOUR (AFRICAN LYMPHOMA). *The Lancet* **283.** PII: S0140673664923451, 238–240. ISSN: 01406736 (1964).

209. Adams, A. Replication of latent Epstein-Barr virus genomes in Raji cells. eng. *Journal of virology* **61.** Journal Article Research Support, Non-U.S. Gov't Journal Article Research Support, Non-U.S. Gov't, 1743–1746. ISSN: 0022-538X. eprint: 3033303 (1987).

210. DSMZ. *RAJI. ACC319* (ed Leibniz Institute) German Collection of Microorganisms and Cell Cultures GmbH. https://www.dsmz.de/collection/catalogue/details/culture/ACC-319 (2022).

211. Engelberts, P. J. *et al.* Type I CD20 Antibodies Recruit the B Cell Receptor for Complement-Dependent Lysis of Malignant B Cells. eng. *Journal of immunology (Baltimore, Md. : 1950)* **197.** Journal Article, 4829–4837. eprint: 27807190 (2016).

212. Fellmann, C. *et al.* An optimized microRNA backbone for effective single-copy RNAi. eng. *Cell reports* **5.** Journal Article Research Support, Non-U.S. Gov't, 1704–1713. eprint: 24332856 (2013).

213. Howard Judelson. *Guidelines for designing primers* https://www.researchgate.net/profile/Maurice_Ekpenyong2/post/How_can_I_design_primers_for_gene_knock_out_by_homologous_recombination/attachment/5c456201cfe4a7645512b6a9/AS%3A717391814205443%401548050945564/download/Primer+design+guidelines.pdf.

214. Sauter, E. J., Kutsche, L. K., Klapper, S. D. & Busskamp, V. Induced Neurons for the Study of Neurodegenerative and Neurodevelopmental Disorders. eng. *Methods in molecular biology (Clifton, N.J.)* **1942.** Journal Article Research Support, Non-U.S. Gov't, 101–121. eprint: 30900179 (2019).

215. Román-Fernández, Á. *et al.* The phospholipid PI(3,4)P2 is an apical identity determinant. eng. *Nature communications* **9.** Journal Article Research Support, N.I.H., Extramural Research Support, Non-U.S. Gov't The authors declare no competing interests., 5041. eprint: 30487552 (2018).

216. Cary, L. C. *et al.* Transposon mutagenesis of baculoviruses: analysis of Trichoplusia ni transposon IFP2 insertions within the FP-locus of nuclear polyhedrosis viruses. eng. *Virology* **172.** Journal Article Research Support, U.S. Gov't, P.H.S., 156–169. ISSN: 0042-6822. eprint: 2549707 (1989).

217. Chen, Q. *et al.* Structural basis of seamless excision and specific targeting by piggyBac transposase. eng. *Nature communications* **11.** Journal Article Research Support, N.I.H., Extramural Research Support, N.I.H., Intramural Research Support, U.S. Gov't, Non-P.H.S. The authors declare no competing interests., 3446. eprint: 32651359 (2020).

218. Mohr, S. *et al.* Hoxa9 and Meis1 Cooperatively Induce Addiction to Syk Signaling by Suppressing miR-146a in Acute Myeloid Leukemia. eng. *Cancer Cell* **31.** Journal Article, 549–562.e11. ISSN: 1535-6108. eprint: 28399410 (2017).

219. Tyanova, S., Temu, T. & Cox, J. The MaxQuant computational platform for mass spectrometry-based shotgun proteomics. eng. *Nature protocols* **11.** Journal Article, 2301–2319. eprint: 27809316 (2016).

220. Paull, K. D. *et al.* The synthesis of XTT: A new tetrazolium reagent that is bioreducible to a water-soluble formazan. *Journal of Heterocyclic Chemistry* **25,** 911–914. ISSN: 0022152X (1988).

221. Roehm, N. W., Rodgers, G. H., Hatfield, S. M. & Glasebrook, A. L. An improved colorimetric assay for cell proliferation and viability utilizing the tetrazolium salt XTT. eng. *Journal of immunological methods* **142.** Comparative Study Journal Article, 257–265. ISSN: 0022-1759. eprint: 1919029 (1991).

222. Jost, L. M., Kirkwood, J. M. & Whiteside, T. L. Improved short- and long-term XTT-based colorimetric cellular cytotoxicity assay for melanoma and other tumor cells. eng. *Journal of immunological methods* **147.** Comparative Study Journal Article Research Support, Non-U.S. Gov't, 153–165. ISSN: 0022-1759. eprint: 1548398 (1992).

223. Laemmli, U. K. Cleavage of structural proteins during the assembly of the head of bacteriophage T4. eng. *Nature* **227.** Journal Article, 680–685. ISSN: 0028-0836. eprint: 5432063 (1970).

224. Weber, K. & Osborn, M. The reliability of molecular weight determinations by dodecyl sulfate-polyacrylamide gel electrophoresis. eng. *The Journal of biological chemistry* **244.** Journal Article, 4406–4412. ISSN: 0021-9258. eprint: 5806584 (1969).

225. Towbin, H., Staehelin, T. & Gordon, J. Electrophoretic transfer of proteins from polyacrylamide gels to nitrocellulose sheets: procedure and some applications. eng. *Proceedings of the National Academy of Sciences of the United States of America* **76.** Journal Article, 4350–4354. eprint: 388439 (1979).

226. Roberts, R. J. Restriction endonucleases. eng. *CRC critical reviews in biochemistry* **4.** Journal Article Research Support, U.S. Gov't, Non-P.H.S. Research Support, U.S. Gov't, P.H.S. Review, 123–164. ISSN: 0045-6411. eprint: 795607 (1976).

227. LePecq, J. B. & Paoletti, C. A fluorescent complex between ethidium bromide and nucleic acids. Physical-chemical characterization. eng. *Journal of molecular biology* **27.** Journal Article, 87–106. ISSN: 0022-2836. eprint: 6033613 (1967).

228. Suzuki, T., Fujikura, K., Higashiyama, T. & Takata, K. DNA staining for fluorescence and laser confocal microscopy. eng. *The journal of histochemistry and cytochemistry : official journal of the Histochemistry Society* **45.** Journal Article Research Support, Non-U.S. Gov't, 49–53. ISSN: 0022-1554. eprint: 9010468 (1997).

229. Watson, J. V., Chambers, S. H. & Smith, P. J. A pragmatic approach to the analysis of DNA histograms with a definable G1 peak. eng. *Cytometry* **8.** Journal Article, 1–8. ISSN: 0196-4763. eprint: 3803091 (1987).

230. Reutelingsperger, C. P. & van Heerde, W. L. Annexin V, the regulator of phosphatidylserine-catalyzed inflammation and coagulation during apoptosis. eng. *Cellular and molecular life sciences : CMLS* **53.** Journal Article Research Support, Non-U.S. Gov't Review, 527–532. ISSN: 1420-682X. eprint: 9230931 (1997).

231. Latt, S. A. Fluorescent probes of chromosome structure and replication. eng. *Canadian journal of genetics and cytology. Journal canadien de genetique et de cytologie* **19.** Journal Article Review, 603–623. ISSN: 0008-4093. eprint: 76502 (1977).

232. Kuwana, T. & Newmeyer, D. D. Bcl-2-family proteins and the role of mitochondria in apoptosis. eng. *Current opinion in cell biology* **15.** Journal Article Review, 691–699. ISSN: 0955-0674. eprint: 14644193 (2003).

233. Kim, H.-E., Du, F., Fang, M. & Wang, X. Formation of apoptosome is initiated by cytochrome c-induced dATP hydrolysis and subsequent nucleotide exchange on Apaf-1. eng. *Proceedings of the National Academy of Sciences of the United States of America* **102.** Journal Article Research Support, N.I.H., Extramural Research Support, Non-U.S. Gov't, 17545–17550. eprint: 16251271 (2005).

234. Ryan, J., Montero, J., Rocco, J. & Letai, A. iBH3: simple, fixable BH3 profiling to determine apoptotic priming in primary tissue by flow cytometry. eng. *Biological chemistry* **397.** Journal Article, 671–678. eprint: 26910743 (2016).

235. Bojarczuk, K. *et al.* Targeted inhibition of PI3Ka/d is synergistic with BCL-2 blockade in genetically defined subtypes of DLBCL. eng. *Blood* **133.** Journal Article Research Support, N.I.H., Extramural Research Support, Non-U.S. Gov't Conflict-of-interest disclosure: M.A.S. has received research funding from Bayer, Bristol-Myers Squibb, and Merck; served as a scientific advisor to Bristol-Myers Squibb; and received honoraria from AstraZeneca. A.L. reports sponsored research and consulting from AbbVie, Novartis, and Astra Zeneca and is a founder and equity holder in Flash Therapeutics and Vivid Bioscience. The remaining authors declare no competing financial interests., 70–80. ISSN: 0006-4971. eprint: 30322870 (2019).

236. Yoshioka, K. *et al.* A novel fluorescent derivative of glucose applicable to the assessment of glucose uptake activity of Escherichia coli. eng. *Biochimica et biophysica acta* **1289.** Journal Article, 5–9. ISSN: 0006-3002. eprint: 8605231 (1996).

237. Yamada, K., Saito, M., Matsuoka, H. & Inagaki, N. A real-time method of imaging glucose uptake in single, living mammalian cells. eng. *Nature protocols* **2.** Journal Article, 753–762. eprint: 17406637 (2007).

238. Strebel, A., Harr, T., Bachmann, F., Wernli, M. & Erb, P. Green fluorescent protein as a novel tool to measure apoptosis and necrosis. *Cytometry* **43,** 126–133. ISSN: 0196-4763 (2001).

239. Métivier, D. *et al.* Cytofluorometric detection of mitochondrial alterations in early CD95/Fas/APO-1-triggered apoptosis of Jurkat T lymphoma cells. Comparison of seven mitochondrion-specific fluorochromes. eng. *Immunology letters* **61.** Comparative Study Journal Article Research Support, Non-U.S. Gov't, 157–163. ISSN: 0165-2478. eprint: 9657269 (1998).

240. Cottet-Rousselle, C., Ronot, X., Leverve, X. & Mayol, J.-F. Cytometric assessment of mitochondria using fluorescent probes. eng. *Cytometry. Part A : the journal of the International Society for Analytical Cytology* **79.** Journal Article Review, 405–425. eprint: 21595013 (2011).

241. Suwa, A. *et al.* Discovery and functional characterization of a novel small molecule inhibitor of the intracellular phosphatase, SHIP2. eng. *British journal of pharmacology* **158.** Journal Article, 879–887. eprint: 19694723 (2009).

242. Griesbeck, O., Baird, G. S., Campbell, R. E., Zacharias, D. A. & Tsien, R. Y. Reducing the environmental sensitivity of yellow fluorescent protein. Mechanism and applications. eng. *The Journal of biological chemistry* **276.** Journal Article Research Support, Non-U.S. Gov't Research Support, U.S. Gov't, P.H.S., 29188–29194. ISSN: 0021-9258. eprint: 11387331 (2001).

243. Torres, R. M., Flaswinkel, H., Reth, M. & Rajewsky, K. Aberrant B cell development and immune response in mice with a compromised BCR complex. eng. *Science (New York, N.Y.)* **272.** Journal Article Research Support, Non-U.S. Gov't, 1804–1808. ISSN: 0036-8075. eprint: 8650582 (1996).

244. Brahmbhatt, H., Uehling, D., Al-Awar, R., Leber, B. & Andrews, D. Small molecules reveal an alternative mechanism of Bax activation. eng. *The Biochemical journal* **473.** Journal Article Research Support, Non-U.S. Gov't, 1073–1083. eprint: 26916338 (2016).

245. Lin, W.-C. *et al.* Helicobacter pylori sensitizes TNF-related apoptosis-inducing ligand (TRAIL)-mediated apoptosis in human gastric epithelial cells through regulation of FLIP. eng. *Cell death & disease* **5.** Journal Article Research Support, Non-U.S. Gov't, e1109. eprint: 24603337 (2014).

246. McIlwain, D. R., Berger, T. & Mak, T. W. Caspase functions in cell death and disease. eng. *Cold Spring Harbor perspectives in biology* **5.** Journal Article Review, a008656. eprint: 23545416 (2013).

247. Walsh, J. G. *et al.* Executioner caspase-3 and caspase-7 are functionally distinct proteases. eng. *Proceedings of the National Academy of Sciences of the United States of America* **105.** Journal Article, 12815–12819. eprint: 18723680 (2008).

248. Tait, S. W. G. & Green, D. R. Mitochondrial regulation of cell death. eng. *Cold Spring Harbor perspectives in biology* **5.** Journal Article Review. eprint: 24003207 (2013).

249. Moldoveanu, T., Follis, A. V., Kriwacki, R. W. & Green, D. R. Many players in BCL-2 family affairs. eng. *Trends in biochemical sciences* **39.** Journal Article Research Support, N.I.H., Extramural Research Support, Non-U.S. Gov't Review, 101–111. ISSN: 0968-0004. eprint: 24503222 (2014).

250. Wei, M. C. *et al.* tBID, a membrane-targeted death ligand, oligomerizes BAK to release cytochrome c. eng. *Genes & development* **14.** Journal Article, 2060–2071. ISSN: 0890-9369. eprint: 10950869 (2000).

251. Moldoveanu, T. *et al.* BID-induced structural changes in BAK promote apoptosis. eng. *Nature structural & molecular biology* **20.** Journal Article Research Support, N.I.H., Extramural Research Support, Non-U.S. Gov't, 589–597. eprint: 23604079 (2013).

252. Czabotar, P. E. *et al.* Bax crystal structures reveal how BH3 domains activate Bax and nucleate its oligomerization to induce apoptosis. eng. *Cell* **152.** Journal Article Research Support, Non-U.S. Gov't, 519–531. eprint: 23374347 (2013).

253. Shamas-Din, A., Brahmbhatt, H., Leber, B. & Andrews, D. W. BH3-only proteins: Orchestrators of apoptosis. eng. *Biochimica et biophysica acta* **1813.** Journal Article Review, 508–520. ISSN: 0006-3002. eprint: 21146563 (2011).

254. Latt, S. A., Stetten, G., Juergens, L. A., Willard, H. F. & Scher, C. D. Recent developments in the detection of deoxyribonucleic acid synthesis by 33258 Hoechst fluorescence. eng. *The journal of histochemistry and cytochemistry : official journal of the Histochemistry Society* **23.** Journal Article Research Support, U.S. Gov't, P.H.S. Review, 493–505. ISSN: 0022-1554. eprint: 1095650 (1975).

255. Gostimskaya, I. S., Grivennikova, V. G., Zharova, T. V., Bakeeva, L. E. & Vinogradov, A. D. In situ assay of the intramitochondrial enzymes: use of alamethicin for permeabilization of mitochondria. eng. *Analytical biochemistry* **313.** Journal Article Research Support, Non-U.S. Gov't, 46–52. ISSN: 0003-2697. eprint: 12576057 (2003).

256. Sarosiek, K. A. *et al.* Developmental Regulation of Mitochondrial Apoptosis by c-Myc Governs Age- and Tissue-Specific Sensitivity to Cancer Therapeutics. eng. *Cancer Cell* **31.** Journal Article Research Support, Non-U.S. Gov't Research Support, N.I.H., Extramural, 142–156. ISSN: 1535-6108. eprint: 28017613 (2017).

257. Kim, D. H. & Rossi, J. J. Strategies for silencing human disease using RNA interference. eng. *Nature reviews. Genetics* **8.** Journal Article Research Support, N.I.H., Extramural Review, 173–184. ISSN: 1471-0056. eprint: 17304245 (2007).

258. Mclaurin, J. D. & Weiner, O. D. Multiple sources of signal amplification within the B-cell Ras/MAPK pathway. eng. *Molecular biology of the cell* **30.** Journal Article Research Support, N.I.H., Extramural Research Support, U.S. Gov't, Non-P.H.S., 1610–1620. eprint: 31042097 (2019).

259. Liu, N. *et al.* BAY 80-6946 is a highly selective intravenous PI3K inhibitor with potent p110a and p110d activities in tumor cell lines and xenograft models. eng. *Molecular cancer therapeutics* **12.** Journal Article Research Support, Non-U.S. Gov't, 2319–2330. eprint: 24170767 (2013).

260. Liu, J. *et al.* ERK-dependent IL-6 positive feedback loop mediates resistance against a combined treatment using danusertib and BKM120 in Burkitt lymphoma cell lines. eng. *Leukemia & lymphoma* **60.** Journal Article Research Support, Non-U.S. Gov't, 2532–2540. eprint: 30947576 (2019).

261. Gururajan, M. *et al.* c-Jun N-terminal kinase (JNK) is required for survival and proliferation of B-lymphoma cells. eng. *Blood* **106.** Journal Article Research Support, N.I.H., Extramural Research Support, U.S. Gov't, P.H.S., 1382–1391. ISSN: 0006-4971. eprint: 15890690 (2005).

262. Lee, S. *et al.* DUSP16 is an epigenetically regulated determinant of JNK signalling in Burkitt's lymphoma. eng. *British journal of cancer* **103.** Journal Article Research Support, Non-U.S. Gov't The authors declare no conflict of interest., 265–274. eprint: 20551953 (2010).

263. Davies, B. R. *et al.* Preclinical pharmacology of AZD5363, an inhibitor of AKT: pharmacodynamics, antitumor activity, and correlation of monotherapy activity with genetic background. eng. *Molecular cancer therapeutics* **11.** Journal Article Randomized Controlled Trial Research Support, Non-U.S. Gov't, 873–887. eprint: 22294718 (2012).

264. Sarbassov, D. D. *et al.* Prolonged rapamycin treatment inhibits mTORC2 assembly and Akt/PKB. eng. *Molecular cell* **22.** Comparative Study Journal Article Research Support, N.I.H., Extramural Research Support, Non-U.S. Gov't Research Support, U.S. Gov't, Non-P.H.S., 159–168. eprint: 16603397 (2006).

265. Kang, S. A. *et al.* mTORC1 phosphorylation sites encode their sensitivity to starvation and rapamycin. eng. *Science (New York, N.Y.)* **341.** Journal Article Research Support, N.I.H., Extramural Research Support, Non-U.S. Gov't Research Support, U.S. Gov't, Non-P.H.S., 1236566. ISSN: 0036-8075. eprint: 23888043 (2013).

266. Ong, S.-E. *et al.* Stable isotope labeling by amino acids in cell culture, SILAC, as a simple and accurate approach to expression proteomics. eng. *Molecular & cellular proteomics : MCP* **1.** Journal Article Research Support, Non-U.S. Gov't, 376–386. ISSN: 1535-9476. eprint: 12118079 (2002).

267. Zhu, H., Pan, S., Gu, S., Bradbury, E. M. & Chen, X. Amino acid residue specific stable isotope labeling for quantitative proteomics. eng. *Rapid communications in mass spectrometry : RCM* **16.** Journal Article Research Support, Non-U.S. Gov't Research Support, U.S. Gov't, Non-P.H.S., 2115–2123. ISSN: 0951-4198. eprint: 12415544 (2002).

268. Chen, L. *et al.* Tonic B-Cell Receptor Signaling Promotes the Survival of Diffuse Large B-Cell Lymphomas: Identification of SYK as a Rational Treatment Target. *Blood* **108,** 226. ISSN: 0006-4971 (2006).

269. Krishan, A. Rapid flow cytofluorometric analysis of mammalian cell cycle by propidium iodide staining. eng. *The Journal of cell biology* **66.** Comparative Study Journal Article Research Support, U.S. Gov't, P.H.S., 188–193. ISSN: 0021-9525. eprint: 49354 (1975).

270. Tanner, L. B. *et al.* Four Key Steps Control Glycolytic Flux in Mammalian Cells. eng. *Cell systems* **7.** Journal Article Research Support, N.I.H., Extramural Research Support, Non-U.S. Gov't DECLARATION OF INTERESTS. The authors declare no competing interests., 49–62.e8. ISSN: 2405-4712. eprint: 29960885 (2018).

271. WARBURG, O. On the origin of cancer cells. eng. *Science (New York, N.Y.)* **123.** Journal Article, 309–314. ISSN: 0036-8075. eprint: 13298683 (1956).

272. Yamada, K. *et al.* Measurement of glucose uptake and intracellular calcium concentration in single, living pancreatic beta-cells. eng. *The Journal of biological chemistry* **275.** Journal Article Research Support, Non-U.S. Gov't, 22278–22283. ISSN: 0021-9258. eprint: 10748091 (2000).

273. Doughty, C. A. *et al.* Antigen receptor-mediated changes in glucose metabolism in B lymphocytes: role of phosphatidylinositol 3-kinase signaling in the glycolytic control of growth. eng. *Blood* **107.** Journal Article Research Support, N.I.H., Extramural, 4458–4465. ISSN: 0006-4971. eprint: 16449529 (2006).

274. Klein, K. *et al.* Role of Mitochondria in Cancer Immune Evasion and Potential Therapeutic Approaches. eng. *Frontiers in immunology* **11.** Journal Article Research Support, N.I.H., Extramural Review, 573326. eprint: 33178201 (2020).

275. Henson, S. M. *et al.* p38 signaling inhibits mTORC1-independent autophagy in senescent human $CD8^+$ T cells. eng. *The Journal of clinical investigation* **124.** Journal Article Research Support, Non-U.S. Gov't, 4004–4016. eprint: 25083993 (2014).

276. Fischer, M. *et al.* Early effector maturation of naïve human CD8+ T cells requires mitochondrial biogenesis. eng. *European journal of immunology* **48.** Journal Article Research Support, Non-U.S. Gov't, 1632–1643. eprint: 30028501 (2018).

277. BROWN, J. Effects of 2-deoxyglucose on carbohydrate metablism: review of the literature and studies in the rat. eng. *Metabolism: clinical and experimental* **11.** Journal Article, 1098–1112. ISSN: 0026-0495. eprint: 13873661 (1962).

278. Desousa, B. R. *et al.* Calculation of ATP production rates using the Seahorse XF Analyzer. eng. *EMBO reports.* Journal Article, e56380. eprint: 37548091 (2023).

279. Pang, Z. *et al.* MetaboAnalyst 5.0: narrowing the gap between raw spectra and functional insights. eng. *Nucleic acids research* **49.** Journal Article Research Support, N.I.H., Extramural Research Support, Non-U.S. Gov't, W388–W396. eprint: 34019663 (2021).

280. Garcia, P. *et al.* The pleckstrin homology domain of phospholipase C-delta 1 binds with high affinity to phosphatidylinositol 4,5-bisphosphate in bilayer membranes. eng. *Biochemistry* **34.** Comparative Study Journal Article Research Support, Non-U.S. Gov't Research Support, U.S. Gov't, Non-P.H.S. Research Support, U.S. Gov't, P.H.S., 16228–16234. ISSN: 0006-2960. eprint: 8519781 (1995).

281. Rizzo, M. A., Springer, G., Segawa, K., Zipfel, W. R. & Piston, D. W. Optimization of pairings and detection conditions for measurement of FRET between cyan and yellow fluorescent proteins. eng. *Microscopy and microanalysis : the official journal of Microscopy Society of America, Microbeam Analysis Society, Microscopical Society of Canada* **12.** Journal Article Research Support, N.I.H., Extramural Research Support, U.S. Gov't, Non-P.H.S., 238–254. ISSN: 1431-9276. eprint: 17481360 (2006).

282. Norris, F. A. & Majerus, P. W. Hydrolysis of phosphatidylinositol 3,4-bisphosphate by inositol polyphosphate 4-phosphatase isolated by affinity elution chromatography. eng. *The Journal of biological chemistry* **269.** Journal Article Research Support, U.S. Gov't, P.H.S., 8716–8720. ISSN: 0021-9258. eprint: 8132601 (1994).

283. Norris, F. A., Atkins, R. C. & Majerus, P. W. The cDNA cloning and characterization of inositol polyphosphate 4-phosphatase type II. Evidence for conserved alternative splicing in the 4-phosphatase family. eng. *The Journal of biological chemistry* **272.** Journal Article Research Support, Non-U.S. Gov't Research Support, U.S. Gov't, P.H.S., 23859–23864. ISSN: 0021-9258. eprint: 9295334 (1997).

284. Ferron, M. & Vacher, J. Characterization of the murine Inpp4b gene and identification of a novel isoform. eng. *Gene* **376.** Journal Article Research Support, Non-U.S. Gov't, 152–161. ISSN: 0378-1119. eprint: 16631325 (2006).

285. Ivetac, I. *et al.* The type Ialpha inositol polyphosphate 4-phosphatase generates and terminates phosphoinositide 3-kinase signals on endosomes and the plasma membrane. eng. *Molecular biology of the cell* **16.** Journal Article Research Support, N.I.H., Extramural Research Support, Non-U.S. Gov't Research Support, U.S. Gov't, P.H.S., 2218–2233. eprint: 15716355 (2005).

286. Brooks, R. *et al.* SHIP1 inhibition increases immunoregulatory capacity and triggers apoptosis of hematopoietic cancer cells. eng. *Journal of immunology (Baltimore, Md. : 1950)* **184.** Journal Article Research Support, N.I.H., Extramural Research Support, Non-U.S. Gov't Disclosures. The authors have no financial conflicts of interest., 3582–3589. eprint: 20200281 (2010).

287. Blake, J. F. *et al.* Discovery and preclinical pharmacology of a selective ATP-competitive Akt inhibitor (GDC-0068) for the treatment of human tumors. eng. *Journal of medicinal chemistry* **55.** Journal Article, 8110–8127. eprint: 22934575 (2012).

288. Pullen, N. *et al.* Phosphorylation and activation of p70s6k by PDK1. eng. *Science (New York, N.Y.)* **279.** Journal Article Research Support, Non-U.S. Gov't, 707–710. ISSN: 0036-8075. eprint: 9445476 (1998).

289. Jensen, C. J. *et al.* 90-kDa ribosomal S6 kinase is phosphorylated and activated by 3-phosphoinositide-dependent protein kinase-1. eng. *The Journal of biological chemistry* **274.** Journal Article Research Support, Non-U.S. Gov't, 27168–27176. ISSN: 0021-9258. eprint: 10480933 (1999).

290. Le Good, J. A. *et al.* Protein kinase C isotypes controlled by phosphoinositide 3-kinase through the protein kinase PDK1. eng. *Science (New York, N.Y.)* **281.** Journal Article Research Support, Non-U.S. Gov't, 2042–2045. ISSN: 0036-8075. eprint: 9748166 (1998).

291. Dutil, E. M., Toker, A. & Newton, A. C. Regulation of conventional protein kinase C isozymes by phosphoinositide-dependent kinase 1 (PDK-1). eng. *Current biology : CB* **8.** Journal Article Research Support, U.S. Gov't, P.H.S., 1366–1375. ISSN: 0960-9822. eprint: 9889098 (1998).

292. Najafov, A., Sommer, E. M., Axten, J. M., Deyoung, M. P. & Alessi, D. R. Characterization of GSK2334470, a novel and highly specific inhibitor of PDK1. eng. *The Biochemical journal* **433.** Journal Article Research Support, Non-U.S. Gov't, 357–369. eprint: 21087210 (2011).

293. Medina, J. R. *et al.* Structure-based design of potent and selective 3-phosphoinositide-dependent kinase-1 (PDK1) inhibitors. eng. *Journal of medicinal chemistry* **54.** Journal Article, 1871–1895. eprint: 21341675 (2011).

294. Elong Edimo, W. *et al.* Evidence of SHIP2 Ser132 phosphorylation, its nuclear localization and stability. eng. *The Biochemical journal* **439.** Comparative Study Journal Article Research Support, Non-U.S. Gov't, 391–401. eprint: 21770892 (2011).

295. Elong Edimo, W., Vanderwinden, J.-M. & Erneux, C. SHIP2 signalling at the plasma membrane, in the nucleus and at focal contacts. eng. *Advances in biological regulation* **53.** Journal Article Research Support, Non-U.S. Gov't Review, 28–37. eprint: 23040614 (2013).

296. Lamkin, T. D. *et al.* Shc interaction with Src homology 2 domain containing inositol phosphatase (SHIP) in vivo requires the Shc-phosphotyrosine binding domain and two specific phosphotyrosines on SHIP. eng. *The Journal of biological chemistry* **272.** Journal Article Research Support, Non-U.S. Gov't Research Support, U.S. Gov't, P.H.S., 10396–10401. ISSN: 0021-9258. eprint: 9099679 (1997).

297. Liu, L., Damen, J. E., Cutler, R. L. & Krystal, G. Multiple cytokines stimulate the binding of a common 145-kilodalton protein to Shc at the Grb2 recognition site of Shc. eng. *Molecular and cellular biology* **14.** Journal Article Research Support, Non-U.S. Gov't, 6926–6935. ISSN: 0270-7306. eprint: 7523859 (1994).

298. Ong, C. J. *et al.* Small-molecule agonists of SHIP1 inhibit the phosphoinositide 3-kinase pathway in hematopoietic cells. eng. *Blood* **110.** Journal Article Research Support, Non-U.S. Gov't, 1942–1949. ISSN: 0006-4971. eprint: 17502453 (2007).

299. Fu, M. *et al.* Elevated expression of SHIP2 correlates with poor prognosis in non-small cell lung cancer. eng. *International journal of clinical and experimental pathology* **6.** Journal Article, 2185–2191. eprint: 24133597 (2013).

300. Zhou, J., Di, M. & Han, H. Upregulation of SHIP2 participates in the development of breast cancer via promoting Wnt/b-catenin signaling. eng. *OncoTargets and therapy* **12.** Journal Article The authors report no conflicts of interest in this work., 7067–7077. ISSN: 1178-6930. eprint: 31564892 (2019).

301. Zhou, X., Liu, Y. & Tan, G. Prognostic value of elevated SHIP2 expression in laryngeal squamous cell carcinoma. eng. *Archives of medical research* **42.** Journal Article, 589–595. eprint: 22079859 (2011).

302. Hoekstra, E. *et al.* Lipid phosphatase SHIP2 functions as oncogene in colorectal cancer by regulating PKB activation. eng. *Oncotarget* **7.** Journal Article CONFLICTS OF INTEREST. None., 73525–73540. eprint: 27716613 (2016).

303. Ecker, V. *et al.* SHIP1 Inhibition As Novel Therapeutic Approach in Chronic Lymphocytic Leukemia. *Blood* **132,** 894. ISSN: 0006-4971 (2018).

304. Hoxhaj, G. & Manning, B. D. The PI3K-AKT network at the interface of oncogenic signalling and cancer metabolism. eng. *Nature reviews. Cancer* **20.** Journal Article Research Support, N.I.H., Extramural Research Support, Non-U.S. Gov't Research Support, U.S. Gov't, Non-P.H.S. Review, 74–88. eprint: 31686003 (2020).

305. Sander, S. *et al.* Synergy between PI3K signaling and MYC in Burkitt lymphomagenesis. eng. *Cancer Cell* **22.** Journal Article Research Support, N.I.H., Extramural Research Support, Non-U.S. Gov't, 167–179. ISSN: 1535-6108. eprint: 22897848 (2012).

306. Li, J. *et al.* PTEN, a putative protein tyrosine phosphatase gene mutated in human brain, breast, and prostate cancer. eng. *Science (New York, N.Y.)* **275.** Journal Article Research Support, Non-U.S. Gov't Research Support, U.S. Gov't, Non-P.H.S. Research Support, U.S. Gov't, P.H.S., 1943–1947. ISSN: 0036-8075. eprint: 9072974 (1997).

307. Steck, P. A. *et al.* Identification of a candidate tumour suppressor gene, MMAC1, at chromosome 10q23.3 that is mutated in multiple advanced cancers. eng. *Nature genetics* **15.** Journal Article Research Support, Non-U.S. Gov't Research Support, U.S. Gov't, P.H.S., 356–362. ISSN: 1061-4036. eprint: 9090379 (1997).

308. Shimobayashi, M. & Hall, M. N. Making new contacts: the mTOR network in metabolism and signalling crosstalk. eng. *Nature reviews. Molecular cell biology* **15.** Journal Article Research Support, Non-U.S. Gov't Review, 155–162. eprint: 24556838 (2014).

309. Choi, Y. *et al.* PTEN, but not SHIP and SHIP2, suppresses the PI3K/Akt pathway and induces growth inhibition and apoptosis of myeloma cells. eng. *Oncogene* **21.** Comparative Study Journal Article Research Support, Non-U.S. Gov't, 5289–5300. ISSN: 0950-9232. eprint: 12149650 (2002).

310. Kerr, W. G. Inhibitor and activator: dual functions for SHIP in immunity and cancer. eng. *Annals of the New York Academy of Sciences* **1217.** Journal Article Research Support, N.I.H., Extramural Research Support, Non-U.S. Gov't Review Conflict of Interest Disclosure: The author currently serves on the Scientific Advisory Board of Aquinox Pharmaceuticals (Vancouver, BC) that is devoted to chemical modulation of SHIP1 expression for therapeutic purposes. The author is also the inventor or co-inventor on patents, both issued and pending, related to modulation of SHIP expression and activity for therapeutic purposes., 1–17. eprint: 21155837 (2011).

311. Frys, S. *et al.* Deregulation of the PI3K/Akt Signal Transduction Pathway Is Associated with the Development of Chemotherapy Resistance and Can be Effectively Targeted to Improve Chemoresponsiveness in Burkitt Lymphoma Pre-Clinical Models. *Blood* **124,** 1769. ISSN: 0006-4971 (2014).

312. Bhatti, M. *et al.* Pre-clinical activity of targeting the PI3K/Akt/mTOR pathway in Burkitt lymphoma. eng. *Oncotarget* **9.** Journal Article CONFLICTS OF INTEREST The authors listed in this paper certify that they have no affiliations with or involvement in any organization or entity with any financial interest (such as honoraria; educational grants; participation in speakers' bureaus; membership, employment, consultancies, stock ownership, or other equity interest; and expert testimony or patent-licensing arrangements), or non-financial interest (such as personal or professional relationships, affiliations, knowledge or beliefs) in the subject matter or materials discussed in this manuscript., 21820–21830. eprint: 29774105 (2018).

313. Schmitz, R. *et al.* Genetics and Pathogenesis of Diffuse Large B-Cell Lymphoma. eng. *The New England journal of medicine* **378.** Journal Article Research Support, N.I.H., Intramural Research Support, Non-U.S. Gov't, 1396–1407. eprint: 29641966 (2018).

314. Gehringer, F., Weissinger, S. E., Möller, P., Wirth, T. & Ushmorov, A. Physiological levels of the PTEN-PI3K-AKT axis activity are required for maintenance of Burkitt lymphoma. eng. *Leukemia* **34.** Journal Article Research Support, Non-U.S. Gov't The authors declare that they have no conflict of interest., 857–871. eprint: 31719683 (2020).

315. Oki, Y. *et al.* Phase II study of an AKT inhibitor MK2206 in patients with relapsed or refractory lymphoma. eng. *British journal of haematology* **171.** Clinical Trial, Phase II Journal Article Research Support, N.I.H., Extramural statements Authors disclosed no conflict of interest., 463–470. eprint: 26213141 (2015).

316. Saurus, P. *et al.* Inhibition of SHIP2 in CD2AP-deficient podocytes ameliorates reactive oxygen species generation but aggravates apoptosis. eng. *Scientific reports* **7.** Journal Article Research Support, Non-U.S. Gov't The authors declare that they have no competing interests., 10731. eprint: 28878342 (2017).

317. Schmid, M. C. *et al.* Receptor tyrosine kinases and TLR/IL1Rs unexpectedly activate myeloid cell PI3kg, a single convergent point promoting tumor inflammation and progression. eng. *Cancer Cell* **19.** Journal Article Research Support, N.I.H., Extramural Research Support, Non-U.S. Gov't, 715–727. ISSN: 1535-6108. eprint: 21665146 (2011).

318. Houslay, D. M. *et al.* Coincident signals from GPCRs and receptor tyrosine kinases are uniquely transduced by PI3Kb in myeloid cells. eng. *Science signaling* **9.** Journal Article Research Support, N.I.H., Extramural Research Support, Non-U.S. Gov't Competing interests: The authors declare that they have no competing interests., ra82. eprint: 27531651 (2016).

319. Fruman, D. A. *et al.* The PI3K Pathway in Human Disease. eng. *Cell* **170.** Journal Article Review, 605–635. eprint: 28802037 (2017).

320. Tuveson, D. A., Carter, R. H., Soltoff, S. P. & Fearon, D. T. CD19 of B cells as a surrogate kinase insert region to bind phosphatidylinositol 3-kinase. eng. *Science (New York, N.Y.)* **260.** Journal Article Research Support, Non-U.S. Gov't Research Support, U.S. Gov't, P.H.S., 986–989. ISSN: 0036-8075. eprint: 7684160 (1993).

321. Otero, D. C., Omori, S. A. & Rickert, R. C. Cd19-dependent activation of Akt kinase in B-lymphocytes. eng. *The Journal of biological chemistry* **276.** Journal Article Research Support, Non-U.S. Gov't Research Support, U.S. Gov't, P.H.S., 1474–1478. ISSN: 0021-9258. eprint: 11042164 (2001).

322. Graf, S. A. & Gopal, A. K. Idelalisib for the treatment of non-Hodgkin lymphoma. eng. *Expert opinion on pharmacotherapy* **17.** Journal Article Research Support, N.I.H., Extramural Review, 265–274. eprint: 26818003 (2016).

323. Madanat, Y. F., Smith, M. R., Almasan, A. & Hill, B. T. Idelalisib therapy of indolent B-cell malignancies: chronic lymphocytic leukemia and small lymphocytic or follicular lymphomas. eng. *Blood and lymphatic cancer : targets and therapy* **6.** Journal Article Disclosure. AA was supported by the CA127264 research grant from National Institutes of Health. BTH has served on an advisory boards with both Genentech and Pharmacyclics. MRS has served on advisory boards with Genentech, Spectrum, and Celgene. The authors report no other conflicts of interest in this work., 1–6. ISSN: 1179-9889. eprint: 27375364 (2016).

324. Mark J Roschewski, M. D. *Copanlisib With Dose-Adjusted EPOCH-R in Relapsed and Refractory Burkitt Lymphoma and Other High-Grade B-cell Lymphomas* (ed National Cancer Institute) https://classic.clinicaltrials.gov/ct2/show/NCT04933617 (2023).

325. Bleckmann, A. *et al.* Treatment response to idelalisib in a patient with immunodeficiency-associated Burkitt lymphoma harboring a PIK3CA H1047R mutation. eng. *Annals of hematology* **100.** Case Reports Letter, 277–279. eprint: 32193631 (2021).

326. Laplante, M. & Sabatini, D. M. mTOR signaling at a glance. eng. *Journal of cell science* **122.** Journal Article Research Support, N.I.H., Extramural Research Support, Non-U.S. Gov't Review, 3589–3594. eprint: 19812304 (2009).

327. Laplante, M. & Sabatini, D. M. Regulation of mTORC1 and its impact on gene expression at a glance. eng. *Journal of cell science* **126.** Journal Article Research Support, N.I.H., Extramural Research Support, Non-U.S. Gov't Review, 1713–1719. eprint: 23641065 (2013).

328. García-Martínez, J. M. & Alessi, D. R. mTOR complex 2 (mTORC2) controls hydrophobic motif phosphorylation and activation of serum- and glucocorticoid-induced protein kinase 1 (SGK1). eng. *The Biochemical journal* **416.** Journal Article Research Support, Non-U.S. Gov't, 375–385. eprint: 18925875 (2008).

329. Marat, A. L. *et al.* mTORC1 activity repression by late endosomal phosphatidylinositol 3,4-bisphosphate. eng. *Science (New York, N.Y.)* **356.** Journal Article Research Support, Non-U.S. Gov't, 968–972. ISSN: 0036-8075. eprint: 28572395 (2017).

330. Cen, O. & Longnecker, R. Rapamycin reverses splenomegaly and inhibits tumor development in a transgenic model of Epstein-Barr virus-related Burkitt's lymphoma. eng. *Molecular cancer therapeutics* **10.** Journal Article Research Support, N.I.H., Extramural Research Support, Non-U.S. Gov't, 679–686. eprint: 21282357 (2011).

331. Ono, K. *et al.* A novel strategy inducing autophagic cell death in Burkitt's lymphoma cells with anti-CD19-targeted liposomal rapamycin. eng. *Blood cancer journal* **4.** Journal Article, e180. ISSN: 2044-5385. eprint: 24510029 (2014).

332. Ippolito, T., Mavis, C., Gu, J., Hernandez-Ilizaliturri, F. J. & Barth, M. J. Omipalisib (GSK458), a Dual an-PI3K/mTOR Inhibitor, Exhibits in Vitro and In Vivo activity in Chemotherapy-Sensitive and -Resistant Models of Burkitt Lymphoma. *Blood* **132,** 2951. ISSN: 0006-4971 (2018).

333. Pearn, L., Fisher, J., Burnett, A. K. & Darley, R. L. The role of PKC and PDK1 in monocyte lineage specification by Ras. eng. *Blood* **109.** Journal Article Research Support, Non-U.S. Gov't, 4461–4469. ISSN: 0006-4971. eprint: 17255356 (2007).

334. Ahmed, N., Riley, C. & Quinn, M. A. An immunohistochemical perspective of PPAR beta and one of its putative targets PDK1 in normal ovaries, benign and malignant ovarian tumours. eng. *British journal of cancer* **98.** Journal Article Research Support, Non-U.S. Gov't, 1415–1424. eprint: 18349831 (2008).

335. Du, J. *et al.* PDK1 promotes tumor growth and metastasis in a spontaneous breast cancer model. eng. *Oncogene* **35.** Journal Article, 3314–3323. ISSN: 0950-9232. eprint: 26455327 (2016).

336. Zeng, X., Xu, H. & Glazer, R. I. Transformation of mammary epithelial cells by 3-phosphoinositide-dependent protein kinase-1 (PDK1) is associated with the induction of protein kinase Calpha. eng. *Cancer research* **62.** Journal Article Research Support, U.S. Gov't, Non-P.H.S. Research Support, U.S. Gov't, P.H.S., 3538–3543. ISSN: 0008-5472. eprint: 12068001 (2002).

337. Filippa, N., Sable, C. L., Hemmings, B. A. & van Obberghen, E. Effect of phosphoinositide-dependent kinase 1 on protein kinase B translocation and its subsequent activation. eng. *Molecular and cellular biology* **20.** Journal Article Research Support, Non-U.S. Gov't, 5712–5721. ISSN: 0270-7306. eprint: 10891507 (2000).

338. Gao, X. *et al.* PI3K/Akt signaling requires spatial compartmentalization in plasma membrane microdomains. eng. *Proceedings of the National Academy of Sciences of the United States of America* **108.** Journal Article Research Support, N.I.H., Extramural Research Support, Non-U.S. Gov't The authors declare no conflict of interest., 14509–14514. eprint: 21873248 (2011).

339. Currie, R. A. *et al.* Role of phosphatidylinositol 3,4,5-trisphosphate in regulating the activity and localization of 3-phosphoinositide-dependent protein kinase-1. eng. *The Biochemical journal* **337 (Pt 3).** Journal Article Research Support, Non-U.S. Gov't, 575–583. eprint: 9895304 (1999).

340. Anderson, K. E., Coadwell, J., Stephens, L. R. & Hawkins, P. T. Translocation of PDK-1 to the plasma membrane is important in allowing PDK-1 to activate protein kinase B. eng. *Current biology : CB* **8.** Journal Article Research Support, Non-U.S. Gov't, 684–691. ISSN: 0960-9822. eprint: 9637919 (1998).

341. Mora, A., Komander, D., van Aalten, D. M. F. & Alessi, D. R. PDK1, the master regulator of AGC kinase signal transduction. eng. *Seminars in cell & developmental biology* **15.** Journal Article Research Support, Non-U.S. Gov't Review, 161–170. ISSN: 1084-9521. eprint: 15209375 (2004).

342. Kobayashi, T. & Cohen, P. Activation of serum- and glucocorticoid-regulated protein kinase by agonists that activate phosphatidylinositide 3-kinase is mediated by 3-phosphoinositide-dependent protein kinase-1 (PDK1) and PDK2. eng. *The Biochemical journal* **339 (Pt 2).** Journal Article Research Support, Non-U.S. Gov't, 319–328. eprint: 10191262 (1999).

343. Vasudevan, K. M. *et al.* AKT-independent signaling downstream of oncogenic PIK3CA mutations in human cancer. eng. *Cancer Cell* **16.** Journal Article Research Support, N.I.H., Extramural Research Support, Non-U.S. Gov't Research Support, U.S. Gov't, Non-P.H.S., 21–32. ISSN: 1535-6108. eprint: 19573809 (2009).

344. Falasca, M. *et al.* Activation of phospholipase C gamma by PI 3-kinase-induced PH domain-mediated membrane targeting. eng. *The EMBO journal* **17.** Journal Article Research Support, Non-U.S. Gov't, 414–422. ISSN: 0261-4189. eprint: 9430633 (1998).

345. Brezski, R. J. & Monroe, J. G. B cell antigen receptor-induced Rac1 activation and Rac1-dependent spreading are impaired in transitional immature B cells due to levels of membrane cholesterol. eng. *Journal of immunology (Baltimore, Md. : 1950)* **179.** Journal Article Research Support, N.I.H., Extramural, 4464–4472. eprint: 17878342 (2007).

346. Gewinner, C. *et al.* Evidence that inositol polyphosphate 4-phosphatase type II is a tumor suppressor that inhibits PI3K signaling. eng. *Cancer Cell* **16.** Journal Article, 115–125. ISSN: 1535-6108. eprint: 19647222 (2009).

347. Sun, H. Q., Yamamoto, M., Mejillano, M. & Yin, H. L. Gelsolin, a multifunctional actin regulatory protein. eng. *The Journal of biological chemistry* **274.** Journal Article Research Support, Non-U.S. Gov't Research Support, U.S. Gov't, P.H.S. Review, 33179–33182. ISSN: 0021-9258. eprint: 10559185 (1999).

348. Marion, E. *et al.* The gene INPPL1, encoding the lipid phosphatase SHIP2, is a candidate for type 2 diabetes in rat and man. eng. *Diabetes* **51.** Journal Article Research Support, Non-U.S. Gov't, 2012–2017. ISSN: 0012-1797. eprint: 12086927 (2002).

349. Falasca, M. *et al.* The role of phosphoinositide 3-kinase C2alpha in insulin signaling. eng. *The Journal of biological chemistry* **282.** Journal Article Research Support, Non-U.S. Gov't, 28226–28236. ISSN: 0021-9258. eprint: 17644513 (2007).

350. Posor, Y. *et al.* Spatiotemporal control of endocytosis by phosphatidylinositol-3,4-bisphosphate. eng. *Nature* **499.** Journal Article Research Support, Non-U.S. Gov't, 233–237. ISSN: 0028-0836. eprint: 23823722 (2013).

351. Gozzelino, L., de Santis, M. C., Gulluni, F., Hirsch, E. & Martini, M. PI(3,4)P2 Signaling in Cancer and Metabolism. eng. *Frontiers in oncology* **10.** Journal Article Review, 360. ISSN: 2234-943X. eprint: 32296634 (2020).

352. Maekawa, M. *et al.* Sequential breakdown of 3-phosphorylated phosphoinositides is essential for the completion of macropinocytosis. eng. *Proceedings of the National Academy of Sciences of the United States of America* **111.** Journal Article Research Support, N.I.H., Extramural Research Support, Non-U.S. Gov't The authors declare no conflict of interest., E978–87. eprint: 24591580 (2014).

353. Hogan, A. *et al.* The phosphoinositol 3,4-bisphosphate-binding protein TAPP1 interacts with syntrophins and regulates actin cytoskeletal organization. eng. *The Journal of biological chemistry* **279.** Journal Article Research Support, Non-U.S. Gov't, 53717–53724. ISSN: 0021-9258. eprint: 15485858 (2004).

354. Gulluni, F., de Santis, M. C., Margaria, J. P., Martini, M. & Hirsch, E. Class II PI3K Functions in Cell Biology and Disease. eng. *Trends in cell biology* **29.** Journal Article Research Support, Non-U.S. Gov't Review, 339–359. eprint: 30691999 (2019).

355. Stoddart, A. *et al.* Lipid rafts unite signaling cascades with clathrin to regulate BCR internalization. eng. *Immunity* **17.** Journal Article Research Support, Non-U.S. Gov't Research Support, U.S. Gov't, P.H.S., 451–462. ISSN: 1074-7613. eprint: 12387739 (2002).

356. Stoddart, A., Jackson, A. P. & Brodsky, F. M. Plasticity of B cell receptor internalization upon conditional depletion of clathrin. eng. *Molecular biology of the cell* **16.** Journal Article Research Support, N.I.H., Extramural Research Support, Non-U.S. Gov't Research Support, U.S. Gov't, P.H.S., 2339–2348. eprint: 15716350 (2005).

357. Rappaport, N. *et al.* MalaCards: an integrated compendium for diseases and their annotation. eng. *Database : the journal of biological databases and curation* **2013.** Journal Article Research Support, Non-U.S. Gov't, bat018. eprint: 23584832 (2013).

358. Hasgall, P. A. *et al.* The putative RNA helicase HELZ promotes cell proliferation, translation initiation and ribosomal protein S6 phosphorylation. eng. *PloS one* **6.** Journal Article Research Support, Non-U.S. Gov't Competing Interests: The authors have declared that no competing interests exist., e22107. eprint: 21765940 (2011).

359. Dowler, S. *et al.* Identification of pleckstrin-homology-domain-containing proteins with novel phosphoinositide-binding specificities. eng. *The Biochemical journal* **351.** Journal Article Research Support, Non-U.S. Gov't, 19–31. eprint: 11001876 (2000).

360. Marshall, A. J., Krahn, A. K., Ma, K., Duronio, V. & Hou, S. TAPP1 and TAPP2 are targets of phosphatidylinositol 3-kinase signaling in B cells: sustained plasma membrane recruitment triggered by the B-cell antigen receptor. eng. *Molecular and cellular biology* **22.** Journal Article Research Support, Non-U.S. Gov't Research Support, U.S. Gov't, P.H.S., 5479–5491. ISSN: 0270-7306. eprint: 12101241 (2002).

361. Wullschleger, S., Wasserman, D. H., Gray, A., Sakamoto, K. & Alessi, D. R. Role of TAPP1 and TAPP2 adaptor binding to PtdIns(3,4)P2 in regulating insulin sensitivity defined by knock-in analysis. eng. *The Biochemical journal* **434.** Journal Article Research Support, N.I.H., Extramural Research Support, Non-U.S. Gov't, 265–274. eprint: 21204784 (2011).

362. Landego, I. *et al.* Interaction of TAPP adapter proteins with phosphatidylinositol (3,4)-bisphosphate regulates B-cell activation and autoantibody production. eng. *European journal of immunology* **42.** Journal Article Research Support, Non-U.S. Gov't, 2760–2770. eprint: 22777911 (2012).

363. Le, A. *et al.* Glucose-independent glutamine metabolism via TCA cycling for proliferation and survival in B cells. eng. *Cell metabolism* **15.** Journal Article Research Support, N.I.H., Extramural Research Support, Non-U.S. Gov't Research Support, U.S. Gov't, Non-P.H.S., 110–121. eprint: 22225880 (2012).

364. Schwarzfischer, P. *et al.* Comprehensive Metaboproteomics of Burkitt's and Diffuse Large B-Cell Lymphoma Cell Lines and Primary Tumor Tissues Reveals Distinct Differences in Pyruvate Content and Metabolism. eng. *Journal of proteome research* **16.** Journal Article Research Support, Non-U.S. Gov't, 1105–1120. eprint: 28161958 (2017).

365. D'Avola, A. *et al.* PHGDH is required for germinal center formation and is a therapeutic target in MYC-driven lymphoma. eng. *The Journal of clinical investigation* **132.** Journal Article Research Support, Non-U.S. Gov't Conflict of interest: KHV is on the board of directors, is a shareholder of Bristol Myers Squibb, is a shareholder of GRAIL Inc., and is on the science advisory board (with stock options) of PMV Pharma, RAZE Therapeutics, and Volastra Therapeutics Inc. She is also on the SAB of Ludwig Cancer. KHV is a cofounder and consultant of Faeth Therapeutics. She has been in receipt of research funding from Astex Pharmaceuticals and AstraZeneca, and she contributed to CRUK Cancer Research Technology filing of Patent Application WO/2017/144877. JGG has received research funding from Celgene, Janssen, and Acerta and honoraria from Abbvie, Acerta, Celgene, Gilead, Janssen, Novartis, Pharmacyclics, and Roche. eprint: 35316216 (2022).

366. Huang, S. *et al.* Novel personalized pathway-based metabolomics models reveal key metabolic pathways for breast cancer diagnosis. eng. *Genome medicine* **8.** Journal Article Research Support, N.I.H., Extramural Research Support, Non-U.S. Gov't, 34. eprint: 27036109 (2016).

367. Anantharaju, P. G. *et al.* Naturally occurring benzoic acid derivatives retard cancer cell growth by inhibiting histone deacetylases (HDAC). eng. *Cancer biology & therapy* **18.** Journal Article, 492–504. eprint: 28506198 (2017).

368. Mycielska, M. E. *et al.* Potential Use of Gluconate in Cancer Therapy. eng. *Frontiers in oncology* **9.** Journal Article, 522. ISSN: 2234-943X. eprint: 31275855 (2019).

369. Garcia-Bermudez, J. *et al.* Aspartate is a limiting metabolite for cancer cell proliferation under hypoxia and in tumours. eng. *Nature cell biology* **20.** Journal Article Research Support, N.I.H., Extramural Research Support, Non-U.S. Gov't, 775–781. eprint: 29941933 (2018).

370. Sullivan, L. B. *et al.* Aspartate is an endogenous metabolic limitation for tumour growth. eng. *Nature cell biology* **20.** Journal Article Research Support, N.I.H., Extramural Research Support, Non-U.S. Gov't, 782–788. eprint: 29941931 (2018).

371. Duan, R. *et al.* Uncovering the Metabolic Origin of Aspartate for Tumor Growth Using an Integrated Molecular Deactivator. eng. *Nano letters* **21.** Journal Article Research Support, Non-U.S. Gov't, 778–784. eprint: 33301328 (2021).

372. Wang, Y. *et al.* Coordinative metabolism of glutamine carbon and nitrogen in proliferating cancer cells under hypoxia. eng. *Nature communications* **10.** Journal Article Research Support, Non-U.S. Gov't The authors declare no competing interests., 201. eprint: 30643150 (2019).

373. Commisso, C. *et al.* Macropinocytosis of protein is an amino acid supply route in Ras-transformed cells. eng. *Nature* **497.** Journal Article Research Support, N.I.H., Extramural Research Support, Non-U.S. Gov't, 633–637. ISSN: 0028-0836. eprint: 23665962 (2013).

374. Kamphorst, J. J. *et al.* Human pancreatic cancer tumors are nutrient poor and tumor cells actively scavenge extracellular protein. eng. *Cancer research* **75.** Journal Article Research Support, N.I.H., Extramural Research Support, Non-U.S. Gov't, 544–553. ISSN: 0008-5472. eprint: 25644265 (2015).

375. Davidson, S. M. *et al.* Direct evidence for cancer-cell-autonomous extracellular protein catabolism in pancreatic tumors. eng. *Nature medicine* **23.** Journal Article, 235–241. eprint: 28024083 (2017).

376. Martínez-Riaño, A. *et al.* Antigen phagocytosis by B cells is required for a potent humoral response. eng. *EMBO reports* **19.** Journal Article Research Support, Non-U.S. Gov't. eprint: 29987136 (2018).

377. Fernandes, S. *et al.* Obesity control by SHIP inhibition requires pan-paralog inhibition and an intact eosinophil compartment. eng. *iScience* **26.** Journal Article W.G.K, S.F., C.P. and J.D.C have patents, pending and issued, concerning the analysis and targeting of SHIP1 and SHIP2 in disease. The other authors have no interests to declare., 106071. eprint: 36818285 (2023).

378. Dempke, W. C. M., Uciechowski, P., Fenchel, K. & Chevassut, T. Targeting SHP-1, 2 and SHIP Pathways: A Novel Strategy for Cancer Treatment? eng. *Oncology* **95.** Journal Article Review, 257–269. eprint: 29925063 (2018).

379. Kerr, W. G., Pedicone, C., Dormann, S., Pacherille, A. & Chisholm, J. D. Small molecule targeting of SHIP1 and SHIP2. eng. *Biochemical Society transactions* **48.** Journal Article Review, 291–300. ISSN: 0300-5127. eprint: 32049315 (2020).

380. Tomska, K. *et al.* Drug-based perturbation screen uncovers synergistic drug combinations in Burkitt lymphoma. eng. *Scientific reports* **8.** Journal Article The authors declare no competing interests., 12046. eprint: 30104685 (2018).

381. Hoelzer, D. *et al.* Improved outcome of adult Burkitt lymphoma/leukemia with rituximab and chemotherapy: report of a large prospective multicenter trial. eng. *Blood* **124.** Clinical Trial Journal Article Multicenter Study Research Support, Non-U.S. Gov't, 3870–3879. ISSN: 0006-4971. eprint: 25359988 (2014).

382. Baumgartener, J. W. SHIP2: an emerging target for the treatment of type 2 diabetes mellitus. eng. *Current drug targets. Immune, endocrine and metabolic disorders* **3.** Journal Article Review, 291–298. ISSN: 1568-0088. eprint: 14683460 (2003).

383. Lehtonen, S. SHIPping out diabetes—Metformin, an old friend among new SHIP2 inhibitors. eng. *Acta Physiologica (Oxford, England)* **228.** Journal Article Review. ISSN: 1748-1708. eprint: 31342643 (2019).

384. Ye, X. *et al.* Selective deletion of SHIP-1 in hematopoietic cells in mice leads to severe lung inflammation involving ILC2 cells. eng. *Scientific reports* **11.** Journal Article Research Support, N.I.H., Extramural Research Support, Non-U.S. Gov't The authors declare no competing interests., 9220. eprint: 33911168 (2021).

385. Helgason, C. D. *et al.* Targeted disruption of SHIP leads to hemopoietic perturbations, lung pathology, and a shortened life span. eng. *Genes & development* **12.** Journal Article Research Support, Non-U.S. Gov't, 1610–1620. ISSN: 0890-9369. eprint: 9620849 (1998).

386. Wada, T. *et al.* Overexpression of SH2-containing inositol phosphatase 2 results in negative regulation of insulin-induced metabolic actions in 3T3-L1 adipocytes via its 5'-phosphatase catalytic activity. eng. *Molecular and cellular biology* **21.** Journal Article Research Support, Non-U.S. Gov't, 1633–1646. ISSN: 0270-7306. eprint: 11238900 (2001).

387. Soeda, Y. *et al.* The inositol phosphatase SHIP2 negatively regulates insulin/IGF-I actions implicated in neuroprotection and memory function in mouse brain. eng. *Molecular endocrinology (Baltimore, Md.)* **24.** Journal Article Research Support, Non-U.S. Gov't, 1965–1977. eprint: 20829391 (2010).

388. Sasaoka, T. *et al.* SH2-containing inositol phosphatase 2 negatively regulates insulin-induced glycogen synthesis in L6 myotubes. eng. *Diabetologia* **44.** Journal Article Research Support, Non-U.S. Gov't, 1258–1267. ISSN: 0012-186X. eprint: 11692174 (2001).

389. Polianskyte-Prause, Z. *et al.* Metformin increases glucose uptake and acts renoprotectively by reducing SHIP2 activity. eng. *FASEB journal : official publication of the Federation of American Societies for Experimental Biology* **33.** Journal Article Research Support, Non-U.S. Gov't, 2858–2869. eprint: 30321069 (2019).

390. Commisso, C., Flinn, R. J. & Bar-Sagi, D. Determining the macropinocytic index of cells through a quantitative image-based assay. eng. *Nature protocols* **9.** Journal Article Research Support, N.I.H., Extramural Research Support, Non-U.S. Gov't The authors declare that they have no competing financial interests., 182–192. eprint: 24385148 (2014).

391. Wang, J. T. H. *et al.* The SNX-PX-BAR family in macropinocytosis: the regulation of macropinosome formation by SNX-PX-BAR proteins. eng. *PloS one* **5.** Journal Article Research Support, Non-U.S. Gov't Competing Interests: The authors have declared that no competing interests exist., e13763. eprint: 21048941 (2010).

392. Wang, J. T. H., Teasdale, R. D. & Liebl, D. Macropinosome quantitation assay. eng. *MethodsX* **1.** Journal Article, 36–41. ISSN: 2215-0161. eprint: 26150932 (2014).

393. Miao, B. *et al.* Small molecule inhibition of phosphatidylinositol-3,4,5-triphosphate (PIP3) binding to pleckstrin homology domains. eng. *Proceedings of the National Academy of Sciences of the United States of America* **107.** Journal Article Research Support, N.I.H., Extramural Research Support, Non-U.S. Gov't Research Support, U.S. Gov't, Non-P.H.S. The authors declare no conflict of interest., 20126–20131. eprint: 21041639 (2010).

394. Riehle, R. D., Cornea, S., Degterev, A. & Torchilin, V. Micellar formulations of pro-apoptotic DM-PIT-1 analogs and TRAIL in vitro and in vivo. eng. *Drug delivery* **20.** Journal Article Research Support, N.I.H., Extramural Research Support, U.S. Gov't, Non-P.H.S., 78–85. eprint: 23495715 (2013).

395. Meyer, S. N., Koul, S. & Pasqualucci, L. Mouse Models of Germinal Center Derived B-Cell Lymphomas. eng. *Frontiers in immunology* **12.** Journal Article Research Support, N.I.H., Extramural Research Support, Non-U.S. Gov't Review The authors declare that the research was conducted in the absence of any commercial or financial relationships that could be construed as a potential conflict of interest., 710711. eprint: 34456919 (2021).